TRAPPED ION STUDIES OF ION-MOLECULE REACTIONS

Thesis by
Peter George Miasek

In Partial Fulfillment of the Requirements
For the Degree of
Doctor of Philosophy

California Institute of Technology
Pasadena, California
1973

(Submitted January 31, 1973)

ACKNOWLEDGEMENTS

Writing a thesis is an all-consuming endeavour, and now at its completion, the number of people who have assisted me in its realization seems endless.

First, I wish to sincerely thank my advisor, Professor J. L. Beauchamp, for his guidance, assistance and encouragement during my graduate career. On a personal level, I will remember Jack for his friendliness and his interest in student welfare outside the laboratory.

I would like to thank all the members of the Beauchamp group, past and present, with whom I have been associated. I have learned from each one and profited from each acquaintance. Special thanks are extended to Terry McMahon, with whom I have collaborated on most of the ICR experiments, and to Ralph Staley, with whom the direct kinetic energy analysis-photoionization experiments were undertaken. I will also remember the responsive ears, helping hands and empty glasses that these two gentlemen always extended.

The technical assistance of Wm. Schuelke, Jim Fetz, Villy Jorgensen and the other members of departmental shops is gratefully acknowledged.

I wish to thank two women who have been very important people to me in recent weeks. They are my typists, Edi Bierce and Mary Lynn Muir.

My loving wife, Donna, deserves special recognition for drawing no less than 60 figures (!) and for assisting me and caring for me in innumerable ways.

Finally, I express my gratitude to the California Institute of Technology and the Department of Chemistry for providing tuition scholarships and graduate teaching assistantships, and to the Atomic Energy Commission which, by grants to JLB, supported this research.

ABSTRACT

Ion-molecule reactions have been studied using a novel high pressure mass spectrometer employing crossed electric and magnetic fields for ion trapping. These studies have been supplemented by ones undertaken using trapped ion-ion cyclotron resonance (ICR) spectrometry.

Reaction rate constants at low ion energies have been measured in many systems, and compare favourably with results of other studies. Correlations of measured rates with theoretical models have characterized certain features of ion-neutral collision processes. Comparisons between chemically similar systems have also provided information about these encounters.

Internal excitation of reactant ions has been shown to induce thermodynamically disallowed reactions. Evidence suggesting the participation of vibrationally excited ions reacting at different rates than their ground state counterparts is presented.

The formation and lifetimes of excited intermediates in ethylene and methanol has been investigated in detail. Relative rates of collisional stabilization of $(C_5H_9^+)^*$ by inert gases have been determined and compared with similar processes in neutral systems. Stabilization of $(C_5H_9^+)^*$ by ethylene itself exhibits different characteristics than those of inert gases.

The equilibrium constant of a reversible ion-molecule reaction has been measured at two temperatures and used to determine the enthalpy and entropy change for the process.

The rates of various thermoneutral proton and charge-transfer reactions have been measured using trapped ion-ion ejection ICR spectrometry. This has enabled a detailed characterization of the collisional phenomena in these systems.

The kinetic energy distribution of CH_3^+ arising from ionization of methyl halides has been determined using ICR spectrometry and photoionization spectroscopy. Inferences about the nature of the dissociative states are presented.

TABLE OF CONTENTS

Chapter		Page
1	Introduction	1
2	Theoretical Models of Ion-Molecule Reactions	6
3	Experimental Techniques of Studying Ion-Molecule Reactions	15
	I. Single Source Mass Spectrometers	15
	II. Tandem Mass Spectrometers	24
4	Design, Construction, and Principles of Operation of the High Pressure Mass Spectrometer	35
	I. General Description	35
	II. Construction of the Spectrometer	35
	II-A. Ion source and lens elements	35
	II-B. Modifications to the quadrupole spectrometer	40
	II-C. Ion source magnets	43
	II-D. Vacuum housing and related aspects	43
	III. Vacuum and Pressure Considerations	48
	IV. Electrical Components	
	IV-A. Filament power supply and emission regulator	52
	IV-B. Plate and lens potentials	58

Chapter Page

IV-C. Timing circuitry 65

V. Operation of the Spectrometer

V-A. Operation of source and lens assembly 68

V-B. Ion motion inside the reaction cavity . 73

V-C. Ion motion through the collimating lens assembly 86

V-D. Effect of ion loss on the determination of reaction rate constants 89

5 Ion-Molecule Reactions in Methane 97

6 Ion-Molecule Reactions in Hydrogen and Binary Mixtures Containing Hydrogen 107

I. H_2, HD, D_2 107

II. H_2-He Mixture 117

III. H_2-CH_4 and H_2-NH_3 Mixtures 124

III-A. $H_2 + CH_4$ 125

III-B. $H_2 + NH_3$ 132

7 Ion-Molecule Reactions in Acetylene 140

8 Ion-Molecule Processes in Ethylene

I. Primary Ion Reactions 154

Chapter		Page
	II. Production of $C_5H_7^+$ and $C_5H_9^+$	163
	III. Thermochemical Predictions	184
9	Ion-Molecule Processes in the Methyl Halides . .	191
	I. Ion-Molecule Reactions in CH_3F	191
	II. Ion-Molecule Reactions in CH_3Cl	197
	III. Ion-Molecule Reactions in CH_3Br	200
	IV. Symmetric Proton Transfer in CH_3Cl	202
	V. Symmetric Charge Exchange in CH_3Br . . .	212
10	Ion-Molecule Reactions in Methanol	220
11	Ion-Molecule Reactions in CH_2F_2 and CHF_3 . . .	242
	I. Methylene Fluoride	242
	II. Fluoroform	250
	III. Methylene Fluoride and Fluoroform	250
12	Ion-Molecule Reactions in Trifluoro Propyne . .	259
13	Charge Exchange in N_2 and CO_2	269
14	Thermoneutral Proton Transfer in CH_2D_2	275
15	Determination of Ion Kinetic Energy Distributions Using ICR Spectrometry	281
	I. Introduction	281

Chapter Page

II. Experimental 292

III. Results 296

IV. Kinetic Energy Distribution of CH_3^+ . . . 305

V. Conclusions 316

16 Comparison of Trapped-Ion Instruments . . . 325

CHAPTER 1

Introduction

The study of ion-molecule reactions in the gas phase is a venerable one, dating back at least as far as J. J. Thomson's early studies of positive rays in his parabolic mass spectrometer.[1] He noted various effects attributable to secondary processes, such as the formation of new ionic species corresponding to no known molecular species, as well as the appearance of certain diffuse lines and bands in his spectra. In particular he observed a species having m/e = 3 in the products of a discharge in hydrogen. Subsequent investigations by other workers[2-5] identified this entity as H_3^+ and ascertained that its mode of formation was via the reaction

$$H_2^+ + H_2 \longrightarrow H_3^+ + H. \tag{1}$$

Reaction (1) is an example of a proton or hydrogen (hydron) transfer reaction, perhaps the most extensively studied type of ion-molecule reaction. Its general form may be written as

$$A + BH^+ \longrightarrow AH^+ + B. \tag{2}$$

Through the years prior to about 1950, there were few direct investigations of ion-molecule reactions. Investigators were primarily concerned with developing the analytical aspects of mass spectrometry, and compiled a large amount of useful information concerning such properties of isolated gaseous ions as ionization potentials, ionic heats of formation and electron affinities. Consequently they directed considerable effort towards avoiding conditions that would lead to secondary ion formation.

Two primary methods of ascertaining whether an observed ion was indeed the result of an ion-molecule reaction were employed. The first involved monitoring the pressure dependence of the various ion intensities; secondary ion currents depended on the square of the pressure while primary ion intensities varied linearly with pressure. Thus early workers used as low a pressure as was compatible with their signal-to-noise requirements, to avoid the appearance of secondary ions. Another, less convenient, method involved variation of the path length traversed by the ions on their way to the exit of the ion source. While primary ion intensity is independent of this length, secondary ion abundances will vary directly with path length.

In 1951, Washburn and co-workers[6] described a third method for the supression of secondary ions from mass spectra. This method makes use of the fact that the reaction probability of an ion decreases as its residence time in the source decreases. Thus Washburn and co-workers found that by raising the ion-repeller voltage in the source, they were able to reduce the secondary ion abundance. This method forms the basis of many of the quantitative methods of the determination of rate constants.

Despite these precautions and endeavours, some interesting and important reactions were discovered, particularly ones resembling Reaction (2). For example, Mann, Hustrulid, and Tate[7] observed the formation of H_3O^+ via Reaction (3).

$$H_2O^+ + H_2O \longrightarrow H_3O^+ + OH \tag{3}$$

while the interesting ion CH_5^+, formed by Reaction (4), was first documented by Tal'roze and Lyubimova[8]

$$CH_4^+ + CH_4 \longrightarrow CH_5^+ + CH_3. \tag{4}$$

In recent years, ion-molecule reactions have been the object of intensive study, both because of the many applications of a knowledge of this subject and because of their importance in basic chemistry. It has long been recognized that such a type of reaction is of considerable importance in many gas-phase processes such as radiation chemistry, electric discharges, and flames. Information on ion-molecule reactions has led to a vastly improved understanding of the earth's atmosphere, particularly the upper regions.[9] The duplication in the gas phase of certain "classical" liquid phase organic reactions such as nucleophilic displacement reactions and acid-catalysed dehydration of alcohols[10] has produced a better realization of the effects of solvation upon these reactions.

Ion-molecule reactions are also very amenable to detailed investigations of the elementary processes of molecular dynamics. While early investigators used only the previously mentioned techniques of pressure or repeller voltage variation, there is now a wide variety of sophisticated experimental procedures at their disposal. These are discussed in Chapter 3. Equally important, there are theoretical models available with which to interpret the experimental results, and these form the basis of the next chapter.

References

1. J. J. Thomson, "Rays of Positive Electricity", Longmans, Green and Co., London, 1933.
2. A. J. Dempster, *Phil. Mag.*, **31**, 438 (1916).
3. F. W. Aston, "Mass Spectra and Isotopes (2nd ed.)", Edward Arnold Publishers, London, 1942.
4. H. D. Smyth, *Phys. Rev.*, **25**, 452 (1925).
5. T. R. Hogness and E. G. Lunn, *Phys. Rev.*, **26**, 44 (1925).
6. H. W. Washburn, C. E. Berry, and L. G. Hall, "Mass Spectrometry in Physics Research", No. 20, *Natl. Bur. Std. Circ.*, 522 (1953).
7. M. M. Mann, A. Hustrulid, and J. T. Tate, *Phys. Rev.*, **58**, 340 (1940).
8. V. L. Tal'roze and A. K. Lyubimova, *Dokl. Akad. Nauk. SSSR*, **86**, 909 (1952).
9. "Physics of the Upper Atmosphere", J. A. Ratcliffe, ed., Academic Press, New York, 1960.
10. D. Holtz, J. L. Beauchamp, and S. D. Woodgate, *J. Amer. Chem. Soc.*, **92**, 7484 (1970); J. L. Beauchamp, *J. Amer. Chem. Soc.*, **91**, 5925 (1969).

CHAPTER 2

Theoretical Models of Ion-Molecule Reactions

The progress of an ion-molecule reaction can be divided into two steps, namely, the formation of the ion-molecule complex $[AB^+]$, and secondly, its subsequent dissociation into products

$$A^+ + B \longrightarrow [AB^+] \longrightarrow C^+ + D. \qquad (1)$$

While other theoretical treatments do exist,[1] the most commonly employed description of the first step was originally formulated by Gioumousis and Stevenson,[2] who applied Langevin's derivation[3] of the classical collision cross section of a charged particle moving in a neutral gas to ion-molecule reactions. The derivation and result have been well presented in numerous reviews[4] and will only be sketched here.

The model assumes that the potential energy function describing the interaction between an ion and a neutral molecule with no dipole moment is

$$V(r) = \frac{-e^2 \alpha}{2 r^4} \qquad (2)$$

where e is the charge of the ion, α is the electric polarizability of the molecule and r is the distance between the ion and molecule. The resulting particle trajectories are of such a form that within a critical impact parameter $b_0 = b_0(g)$, where g is the relative velocity, the ion will always spiral into the molecule and undergo a "hard" collision. Defining $\sigma(g)$ as the collision cross section and setting $\sigma(g) = \Pi b_0^2(g)$, there results

$$\sigma(g) = \frac{2\Pi e}{g}\left(\frac{\alpha}{\mu}\right)^{1/2} \tag{3}$$

where μ is the reduced mass of the ion-molecule pair.

This represents a velocity dependent ion-molecule collision cross section. If it is assumed that all hard collisions inevitably lead to reaction, $\sigma(g)$ may be treated as a reaction cross section. This assumption eliminates any possible dependence of the reaction cross section on the energy distribution between the internal coordinates, and precludes any requirement of interaction between the internal coordinates of the reactants. In addition, this assumption implies that no activation barrier to reaction exists.

The reaction rate constant k is defined as

$$k = \langle g\sigma(g)\rangle_{Av} \tag{4}$$

where the average is taken over the entire range of ionic and molecular velocities. Since the quantity $g\sigma(g)$ is independent of g, the averaging is straightforward, and there results

$$k = 2\Pi e\sqrt{\frac{\alpha}{\mu}}\,. \tag{5}$$

Equations (3) and (5) have been used extensively to interpret ion-molecule reaction data, both at thermal energies and at the higher energies employed in the repeller field studies discussed earlier.

At thermal ion energies, Equation (5) has had good success in reproducing experimental rate constants for simple systems involving no large geometric changes or other complicating effects.[2]

In cases where the neutral molecule has a dipole moment μ_D, an additional important term appears in the ion-molecule attractive potential, which then becomes

$$V(r) = \frac{-e^2\alpha}{2r^4} - \frac{e\,\mu_D \cos\theta}{r^2} \tag{6}$$

where θ is the angle between the dipole and the radius vector between the particles. Using the simplifying assumption that the dipole always aligns itself with the ion field, Moran and Hamill[5] have shown the cross section to become

$$\sigma(g) = \frac{2\Pi e}{g}\left[\sqrt{\frac{\alpha}{\mu}} + \frac{\mu_D}{\mu g}\right]. \tag{7}$$

At thermal velocities, Gupta _et al._[6] have shown that the rate constant then is

$$k = 2\Pi e\sqrt{\frac{\alpha}{\mu}} + \frac{2\Pi e\,\mu_D}{\mu}\left(\frac{2\mu}{\pi k_B T}\right)^{1/2}, \tag{8}$$

where k_B is the Boltzmann constant.

This model accounts for the substantial increase in cross section for polar molecules often noted at low energies, though quantitatively its results are inevitably too high. A more elaborate treatment using computer simulation of the particle trajectories has been developed by Dugan and Magee.[7]

Under certain experimental conditions, particularly those where a beam of ions is injected into a reaction chamber, the determination of the reaction rate constant is difficult and impractical. In this case, the reaction cross section $\sigma(g)$ is usually determined. Many reactions have been found that obey the simple dependence of reaction cross section on energy given in Equation (3) over a considerable range of energies. However the simple form has two drawbacks. At very high energies, it is seen that the Langevin cross section would become less than the hard sphere collision cross section, σ_h, and it is in this energy region that interpretation of the cross section in Equation (3) as a reaction cross section breaks down. In addition, many other reactions have been found that display a more complex behaviour even at lower energies. This has led to numerous attempts to modify Equation (3), first by introduction of the hard sphere cross section, σ_h, at large energies, and also by introduction of certain arbitrary reaction probabilities.[5,8,9] These efforts have not received widespread usage.

The experimental results presented in this thesis were all obtained under quasi-thermal conditions where electric fields influencing the ion velocities were low. The simple Langevin treatment should approximate the rate constant for simple systems. For more complex systems having numerous reactive channels, the Langevin rate gives, of course, only an indication of the encounter rate between the ion and molecule. There are a variety of different theoretical approaches that attempt to provide a detailed description of the fate of the intermediate complex thus formed.

The most detailed of these are the phase space theory of J. C. Light[10, 11] and other related statistical approaches.[12, 13] The basic postulate of these theories is that in the initial formation of the complex, it loses much or all information about its initial states, and that the probability of a product is then governed mainly by the amount of phase space available, consistent with conservation of energy and angular momentum. This approach is valid if the complex is long lived and if translational-vibrational energy exchange occurs. For ion-molecule reactions this is probably the case, as strong attractive forces exist. Unfortunately, there is no straightforward procedure for extending these statistical treatments to molecules of more than two atoms. For more complex molecules of chemical interest, less vigorous approaches are required.

The quasi-equilibrium theory (QET) of unimolecular fragmentation of polyatomic ions is such an approach. This theory was originally derived[14] for the unimolecular dissociation of molecules which were excited by electron impact. Thus it predicted the fragmentation pattern of a molecule-ion as a function of electron energy. The fundamental assumption was that the ion was formed by vertical ionization, but that there followed a period of time where this initially localized excitation energy was redistributed over various other degrees of freedom, including the one which corresponded to the eventual dissociation.

Clearly the theory can be extended to the situation where the initial excitation energy is due to the collision of an ion with a neutral to form a randomized complex of significant lifetime. Dissociation then occurs unimolecularly.

The decomposition is accomplished by the translation of the intermediate along the reaction coordinate to an activated state, and then on to products. The rate constant for the decomposition of a molecule by this mechanism is simply the ratio of the number of possible ionic states in the activated configuration to the number of states of the intermediate. State densities are generally calculated from formulae that use continuous functions as an approximation to the number of discrete levels.

For an intermediate having various modes of decomposition (including the route returning to the starting materials), this calculation would be undertaken for a variety of activated configurations, one for each dissociative channel. Each activated complex is characterized by its own geometry, its own set of vibrational frequencies and by its own potential energy, ϵ_0. In a calculation for the relative probabilities of each channel, the density of states in the intermediate cancels out.

Five pieces of information are thus required before the QET can be applied to obtain relative rates:

(1) The geometry of the various activated complexes and the selection of the reaction coordinates for each dissociative mode. This is the major area of uncertainty in the successful application of the theory.

(2) The state density functions for each complex.

(3) The activation energy for decomposition of the intermediate, ϵ_0, for each complex.

(4) The vibrational frequencies of each activated complex.

(5) The total available energy E.

The reaction intermediate is assumed to be the most stable ion structure with the correct formula. Vibrational frequencies for ions are almost unknown, so the vibrational frequencies for the corresponding neutral molecules must be used instead. The vibrational frequencies in the activated complex are generally regarded as unchanged, except for the degrees of freedom involved in the reaction coordinate. Reasonable guesses are made for these frequencies. Benson[15] has given some general principles for neutral transition states that can be followed. The density functions are usually calculated using one of a variety of classical approximations.[16] The activation energy ϵ_0 is estimated from appearance potential measurements, while the energy E is obtained from thermochemical considerations, assuming, again, the most stable possible chemical structure for the intermediate.

While the successful application of the QET requires the arbitrary assignment of numerous parameters. Buttrill[17] has recently shown that it is possible to obtain good agreement with experiment when determining the ratio of the rates of two different reactions arising from the same intermediate, even when few arbitrary frequency assignments are made. His analysis accurately predicted isotope effects in ion molecule reactions, and is the most successful application of QET to date.

References

1. K. Yang and T. Ree, *J. Chem. Phys.*, **35**, 588 (1961).
2. G. Gioumousis and D. P. Stevenson, *J. Chem. Phys.*, **29**, 294 (1958).
3. M. P. Langevin, *Ann. Chim. Phys.*, **5**, 245 (1905).
4. J. H. Futrell and T. O. Tiernan, in "Fundamental Processes in Radiation Chemistry", P. Ausloos, ed., Interscience, New York, 1968.
5. T. F. Moran and W. H. Hamill, *J. Chem. Phys.*, **39**, 1413 (1963).
6. S. K. Gupta, E. G. Jones, A. G. Harrison, and J. J. Myher, *Can. J. Chem.*, **45**, 3107 (1967).
7. J. V. Dugan and J. L. Magee, *J. Chem. Phys.*, **47**, 3103 (1967).
8. R. P. Pottie, A. J. Lorquett, and W. H. Hamill, *J. Amer. Chem. Soc.*, **84**, 529 (1962).
9. N. Boelrijk and W. H. Hamill, *ibid.*, **84**, 730 (1962).
10. J. C. Light, *J. Chem. Phys.*, **40**, 3221 (1964).
11. J. C. Light and J. Lin, *ibid.*, **43**, 3209 (1965).
12. A. Tannenwald, *Proc. Phys. Soc.*, **87**, 109 (1966).
13. F. A. Wolf, *J. Chem. Phys.*, **44**, 1619 (1966).
14. H. M. Rosenstock, M. B. Wallenstein, A. L. Wahrhaftig, and H. Eyring, *Proc. Nat. Acad. Sci.*, **38**, 667 (1952).
15. S. W. Benson, "Thermochemical Kinetics", Wiley, New York, 1968.
16. M. Vestal, A. L. Wahrhaftig, and W. H. Johnson, *J. Chem. Phys.*, **37**, 1276 (1962).
17. S. E. Buttrill, Jr., *ibid.*, **52**, 6174 (1970).

CHAPTER 3

Experimental Techniques of Studying Ion-Molecule Reactions

There are a large number of excellent and very comprehensive reviews that discuss current experimental techniques used to investigate ion-molecule reactions.[1,2] Consequently this chapter will provide only a cursory review that describes the general features of some apparatuses rather than detailed experimental techniques. The types of results obtained will also be considered.

I. Single Source Mass Spectrometers

Until rather recently, only conventional single source mass spectrometers were available for studying ion-molecule reactions.[3] In these studies, three types of measurements are generally employed:

(1) variation of ion intensity with pressure,

(2) variation of ion intensity with electric field in the ionization chamber due to the ion repeller, and

(3) measurement of the appearance potentials of the various ions.

In general, the pressure variation is used to differentiate primary from secondary from tertiary ions, and in cases where ion residence times can be estimated, rate constants can be determined. Repeller field data is also utilized to separate reactants from products and, in addition, affords some insight into the kinetic energy dependence of the reaction. Appearance potential measurements are used, in favourable cases, to ascertain the identity of the reactant ion responsible for a particular product.

While lacking much of the sophistication of the more recent instruments to be described later, these techniques have provided the bulk of ion-molecule reaction data. Recently improved techniques of differential pumping have permitted very high source pressures to be reached. At these pressures, reaction times and ion kinetic energies are ill-defined. Consequently, meaningful rate constant measurements are difficult to make. However, in some cases, it is now possible to investigate systems under conditions more closely approximating those present in high pressure radiolysis.[4, 5] In addition, interesting thermodynamic data on ionic solvation has been obtained at high pressures.[6, 7] Finally, Field[8] has devised systems where methane is present at a pressure of more than one torr, and to which traces of other compounds are added. The dominant ion under these conditions is CH_5^+, which is then able to donate a proton to the trace component. In most cases, this results in a degree of fragmentation of that substance similar to an electron bombardment cracking pattern, but differing in detail. This process has been named chemical ionization, and is an important application of ion-molecule reactions to structure analysis.

While most mass spectrometers continue to use electrons emitted from a hot filament as the source of ionization, some investigators[9, 10] have employed particles emitted from radioactive materials to ionize the gas. This avoids the difficulties arising from pyrolysis of the gas on the hot filament surface. One drawback of this form of ionization is that it is impossible to vary the ionizing energy, which is usually very high. This precludes appearance potential measurements.

Many investigators have employed the direct ionization of gases by photons in ion-molecule reaction studies.[11, 12] Photoionization has several important advantages over ionization by electron impact:

(1) Pyrolysis of the gas on the filament is avoided.

(2) Excellent ionizing energy resolution is achieved. In favourable cases, it is possible to selectively ionize a molecule into a certain state or group of states and study the dependence of rate constants on internal energy.[11, 13] This is much more difficult for electron ionization, as the energy spread is larger.

(3) Ionization cross sections just above threshhold are much higher for photoionization than electron impact ionization.

(4) There is no electron space charge effect, and there is no need for a collimating magnetic field.

The primary difficulties associated with the photoionization technique are:

(1) Photon beam intensities are lower than electron beam intensities.

(2) It is more difficult to change the energy of a photon beam than an electron beam.

(3) Photon beams are inconvenient for negative ion studies. Negative ions can be produced by dissociation of a molecule into two oppositely charged fragments, but the cross sections for these processes are generally low.

There are a variety of pulsed ion sources that have been devised that permit an accurate determination of reaction times and enable almost field free conditions to exist during the reactive period. The instruments are designed to reduce the energy of the reactant ions, thus circumventing one of the primary objections to conventional mass spectrometric investigations. One instrument having this capability was constructed in these laboratories as part of this program of research, and will be described more fully in later chapters. Another such instrument is the trapped ion ICR cell discussed later in this chapter.

Ryan and Futrell[14] have built a pulsed instrument where ions are allowed to react under the influence of a small dc field for a selected time. The reaction is then quenched by application of a large repeller pulse superimposed on the dc repeller field. The delay time between the ionization pulse and the quenching pulse can be related to the average kinetic energy possessed by the ions during reaction. In this way, the reactions of a nearly monoenergetic packet of ions having a controllable and well-defined kinetic energy can be studied. The energy range extends from about .1 to 1.5 eV. Their results indicated that the rate constants for proton transfer in systems with no dipole moment (CH_4, C_2H_4) were dependent of ion velocity, as predicted by the Langevin theory. Proton transfer rates in systems having a permanent dipole moment (H_2O, NH_3, HCl) obeyed the formulation of Moran and Hamill outlined in Chapter 2.

Harrison[15] has developed an ion source where positive ions are trapped in the space charge potential of a low energy, high current electron beam. Positive ions are formed by a short ionizing pulse burst and allowed to react for a variable reaction time. They are then extracted by application of a large dc repeller field. Ion energies in this source have been estimated to be about .5 eV. Typical reaction times are 0-2 msec, and typical pressures are about .1 to .3 microns. Secondary, tertiary and quaternary products can easily be observed. Rate constants are determined by monitoring relative ion abundances as a function of reaction time.

Tal'roze[16] has constructed a similar apparatus where trapping is achieved in the region between an outer cylinder and an axial wire, held at a lower voltage than the cylinder.

One of the newest and most versatile single-source techniques for studying ion-molecule reactions is based on the phenomenon of ion cyclotron resonance (ICR). A schematic of a ICR cell constructed by Varian Associates[17] is provided in Figure 1. Ions are formed in the source region by electron bombardment from a hot filament and are drifted down the cell in the -y direction through the resonance or detection region to an ion collector measuring the total ion current.

Figure 1

Schematic drawing of the ICR cell.

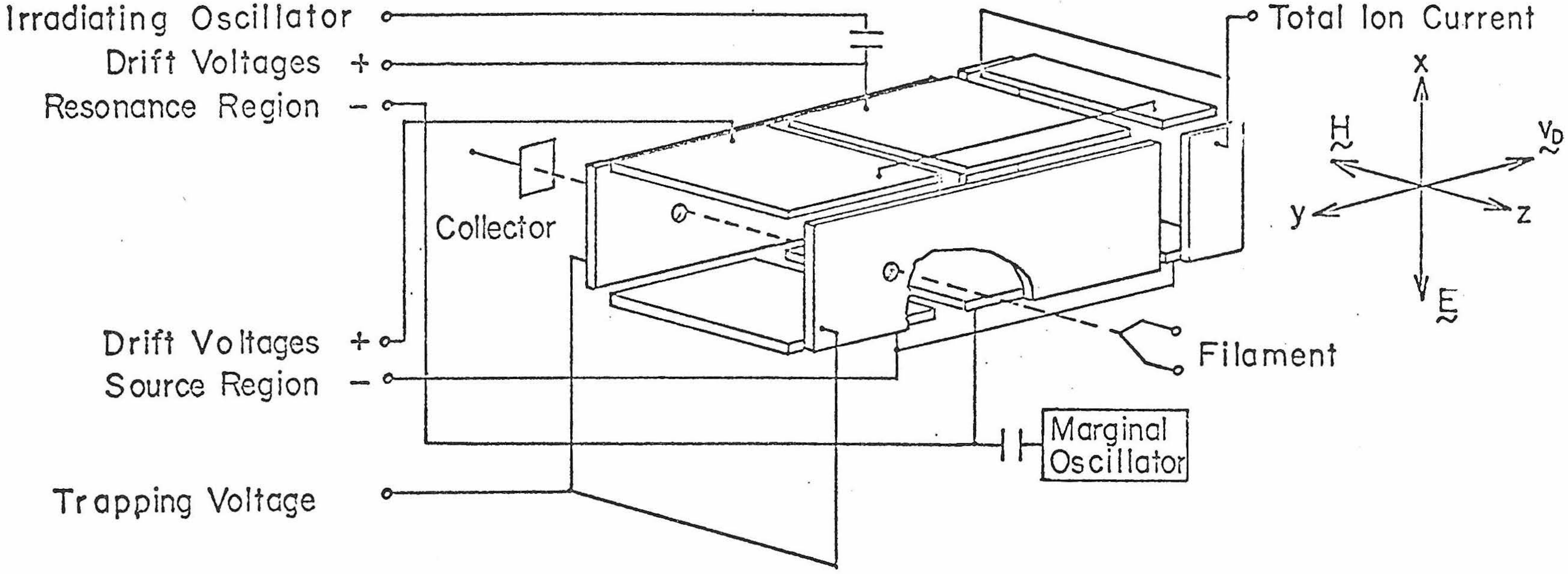
Irradiating Oscillator
Drift Voltages +
Resonance Region −
Drift Voltages +
Source Region −
Trapping Voltage
Collector
Total Ion Current
Filament
Marginal Oscillator
x
H
v_D
y
z
E

The drift motion arises from the action of crossed electric and magnetic fields; the drift velocity in the crossed field geometry is given by Equation (1)

$$V_D = \frac{cE}{B} \tag{1}$$

where E is the strength of the static electric field. Gaussian units are used throughout this analysis. Typical drift velocities are around 10^4 cm/sec, corresponding to ion transit times of about 1 msec. The ions are detected by their power absorption from an rf electric field applied in the resonance region at the cyclotron frequency of the ion, ω_c. This frequency, given in Equation (2), is dependent on the mass and charge of the ion

$$\omega_c = \frac{qB}{mc}. \tag{2}$$

With a fixed observing frequency, a spectrum linear in mass is obtained by sweeping the magnetic field. Ionic abundances are determined by the magnitude of the power absorption, as detected by a marginal oscillator. Trapping voltages are applied to the sides of the cell to confine the ion motion in the z direction, but do not seriously alter the drift motion of the ions. A more comprehensive review of the principles of ICR spectrometry has been given by Beauchamp.[18]

The ICR mass spectrometer has two features making it well suited to the study of ion-molecule reactions at low pressures. First, since the ions have a long transit time, reactions producing secondary ions are readily seen at rather low pressures. Typically, pressures less than $.02\mu$ are sufficient to observe reactions like those in Chapter 1. Tertiary and higher order reaction products are detectable at higher pressures. The drift time can easily be varied in a quantitative fashion to permit the determination of rate constants.[19] Alternatively, the pressure can be varied to yield this information.[20]

Secondly, the possibility of simultaneously irradiating the ions with two or more oscillators provides a sensitive probe for coupled chemical reactions. In this double resonance technique,[18] one rf oscillator is set at the cyclotron frequency of a given ion and a second, variable frequency oscillator is swept as an analyzer. In this way, the effect on the remainder of the mass spectrum of translationally exciting a particular ion may be directly observed. If two ions are coupled as reactant and product of an ion-molecule reaction, the only requirement for an effect to be observed is that the rate constant be a function of ion velocity. While not predicted by the Langevin theory, this is nevertheless often the case. Accordingly, complex reaction sequences may be unravelled. This technique has also been used to selectively eject an ion from the system to determine its contribution to the products in the mass spectrum.[21] Quantitative determinations of the effect of ion velocity on rate constants have also been made using double resonance.[22]

Recently a number of novel trapped ion ICR cells have been devised.[23, 24] In the one currently in use in our laboratory, a short pulse of ions is formed in the source region of the conventional cell by appropriately pulsing the electron energy. The ions are then trapped in this region for a known and variable reaction time τ and are then ejected by allowing them to drift into the resonance region in the normal fashion, where they are detected. Trapping is effected by application of the appropriate dc voltages on the various plates of the cell. Trapping times as long as 10 seconds have been achieved, and times of 500 msec are routinely used with no significant ion loss. At pressures between 10^{-6} and 10^{-5} torr, secondary and tertiary ions are thus readily seen. The variation of ion abundances with τ yields ion-molecule reaction rate constants for near-thermal ions directly. Rate constants determined by this method have agreed well with determinations by other techniques. The possibility of exciting or ejecting certain ions using the trapped ion technique still exists. Trapped ion ICR techniques were employed for some of the studies described in later chapters. A more complete description will be found there.

II. Tandem Mass Spectrometers

The techniques discussed in this section permit the study of ion-molecule reactions under conditions quite different from those previously described. Here, a nearly monoenergetic, mass selected beam of ions is either passed through a gas filled collision chamber or allowed to intersect a beam of molecules of a known species. The primary and secondary ions emerging from the collision region are energy and mass analyzed before detection. In many cases, the angular distribution of scattered ions can also be determined by rotation of the entire product ion analysis system. A schematic diagram of an ideal experimental arrangement employing a collision chamber is provided in Figure 2.

The advantages offered by the use of beam techniques are important and several in number. Foremost among these is the ease of selection of the incident ions, eliminating the difficulties from interference of other primary ions that are present in single source experiments. The separation of the ion source and the reaction region also permits difference gases to be used in each. Furthermore, various gases can be used in the source to produce ions of a given type but in various energy states. For example, the populations of O^+ ions in the ^4S, ^2D and ^2P excited states are different, depending on whether the ions originated from CO or CO_2.[25]

Another important advantage is that the energy of the primary beam is readily selected. The present lower limit of attainable ion energies is about 1 eV in the laboratory frame of reference, meaning that thermal conditions cannot be duplicated by beam techniques. In favourable cases, however, where a heavy ion collides with a light molecules, the energy in the centre of mass frame is nearly thermal. The possibility of determining the angular and/or the kinetic energy distribution of the products means that a great deal

Figure 2

Schematic drawing of an "ideal" single-beam static gas apparatus for the study of ion-molecule reactions. The energy analyzer, mass analyzer and ion detector may be rotated as a unit about the centre of the collision region.

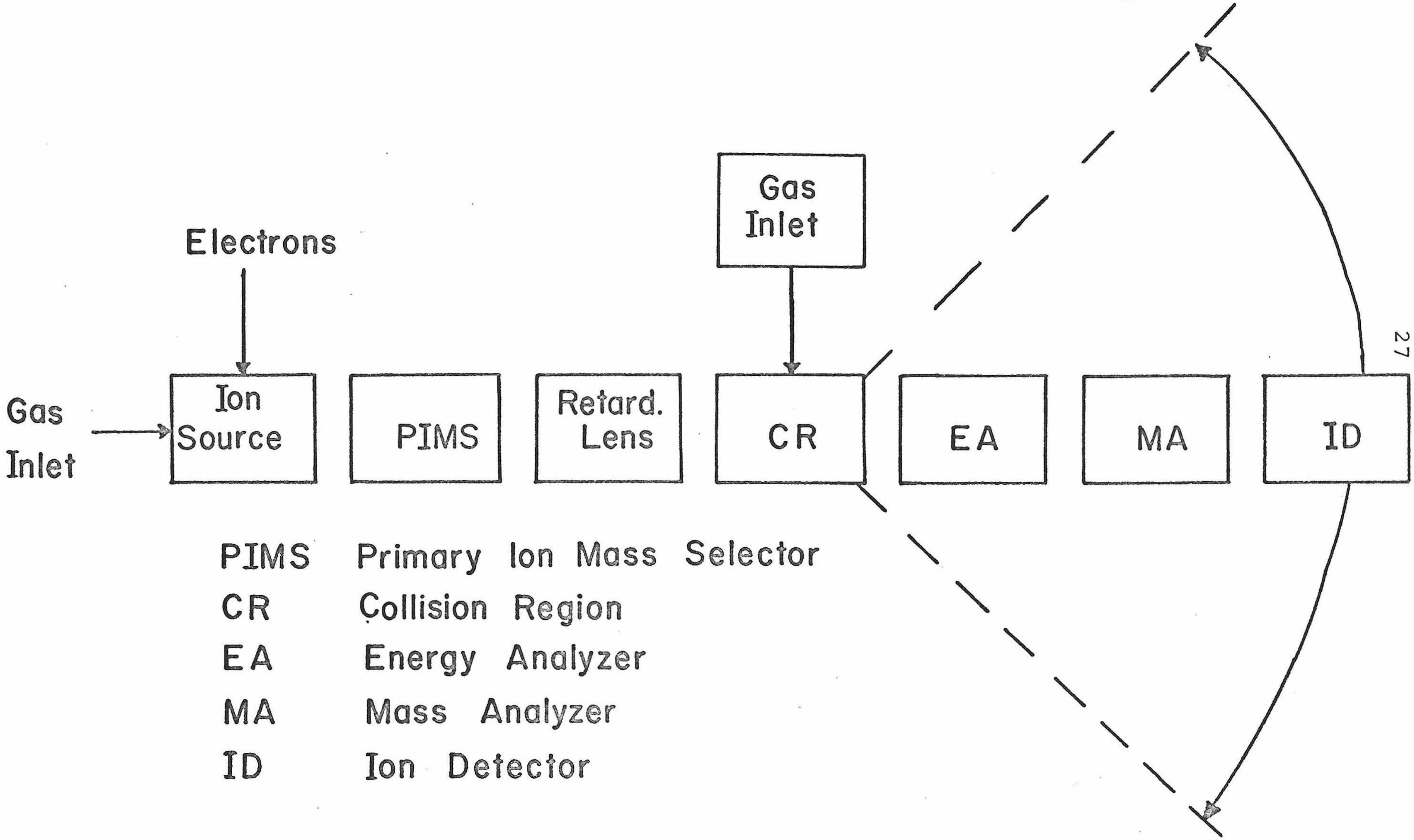
Gas Inlet
Electrons
Ion Source
PIMS
Retard. Lens
Gas Inlet
CR
EA
MA
ID
PIMS Primary Ion Mass Selector
CR Collision Region
EA Energy Analyzer
MA Mass Analyzer
ID Ion Detector

can be inferred about the reaction mechanism and energetics.

For example, Henglein[26] has used the simple apparatus consisting of an energy analyzed primary beam reacting with molecules in a field-free collision chamber. The forward scattered ions were velocity analyzed in a Wien filter. Systems under investigation included hydrogen atom transfer reactions such as

$$Ar^+ + H_2 \longrightarrow ArH^+ + H \qquad (3)$$

$$N_2^+ + H_2 \longrightarrow N_2H^+ + H \qquad (4)$$

The experimental results for primary ion energies above 20 eV were well predicted from a stripping model, in which the primary ion reacts only with one atom of the molecule, leaving the other atom unperturbed. For example, in Reaction (3), if the original velocity of Ar^+ were V_0, then by conservation of momentum, the velocity of ArH^+ is predicted to be $.976\ V_0$. The experimental velocity was close to this and verified the applicability of the model.

Instruments having a collision chamber where the product ion beam is detected in a direction transverse to that of the primary ions have also been constructed. Lindholm[27] has used such an apparatus to study charge-transfer processes, particularly those involving production of fragment ions via dissociative charge transfer from pre-selected ions. The dependence of the fragmentation pattern on the excitation energy of the parent molecular ions was studied. Proton and hydride transfers were also observed. Transverse instruments of this type strongly discriminate against ions with a velocity component along the direction of the primary beam. This renders them unsuitable for heavy particle transfer studies, unless appropriate extraction plates are used.[28] Use of extraction voltages precludes any meaningful kinetic energy analysis of the products.

Futrell and co-workers[29] have devised an extremely versatile longitudinal beam instrument. It has been used to investigate isotope effects in reactions with known ionic species, to measure reactive cross sections for a large variety of processes as a function of impact ion energy and to study the conversion of the translational energy of primary ions into internal energy. For example, in ethylene[30] they examined the reactions of the parent molecule and its deuterated analogue with $C_2H_4^+$, $C_2H_3^+$, $C_2H_2^+$, and C_2H^+. Relative cross sections for each product channel arising from these primary ions were determined. The variation of product ion abundance with the pressure of ethylene in the collision chamber was used to identify the reaction order of these ions. In addition, $C_2H_4^+$ ions were produced in the collision chamber by charge-transfer reactions between ions of appropriate recombination energy and ethylene. Ion-molecule reactions of $C_2H_4^+$ with C_2H_4 were then induced by elevating the collision chamber pressure. Finally, reactions between ethylene and $C_2H_5^+$, $C_3H_5^+$, and $C_4H_7^+$, which are major second-order reaction products in ethylene, were investigated. They were produced using 1-butene and neopentane in the primary beam source. The results of these experiments served to elucidate many of the ion-molecule reaction processes in ethylene. A lifetime for the $(C_4H_8^+)^*$ collision complex was also estimated.

These examples illustrate the kind of detailed information available from collision chamber-beam instruments. Angular distributions have also been mapped, particularly for systems involving heavy ion impact on light molecules. Mahan and co-workers[31] have mapped the angular dependence of product ion intensity from Reaction (5) at incident beam

$$N_2^+ + D_2 \longrightarrow N_2D^+ + D \tag{5}$$

energies between 35 and 120 eV. The kinetic energy of the products at each angle was also measured. The results manifested scattering in the direction of the ion and generally suggested a spectator stripping mechanism with some backward scattering by a rebound mechanism. The reaction was found to be translationally endothermic, with much of the relative kinetic energy of the reactants being stored as internal energy of the product ions.

Wolfgang and associates[32] have also studied this system using a crossed beam apparatus and lower incident ion energies. Their results were in harmony with those of Mahan et al., though at low incident energies the reaction was found to release kinetic energy.

The measurement of the angular distribution of product ions clearly provides much information about the dynamics of ion-molecule reactions. Thus, product ions having an isotropic angular distribution indicate that the reaction intermediate has a lifetime of at least a few rotational periods (10^{-10} sec). Pronounced forward scattering suggests a stripping mechanism, while backward scattering implies rebound mechanisms, generally occurring at small impact parameters.

References

1. J. H. Futrell and T. O. Tiernan, in "Fundamental Processes in Radiation Chemistry", P. Ausloos, ed., Interscience, New York, 1968.
2. E. W. McDaniel, V. Čermák, A. Dalgarno, E. E. Ferguson, and L. Friedman, "Ion-Molecule Reactions", Chapter 2, Wiley-Interscience, New York, 1970.
3. F. W. Lampe, J. L. Franklin, and F. H. Field, in "Progress in Reaction Kinetics", Vol. 1, G. Porter, ed., Pergamon Press, New York, 1961.
4. S. Wexler and L. G. Pobo, *J. Amer. Chem. Soc.*, **91**, 7233 (1969).
5. P. Ausloos and S. G. Lias, *ibid.*, 92, 5037 (1970); G. J. Collin and P. Ausloos, *ibid.*, **93**, 1336 (1971).
6. R. Yamdagni and P. Kebarle, *ibid.*, **94**, 2940 (1972) and references contained therein; A. Good, D. A. Durden, and P. Kebarle, *J. Chem. Phys.*, **52**, 212 (1970) and references contained therein.
7. D. P. Beggs and F. H. Field, *J. Amer. Chem. Soc.*, **93**, 1567 (1971).
8. F. H. Field, *Acc. Chem. Res.*, **1**, 42 (1968).
9. C. E. Melton and P. S. Rudolph, *J. Chem. Phys.*, **30**, 847 (1959).
10. V. Aquilanti, A. Galli, A. Giardini-Guidoni, and G. G. Volpi, *J. Chem. Phys.*, **43**, 1969 (1965).
11. W. A. Chupka, M. E. Russell, and K. Refaey, *J. Chem. Phys.*, **48**, 1518 (1968).
12. L. W. Sieck, S. Searles, and P. Ausloos, *J. Chem. Phys.*, **54**, 91 (1971).
13. L. W. Sieck, L. Hellner, and R. Gorden, Jr., *Chem. Phys. Lett.*, **10**, 502 (1971).

14. K. R. Ryan and J. H. Futrell, *J. Chem. Phys.*, **43**, 3009 (1965).

15. A. A. Herod and A. G. Harrison, *Int. J. Mass. Spec. Ion Phys.*, **4**, 415 (1970).

16. V. L. Tal'roze and G. V. Karachevtsev, "Ion-Molecule Reactions", in "Advances in Mass Spectrometry" (W. L. Mead, ed.), Vol. 3, Institute of Petroleum, London, 1966.

17. Varian V-5900 series ICR spectrometers, Varian Associates, Palo Alto, California.

18. J. L. Beauchamp, *Ann. Rev. Phys. Chem.*, **22**, 527 (1971) and references contained therein.

19. M. T. Bowers, D. D. Elleman, and J. King, Jr., *J. Chem. Phys.*, **50**, 4787 (1969).

20. A. G. Marshall and S. E. Buttrill, Jr., *J. Chem. Phys.*, **52**, 2752 (1970).

21. J. L. Beauchamp and R. C. Dunbar, *J. Amer. Chem. Soc.*, **92**, 1477 (1970).

22. W. T. Huntress, Jr., M. M. Mosesman, and D. D. Elleman, *J. Chem. Phys.*, **54**, 843 (1971).

23. R. T. McIver, Jr., *Rev. Sci. Instrum.*, **41**, 555 (1970).

24. T. B. McMahon and J. L. Beauchamp, *Rev. Sci. Instrum.*, **43**, 509 (1972).

25. P. Wilmenius and E. Lindholm, *Arkiv. Fysik.*, **21**, 97 (1962).

26. A. Henglein, "Stripping Effects in Ion-Molecule Reactions" in "Ion-Molecule Reactions in the Gas Phase", Advances in Chemistry Series, No. 58, American Chemical Society, 1966.

27. E. Lindholm, *Z. Naturforsch.*, **9a**, 535 (1954).

28. E. R. Weiner, G. R. Hertel, and W. S. Koski, *J. Amer. Chem. Soc.*, **86**, 788 (1964).

29. J. H. Futrell and C. D. Miller, *Rev. Sci. Instrum.*, **37**, 1521 (1966).

30. T. O. Tiernan and J. H. Futrell, J. Phys. Chem., **72**, 3080 (1968).

31. B. H. Mahan, Acc. Chem. Res., **1**, 217 (1968).

32. Z. Herman, J. Kersetter, T. Rose, and R. W. Wolfgang, Disc. Faraday Soc., **44**, 137 (1967).

Chapter 4

Design, Construction, and Principles of Operation of the High Pressure Mass Spectrometer

This chapter describes the design, construction, and principles of operation of a high pressure pulsed mass spectrometer that has been built in these laboratories as part of the present program of research.

I. General Description

The instrument is comprised of a specially designed trapped-ion source and a quadrupole mass spectrometer. Ions are formed in the source by a pulsed electron beam and are trapped by a combination of electric and magnetic fields for a known and variable reaction time. They are then ejected by application of a suitable ejection pulse and pass through a series of collimating electrostatic lenses before entering the mass spectrometer. The mass filtered ion current is amplified by an electron multiplier and this signal is fed to a preamplifier and then finally to a boxcar integrator for final processing.

II. Construction of the Spectrometer

II-A. Ion source and lens elements. The ion source is sketched in Figure 1. The filament is a rhenium ribbon (.030" wide, .0012" thick) and is mounted on a rectangular boron nitride block

Figure 1

The Ion Source

F -- Boron nitride filament block

P1 -- Anode plate

P2 -- Control plate

P3 -- Electron-entry plate

P4 -- Ion-exit plate

P5 -- Drawout plate

S -- Ion energy screen

SS -- Shielding screen

BN -- Boron nitride mounting discs

V -- Vespel mounting brackets

GI -- Gas inlet tube

PG -- Pressure gauge tube

FL -- Conflat flange (A2)

EL -- Electrical feedthrough

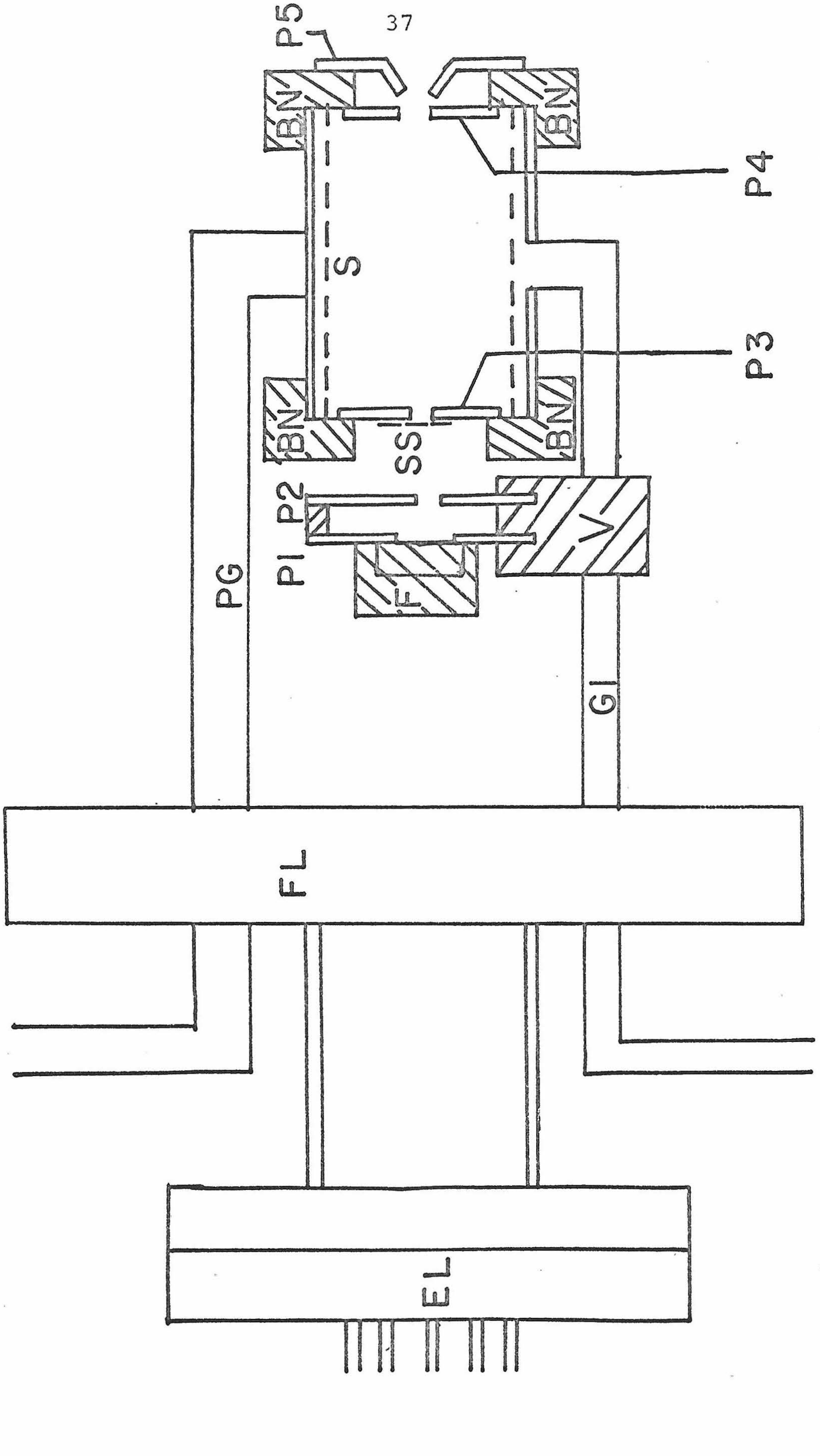
P5
BN
BN
P4
S
P3
BN
BN
SS
P2
P1
PG
F
V
GI
FL
EL

which is supported on plate P1. The block is designed to permit easy access to the filament, in the event that filament replacement is required. Two circular plates, each consisting of a .030" copper base which is silver coated and rhodium flashed, are interposed between the filament and the high pressure chamber. A specially machined Vespel (A1) bracket, which is clamped onto the gas inlet tube, holds the plates in position. These plates control the electron current into the chamber. The cylindrical reaction chamber has a stainless steel outer can, to which are welded the gas inlet (3/16" diameter) and pressure gauge (1/4" diameter) tubes. Inside the can, and electrically insulated from it, is a cylindrical copper mesh (40 mesh), also silver coated and rhodium flashed. The screen is 1 1/2" long and 3/4" in diameter. This mesh has an electrical connection to it, and controls the energy of the ions with respect to the quadrupole filter. Trapping plates are mounted on the ends of the chamber on boron nitride discs, so that the entire cavity has no signficant leaks apart from the electron entrance and ion exit apertures in the centre of these plates. The boron nitride discs also support the screen described above. Mounted on the ion exit disc is a draw out plate, shaped in the form of an inverted cone. A 90% transparent gold screen covers the electron entry aperture to prevent penetration of the electron pulsing potentials into the reaction chamber. Table I gives the pertinent aperture dimensions for each of the five plates.

Table I

Aperture Dimensions in the Ion Source

Plate	Commonly used name	Diameter of central hole (mm)
P1	anode	3
P2	control	2
P3	electron-entry	1
P4	ion-exit	2.5
P5	drawout	2.5

The entire ion source is supported on the gas inlet and pressure monitoring tubes, which are welded to the rear flange. A Varian eight pin feedthrough (A2) is also attached to this flange and provides electrical connections to the seven elements (two connections are needed for the filament) of the source. The entire source is very sturdy and can easily be disassembled.

There are five identical cylindrical stainless steel collimating lenses located directly beyond the ion source. They are 1 1/2" long, with an inner diameter of 1/2" and an outer diameter of 15/16". The gap between successive lenses is 1/2" and the distance between the final plate of the source and the first lens is 1/4". The lenses rest on two long ceramic rods which are held in place by two mounting rings that fit inside the inner wall of the vacuum housing. Three rods connect the two rings to maintain rigidity. One ring has three trapped screws that abut against the inner wall of the vacuum housing. These are provided to align the lens assembly. Figure 2 illustrates the lens assembly.

II-B. Modifications to the quadrupole spectrometer. After passing through the lens system, the ions enter an EAI Quad 250B (A3) quadrupole mass spectrometer. This spectrometer was used as supplied, except that a 3/4" hole was drilled in the back of its ion source to permit entry of the ion beam.

Figure 2

Collimating Lens Assembly

Figure (2A) -- Side view

Figure (2B) -- End view

L -- Lens

C -- Ceramic rod

R -- Support rod

MR -- Mounting ring

S -- Alignment screw

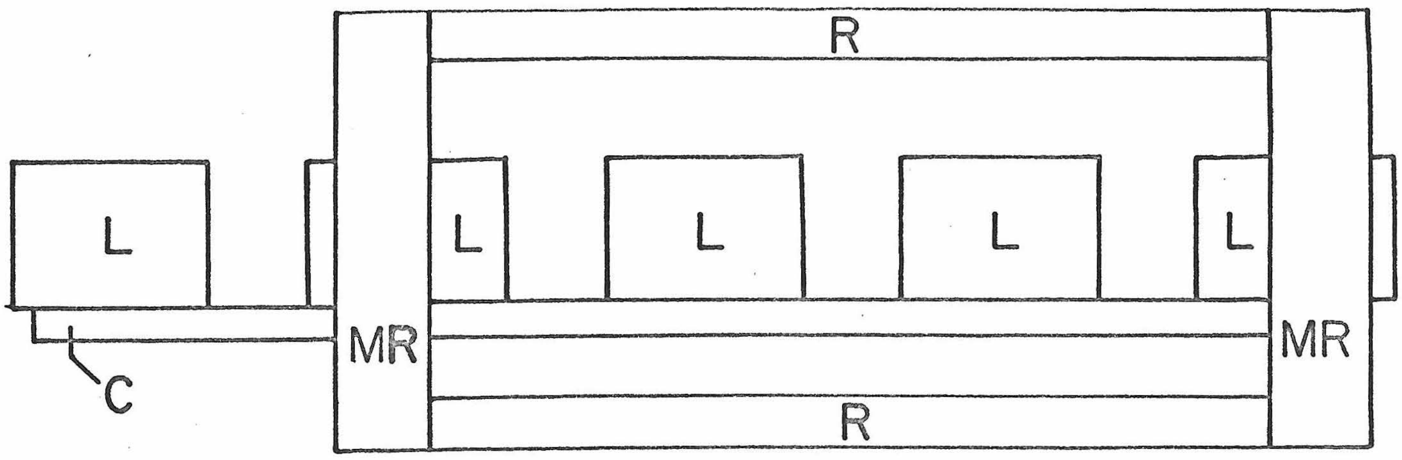
R
L
L
L
L
L
MR
MR
C
R

A

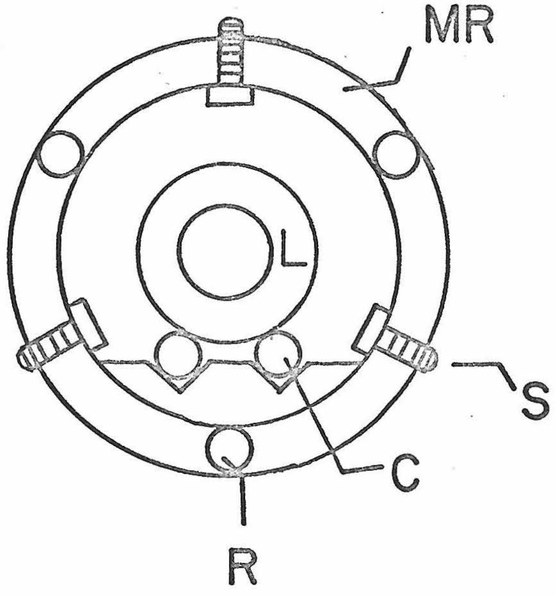

B

II-C. Ion source magnets. The ion source is mounted on a 4 1/2" conflat flange and is enclosed inside a stainless steel tube having an outer diameter of 2" and a length of 6". Surrounding this tube are three permanent torroidal magnets (A4) and two aluminum support discs. Three long bolts, extending between the aluminum plates, surround the magnets and keep the entire assembly, comprising the magnets and the two plates, rigid. Since proper orientation of the magnets is critical for the successful operation of the ion source, special care was taken to design a mechanism to orient the magnets. Three equally spaced bolts extend radially inward through the centre of each aluminum end plate, and abut against the outer wall of the vacuum housing. Reorientation of the magnets is effected by appropriately retracting or extending particular bolts. Figure 3 is a sketch of this arrangement.

II-D. Vacuum housing and related aspects. Figure 4 is a sketch of the entire vacuum system, including the gas inlet system and the pressure measuring apparatus. An NRC (A6) pumping stack, consisting of a 15 CFM roughing pump, a 1200 liter/sec oil diffusion pump, a chevron cyrobaffle, a gate valve, as well as assorted roughing valves, vent valves and pressure gauges provides the bulk of the pumping to the system. In addition, a 50 liter/sec Varian ion pump is connected directly to the housing surrounding the quadrupole rods and serves to keep the rods and the electron multiplier at a low pressure. As the clearance between the spectrometer and its housing

Figure 3

Magnet Assembly

Figure (3A) -- End view

Figure (3B) -- Side view

P -- Aluminum end plates

M -- Magnets

B -- Bolts surrounding magnets

AB -- Alignment bolts

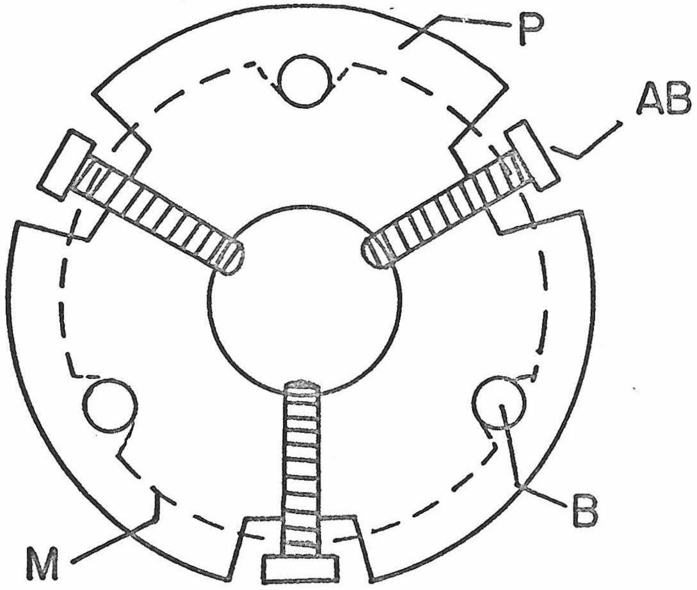

A

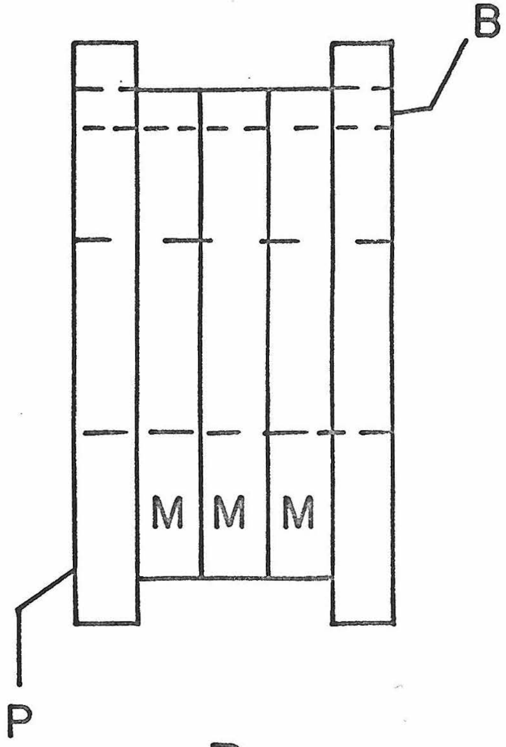

B

Figure 4

Sketch of Vacuum Housing and Related Aspects

Part	Name	Vendor or manufacturer
CM	Capacitance manometer	A5
CT	Chevron cyrobaffle cold trap	A6
DP	Diffusion pump	A6
GV	Gate valve	A6
IG	Ionization gauge	A6
IP1	Spectrometer ion pump	A2
IP2	Manometer ion pump	A2
LV	Sample leak valve	A7
M	Ion source magnets	A4
R1	System roughing pump	A6
R2	Sample roughing pump	A8
S	Ion source	-
SP	Spool piece	-
TC1	Foreline thermocouple gauge	A6
TC2	System thermocouple gauge	A6
TC3	Sample foreline thermocouple gauge	A9
V1	Diffusion pump roughing valve	A6
V2	System roughing valve	A6
V3	Foreline vent valve	A10
V4	System vent	A6
V5	Gas inlet valve	A11
V6	Sample roughing valve	A11
V7	Source-manometer valve	A12
V8	Manometer equalization valve	A12

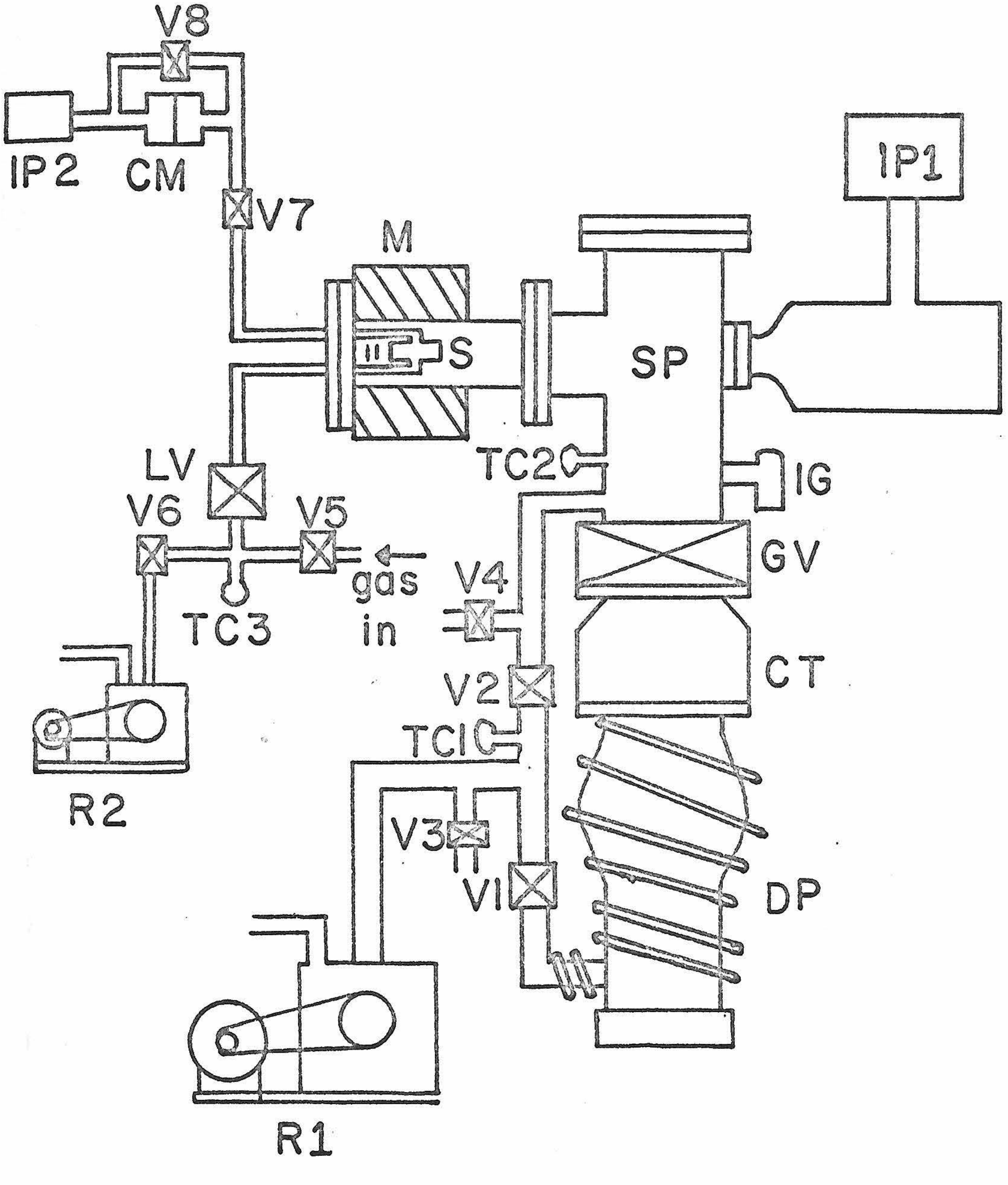
V8
IP2
CM
IP1
V7
M
S
SP
TC2
IG
LV
V6
V5
gas
in
GV
TC3
V4
V2
CT
R2
TC1
V3
V1
DP
R1

in the region near the spool piece is very small, this pump makes only a small contribution to the evacuation of the spool piece and ion source. The gas inlet system uses a Granville Phillips (A7) variable leak valve to regulate the flow of sample gas into the reaction chamber. Appropriate roughing valves are located as shown in Figure 4, and the system has its own roughing pump. A thermocouple gauge monitors the sample foreline pressure.

The accurate measurement of the pressure in the reaction chamber is of critical importance for reliable determinations of rate constants. An MKS (A5) capacitance manometer was used for the present investigations. The reference side of the manometer was kept at a pressure of less than 10^{-8} torr by a 1 liter/sec ion pump.

III. Vacuum and Pressure Considerations

The reaction chamber is differentially pumped, with gas entering through the gas inlet and effusing through the small holes in the trapping plates.

The conductance of these two holes may be estimated from the empirical equation[1]

$$C = 60\, d^2 \ \ \text{l/sec} \tag{1}$$

where C is the conductance and d is the diameter of a hole in inches. The total conductance of the two holes is thus calculated to be .70 l/sec.

Now if the pressure in the chamber is P_2, and the external pressure is P_1, then the net flow of gas molecules through the orifices is

$$C(P_2 - P_1) \quad \text{particles/sec}. \tag{2}$$

This flow is balanced by the pumping action of the diffusion pump. The pumping action is defined by the equation[1]

$$-\frac{dP_1}{dt} = \frac{S}{V}(P_1 - P_S) \tag{3}$$

where S is the pumping speed, V is the volume to be exhausted and P_S is the ultimate low pressure attainable. The number of particles pumped every second is $\frac{-dP_1}{dt}V$. At equilibrium, the amount of gas pumped is equal to the amount of gas flowing through the orifices

$$\left|\frac{dP_1}{dt}V\right| = C(P_2 - P_1). \tag{4}$$

Using Equation (2), Equation (4) becomes

$$C(P_2 - P_1) = S(P_1 - P_S).$$

Assuming $P_2 \gg P_1$ and $P_1 \gg P_S$, we have thus

$$P_2/P_1 = S/C. \tag{5}$$

Equation (5) indicates the extent of differential pumping that can be achieved.

The effective pumping speed S_{eff} of the pumping stack is reduced from its nominal value of 1200 liter/sec because of the non-infinite conductance of the cold trap. The conductance of this trap has been rated at 950 liter/sec. Since

$$\frac{1}{S_{eff}} = \frac{1}{S_{nominal}} + \frac{1}{C}, \tag{6}$$

it is therefore concluded that $S_{eff} = 550$ liter/sec. In addition, the spool piece has only a finite conductance, reducing the pumping speed at the reaction chamber even further. The conductance of this portion of the system may be estimated from Equation (7),[1]

$$C = 80 \frac{d^3}{H + 4d/3} \text{ liter/sec} \tag{7}$$

where H is the length of tubing in inches and d is its diameter in inches. This works out to about 200 liter/sec. The effective pumping speed near the source is thus approximately 200 l/sec. From Equation (5), it is seen that

$$P_2/P_1 \sim 3 \times 10^2 . \tag{8}$$

It should be remarked that this ratio is a lower limit, as the pressure outside the reaction chamber will clearly be dependent on the distance from the cell. At large distances from the source, the pressure differential will be greater, as the pumping speed at these points is larger than that calculated above.

The pressure in the source, P_2, is measured by a capacitance manometer that is connected to the cell by a 10 inch section of 1/4" tubing. The conductance of this tubing, unfortunately, is rather low. It may be calculated from Equation (7) to be about .15 liter/sec, which is comparable to the conductance of the electron entry and ion exit apertures. There thus arises the question as to whether the manometer will measure a true pressure.

An answer may be proposed by ascertaining the nature of the gas flow inside the chamber. If the gas flow through the apertures is viscous flow, then there would be a wide distribution of pressures throughout the entire volume of the chamber, and pressures measured at the manometer would differ from those in other regions of the cell. However, in molecular flow, the number of bimolecular collisions is insignificant compared to the number of molecular collisions with walls. In this case, there is no pressure differential throughout the entire source-manometer assembly. Two criteria have been established[2] to define molecular flow through an aperture of diameter D. These are

$$P_2D < 6\ \mu\ \text{in}$$

$$\ell > D/3$$

where ℓ is the mean free path. For air, these criteria are met at source pressures less than 50 μ. Since source pressures never exceeded 10 μ in any studies reported in this thesis, evidently the manometer reading will accurately reflect the source pressure.

It remains to define the permissible valves of P_2 and P_1. The primary consideration is that the ions do not suffer a collision as they travel towards the rods. The time T for a typical ion of mass 25 amu to traverse a distance L of 20 cm with an average energy E of 50 eV is

$$T = \frac{L}{V} = L\sqrt{\frac{m}{2E}} \approx 10\,\mu\text{sec}. \tag{9}$$

The time between collisions of an ion with a neutral at thermal energy is

$$t = \frac{\ell}{V_{\text{thermal}}} = \frac{1}{n\sigma V_{\text{thermal}}} \tag{10}$$

where ℓ is the mean free path, σ is the collision cross section and n is the pressure of the neutral gas. Cross sections may be derived from the Langevin formulation, but are certainly less than 100 Å^2. Accordingly, the times T and t for various pressures are as given in Table II. There it is seen that for source pressures less than 30 μ, the probability of a collision of this kind occurring is less than .01.

IV. Electrical Components

IV-A. Filament power supply and emission regulator.

The filament power supply is a Kepco JQE6-10M (A13) model with an output range of 0-6 volts DC and 0-10 amps. The power supply may be programmed to provide regulation of the filament current. An emission regulation circuit was designed and constructed for this purpose.

Table II

Characteristic Times at Different Pressures[a]

P_2 (torr)	P_1 (torr)	T (μsec)	t (msec)	Probability of collision
3×10^{-5}	10^{-7}	10	600	.00001
3×10^{-4}	10^{-6}	10	60	.0001
3×10^{-3}	10^{-5}	10	6	.001
3×10^{-2}	10^{-4}	10	.6	.01

[a] Quantities P_2, P_1, T, t defined in text.

An understanding of this circuit requires first a cursory knowledge of the general principles of power supply regulation. Most modern operational power supplies can be treated as a simple high gain, three terminal amplifier. If this amplifier is provided with an input and feedback impedance (R_{in} and R_f), as in Figure 5A, then the equation of output in terms of input is simply

$$E_{out} = E_{in} \cdot \frac{R_f}{R_{in}}. \tag{11}$$

This equation demonstrates how the output voltage will track the input signal.

One of the very important features of operational amplifiers is that the point X is very close to ground potential. This called a virtual ground. It is fruitful to describe operational amplifiers in terms of input currents rather than voltages. Since point X is at virtual ground, the input current I_{in} is simply E_{in}/R_{in}. Therefore, from Equation (11)

$$E_{out} = I_{in} \cdot R_f. \tag{12}$$

For emission regulation, the input current must reflect the emission characteristics. This is done by passing the emission current, i_e, across a resistor R_e to produce a voltage $i_e R_e$. As the emission resistor R_e is usually large, the voltage $i_e R_e$ is not immediately suitable for programming, since the input impedance of the amplifier, R_{in}, is considerably smaller than R_e. This problem is

Figure 5

Elements of the Emission Regulation Circuit

Figure 5A -- Operational amplifier

Figure 5B -- Impedance transformer

Figure 5C -- Basic emission regulation circuit

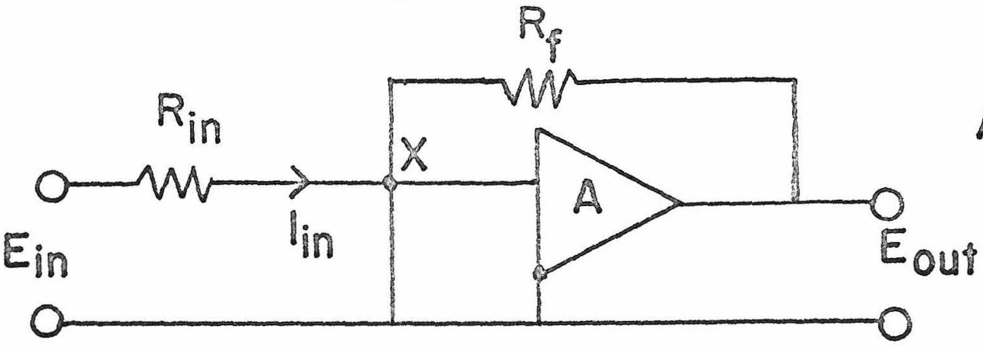
R_f
R_{in}
X
A
E_{in}
I_{in}
E_{out}

A

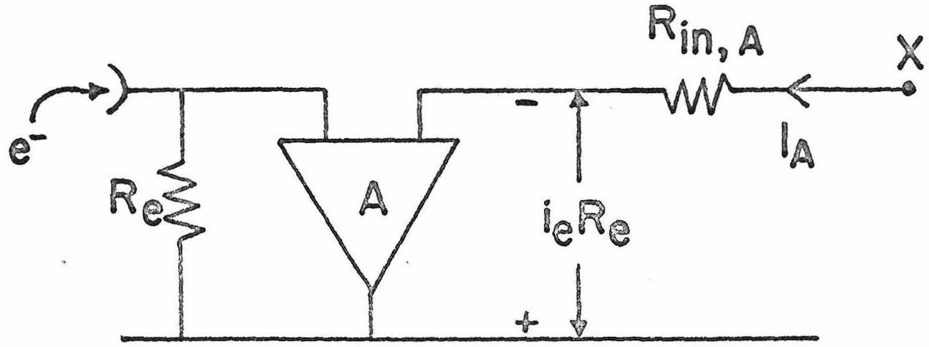
e^-
R_e
A
−
$R_{in,A}$
X
I_A
i_eR_e
+

B

C

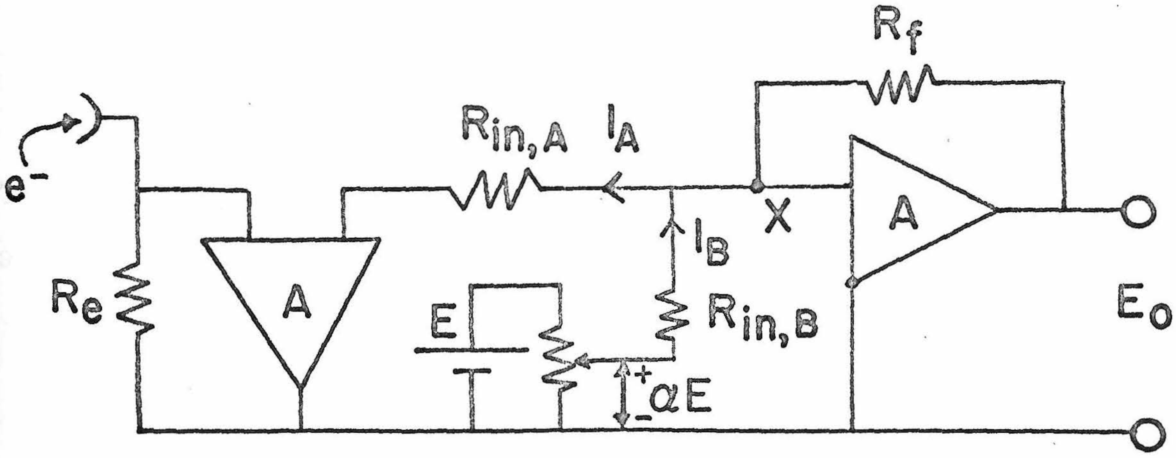
R_f
e^-
$R_{in,A}$
I_A
X
A
I_B
R_e
A
E
$R_{in,B}$
E_o
+
αE
−

circumvented by employing another amplifier as an impedance transformer or voltage follower,[3] as in Figure 5B. An impedance transformer simply repeats the input signal but renders it suitable for programming by reducing the output impedance of the system. Employing an input resistance $R_{in, A}$, the programming current I_A is then

$$I_A = \frac{i_e R_e}{R_{in, A}}. \tag{13}$$

This current is then added to another current, I_B, produced from a variable DC voltage, αE, where $0 \leq \alpha \leq 1$

$$I_B = \frac{\alpha E}{R_{in, B}}. \tag{14}$$

The difference between these currents becomes the input programming current of the amplifier

$$I_{in} = \frac{\alpha E}{R_{in, B}} - \frac{i_e R_e}{R_{in, A}}. \tag{15}$$

The final circuit is given in Figure 5C. The output voltage supplied across the filament is then

$$E_0 = \left(\frac{\alpha E}{R_{in, B}} - \frac{i_e R_e}{R_{in, A}}\right) R_f . \tag{16}$$

It is seen that should the emission current unaccountably increase, E_0 is correspondingly reduced. In this way, the emission current is regulated. A desired increase or decrease in i_e is effected by increasing or decreasing α.

A schematic of the complete emission regulation and filament power circuit is given in Figure 6. The principles of operation are identical to the simplified case discussed above. A 22.4 V battery is included in the circuit to keep the anode at a more positive potential than the filament at all electron energies. The ammeter A reads the current I_A, which can be directly related to the emission current using Equation (13). Three different emission resistors R_e are employed to provide differing degrees of programming sensitivity. Good emission regulation has been achieved for currents ranging between .01 μA and 10 μA.

The Kepco power supply has a current-limit mode which defines the maximum safe filament current (presently set at 4.5 A). If the programming circuit produces a signal demanding a filament current greater than 4.5 A, the current limit mode disables the programming capability and maintains the current at 4.5 A until the programming overload ceases.

IV-B. Plate and lens potentials. An electrical circuit was designed and constructed to supply voltages to the various elements of the source and lens assembly. A variety of pulsing circuits were used, as well as standard potentiometric circuits supplying dc voltages.

The electron current from the filament into the chamber is controlled by a control plate. The voltage on this plate is pulsed

Figure 6

Emission Regulation and Filament Power Circuit

Circuit elements shown inside shaded box were part of the Kepco Power Supply. Connections were made to these elements using nine terminals mounted on the rear of the supply. The internal programming input (terminals 3, 4, 5) was disabled to permit remote programming.

Circuit element	Name	Vendor or manufacturer
A	1557/15 amplifier	A14
E	22.4 V battery	A15
PS1	19 V power supply	A16
PS2	15 V power supply	A17
PS3	15 V power supply	A17
R1	20 M resistor	
R2	500 K resistor	
R3	50 K resistor	
R4	5 K resistor	
R5	1 K potentiometer	
R6	10 K resistor	
R7	6 K resistor	
R8	6 K resistor	

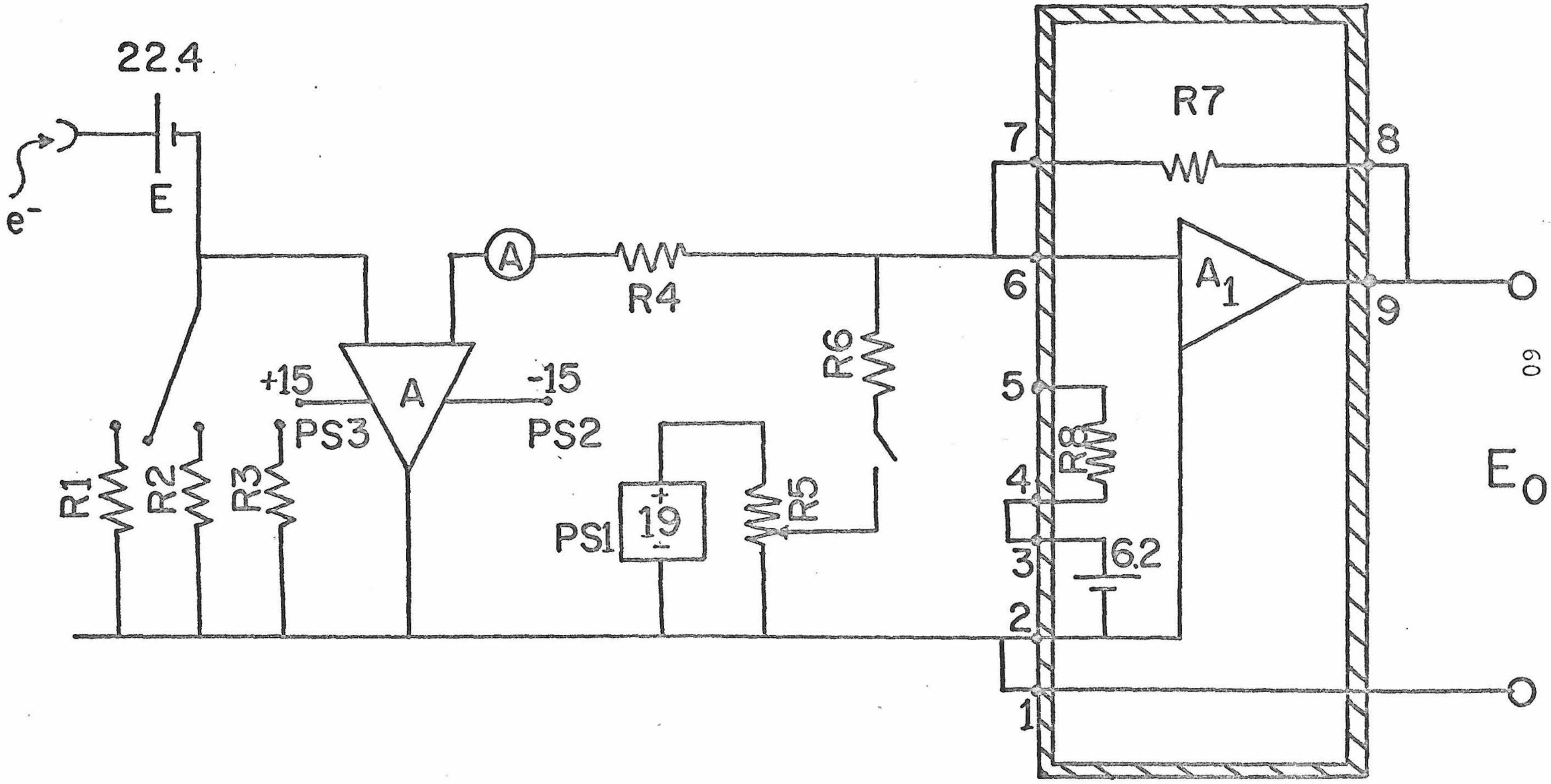
22.4
e-
E
R1
R2
R3
+15
PS3
A
-15
PS2
Ⓐ
R4
R6
PS1
+
19
-
R5
7
6
5
4
3
2
1
R7
R8
6.2
A_1
8
9
E_0

between a negative value (with respect to the filament potential) that prevents the beam from entering the chamber, and a positive value that permits electrons to pass into the cell. These pulses are supplied by one of two possible circuits, depending on whether the filament bias is above or below ground. Under most operating conditions, the bias of the screen is set at +50 V, as this ion energy ensures the best transmission of ions through the lens system to the quadrupole. In situations when the electron energy is to be greater than 50 eV, the filament potential must then be negative.

Figure 7A sketches the pulsing circuit used in this case. At low electron energies the filament is at positive potentials, and the control circuit of Figure 7A is unsuitable, as electrons are repelled at all voltages. In this case the circuit of Figure 7B is employed. Both circuits use a negative going input pulse supplied by an external pulse generator.

Ions are ejected from the chamber by simultaneously reducing the ion exit and drawout plate potentials from V_T to a lower value. The pulsing circuit for this uses a negative going input pulse supplied by a pulse generator. Figure 7C gives a schematic of this circuit.

The remaining elements have variable dc voltages supplied by standard potentiometric circuits. Originally cathode follower circuits were used, but no operational change was observed when these circuits were replaced by the simpler potentiometric ones. Alternate members of the lens assembly are shorted together, with three elements having a variable negative voltage and two having a variable

Figure 7

Pulsing Circuits

Figure 7A -- Emission current pulsing circuit used for high electron energies (>50 eV).

Figure 7B -- Emission current pulsing circuit used for low electron energies (< 50 eV).

Figure 7C -- Ion ejection pulsing circuit.

A

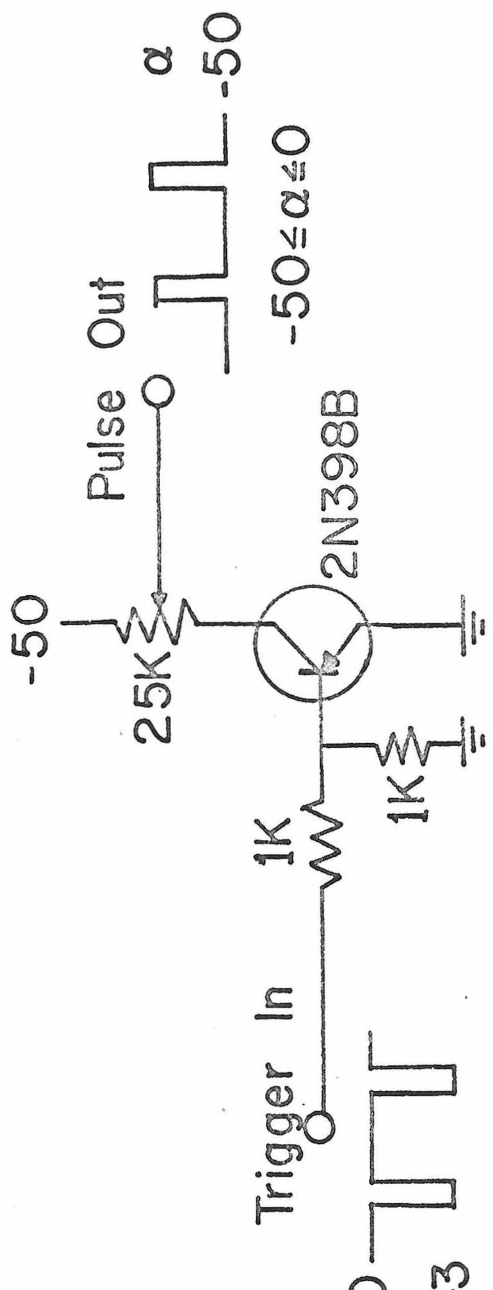

Trigger In
0
-3
1K
1K
2N398B
-50
25K
Pulse Out
α
-50
-50≤α≤0

B

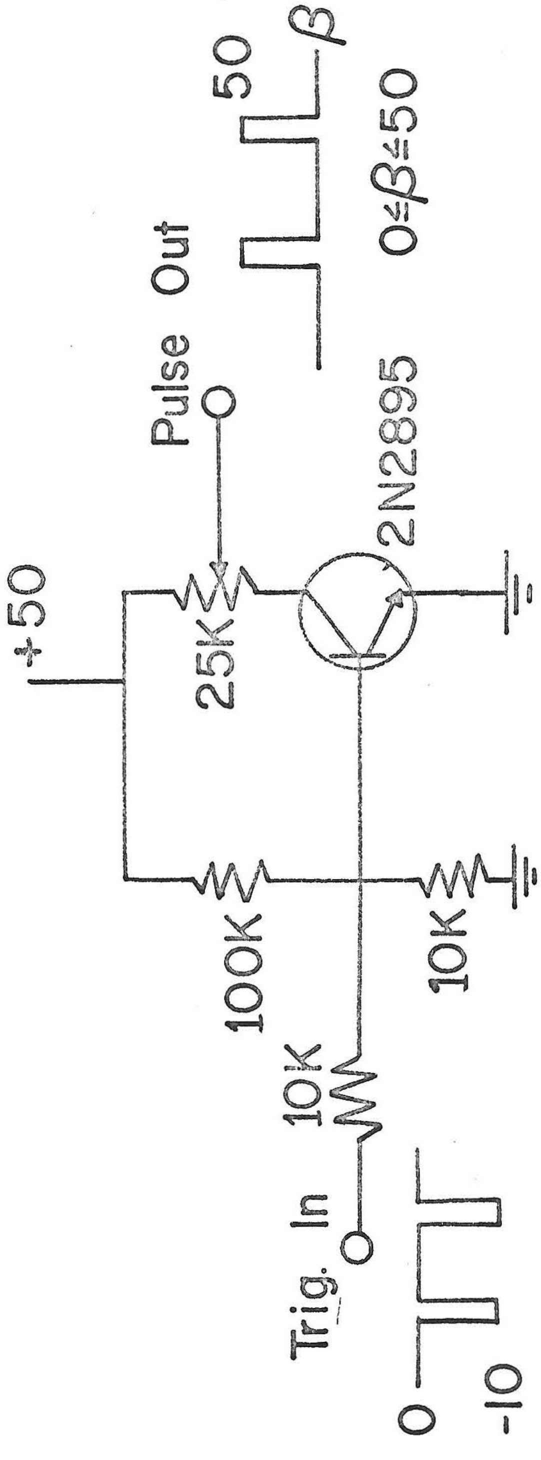

Trig. In
0
-10
10K
100K
10K
+50
25K
2N2895
Pulse Out
50
β
0≤β≤50

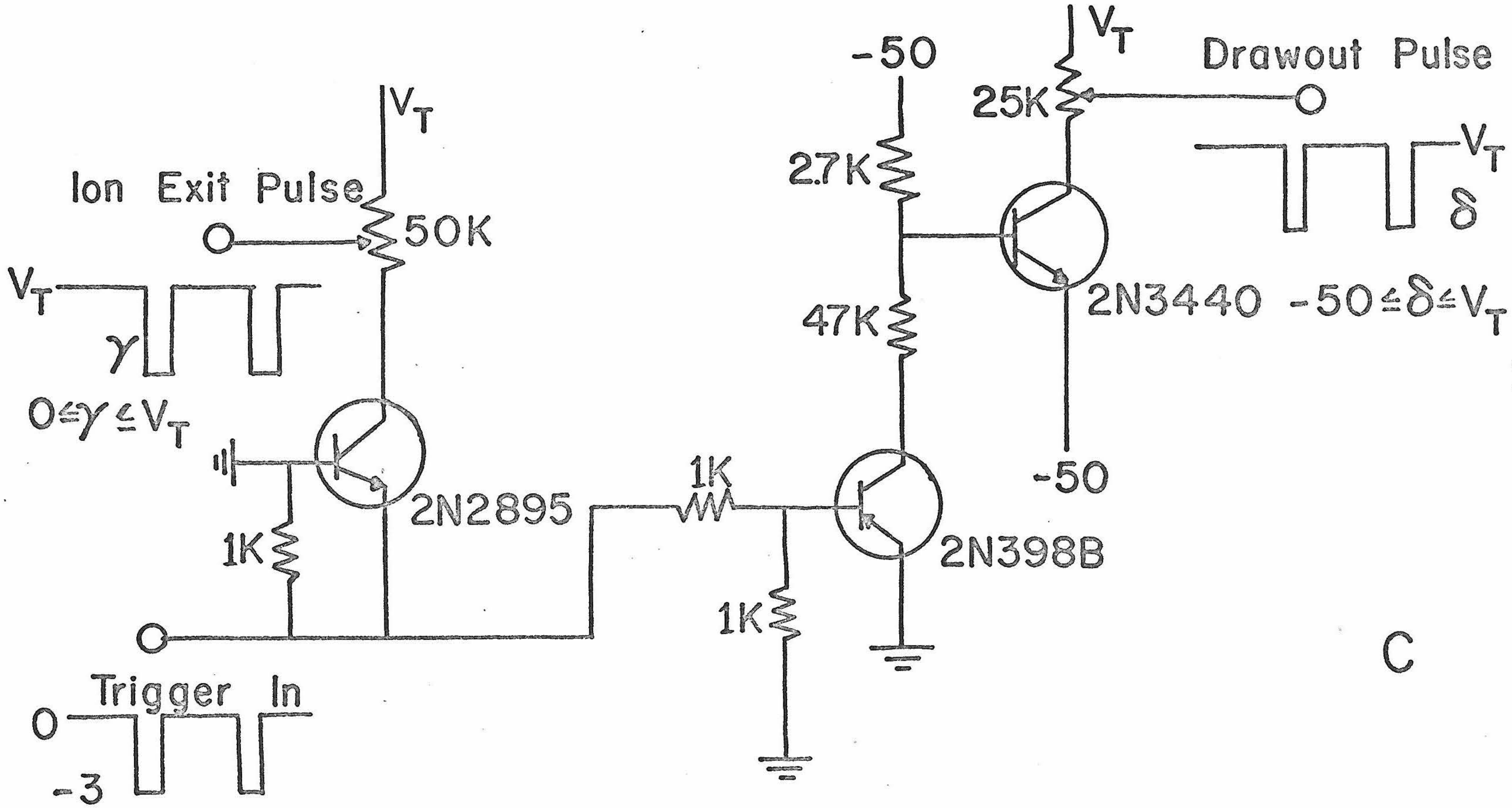
Ion Exit Pulse
V_T
50K
V_T
γ
$0 \leq \gamma \leq V_T$
1K
2N2895
Trigger In
0
-3
1K
1K
2N398B
-50
2.7K
47K
V_T
25K
Drawout Pulse
V_T
δ
2N3440
$-50 \leq \delta \leq V_T$
-50

C

positive voltage. Table III lists the range of voltages available for each element. The performance of the circuits is more readily evaluated when described in terms of commonly used parameters, such as the electron energy, ion energy, and trapping voltage. Table IV shows the range of available voltages for these parameters. The potentiometric circuits are designed so that the parameters listed in Table IV are each directly controllable with one potentiometer.

IV-C. Timing circuitry. The timing sequence commences with a negative going input pulse with a typical width of 5 μsec that is applied to the emission current control circuit. A Tektronix (A18) Model 162 Sawtooth generator and Model 161 pulse generator are used to supply the pulse. The control circuit accordingly permits a pulse of electrons 5 μsec wide to enter the reaction chamber. Simultaneously, the negative trigger is applied to the "trigger in" input of a PAR Model CW-1 (A19) boxcar integrator. A boxcar integrator is a detector that samples an input signal using a variable width, variable delay gate. It has particular utility for input signals consisting of a repetitive waveform of interest plus noise. In addition to activating the sampling amplifiers, the gate is used to trigger another Tektronix pulse generator, which in turn applies a negative pulse used to trigger the ejection circuitry. The sampling gate width is determined by the

Table III

Available Voltages for Spectrometer Elements

Element	Voltage range[a]
Filament	-50 to +70
Control plate	pulsed, see Figures 7A and 7B
Electron entrance	+10 to +90
Screen	+10 to +80
Ion exit	pulsed, see Figure 7C
Drawout	pulsed, see Figure 7C
Negative lenses	0 to -50
Positive lenses	0 to +80

[a] All voltages referenced to ground.

Table IV

Available Voltage Range for Spectrometer Parameters

Parameter	Voltage range
Electron energy	7 to 130
Ion energy	10 to 80
Trapping voltage	0 to 10
Negative lenses	0 to -50
Positive lenses	0 to +80

sum of the flight time of the ions from the source to the multiplier (typically 20 μ sec) plus the width of the output signal from the detector (typically 50 μsec). The variable delay function of the integrator is used to slowly scan delay times and thus reaction times. Usually, scan times of 2 minutes are used and maximum delay times of .5 to 4 msec are employed. Figure 8 is a block diagram of the important features of the timing circuitry.

V. Operation of the Spectrometer

This section describes theoretical and actual operating conditions of the spectrometer.

V-A. Operation of source and lens assembly. For most kinetic measurements, typical emission currents measured at the anode were in the range of .1 to 1 μA. Under conditions where the beam was not repelled by the control plate, it was found that about 50% of this current passed through the electron entry plate into the reaction chamber. Usually an electron gate width of 5 μsec was used. There is thus relatively little uncertainty in the time of formation of the ions.

Virtually all experiments used an electron energy of 70 eV, as the source operated most reliably at this energy. Lower electron energies, even at larger emission currents, generally resulted in intensity losses and reduced trapping efficiencies. The ion energy was usually maintained at the relatively high value of 50 eV, as the transmission of ions to the quadrupole was maximum at this value.

Figure 8

Block Diagram of Timing Circuitry

Unit	Name	Vendor or manufacturer
1	Saw tooth generator	A18
2	Pulse generator	A18
3	Box car integrator	A19
4	Pulse generator	A18
5	Source and lens voltage control	–

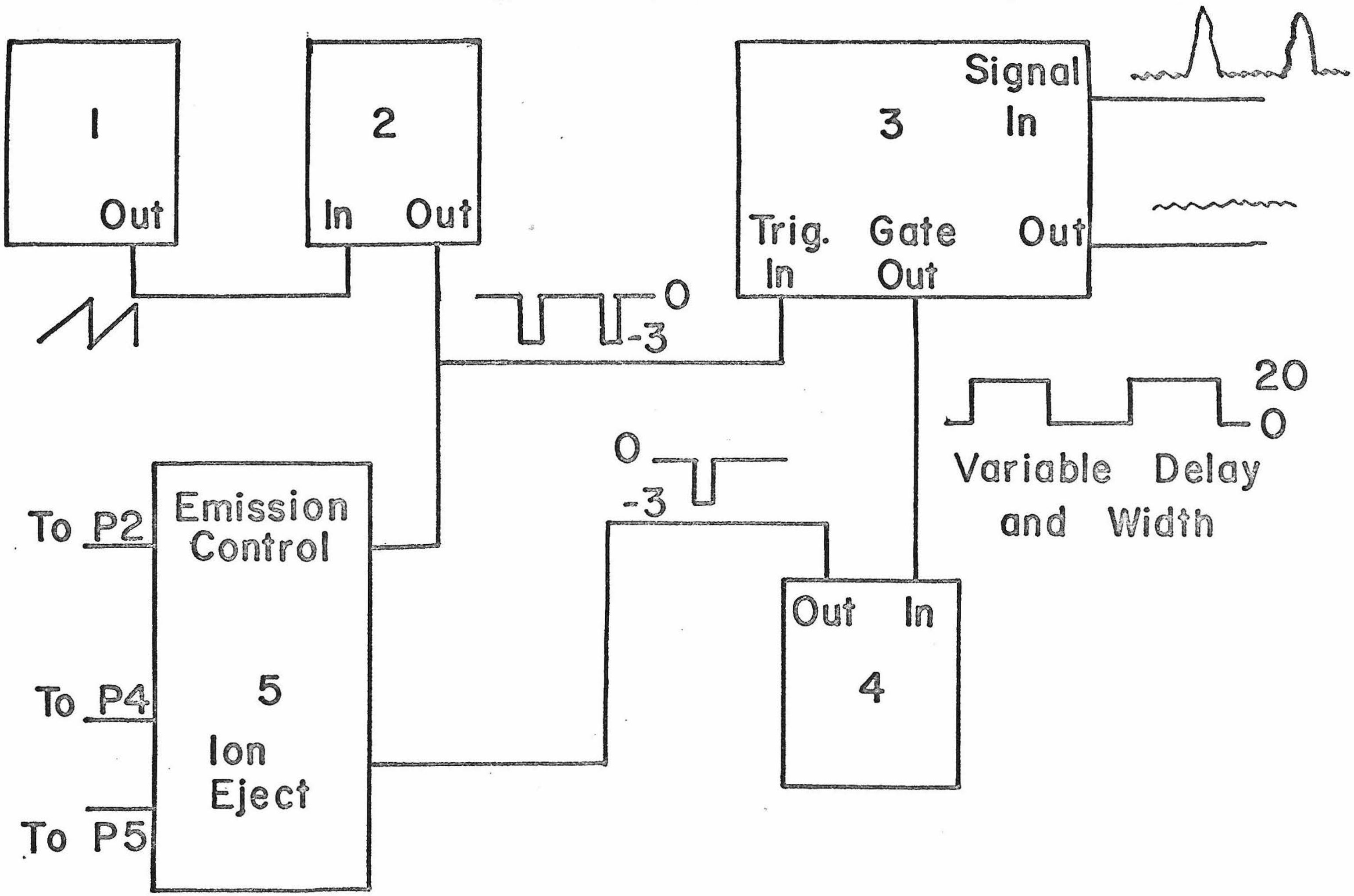
1
Out
2
In
Out
3
Signal
In
Trig.
In
Gate
Out
Out
0
-3
20
0
Variable Delay
and Width
0
-3
Out
In
4
Emission
Control
5
Ion
Eject
To P2
To P4
To P5

Accordingly, the filament generally had a negative bias with respect to ground, and thus the control circuit of Figure 7A was usually used to pulse the emission current.

The mass resolution of the quadrupole filter was observed to be around 100 for most experiments. This rather poor resolution is due to two effects:

(1) The relatively high ion kinetic energy adversely affects resolution.

(2) The most efficient ejection of ions from the source was effected with ejection pulse depths of 10 to 20 volts. The actual potential profile in the chamber during trapping and ejection is discussed later, but this obviously introduces a spread in ion kinetic energies, which reduces quadrupole resolution.

The resolution was adequate, however, for the experiments discussed in this thesis.

Ion trapping efficiencies were found to be very sensitive to the orientation of the magnets surrounding the ion source and great care was exerted to achieve an optimum orientation. One of the most effective methods of magnet alignment involved maximizing the electron current that was collected on the first collimating lens. The lens was maintained at a +100 volt bias for the purpose. It is reasoned that this condition results in a nearly axial magnetic field well suited for ion trapping.

Trapping efficiencies depended markedly on the magnitude of the trapping voltage. At voltages lower than 2 volts, only untrapped ions were detected at the spectrometer. Ions were characterized as untrapped by their anomalously early arrival time at the spectrometer. At trapping voltages between 3 and 6 volts, the ratio of trapped to untrapped ions was about 20:1 for most systems. Above 6 V, the intensities of signals generally decreased somewhat, and greater relative ion loss was observed. Usually, higher trapping voltages were required for efficient trapping of lighter mass ions.

Virtually all trapped-ion experiments undertaken with the instrument were characterized by some degree of loss of trapped-ion current with time. The mechanism for this ion loss is presumably one in which the ions random walk towards the walls of the chamber by a succession of collisions with neutral molecules. Plots of total ion current versus trapping time show an initial sharp drop at very short trapping times (less than 50 μsec) and a more gentle decrease throughout the remainder of the scan. Ion loss rates are usually very dependent on pressure but depend also on other source conditions, such as trapping voltage. In many systems, however, minimal ion loss is observed at low pressures near 10^{-5} torr. This lends credence to the collisional loss mechanism proposed above. The initial steep fall in ion current may well be due to space charge blowup of the initial ion packet. Immediately after formation, under typical conditions,[4] there is an ion density of about 10^6 ions/cc in the narrow cylinder traversed by the electron beam. This density is sufficient to cause some space charge blowup of the ion distribution. The effect of ion loss on the calculation of ion-molecule reaction rates is discussed in Section V-D.

Untrapped ions were also observed when the potential of the positive lenses was below +20 volts. Presumably these ions arise from ionization occurring outside the cell, in the region between the ion exit plate and the first lens. At lens voltages greater than +20 V, untrapped ions were not detected. When the positive lens voltage approached the ion energy, there was a marked diminution of signal. Usually the positive lens voltage was about 25 volts, and negative lens voltages were near -50 volts. The focussing properties of the lens system will be discussed in more detail in a later section.

V-B. Ion motion inside the reaction cavity. It is of interest to know the nature of the electric potential inside the chamber. Using LaPlace's equation in cylindrical coordinates, it is found[5] that the electric potential Φ inside a chamber having length l, radius a, a voltage V_1 applied at $z = 0$ and V_2 applied at $z = l$ is

$$\Phi(r, z) = 2 \sum_{\alpha} \left[\frac{J_0(\frac{\alpha r}{a})}{\alpha J_1(\alpha) \sinh \frac{\alpha \ell}{a}} \left| V_1 \sinh \frac{\alpha(\ell - z)}{a} + V_2 \sinh \frac{\alpha z}{a} \right| \right] \quad (17)$$

where J_i is the Bessel function of order i. The various values of α are determined from the solution to

$$J_0(\alpha) = 0. \quad (18)$$

The first few values of α are 2.405, 5.520, 8.654, 11.794, 14.9 and the corresponding values of $J_1(\alpha)$ are .52, -.34, .27, -.23, and .21.

Since ions are formed along the line $r = 0$, it is of particular interest to know $\Phi(0, z)$. Using Equation (17) and substituting $l = 1.5''$, $a = .375''$ this is found to be

$$\Phi(0, z) = 2\sum_{\alpha} \frac{1}{\alpha J_1(\alpha)} \frac{V_1 \sinh 4\alpha(1 - z/\ell) + V_2 \sinh \frac{4\alpha z}{\ell}}{\sinh 4\alpha} \tag{19}$$

The axial voltage profile during trapping can be determined by letting $V_1 = V_2 = V_T$. This profile is illustrated in Figure 9.

Ions initially formed along the entire length of the axis will oscillate in the trapping field. This characteristic oscillatory frequency along the z axis can be estimated by using a simplified form of the potential Φ. One form particularly amenable to simple calculations is

$$\Phi(z) \approx V_T(.025 + 3.90\,(z - \ell/2)^2/\ell^2). \tag{20}$$

This approximate potential is also plotted in Figure 9.

The equation of motion of an ion of mass m and charge q is

$$m\ddot{z} = -q\frac{\partial\Phi}{\partial z}. \tag{21}$$

Substitution of Equation (20) and redefining $z = 0$ as the centre of the cylinder gives

Figure 9

Axial Voltage Profile in Reaction Chamber

when Trapping Voltage = V_T

The solid line indicates the exact profile calculated from Equation (19). The dashed line indicates the approximate profile of Equation (20).

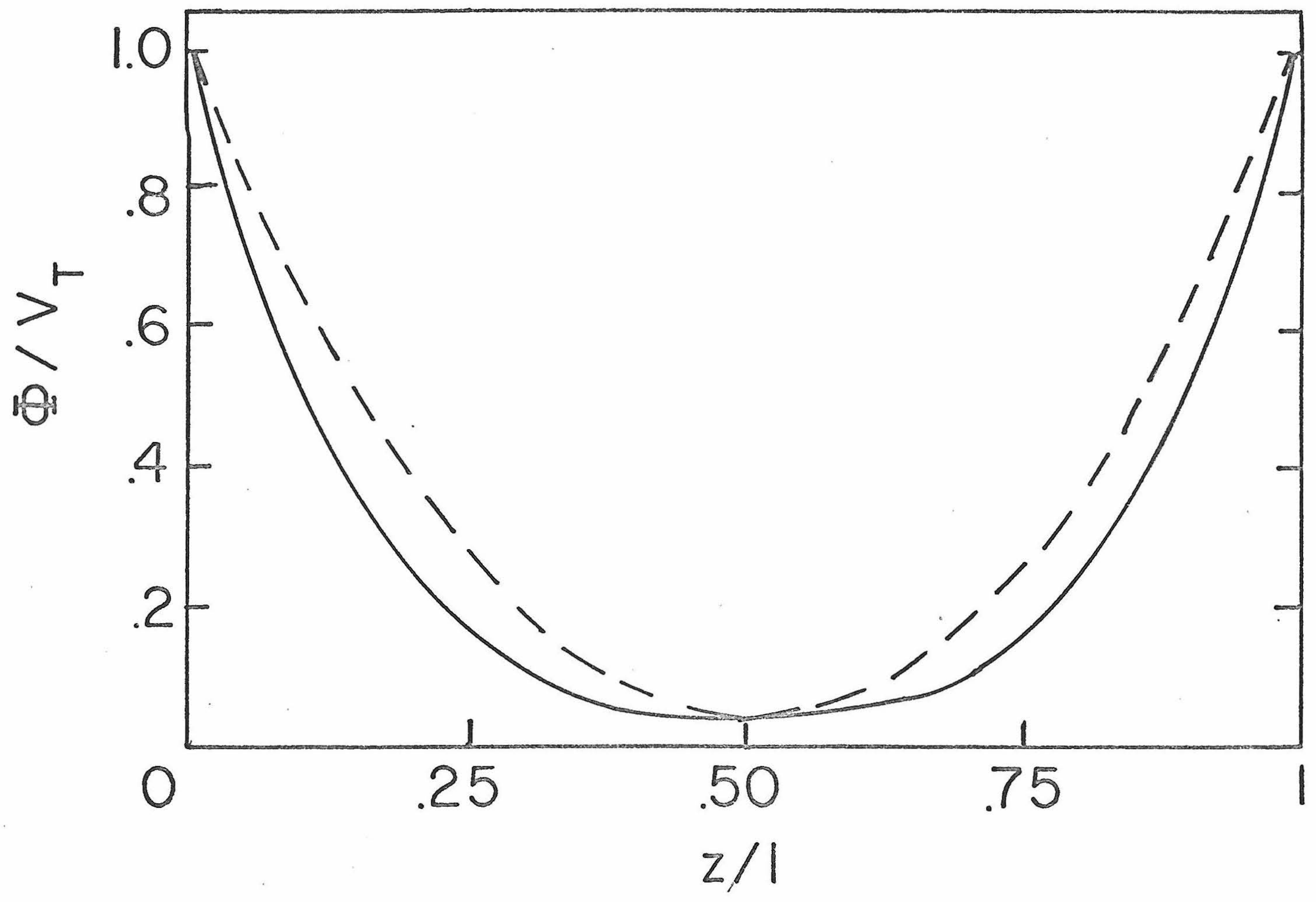

1.0
.8
.6
.4
.2
0
.25
.50
.75
1
Φ / V_T
z/l

$$\ddot{z} = -\frac{7.80\, q\, V_T}{m\ell^2} z. \qquad (22)$$

Defining

$$\omega_T^2 = \frac{7.80\, q\, V_T}{m\ell^2} \qquad (23)$$

there results

$$z = -\omega_T^2 z. \qquad (24)$$

Equation (24) demonstrates that the motion of an ion along the z axis is an oscillatory one with characteristic frequency $\nu_T = \omega_T/2\pi$. The period of oscillation τ_T is simply $1/\nu_T$ and can be shown to be

$$\tau_T = 8.73\sqrt{\frac{M}{V_T}}\ \mu\text{sec} \qquad (25)$$

where M is in amu and V_T is in practical volts. Typical periods of oscillation for conditions described earlier thus range from 10 to 40 μsec.

Trapping of positive ions in the z direction occurs whenever positive trapping voltages are used. Radial trapping of the ions is effected by the homogeneous axial magnetic field, which constrains the ions to move in a circular orbit in a plane perpendicular to the axis. The rotational period, τ_c, is $2\pi/\omega_c$, where

$$\omega_c = \frac{qB}{mc}. \qquad (26)$$

The magnetic field B was measured with a gaussmeter as 700 gauss. Accordingly, cyclotron frequencies will be in the range 100 to 13 KHz for ions in the mass range of 10-80 amu. The corresponding radii of curvature may be estimated for ions of thermal energy using

$$r = \frac{1}{\omega_c} \cdot \sqrt{\frac{2kT}{m}} \qquad (27)$$

and vary from .1 to .3 cm. This is to be compared to the .9 cm radius of the ion source. For thermal ions of large mass, the cyclotron radii are almost comparable to the radius of the reaction chamber. Accordingly only a relatively small number of collisions that redefine the centre of the rotational motion would cause these ions to strike the cylinder walls. (Random walk statistics predict an average of 10 collisions would be sufficient for a mass 80 ion). For smaller ions, a larger number of collisions is required. Thus this mechanism of ion loss predicts that heavier mass ions are more difficult to trap for long periods of time and that ion loss rates are not independent of mass. This effect has been observed experimentally and significantly affects kinetic calculations (see Section V-D).

When the ions are ejected, the potential of the ion exit trapping plate is suddenly lowered. The voltage profile in the chamber of this new arrangement can be determined from Equation (19). Typical cases are illustrated in Figure 10. There is thus the possibility of a wide distribution of ion kinetic energies, depending on the ion distribution along the z-axis at the instant that the ejection pulse is applied.

Figure 10

Axial Voltage Profiles during Ion Ejection

The solid curve shows the profile when electron entry plate voltage = V_T and ion exit plate voltage = $-V_T$. The dashed curve shows the changes in the profile when the ion exit plate voltage = $-2\,V_T$.

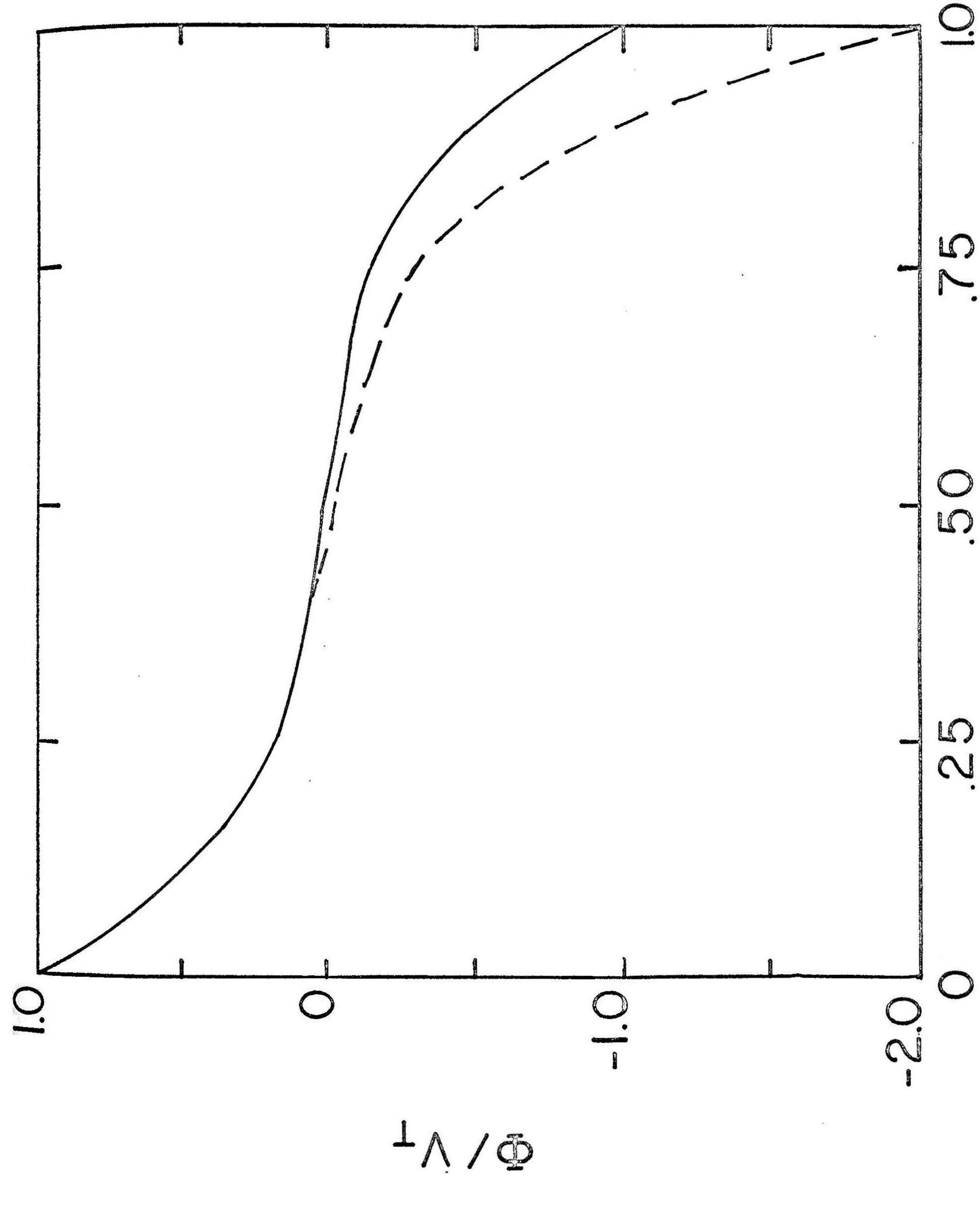
1.0
0
-1.0
-2.0
0
.25
.50
.75
1.0
z / l
Φ / V_T

If no randomizing collisions occur, Equation (25) shows that there are times when all the ions are concentrated at $z = \ell/2$. These times occur at $\tau_T/4$, $3/4\ \tau_T$, $5/4\ \tau_T \cdots$ after the initial formation pulse. If the ejection pulse is applied at any of these times, there should be little spread of ion kinetic energies. Alternatively, the ionic distribution at the times $\tau_T/2$, $\tau_T \cdots$ will be a uniform one along the entire length of the z axis, and there will be a resultant large spread in ion kinetic energies.

In addition, the differing ionic distributions will likely have different ejection efficiencies, as one of the ionic distributions will be less favourable for effective ion withdrawal. This effect has been observed for non-reactive ions at low pressure. A typical spectrum is given in Figure 11. The time between successive maxima is predicted to be $\tau_T/2$. For the conditions described in Figure 11, $\tau_T/2$ is calculated to be 14 μsec. The measured time interval is measured as 18 ± 3 μsec. At a pressure of 1.5×10^{-4} torr, these oscillations were not seen, indicating that collisions had randomized the ion distribution.

Spectra exhibiting oscillations of this nature have been observed for numerous systems at low pressures. In most cases, however, the time intervals between successive maxima are considerably larger than those predicted from Equation (25). Low pressure curves for N_2^+ and He^+ are given in Figure 12. The reason for the discrepancy is not known, but may result from a combination of the cyclotron rotation and the trapping well oscillation. These two

Figure 11

Variation of Ion Intensity with Trapping Time for N_2^+

The pressure was 3×10^{-5} torr and the trapping voltage was 3 volts.

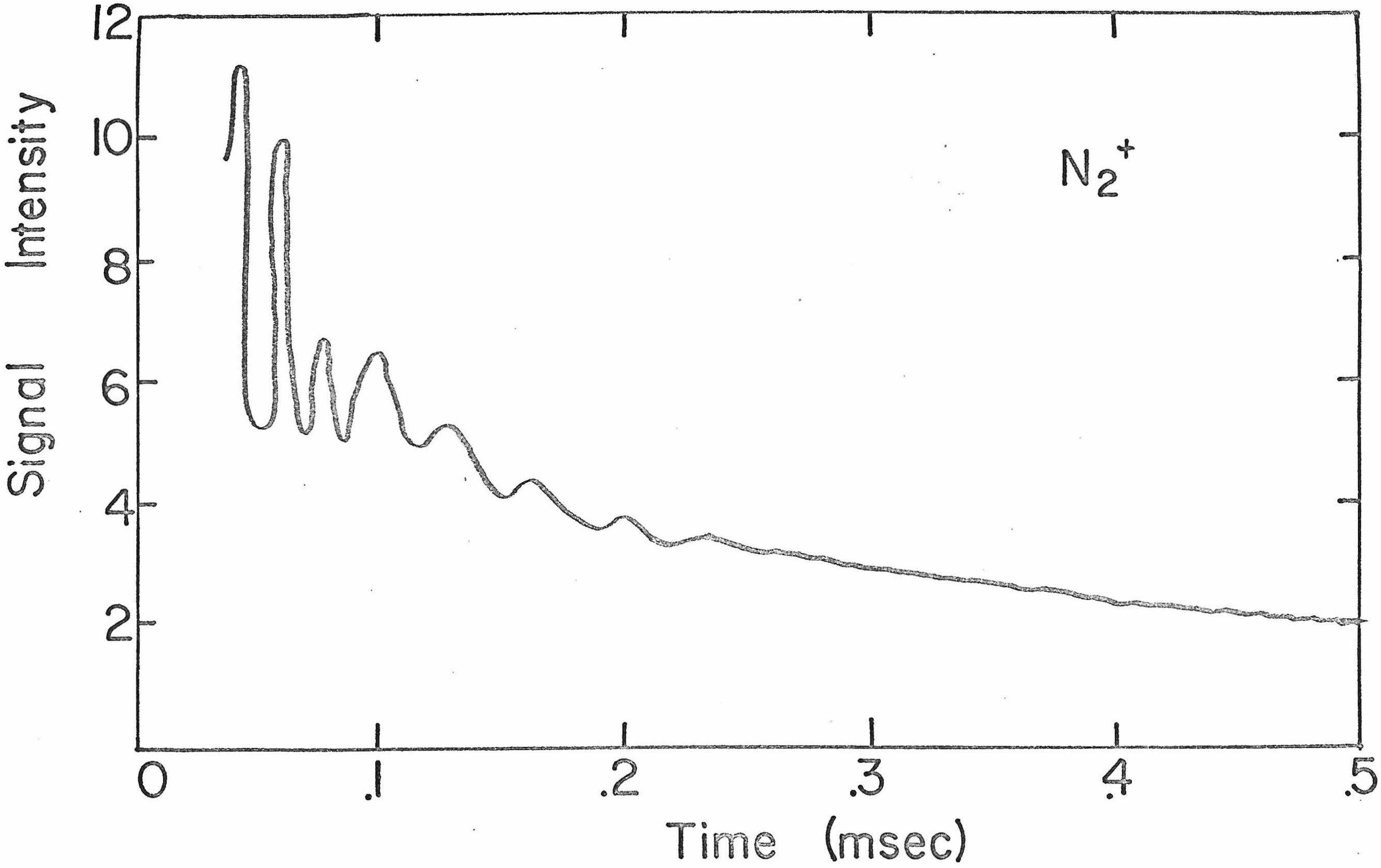
Signal Intensity
12
10
8
6
4
2
0
.1
.2
.3
.4
.5
Time (msec)
N_2^+

Figure 12

Low Pressure Intensity Versus Trapping

Time Spectra for He^+ and N_2^+

Trapping voltages were 9 and 7 volts, respectively.

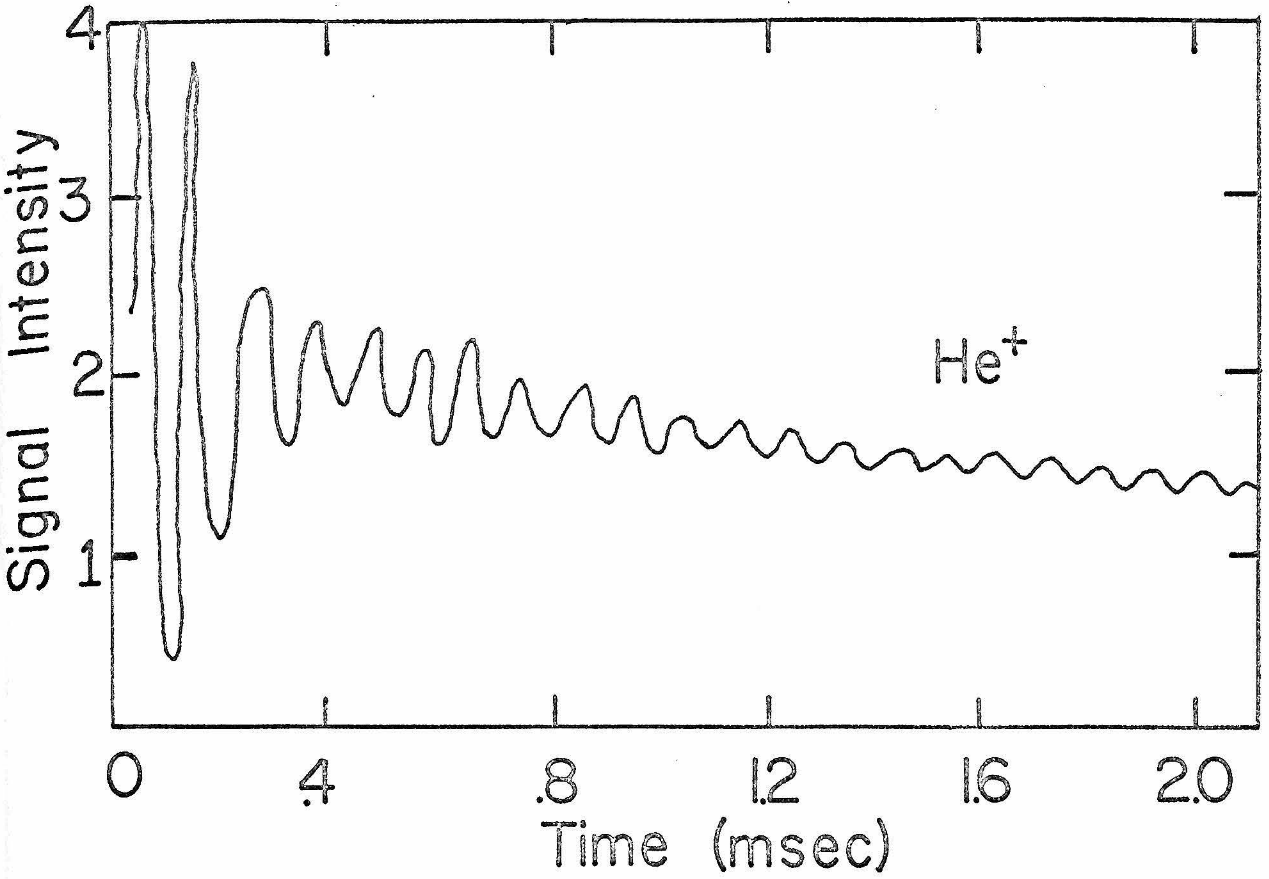
Signal Intensity
1
2
3
4
He$^+$
0
.4
.8
1.2
1.6
2.0
Time (msec)

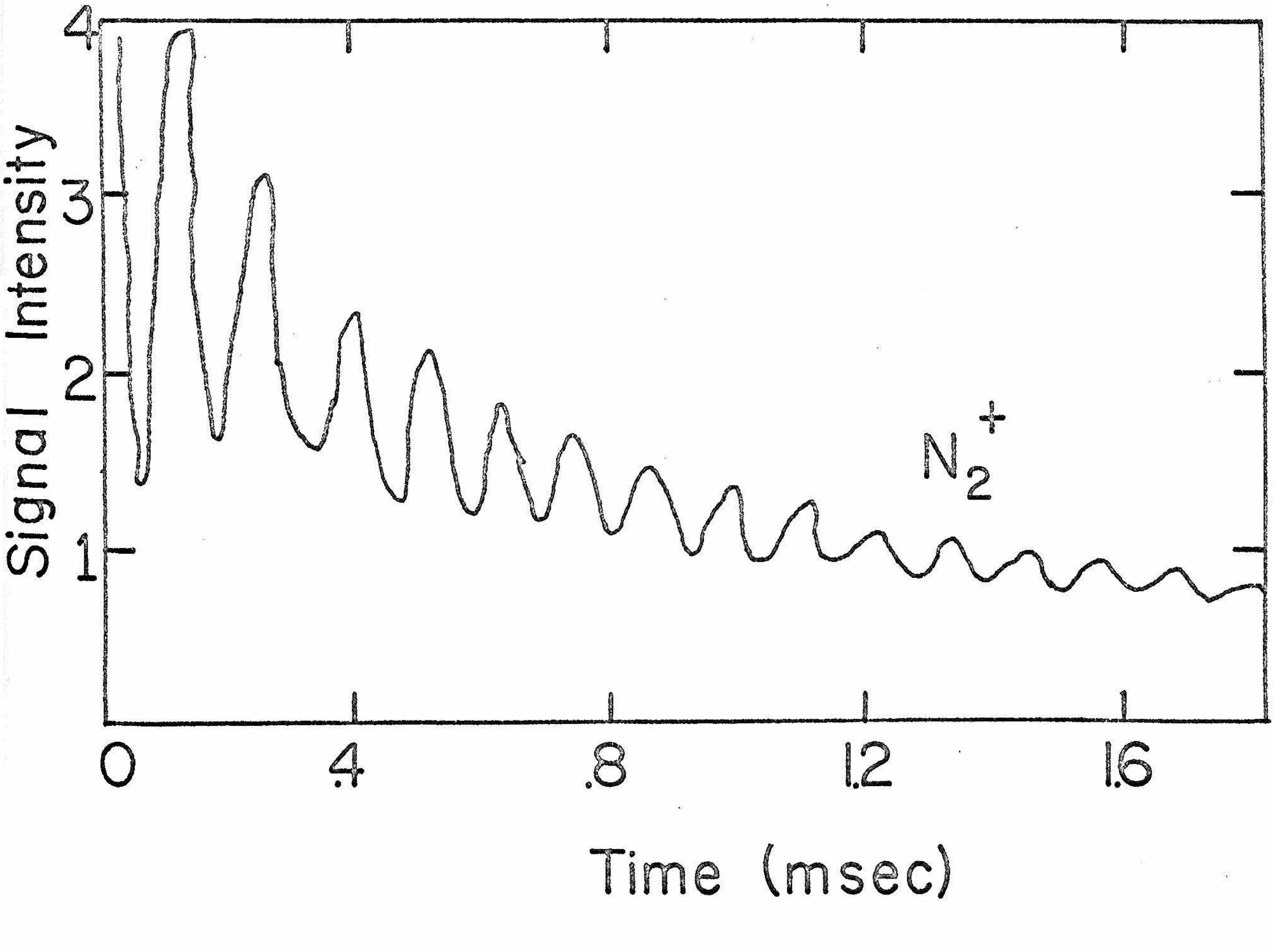
Signal Intensity
1
2
3
4
N$_2^+$
0
.4
.8
1.2
1.6
Time (msec)

independent effects could act together producing ionic distributions with differing collection efficiencies. Successive maxima should then occur at a certain beat frequency of these two periodic motions. The beat interval should then be given by Equation (26)

$$\text{Beat interval} \approx n\tau_c \approx m\frac{\tau_T}{2} \qquad (26)$$

$$m,\ n \text{ integers}.$$

The exact determination of the beat interval is not possible, since τ_c and τ_T are not known with sufficient accuracy. In addition, the degree to which the equality in Equation (26) must be obeyed is unknown. However, rough calculations generally predict beat intervals within 30% of the observed period for a variety of well depths and ionic masses.

V-C. Ion motion through the collimating lens assembly.

The alternating positive-negative voltage configuration of the collimating lenses ensures that the ejected ion beam does not diverge en route to the quadrupole spectrometer. The focussing properties of two cylindrical elements with differing voltages have been investigated in detail by Spangenberg.[6] This discussion will be qualitative only. The shape of the potential surfaces between two cylinders of the appropriate dimensions are sketched in Figure 13. Typical ion trajectories are shown for an ion beam that is divergent at point A. It is seen that the initially divergent beam is refocussed to a point B further down the ion path. This process is repeated at each of the lens interfaces

Figure 13

Equipotential Surfaces and Ion Trajectories in the Lens Assembly

The surfaces were calculated with the aid of Equation (13.28) of Reference 5. All voltages are referenced to $\frac{V_- + V_+}{2}$ being defined as 0, where V_- and V_+ are the negative and positive lens voltages used in actual operation. Equipotential surfaces are shown for $V = 0$, $V = \pm .5\ V$ and $V = \pm .9\ V$. Ion trajectories are shown as dashed lines.

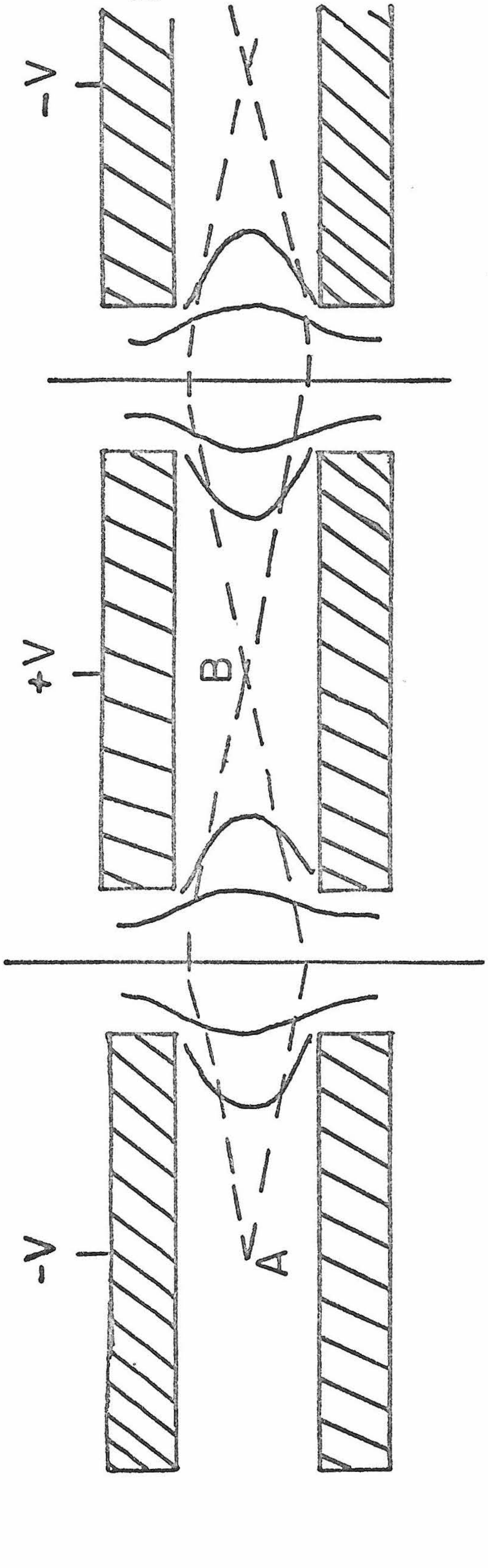
-V
+V
-V
B
A

and in this fashion the beam remains well collimated over the length of the lens assembly.

V-D. Effect of ion loss on the determination of reaction rate constants. Consider the generalized ion molecule reaction given in Equation (27)

$$A^+ \xrightarrow{k} B^+ . \tag{27}$$

Each ion is characterized by an ion loss rate constant Q_A and Q_B which may or may not depend upon pressure. The time dependence of the ionic abundances is

$$\frac{d[A^+]}{dt} = -nk\,[A^+] - Q_A[A^+] \tag{28}$$

$$\frac{d[B^+]}{dt} = nk.[A^+] - Q_B[B^+] \tag{29}$$

where n is the pressure of the neutral reactant. These equations can be solved using standard techniques giving

$$A^+(t) = A_0\, e^{-(nk + Q_A)t} \tag{30}$$

$$B^+(t) = B_0\, e^{-Q_B t} - \frac{nk A_0 [1-e^{(Q_B - Q_A - nk)t}]}{Q_B - Q_A - nk}\, e^{-Q_B t} \tag{31}$$

where A_0 and B_0 are the initial abundances of the two ions. In order to determine the rate constant k, it is instructive to consider the quantity $A^+/(A^+ + B^+)$. Under conditions where $B_0 = 0$, this ratio can be reduced to a particularly useful form

$$A^+/\Sigma \equiv \frac{A^+}{A^+ + B^+} = \frac{1}{1 + \frac{nk[e^{(nk+\delta)t} - 1]}{nk + \delta}} \qquad (33)$$

where

$$\delta = Q_A - Q_B \qquad (33)$$

and reflects the difference in ion loss rates for the two ions. If $\delta \ll nk$, then

$$A^+/\Sigma \approx e^{-nk\,t} \qquad (34)$$

and a plot of the logarithm of this quantity versus time is a straight line with slope -nk. Knowledge of the pressure then yields the rate constant directly. It follows therefore that ion loss does not affect the determination of k if all ions in the system are lost at the same rate.

For larger values of δ, the slope of the log of the normalized abundance of A^+ begins to deviate from the ideal value of -nk, leading to progressively larger errors in the apparent rate constant. Figure 14 shows curves of A^+/Σ for various values of δ and Table V lists the magnitude of the error in the apparent rate constant if Equation (34) is uncritically applied. For values of δ less than .2 nk, the error is less than 10%. This will be taken as the acceptable upper limit for δ.

Figure 14

Plots of the logarithm of A^+/Σ versus time for various values of δ, the quantity measuring the difference in ion loss rates for reactant and product.

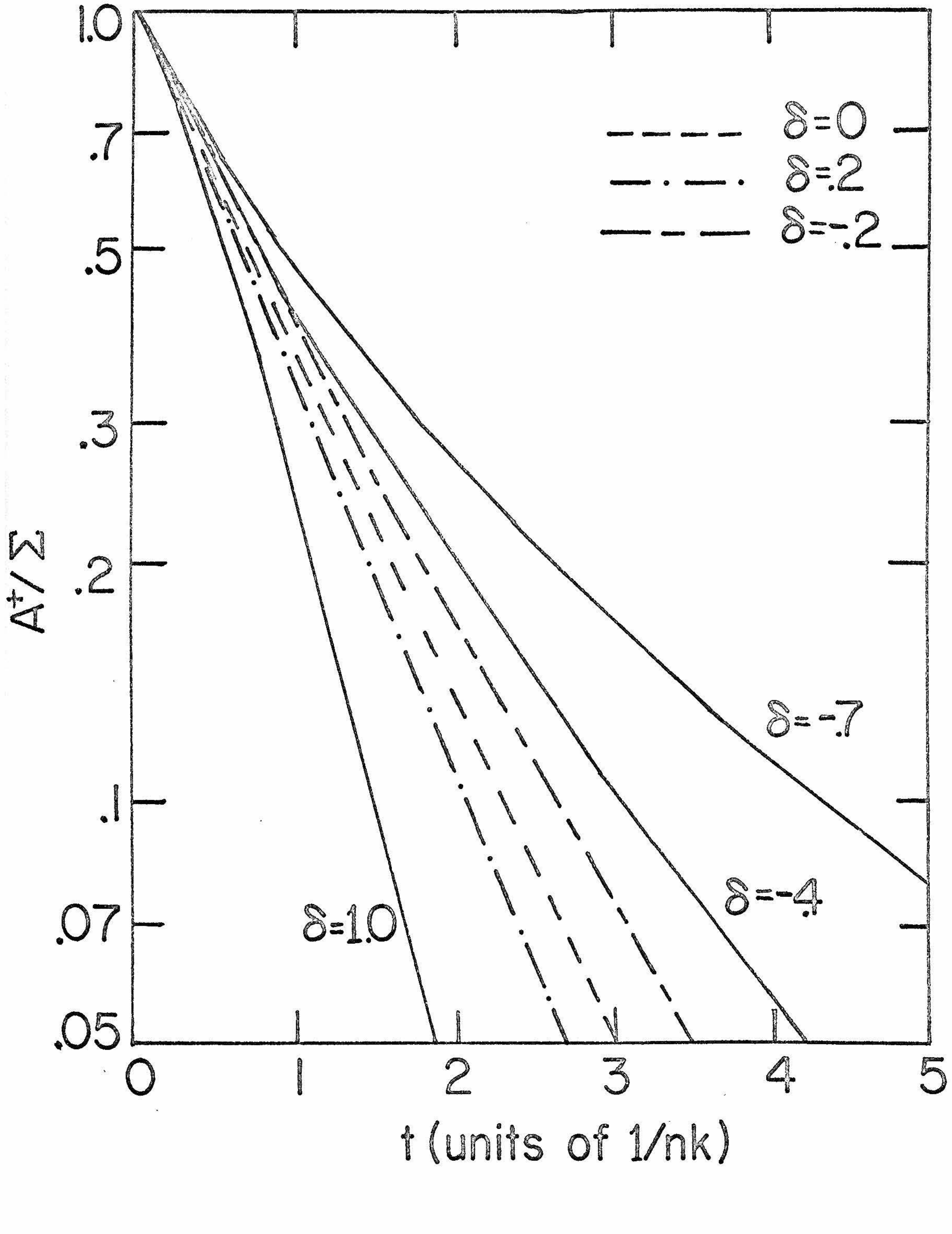
1.0
.7
.5
.3
.2
.1
.07
.05
A⁺/Σ
0
1
2
3
4
5
t (units of 1/nk)
δ=0
δ=.2
δ=-.2
δ=-.7
δ=-.4
δ=1.0

Table V

Errors in the Apparent Rate Constant for Various Values of δ[a]

δ[b]	$k_{apparent}$[c]
0	1
+.2	1.1
+.4	1.2
+1.0	1.6
-.2	.9
-.4	.8
-.7	.55

[a] Defined in text.

[b] Units of nk.

[c] Expressed in units of k_{actual}.

The magnitude of δ may be estimated by determining Q_A and Q_B. If it is initially assumed that Equation (34) is indeed valid for a particular reactive system, then Q_A is readily estimated by comparing the slopes of $\ell n\, A^+$ (Equation (30)) and $\ell n\, A^+/\Sigma$ (Equation (34)) versus time. Secondly, Q_B may be evaluated by noting the time when $\frac{dB^+}{dt} = 0$. At this time

$$Q_B = \frac{A^+}{B^+} nk \tag{35}$$

An approximate value of δ then follows directly. If this value is less than .2 nk, then the original assumption about the applicability of Equation (34) is valid and the entire analysis is self-consistent.

References

1. S. Dushman, in "Scientific Foundations of Vacuum Technique," Section 2, J. M. Lafferty, ed., Wiley and Sons, New York, 1962.

2. A. Guthrie, "Vacuum Technology," Wiley and Sons, New York 1963.

3. H. V. Malmstadt and C. G. Enke, "Electronics for Scientists," Benjamin, Inc., New York, 1962.

4. Emission current = .5 μA, pressure = 10^{-4} torr, ionization cross section = 10 Å^2.

5. F. Bowman, "Introduction to Bessel Functions," p. 46, Dover, New York, 1958.

6. K. R. Spangenberg, "Vacuum Tubes," Chapter 13, McGraw-Hill Book Co., New York, 1962.

Names of Vendors and Manufacturers

A1 -- E. I. du Pont de Nemours & Co., Wilmington, Del.
A2 -- Varian Associates, Palo Alto, Ca.
A3 -- Electronic Associates Inc., Palo Alto, Ca.
A4 -- Permag Corp., Jamaica, N. Y.
A5 -- MKS Instruments, Burlington, Mass.
A6 -- Varian (NRC) Associates, Palo Alto, Ca.
A7 -- Granville Phillips Co., Boulder, Colo.
A8 -- Welch Scientific Company, Skokie, Ill.
A9 -- Hastings-Raydst, Hampton, Va.
A10 -- CHA Industries, Menlo Park, Ca.
A11 -- Airco Temescal, Berkeley, Ca.
A12 -- Hoke, Inc., Cresskill, N. J.
A13 -- Kepco, Inc., Flushing, N. Y.
A14 -- Burr-Brown Research Corp., Tucson, Arizona
A15 -- Eveready Battery, Union Carbide, N. Y.
A16 -- Dressin-Barnes Electronics, Pasadena, Ca.
A17 -- Consolidated Electronics Corp., Pasadena, Ca.
A18 -- Tektronix, Inc., Beaverton, Oregon
A19 -- Princeton Applied Research Corp., Princeton, N. J.

Chapter 5

Ion-Molecule Reactions in Methane

The ion-molecule reactions in methane have been studied extensively using most of the techniques described in Chapter 3. McAskill[1] has summarized much of the pertinent recent work. The reactions of the major ions are well characterized and were reinvestigated here primarily to evaluate the reliability of the high pressure mass spectrometer for the determination of ion-molecule reaction rates. The two major ions, CH_4^+ and CH_3^+ undergo reactions (R1) and (R2) shown below.

$$CH_4^+ + CH_4 \xrightarrow{R1} CH_5^+ + CH_3 \qquad (R1)$$

$$CH_3^+ + CH_4 \xrightarrow{R2} C_2H_5^+ + H_2 \qquad (R2)$$

These two product ions do not react further with CH_4^+. Mass discrimination effects at the electron multiplier were investigated by comparing the ratio $[CH_4^+]/[CH_3^+]$ at short times (1.30) to the ratio $[CH_5^+]/[C_2H_5^+]$ at long times when reaction is nearly complete (1.25). As $C_2H_5^+$ arises solely from CH_3^+, while CH_5^+ is the only product of CH_4^+, the difference in the above ratios should reflect any difference in mass sensitivity of the multiplier for mass 29 versus masses 15-17. Discrimination was judged to be negligible.

The variation of ion abundances with reaction time for the system is shown in Figure 1. An analysis of these curves using methods described earlier indicates that discriminatory ion loss is minimal. The measured rate constants are reported in Table I, together with determinations by other workers. The values reported here represent the average of many determinations using pressures ranging from 3×10^{-5} torr to 10^{-3} torr. The uncertainty arises mainly from errors in pressure measurements and from ambiguities in determining the slopes of decay curves. While the agreement with previous results is satisfactory, our results were persistently about 10-15% lower than most other published values. However the relative rates of R1 and R2 are in good agreement. Considerable effort has been expended in an attempt to find a reason for the discrepancy, which appears to be unique to methane. No satisfactory answer has been found. The magnitude of the effect is not large enough to significantly alter any conclusions presented in other sections of this thesis.

The variation of the rate of R1 with well depth was also investigated. Previous work by Clow and Futrell[7] using a pulsed ICR technique, has shown that this rate decreases slightly with increasing kinetic energy, reaching 80% of the thermal rate at 1 eV centre of mass kinetic energy. The results of our study for R1 at trapping voltages between 2.5 and 9.5 volts are shown in Figure 2. It was not possible to operate at trapping voltages below 2.5 volts. Converting to average centre of mass kinetic energies, $\langle E_{cm} \rangle_{AV}$,

Figure 1

A -- Time dependence of ionic abundances for the major ions in CH_4. Electron energy = 70 eV, ionizing pulse width = 15 μsec, pressure = 4.6×10^{-5} torr, trapping voltage = 4.5 volts.

B -- Time dependence of the logarithm of normalized ion abundances in CH_4. Data is from Figure 1A.

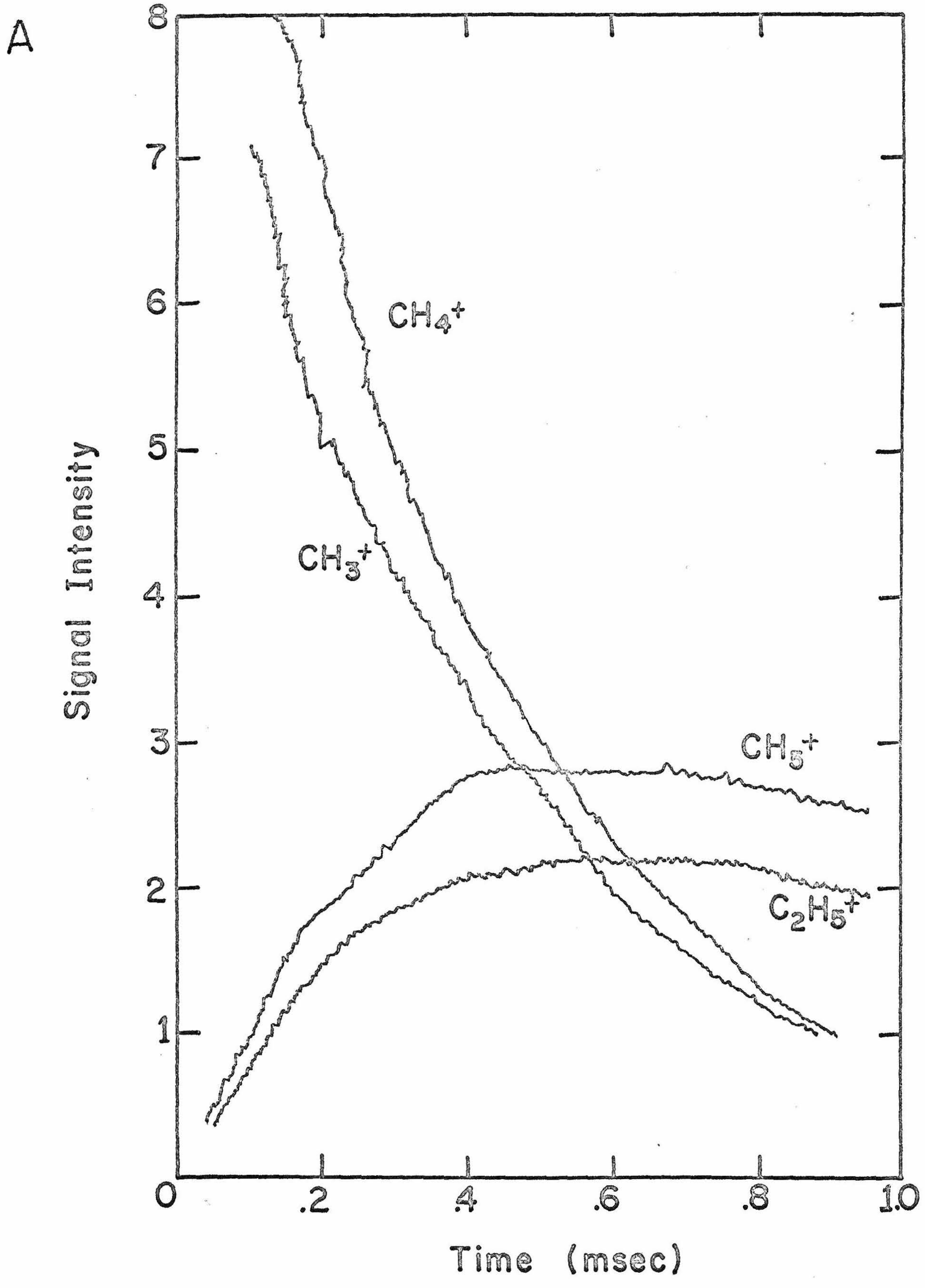
A
Signal Intensity
Time (msec)
0
1
2
3
4
5
6
7
8
.2
.4
.6
.8
1.0
CH_4^+
CH_3^+
CH_5^+
$C_2H_5^+$

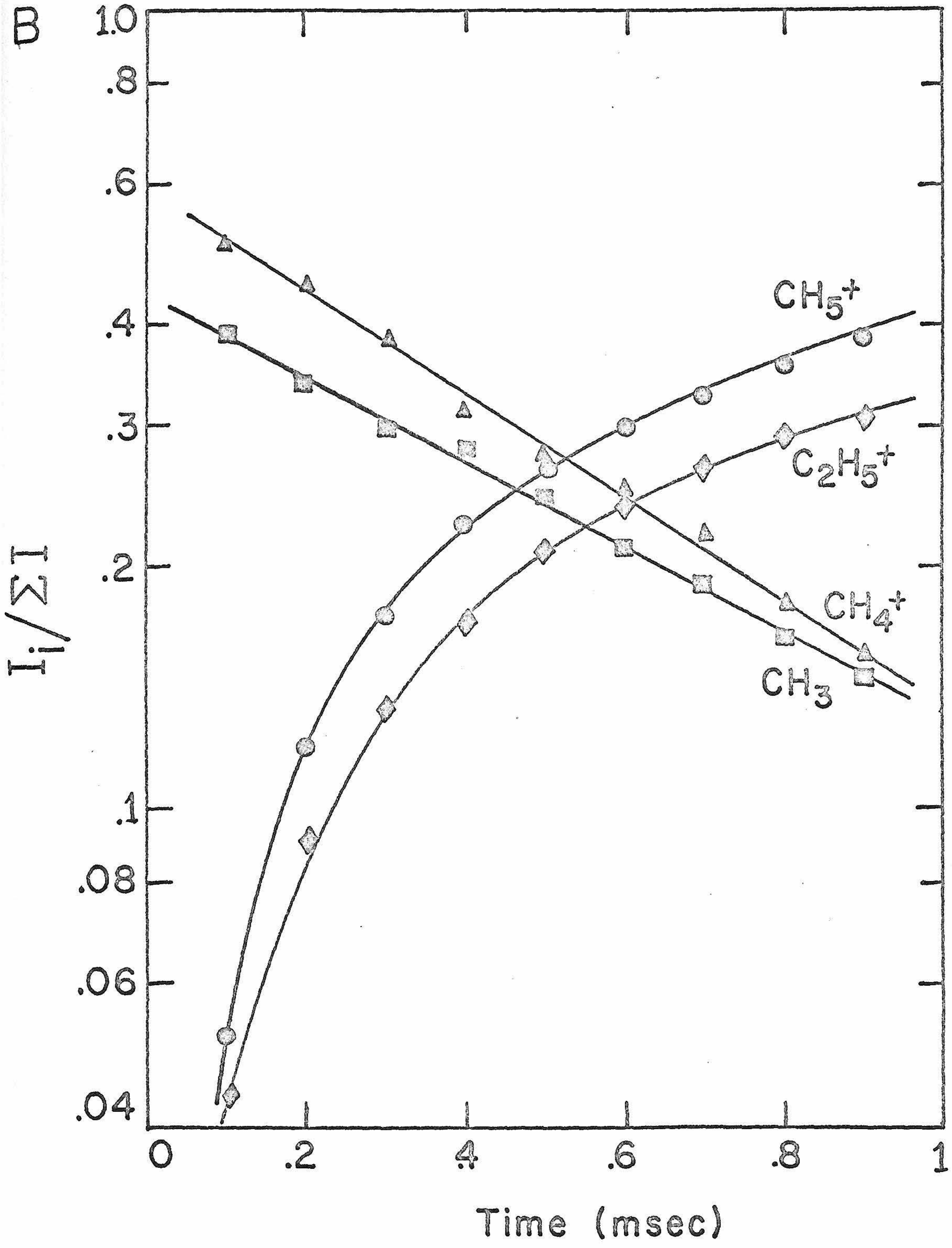
B
1.0
.8
.6
.4
.3
.2
.1
.08
.06
.04
$I_i/\sum I$
CH_5^+
$C_2H_5^+$
CH_4^+
CH_3
0
.2
.4
.6
.8
1
Time (msec)

Table I

Rate Constants in CH_4

Reaction	Rate constant cm^3 molecule^{-1} sec^{-1} × 10^{-9} this work	high press. m.s.[a]	trapped ion m.s.[b]	high press. m.s.[c]	tandem m.s.[d]	ICR[e]	high press. m.s.[f]
$CH_4^+ + CH_4 \rightarrow CH_5^+ + CH_3$	1.05 ± .15	1.23	1.20	1.03	1.12	1.15	1.22
$CH_3^+ + CH_4 \rightarrow C_2H_5^+ + H_2$	.95 ± .15	1.05	1.15	.82			

[a] Reference 1.

[b] Reference 2. The value of 1.20×10^{-9} cm^3 molecule^{-1} sec^{-1} was assumed to be the rate of R1. The rate of R2 was then calculated relative to this value.

[c] Reference 3. [d] Reference 4.

[e] Reference 5. [f] Reference 6.

Figure 2

Variation of the rate constant for the reaction $CH_4^+ + CH_4 \rightarrow CH_5^+ + CH_3$ with trapping voltage and with centre of mass kinetic energy (calculated from trapping voltage). The different symbols represent independent experiments. For each experiment, the value of k at V_T = 2.5 V or 3V was taken as unity and other rates were calculated relative to this value.

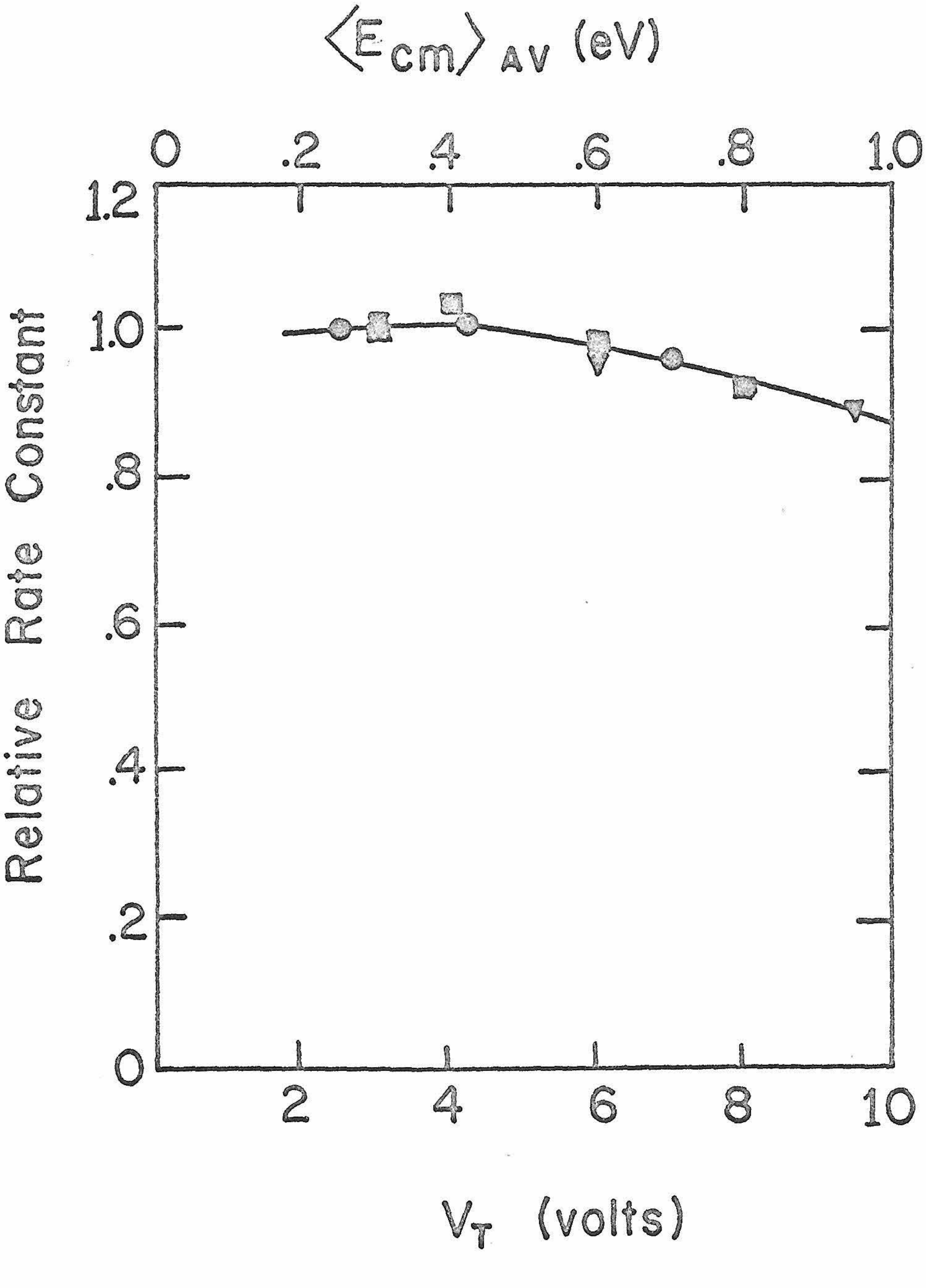
$\langle E_{cm} \rangle_{AV}$ (eV)
0
.2
.4
.6
.8
1.0
Relative Rate Constant
1.2
1.0
.8
.6
.4
.2
0
2
4
6
8
10
V_T (volts)

it is seen that the results are in good agreement with the findings of Clow and Futrell.

The variation of the rate of R2 was also studied and appeared to exhibit a very similar dependence. In this case, the interpretation is less straightforward, as relative ion extraction efficiencies for masses 15 and 29 could presumably vary with trapping voltage. Clow and Futrell also investigated the kinetic energy dependence of R2 and found very similar behaviour to that of R1, thus suggesting that there is, in fact, no variation of relative ionic extraction efficiency on V_T.

References

1. N. A. McAskill, Aust. J. Chem., 22, 2267 (1969).
2. A. A. Herod and A. G. Harrison, Int. J. Mass Spec. Ion Phys., 4, 415 (1970).
3. F. H. Field, J. L. Franklin, and M. S. B. Munson, J. Amer. Chem. Soc., 85, 3575 (1963).
4. J. H. Futrell, T. O. Tiernan, F. P. Abramson, and C. D. Miller, Rev. Sci. Inst., 39, 340 (1968).
5. M. B. Comisarow, J. Chem. Phys., 55, 205 (1971).
6. S. K. Gupta, E. G. Jones, A. G. Harrison, and J. J. Myher, Can. J. Chem., 45, 3107 (1967).
7. R. P. Clow and J. H. Futrell, Int. J. Mass Spec. Ion Phys., 4, 165 (1970).

Chapter 6

Ion-Molecule Reactions in Hydrogen and Binary Mixtures Containing Hydrogen

I. H_2, HD, D_2

Ions studied in these systems had masses ranging from 2 to 6. To correct for possible mass discrimination effects at the electron multiplier, a mixture of H_2, HD and D_2 was run at low pressures and short reaction times. Under these conditions, no significant amount of ion-molecule reaction products were observed. The resulting spectra were compared with ones run for the same mixture under similar source conditions in an ion cyclotron resonance spectrometer. The ICR spectrometer is well suited for the determination of primary ion abundances as the method of ion detection precludes any mass discrimination. The apparent ion concentrations obtained from the two instruments agreed within 10% and the differences exhibited no systematic variation with mass. This suggests minimal mass discrimination for masses 2, 3 and 4. The assumption was then made that this condition would prevail for masses 5 and 6.

The ion-molecule reactions occurring in each pure gas were investigated separately. The major primary ion in each system is the parent ion, which reacts with the neutral in reactions R1-R3 to produce an $(H, D)_3^+$ entity.

$$H_2^+ + H_2 \longrightarrow H_3^+ + H \qquad \text{(R1)}$$

$$D_2^+ + D_2 \longrightarrow D_3^+ + D \qquad \text{(R2)}$$

$$HD^+ + HD \begin{cases} \longrightarrow H_2D^+ + D & \text{(R3a)} \\ \longrightarrow D_2H^+ + H & \text{(R3b)} \end{cases}$$

The variation of ionic abundances with reaction time for each system is shown in Figures 1-3. The oscillatory behaviour, particularly evident at very low pressures such as that for H_2, reflects the variation of ejection efficiencies with trapping time, as discussed in Chapter 4. Plots of the logarithm of the normalized ion signals versus time are given in Figures 1-3. These curves are unaffected by the oscillations of the signal, suggesting that the variation in extraction efficiency is relatively insensitive to changes in mass. An analysis of the intensity data indicates that discriminatory ion loss is insignificant, and that the slope of the normalized primary ion abundance should thus accurately reproduce the rate constant. The rate constants, together with the results of other investigatiors, are listed in Table I. Uncertainties in our values arise from errors in pressure measurements and in ambiguities in determining the exact decay slopes.

The measured parent ion disappearance rate constants in all three systems are in good agreement with the predicted Langevin rates and indicate that virtually all spiraling collisions lead to reaction. This is a common feature of many proton or hydrogen

Figure 1

A -- Variation of ion abundance with reaction time for H_2^+ and H_3^+ in H_2. Ionizing energy = 70 eV, ionizing pulse width = 15 μsec, pressure = 3.5×10^{-5} torr, trapping well depth = 7 volts. The ion loss rate constants are $Q_{H_2^+} = .30$ nk, $Q_{H_3^+} = .36$ nk, giving $\delta = .06$ nk.

B -- Variation of logarithm of normalized ion abundances in H_2 with time. Data from Figure 1A.

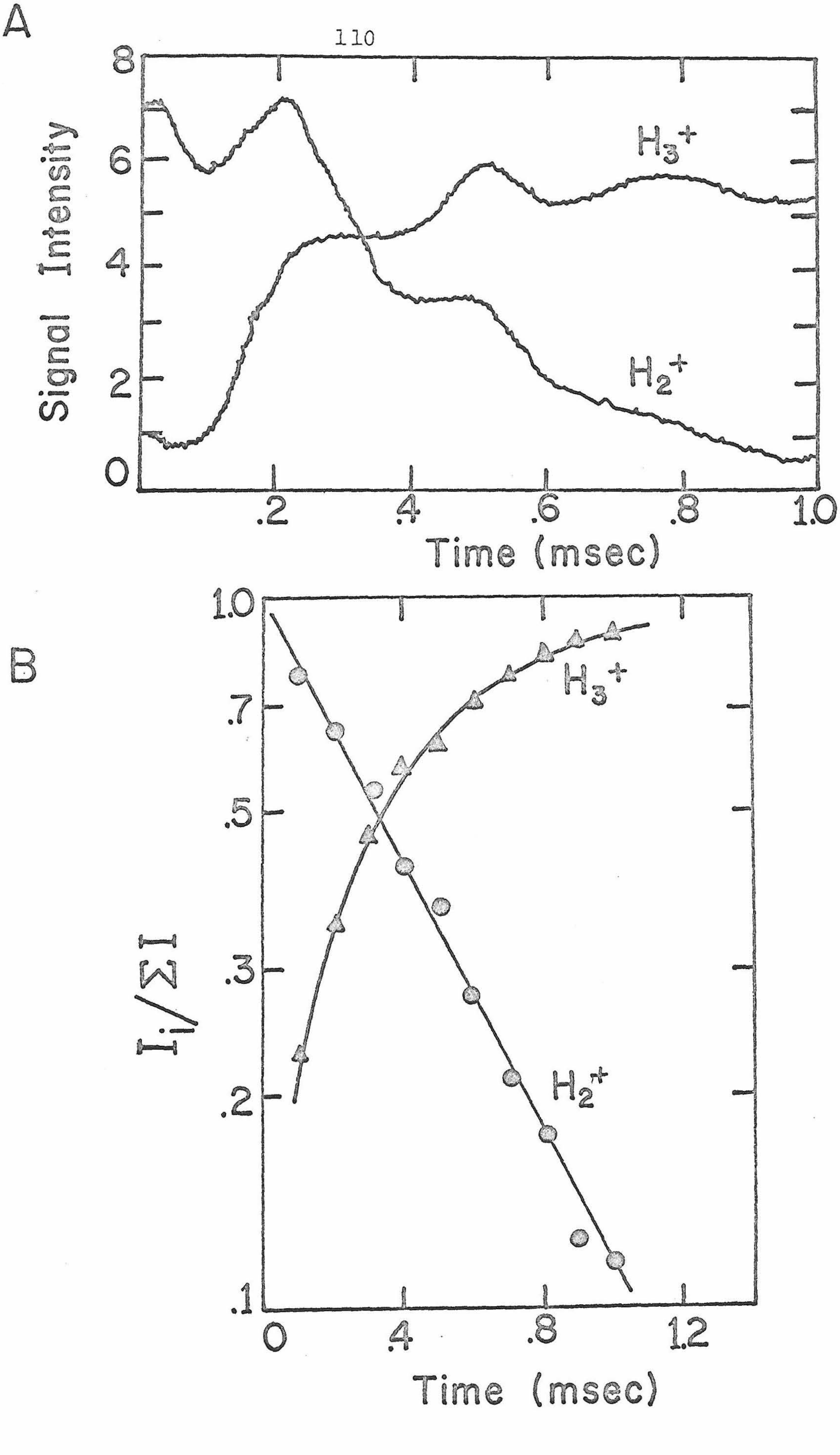
A
8
6
4
2
0
Signal Intensity
.2
.4
.6
.8
1.0
Time (msec)
H_3^+
H_2^+
B
1.0
.7
.5
.3
.2
.1
$I_i/\Sigma I$
0
.4
.8
1.2
Time (msec)
H_3^+
H_2^+

Figure 2

A -- Variation of ion abundance with reaction time for major ions in D_2. Ionizing energy = 70 eV, ionizing pulse width = 15 μsec, pressure = 8×10^{-5} torr, trapping voltage = 5.5 volts. The ion loss rate constants are $Q_{D_2^+} = .46$ nk, $Q_{D_3^+} = .43$ nk, giving $\delta = .03$ nk.

B -- Variation of logarithm of normalized ion abundances in D_2 with time. Data from Figure 2A.

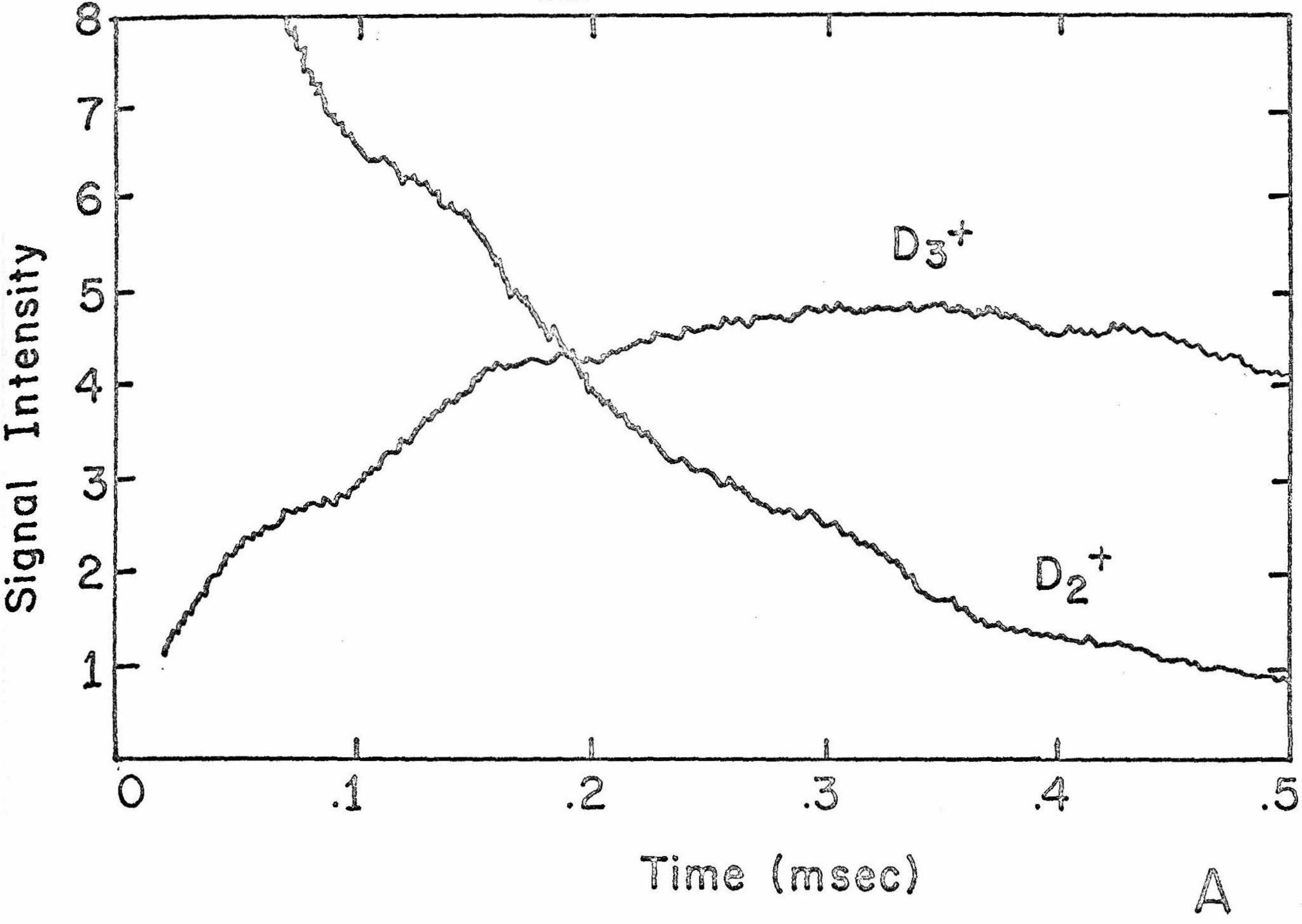
Signal Intensity
8
7
6
5
4
3
2
1
0
.1
.2
.3
.4
.5
Time (msec)
D_3^+
D_2^+
A

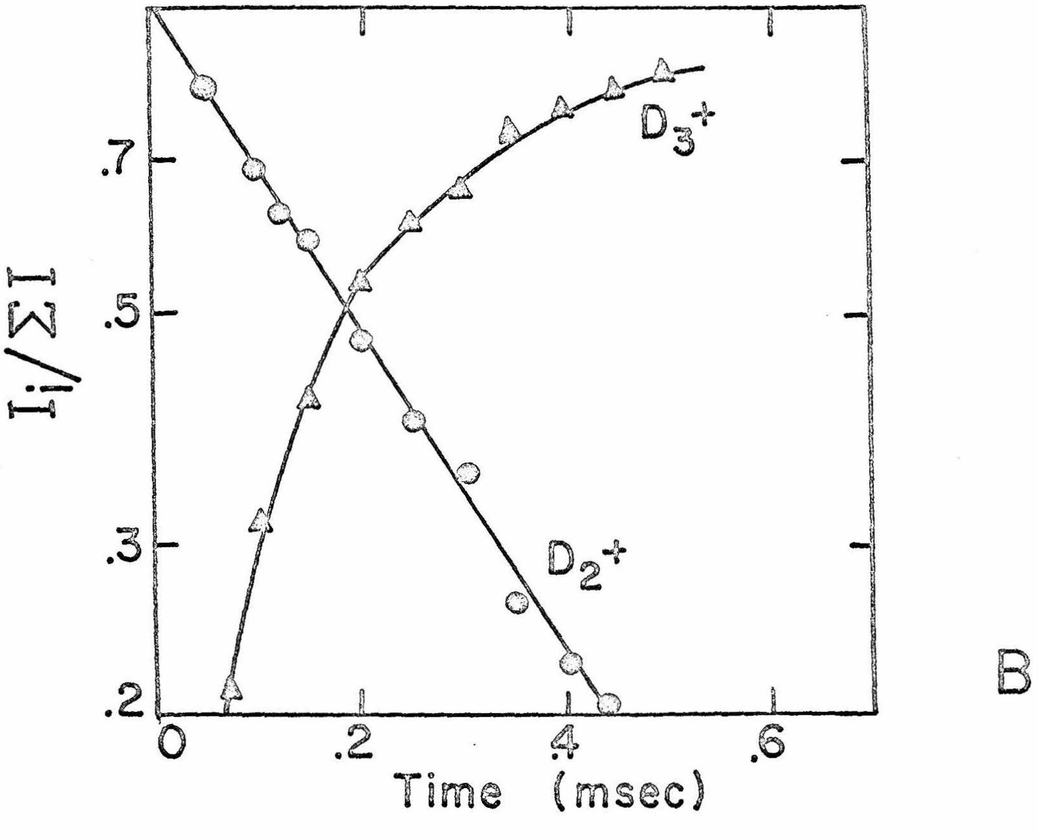
$I_i/\Sigma I$
.7
.5
.3
.2
0
.2
.4
.6
Time (msec)
D_3^+
D_2^+
B

Figure 3

A -- Time dependence of ionic abundances in HD. Ionizing energy = 70 eV, ionizing pulse width = 15 μsec, pressure = 1.2×10^{-4} torr, trapping voltage = 5.5 volts. The ion loss rate constants are $Q_{HD^+} = .55$ nkT, $Q_{H_2D^+} = .35$ nk_T, $Q_{D_2H^+} = .37$ nk_T, where k_T is the total reaction rate of HD^+. This leads to $\delta \approx .19$ nk_T.

B -- Variation of logarithm of normalized ion abundances in HD with time. Data taken from Figure 3A.

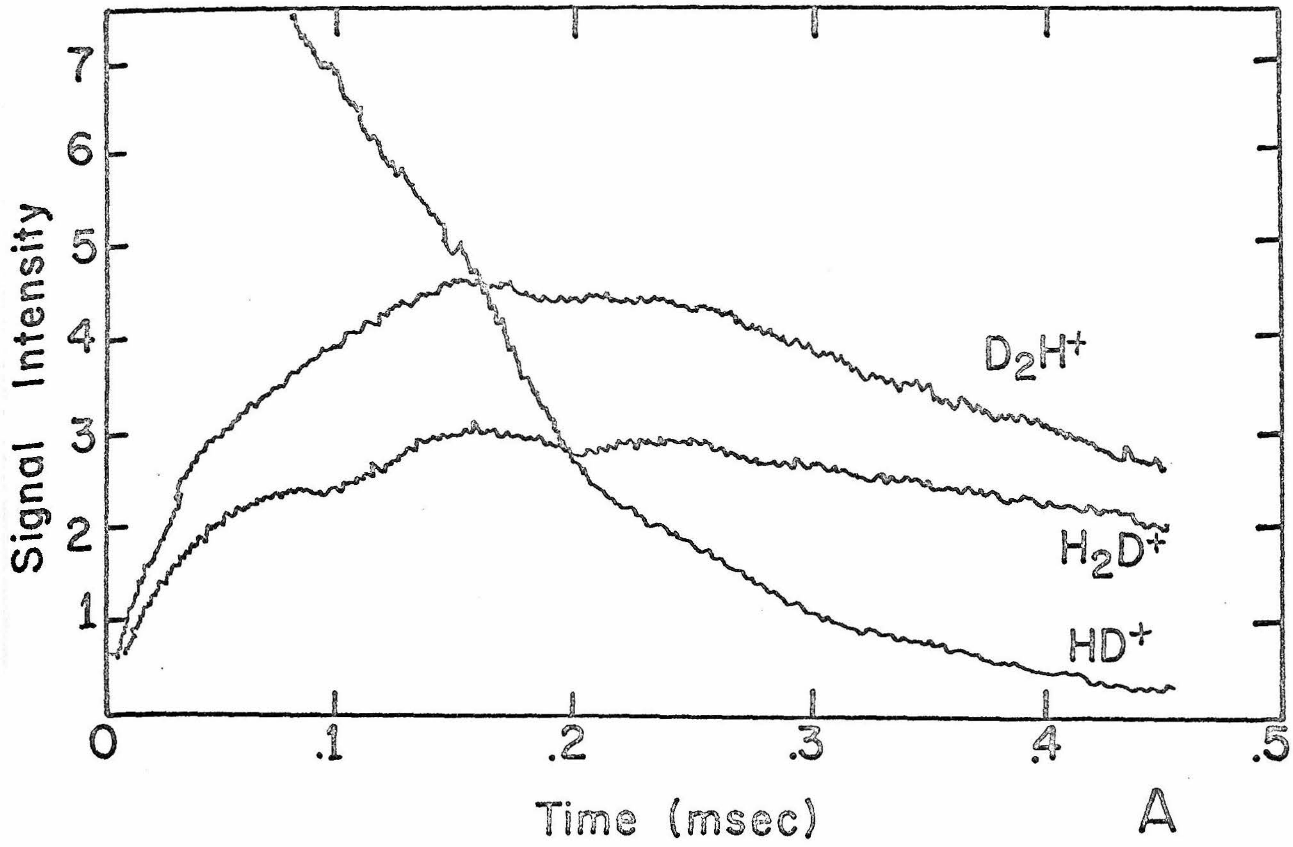
Signal Intensity
1
2
3
4
5
6
7
Time (msec)
0
.1
.2
.3
.4
.5
D$_2$H$^+$
H$_2$D$^+$
HD$^+$
A

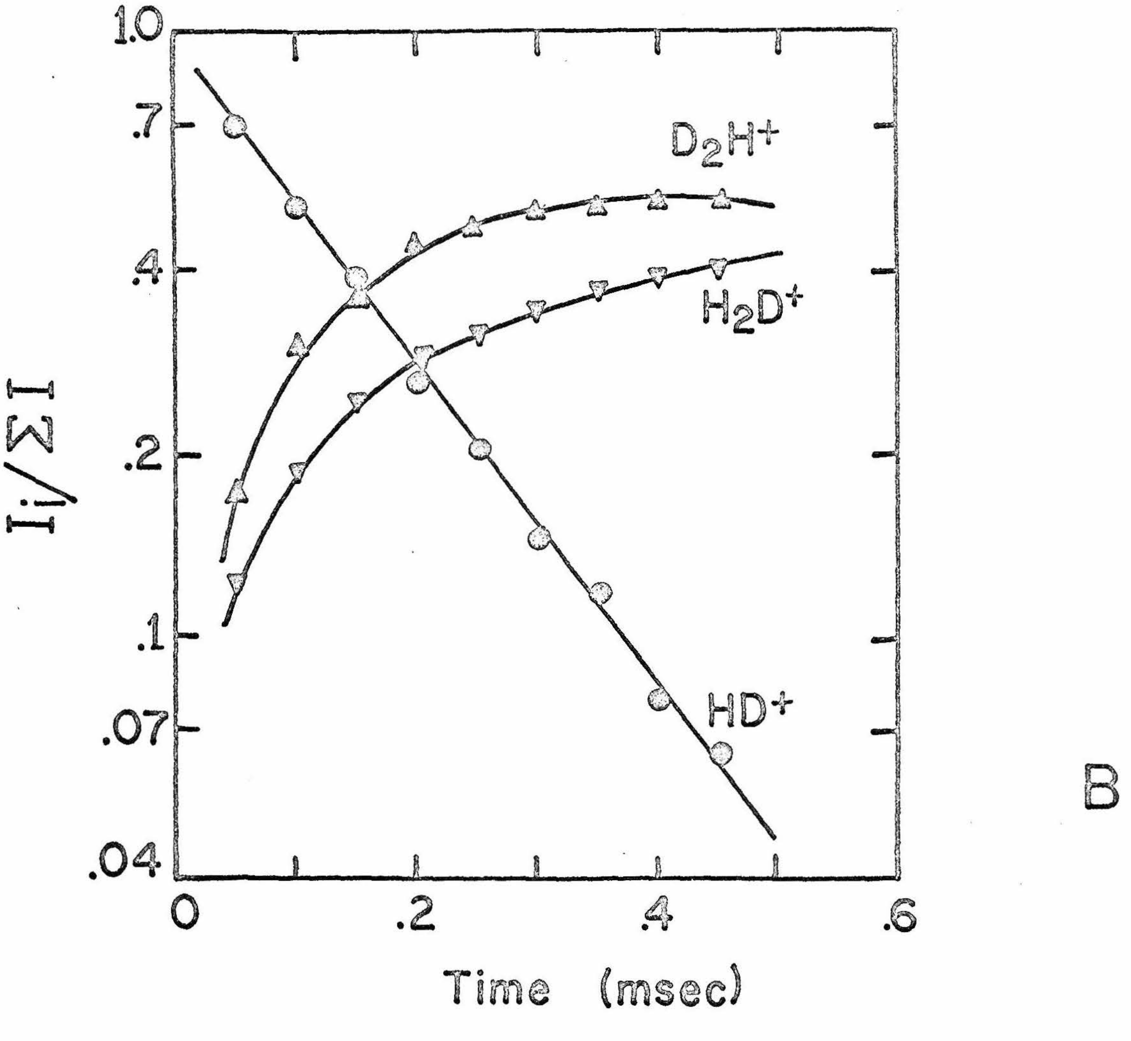
I$_i$/ΣI
1.0
.7
.4
.2
.1
.07
.04
Time (msec)
0
.2
.4
.6
D$_2$H$^+$
H$_2$D$^+$
HD$^+$
B

Table I

Rate Constants in H_2, D_2 and HD

	Rate constant $cm^3\ molecule^{-1}\ sec^{-1} \times 10^{-9}$				
Reaction	This work	ICR[a]	High pressure[b] m. s.	ICR[c]	Theory[d]
$H_2^+ + H_2 \rightarrow H_3^+ + H$	2.00 ± .2	2.11	2.02	2.0	2.08
$D_2^+ + D_2 \rightarrow D_3^+ + D$	1.35 ± .1	1.60	1.44	1.6	1.45
$HD^+ + HD \rightarrow H_2D^+ + D$	.60 ± .1	.75	1.66	.80	1.66
$HD^+ + HD \rightarrow D_2H^+ + H$	1.00 ± .1	1.05		1.00	

[a] Reference 1. [b] Reference 2. [c] Reference 3.

[d] Langevin rate, using $\alpha_{H_2} = \alpha_{D_2} = \alpha_{HD} = .79\ \mathring{A}^3$.

transfer reactions where structural rearrangement is not large.

The determination of the relative rates of R3a and R3b is complicated by the interconversion of the $(H, D)_3^+$ entities via thermoneutral proton or deuteron transfer to neutral HD. These processes have been investigated in detail using ICR spectroscopy,[4] where it has been shown that the rate constants for the transfer are about 3×10^{-10} cm^3 molecule^{-1} sec^{-1}. This interconversion slightly favours H_2D^+ and accounts for the slowly decreasing $[D_2H^+]/[H_2D^+]$ ratio at long times. An extrapolation of this ratio back to zero time yields $([D_2H^+]/[H_2D^+])_{\tau=0} = 1.65$, which represents the ratio of the rates of R3b and R3a. This value is somewhat larger than values of 1.2 to 1.4 found by ICR,[1, 3] high pressure,[2] and tandem mass spectrometry.[5] The kinetic energy dependence of these two rates has been measured using tandem mass spectrometry[5] and ICR spectroscopy.[3, 6] The results indicate that k_{3b}/k_{3a} decreases with increasing ion energy. Accordingly, the rather high value of this ratio cannot be due to "non-thermal" ion energies in this instrument. The discrepancy may arise from different degrees of interconversion between the $(H, D)_3^+$ moities in each experiment.

The dependence of the rates of R1 and R2 on trapping voltage was briefly investigated. There is general agreement that these rates increase very slightly with ion energy, reaching a maximum of 1.1 times the thermal rate at centre of mass ion energies of .5 eV. Clow and Futrell[3] have recently summarized much of the pertinent work. Our results showed no significant variation for time and space averaged centre of mass ion energies up to 1 eV. This is likely a consequence of the very large energy spread in the trapping well.

II. H_2-He Mixture

This very interesting system provides a good illustration of the effects of internal and kinetic energy on ion-molecule reactions. Irradiation of a binary mixture of H_2 and He with 70 eV electrons produces two major primary ions which can undergo a variety of ion-molecule reactions.

$$H_2^+ + H_2 \longrightarrow H_3^+ + H \qquad (R4)$$

$$H_2^+ + He \longrightarrow HeH^+ + H \qquad (R5)$$

$$He^+ + H_2 \longrightarrow H_2^+ + He \qquad (R6)$$

$$He^+ + H_2 \longrightarrow HeH^+ + H \qquad (R7)$$

Reaction (R4) has been studied in detail earlier and is known to proceed with a rate constant of $2.0 \pm .2 \times 10^{-9}$ cm^3 molecule^{-1} sec^{-1}. Using a proton affinity for He of 42 kcal/mole [7] and the known values of the ionization potential and dissociation energy of H_2, Reaction (R5) is found to be 20 kcal/mole endothermic for ground state H_2^+. Reaction (R6) is a highly exothermic charge transfer and, as such, likely has a negligible rate since it is impossible for the products to accommodate the 9.2 eV of released energy. Reaction (R7) is also very exothermic, but is known to proceed only at an extremely slow rate. Giese and Maier [8] have estimated the reaction cross section at 1 eV to be 7×10^{-18} cm^2, or .003 of the Langevin cross section at this energy.

Mahan[9] has given a molecular orbital analysis of some simple ion-molecule reactions, including R5 and R7. His model suggests that correlation diagrams between reactants and products may predict the occurrence or non-occurrence of a reaction. Mahan predicts that R5 should occur (when exothermic) and that R7 should not occur, being supplanted by the dissociation of H_2, if sufficient kinetic energy is available.

The variation of ion abundance with time for an 8:1 He–H_2 mixture is shown in Figure 4. The mixture was prepared in one gas bulb. Approximately 50 torr of H_2, read with a mercury manometer, was admitted to one portion of a vacuum line of known volume. A measured pressure of He was introduced to another part of the line of known volume. The two gases were permitted to mix and equilibrate for one hour. Partial pressures were then calculated using the ideal gas law. The composition of the mixture was also measured using a low pressure, single resonance ICR spectrum at 70 eV. Ionization cross sections of H_2 and He of 1.01 $\mathring{A}^2$ and .38 $\mathring{A}^2$, respectively, were employed. Rather remarkably, the two determinations were in good agreement.

The electron multiplier was operated at the same voltage as for the H_2, D_2 and HD systems described earlier; thus no mass discrimination is anticipated.

Figure 4

Variation of ion abundances with trapping time for an 8:1 He–H_2 mixture. Electron energy = 70 eV, ionizing pulse width = 15 μsec, pressure = 2.6×10^{-4} torr, trapping voltage = 7 volts.

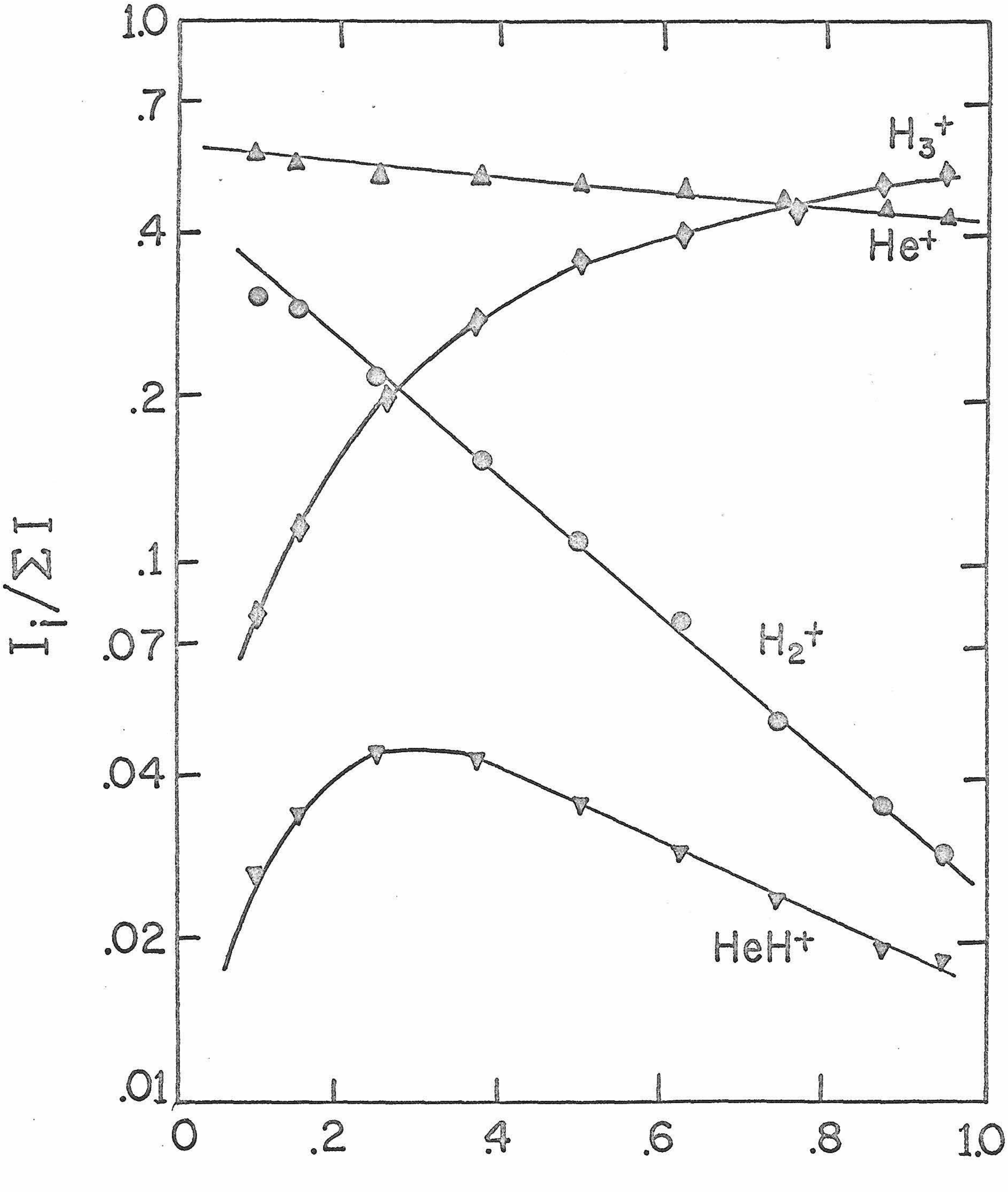
1.0
.7
.4
.2
.1
.07
.04
.02
.01
$I_i/\Sigma I$
0
.2
.4
.6
.8
1.0
Time (msec)
H_3^+
He^+
H_2^+
HeH^+

The disappearance rate of H_2^+ was found to be 3.42×10^{-10} cm^3 molecule^{-1} sec^{-1}. Ignoring any contribution of R6 to the H_3^+ abundance, the rate constant for R5, k_{R5}, may be extracted from this value and from the known value of the rate of R4, k_{R4}. Thus

$$3.42 \times 10^{-10}\ \mathrm{cm^3\,molecule^{-1}\,sec^{-1}} = f_{H_2} k_{R4} + f_{He} k_{R5}, \qquad (1)$$

where f_{H_2} is the fraction of the total pressure comprising H_2 (.11) and f_{He} is the fraction of He (.89). Using $k_{R4} = 2.0 \times 10^{-9}$ cm^3 molecule^{-1} sec^{-1}, k_{R5} is then found to be 1.37×10^{-10} cm^3 molecule^{-1} sec^{-1}. The error in this determination is rather large, as k_{R5} is the small difference of two larger numbers. The value of k_{R5} = $1.4 \pm .3 \times 10^{-10}$ cm^3 molecule^{-1} sec^{-1} best summarizes the results of this work using two different mixtures of gases and a variety of pressures and reaction times.

This reaction is nominally endothermic by 20 kcal/mole and thus the observation of a measurable rate constant reflects the presence of sufficient internal energy or kinetic energy of H_2^+ to cause reaction. Friedman[10] has calculated the distribution of vibrational energy in H_2^+ arising from 50 eV electron impact. These calculations were made for an electron energy far exceeding the various excited ion thresholds of H_2^+, so that excitation to a particular quantum state was considered independent of electron energy and determined primarily by the vibrational wavefunction overlap. Accordingly, the calculations are also valid for impact by 70 eV electrons. States with more than 20 kcal/mole internal energy have vibrational quantum numbers of 5 or more and comprise about 30% of the H_2^+ ionization. In the absence of kinetic energy effects, this suggests that a maximum of 30% of the H_2^+–He collisions could lead to HeH^+ formation. Our observed rate is about 20% of the theoretical Langevin rate of 7.8×10^{-10} cm^3 $molecule^{-1}$ sec^{-1}, in reasonable agreement with this model.

The kinetic energy dependence of R5 has been investigated by Chupka and Russell,[11] and recently by D'Amico.[12] These studies employed photoionization to selectively generate H_2^+ in definite vibrational states. The reaction rate of R5 was then determined at varying repeller voltages. It was found that the minimum quantum number, v, for reaction to occur at zero kinetic energy was 4. This is in good agreement with Friedman's results. At higher kinetic energies, this threshold dropped significantly, indicating that kinetic energy is effective in inducing R5. At 1.5 eV lab energies, corresponding to the average ion energies used in our studies, the total cross section for HeH^+ formation by H_2^+ with vibrational quantum numbers $V = 0, 1, 2$ and 3 was almost as large as the total cross section for $V = 4$ and $V = 5$. Thus, the contribution of these normally endothermic channels is significant, and the simple model of Friedman appears to apply only at near-thermal energies. It thus follows that under our experimental conditions, somewhat more than 30% of the H_2^+–He collisions have sufficient energy to be reactive. The experimental value of 20% indicates that many non-reactive collisions occur in this system.

If the contribution of R7 towards HeH^+ production is neglected, then the rate of disappearance of HeH^+ via R8

$$HeH^+ + H_2 \longrightarrow H_3^+ + He \qquad (R8)$$

$$\Delta H = -60 \text{ kcal/mole}$$

is directly obtainable from the slope of the HeH^+ decay in Figure 5 at long times. The rate is found in this manner to be $1.62 \pm .25 \times 10^{-9}$ cm^3 molecule^{-1} sec^{-1}, in good agreement with a predicted Langevin rate of 1.75×10^{-9} cm^3 molecule^{-1} sec^{-1}. To our knowledge, this rate has not been previously measured.

The only reactive mechanism contributing to the disappearance of He^+ is R7. If this is the case, then the rate for this reaction is determined to be 1.3×10^{-10} cm^3 molecule^{-1} sec^{-1}, or about 1/10 of the Langevin rate. This value is about 30 times larger than that predicted from the cross sections of Giese and Maier. Accordingly, it is more likely that the primary mode of He^+ loss arises from discriminatory ion loss. Since He^+ is heavier than the other two major ions in the system, it should possess a larger ion loss rate constant. However the disappearance rate is slow (only 25% over 1 msec) and thus it is unlikely that the rate constants measured in this system are greatly altered by ion loss effects, although the rate of R8 may be slightly too high because of similar ion loss discrimination. This is the reason for the large uncertainty reported for this rate. Alternatively, the disappearance of He^+ may arise from charge-transfer reactions with impurities.

III. H_2–CH_4 and H_2–NH_3 Mixtures

The dominant feature of the ion chemistry of dilute mixture of methane or ammonia in hydrogen concerns the reactions of H_3^+ with these minor constituents. Leventhal and Friedman[13] have shown that this entity, formed by reaction R9, initially contains about 2 eV excess

$$H_2^+ + H_2 \longrightarrow (H_3^+)^* + H \qquad \text{(R9)}$$

internal energy. Complete deactivation of $(H_3^+)^*$ may be effected by as few as one subsequent collision with H_2, and presumably occurs *via* a symmetric proton transfer in which a proton carrying no excess energy is transferred

$$(H_3^+)^* + H_2 \longrightarrow H_2^* + H_3^+ . \qquad \text{(R10)}$$

Previous studies have shown that the reactivity of H_3^+ with various substituted methanes[14] is strongly dependent on the internal energy content of H_3^+. In addition, these systems are of interest in the understanding of the evolution of the earth's primitive reducing atmosphere and in the study of the Jovian atmosphere.[15]

III-A. $H_2 + CH_4$

The hydrogen-methane system has been studied by several authors,[16-18] the most recent work being by Bowers and Elleman using ion cyclotron resonance spectroscopy. There is general agreement that reactions between H_3^+ and CH_4 result in either CH_3^+ or CH_5^+ formation. This is assumed to occur via a $(CH_5^+)^*$ intermediate which can either be collisionally stabilized by H_2 or unimolecularly fragment to CH_3^+. Bowers and Elleman have proposed a more complex mechanism involving two states of $(CH_5^+)^*$ and also the direct reaction of H_3^+ to form CH_3^+.

The variation of ion abundance with reaction time for a 14:1 mixture of H_2 and CH_4 at 70eV ionizing energy has been investigated using the high pressure mass spectrometer. Typical results are given in Figure 5. Mixtures were prepared using the method described earlier for H_2-He mixtures, and involved admitting known pressures of gases into different portions of a vacuum line of known volumes. The two gases were then permitted to mix and equilibrate for one hour. Partial pressures were calculated using the ideal gas law.

Mass discrimination at the electron multiplier was checked by operating the source in a continuous mode where the ion exit and drawout plates were continuously biased for ejection. Normalized ion intensities found in this way were $[H_2^+] = .75$, $[CH_4^+] = .14$, $[CH_3^+] = .11$. No significant abundance of other ions was detected. Using 70 eV ionization cross sections[19] of $1.1\,Å^2$ and $4.6\,Å^2$ for H_2

Figure 5

Variation of ion abundance with reaction time for a 14 ± 1:1 mixture of H_2 and CH_4. Electron energy = 70 eV, ionizing pulse width = 15 μsec, pressure = 3.6×10^{-4} torr, trapping voltage = 6 volts. The $C_2H_5^+$ ion abundance was not monitored, but is expected to rise to ~.05 of the total ionization at 1 msec. The ion H_2^+ was observed to decay rapidly at short times.

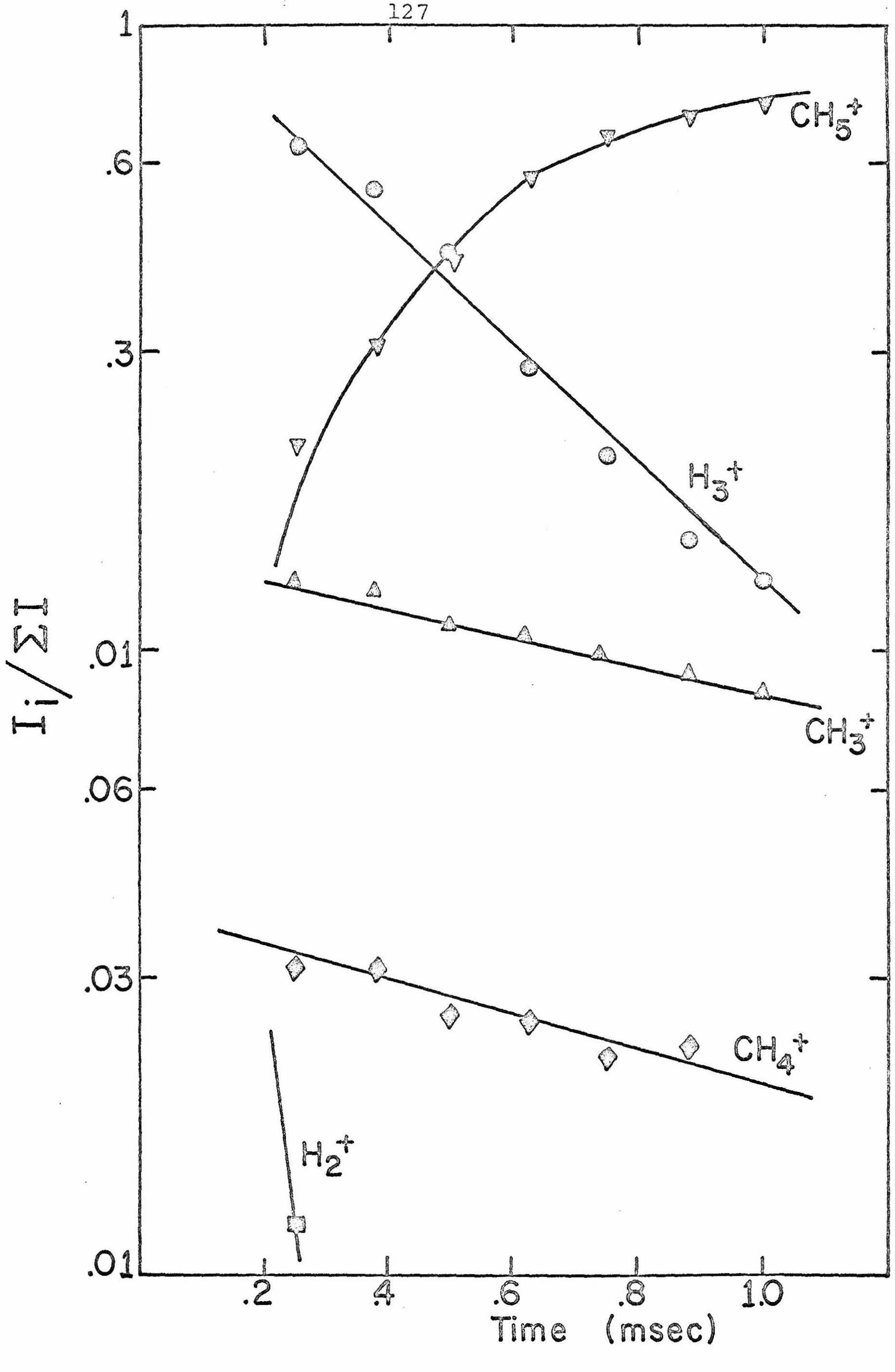
1
.6
.3
.01
.06
.03
.01
.2
.4
.6
.8
1.0
Time (msec)
$I_i/\Sigma I$
CH_5^+
H_3^+
CH_3^+
CH_4^+
H_2^+

and CH_4, respectively, the neutral ratio is thus calculated to be $H_2:CH_4 = 12:1$. The disagreement with the manometric determination is about 15%, and may arise either from mass discrimination favouring the methane peaks or from an incorrect value for the neutral pressure ratio. Similar studies using H_2-NH_3 mixtures, reported later, were found to exhibit an enhancement of the NH_3 peaks by about 20%. Since the H_2-NH_3 mixtures were prepared using a method of greater reliability, and are thus less subject to large errors, this suggests that discriminatory effects at the electron multiplier are responsible for the deviations. Appropriate corrections have been applied to the results of our work, although the qualitative conclusions remain unchanged and the values of reported rate constants are changed by only 10%.

The results of Figure 5 display an abundance of CH_4^+ and CH_3^+ at short times that is significantly lower than that found using the continuous mode of operation, as described above. There, roughly 15% of the total ion current constituted CH_4^+ while in Figure 5, this fraction is only about 4%. This discrepancy must arise from substantially differing ion loss rates of CH_4^+ (and CH_3^+) and H_2^+. The reason for the difference is not known, but may be a consequence of the large difference in masses of these ions. As discussed in Chapter 4, the time dependence of unreactive ion concentrations characteristically exhibits a very steep initial decline between 0 and 50 μsec, followed by a slower decrease at longer times. The mechanism of ion loss at long times probably involves collisional phenomena. The initial decline may arise from a different source, that of space-charge "blowup" of the initial ionic distribution. Ionic densities along the path of the electron beam immediately following ionization are typically[20] 6×10^5 ions/cm^3, large enough to introduce significant space charge effects. If ion loss due to space charge blowup is strongly mass dependent, this could cause ions of masses 15 or 16 to be preferentially lost compared to ions of mass 2. The behaviour of the system would thus resemble one in which little primary ionization of CH_4 occurred. Similar effects have not been noted in other systems since there all primary ion masses were comparable, within a factor of 2. In H_2-CH_4, this factor is 8.

Although this mechanism qualitatively explains the short-time ion abundances in Figure 5, there is still sufficient uncertainty in our results that many quantitative interpretations concerning the extent of CH_3^+ and CH_5^+ formation from $(H_3^+)^*$ and H_3^+ must be foregone.

The determination of the rate of reaction of H_3^+ in formation of CH_3^+ and CH_5^+

$$\left.\begin{array}{l}(H_3^+)^* \\ (H_3^+)\end{array}\right\} + CH_4 \longrightarrow \begin{cases} CH_3^+ + 2H_2 & \text{(R9)} \\ CH_5^+ + H_2 & \text{(R10)} \end{cases}$$

is unaffected by the uncertainty in the initial abundances of these ions, and can be found in a routine manner from the slope of the H_3^+ decay in Figure 6. This value is $2.5 \pm .5 \times 10^{-9}$ cm^3 molecule^{-1} sec^{-1}, in excellent agreement with the Langevin collision rate of 2.42×10^{-9} cm^3 molecule^{-1} sec^{-1}. The uncertainty arises primarily from the possible error in the neutral ratio of the mixture. The disappearance rate of H_3^+ in reactions with CH_4 has been measured by Burt et al.[21] using a flowing afterglow technique. Their value of 1.6×10^{-9} cm^3 molecule^{-1} sec^{-1} is in reasonable agreement with the results of this investigation. Burt et al. claim only 30% accuracy in their measured values, due to uncertainties in the flow hydrodynamics.

From Figure 5, it is seen that the CH_4^+ abundance decreases steadily due to reactions with CH_4. Assuming reaction only with CH_4 neutrals,[22] the disappearance rate of CH_4^+ can be calculated to be 9×10^{-10} cm^3 molecule^{-1} sec^{-1}, only slightly smaller than values found in pure methane. This demonstrates that there is no production of CH_4^+ at these times via charge transfer from H_3^+

$$H_3^+ + CH_4 \not\longrightarrow CH_4^+ + H_2 + H.$$

This reaction is calculated to be 91 kcal/mole endothermic for ground state H_3^+ and ~45 kcal/mole endothermic[23] for $(H_3^+)^*$.

The production of CH_3^+ by reactions of $(H_3^+)^*$ or H_3^+ clearly is an important reactive process since the $[CH_3^+]/[CH_4^+]$ ratio is roughly 5 times larger than that in pure methane. Bowers and Elleman note that both CH_3^+ and CH_4^+ are produced by reactions of H_2^+ with CH_4, but do not report relative probabilities for these two channels. However the abundance of CH_3^+ is too large to arise solely from the reaction of H_2^+. Methyl cation subsequently disappears slowly by reaction with CH_4. Assuming reaction only with CH_4 neutrals,[22] the disappearance rate is found to be 8×10^{-10} cm^3 molecule^{-1} sec^{-1}, only slightly smaller than the rate in pure methane. The determination of this rate constant is relatively independent of any mass discrimination or ion loss effects. The good agreement of the disappearance rate of CH_3^+ to that in CH_4 implies that minimal CH_3^+ production occurs at long times by reactions of H_3^+. This absence of CH_3^+ formation at long times, when all $(H_3^+)^*$ entities have deactivated to H_3^+, suggests that only $(H_3^+)^*$ is capable of producing CH_3^+. This is in contrast to the mechanism proposed by Bowers and Elleman, who included formation of CH_3^+ by ground state H_3^+. The enthalpies of reaction of these two modes of CH_3^+ formation are[23]

$$(H_3^+)^* + CH_4 \longrightarrow CH_3^+ + 2\,H_2 \qquad \Delta H = -1.2 \text{ eV}$$

$$H_3^+ + CH_4 \longrightarrow CH_3^+ + 2\,H_2 \qquad \Delta H = +.8 \text{ eV}$$

thus demonstrating that the internal excitation of $(H_3^+)^*$ is sufficient to induce a reaction which is endothermic for ground state H_3^+.

In conclusion, the disappearance rate of H_3^+ by reaction with CH_4 to form CH_3^+ and CH_5^+ has been measured to be $2.5 \pm .5 \times 10^{-9}$ cm^3 $molecule^{-1}$ sec^{-1}, which is close to the Langevin limit for this process. The data suggest that CH_3^+ formation occurs only by reactions of $(H_3^+)^*$. By contrast, CH_5^+ can be formed from either reactive state. This is in agreement with the results of Burt et al. who observed only CH_5^+ in their flowing afterglow apparatus under conditions where all H_3^+ entities are likely to be deactivated.

This system also demonstrates the utility of the high pressure mass spectrometer for chemical ionization. It is evident that considerably more CH_5^+ is formed than could arise directly from reactions of CH_4^+, and that after 1 msec, conversion to CH_5^+ is almost quantitative.

III-B. $H_2 + NH_3$

The ion chemistry of this system has not previously been investigated in detail. Harrison and Thynne[24] have measured rate constants between D_2^+ and NH_3 and between NH_3^+ and D_2. No reactions of D_3^+ were reported. In dilute mixtures, there are marked similarities to the H_2-CH_4 system discussed earlier. The variation of ion abundances with time for an 8:1 mixture of H_2 and NH_3 at 70 eV ionizing energy is given in Figure 6. The behaviour of a 16:1 mixture was also investigated. The mixtures were prepared in one gas bulb by first freezing an appropriate quantity of NH_3 in a cold finger attached to the bulb and then adding the required amount of H_2. Mixing was then induced by permitting the solid NH_3 to evaporate, and was promoted by heating the bulb to create thermal currents. This method ensures reasonable accuracy in the determination of partial pressures.

Mass discrimination at the electron multiplier was investigated using the continuous mode of operation described earlier. For the 16:1 mixture, the normalized ion currents were: $[H_2^+] = .79$, $[NH_3^+] = .13$, and $[NH_2^+] = .08$. No significant quantities of other ions were observed. Using ionization cross sections[19] of $1.1\,Å^2$ and $3.5\,Å^2$ for H_2 and NH_3, respectively, the neutral ratio is predicted to be 12.8.

Figure 6

Variation of ion abundance with reaction time for a 8:1 mixture of H_2 and NH_3. Electron energy = 70 eV, ionizing pulse width = 15 μsec, pressure = 2.0×10^{-4} torr, trapping voltage = 6 volts. The ion H_2^+ was observed to decay rapidly at short times.

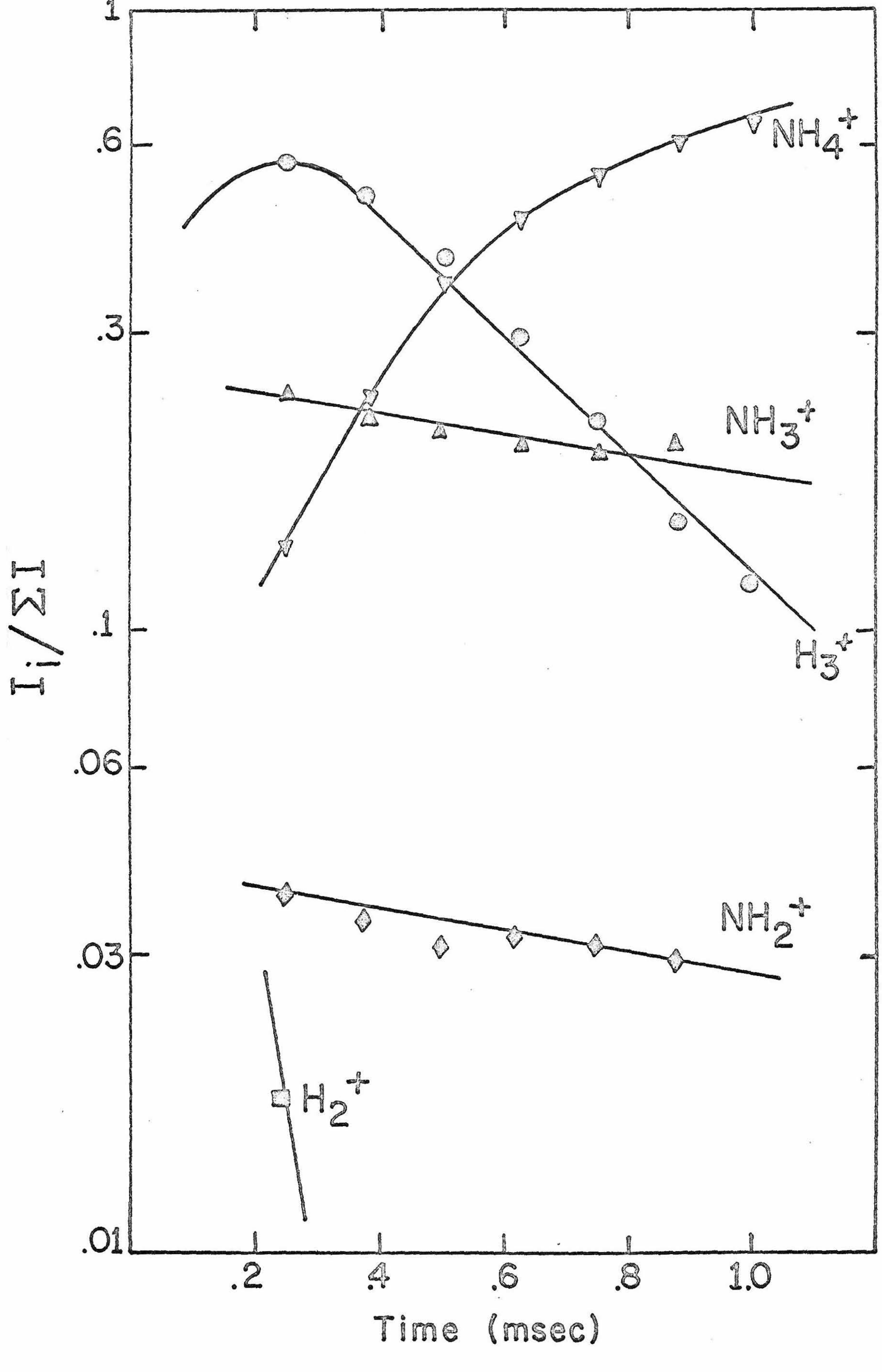
1
.6
.3
.1
.06
.03
.01
$I_i/\Sigma I$
.2
.4
.6
.8
1.0
Time (msec)
NH_4^+
NH_3^+
H_3^+
NH_2^+
H_2^+

This differs by 20% from the known ratio and indicates the extent of mass discrimination. These results are consistent with those from the H_2-CH_4 mixture. Appropriate corrections have been applied to our results, although the qualitative conclusions remain unaltered and the values of the rate constants change by less than 10%.

The results of Figure 6 display abundances of NH_3^+ and NH_2^+ at short times that are considerably lower than those found using the continuous mode of operation. The reasons for this discrepancy have been discussed for the H_2-CH_4 system, where similar behaviour was observed. Again, this effect precludes many of the quantitative interpretations concerning the extent of NH_3^+ and NH_4^+ from $(H_3^+)^*$ and H_3^+.

The disappearance rate of H_3^+ can be routinely calculated from the slope of the H_3^+ decay in Figure 6, and is found to be $3.8 \pm .4 \times 10^{-10}$ cm^3 $molecule^{-1}$ sec^{-1}. The uncertainty arises primarily from possible errors in the neutral ratios. This value is in very good agreement with that of 3.6×10^{-9} cm^3 $molecule^{-1}$ sec^{-1} obtained by Burt et al.[21] using a flowing afterglow technique. The uncertainty in their measurement, however, is large. This rate is much larger than the Langevin rate of 2.2×10^{-9} cm^3 $molecule^{-1}$ sec^{-1}. The locked dipole rate for this system is 8.0×10^{-9} cm^3 $molecule^{-1}$ sec^{-1}, indicating that while a significant ion-dipole attraction exists, locking does not occur. Ion-dipole locking should be most probable if the ion is sufficiently light that it is able to follow the rotational motion of the neutral molecule without greatly increasing its angular momentum.

The absence of locking in this nearly ideal system suggests that it is extremely unlikely for any reasonable chemical systems.

The production of NH_2^+ must arise solely from primary ionization or from dissociative charge transfer from H_2^+, as the reaction of H_3^+ forming NH_2^+ is endothermic, even for $(H_3^+)^*$ as the reactant ion.

By contrast, large quantities of NH_3^+ are formed, suggesting both H_2^+ and H_3^+ as possible precursors. However, only the excited state of H_3^+ is able to form this ion, as reaction

$$(H_3^+)^* + NH_3 \longrightarrow NH_3^+ + H_2 + H \qquad \Delta H = -1.0 \text{ eV}$$

$$H_3^+ + NH_3 \longrightarrow NH_3^+ + H_2 + H \qquad \Delta H = +1.0 \text{ eV}$$

with ground state H_3^+ is endoergic [23] by 1.0 eV. This conclusion is verified by calculating the disappearance rate of NH_3^+. Assuming reaction only with neutral ammonia, [25] the rate of disappearance is 8×10^{-10} cm^3 $molecule^{-1}$ sec^{-1}, in fair agreement with rates measured in NH_3, [26-28] which range between 1.3 and 1.9×10^{-9} cm^3 $molecule^{-1}$ sec^{-1}. The difference may reflect the effect of internal excitation of NH_3^+ on the rate of protonation. The ammonia ion, formed by $(H_3^+)^*$, can have up to 22 kcal/mole internal energy. Chupka and Russell [29] have shown that the rate of NH_4^+ production from NH_3^+ is very sensitive to the vibrational energy content in NH_3^+. For an internal energy of 20 kcal/mole, the rate is only 60% that of ground state NH_3^+.

The results of these investigations have shown that reaction between H_3^+ and NH_3 is extremely rapid. In concurrence with thermodynamic predictions, NH_3^+ is formed only by $(H_3^+)^*$ containing at least 1 eV internal energy. By contrast, NH_4^+ can be formed from either state of H_3^+. Chemical ionization of ammonia by H_3^+ is found to occur rapidly and efficiently at H_2 pressures of $.2\,\mu$, leading essentially to complete conversion to NH_4^+ after 1 msec reaction time.

References

1. M. T. Bowers, D. D. Elleman, and J. King, Jr., *J. Chem. Phys.*, **50**, 4787 (1969).
2. B. G. Reuben and L. Friedman, *J. Chem. Phys.*, **37**, 1636 (1963).
3. R. P. Clow and J. H. Futrell, *Int. J. Mass Spec. Ion Phys.*, **8**, 119 (1972).
4. T. B. McMahon and P. G. Miasek, unpublished results.
5. J. H. Futrell and F. P. Abramson, *Adv. Chem. Ser.*, **58**, 107 (1966).
6. W. T. Huntress, D. D. Elleman, and M. T. Bowers, *J. Chem. Phys.*, **55**, 5413 (1971).
7. J. L. Beauchamp, *Ann. Rev. Phys. Chem.*, **22**, 527 (1971).
8. C. F. Giese and W. B. Maier II, *J. Chem. Phys.*, **39**, 739 (1963).
9. B. H. Mahan, *J. Chem. Phys.*, **55**, 1436 (1971).
10. L. Friedman, *Adv. Chem. Ser.*, **58**, 87 (1966).
11. W. A. Chupka and M. E. Russell, *J. Chem. Phys.*, **49**, 5426 (1968).
12. P. M. D'Amico and W. A. Chupka, unpublished results.
13. J. J. Leventhal and L. Friedman, *J. Chem. Phys.*, **49**, 1975 (1968); *ibid.*, **50**, 2928 (1969).
14. M. T. Bowers and W. T. Huntress, unpublished results.
15. G. P. Kuiper, "The Atmosphere of the Earth and Planets", University of Chicago Press, Chicago, 1952.
16. S. Wexler, *J. Amer. Chem. Soc.*, **85**, 272 (1963).
17. V. Aquilanti and G. G. Volpi, *J. Chem. Phys.*, **44**, 2307 (1966).

18. M. T. Bowers and D. D. Elleman, *J. Amer. Chem. Soc.*, **92**, 1847 (1970).

19. Cross sections taken from J. A. Beran and L. Kevan, *J. Phys. Chem.*, **73**, 3866 (1969), and from R. W. Kiser, "Introduction to Mass Spectrometry and Its Applications," Prentice-Hall, Englewood Cliffs, N. J., 1965.

20. Typical conditions: emission current = .1 μA, ionizing pulse width = 15 μsec, pressure = 3×10^{-4} torr, ionization cross section = 5 Å^2, electron beam diameter = 1 mm.

21. J. A. Burt, J. L. Dunn, M. J. McEwan, M. M. Sutton, A. E. Rache, and H. I. Schiff, *J. Chem. Phys.*, **52**, 6062 (1970).

22. No reaction of CH_4^+ with H_2 has been observed, M. S. Foster and J. L. Beauchamp, unpublished results.

23. Proton affinities obtained from Reference 7. Internal energy content of $(H_3^+)^*$ assumed to be 2 eV.

24. A. G. Harrison and J. C. J. Thynne, *Trans. Faraday Soc.*, **64**, 945 (1968).

25. The rate between NH_3^+ and D_2 was found to be $.76 \times 10^{-10}$ cm^3 molecule^{-1} sec^{-1} (Reference 24). However, A. Giardini-Guidoni and G. G. Volpi, *Nuovo Cimento* **17**, 919 (1960), determined this rate to be less than $.1 \times 10^{-10}$ cm^3 molecule^{-1} sec^{-1}.

26. G. A. W. Derwish, A. Galli, A. Giardini-Guidoni, and G. G. Volpi, *J. Chem. Phys.*, **39**, 1599 (1963).

27. C. E. Melton, *ibid.*, **45**, 4414 (1966).

28. W. T. Huntress, M. M. Mosesman, and D. D. Elleman, *ibid.*, **54**, 843 (1971).

29. W. A. Chupka and M. E. Russell, *J. Chem. Phys.*, **48**, 1527 (1968).

Chapter 7

Ion-Molecule Reactions in Acetylene

The ion chemistry of acetylene provides an interesting illustration of the effect of an anisotropic polarization interaction upon the rates of ion-molecule reactions. Numerous studies investigating the enhancement of rates due to a permanent dipole moment have been undertaken[1] using the formalism presented in Chapter 2. However ion-molecule reactions with non-polar but highly anisotropic molecules have not been studied in this light. Acetylene is such a molecule, having an axial polarizability,[2] $\alpha_{\parallel}$, of 5.12 Å^3 and a perpendicular polarizability, $\alpha_{\perp}$, of only 2.43 Å^3, leading to an angle averaged polarizability, $\alpha = 1/3\,(\alpha_{\perp} + 2\,\alpha_{\parallel})$, of 3.33.

The results of trapped ion experiments at 70 eV electron energy in acetylene are given in Figure 1. Mass discrimination effects at the electron multiplier were examined by comparing a mass spectrum of isopentane at 70 eV and low pressure with published spectra. Minimal discrimination was observed.

The logarithmic plot for the disappearance of the primary ions was linear over more than two orders of magnitude. Two major secondary ions were formed, $C_4H_2^+$ and $C_4H_3^+$, in a ratio of 0.50:1. This may be compared to ratios of 0.44,[3] 0.40,[4] 0.50,[5] 0.45[6] and 0.40[7] found using other trapped ion and mass spectroscopic techniques under conditions where $C_2H_2^+$ was the only primary ion.

Figure 1

Time dependence of ion abundances in acetylene. Electron energy = 70 eV, ionizing pulse width = 15 μsec, trapping voltage = 4 V, pressure = 4.2×10^{-4} torr.

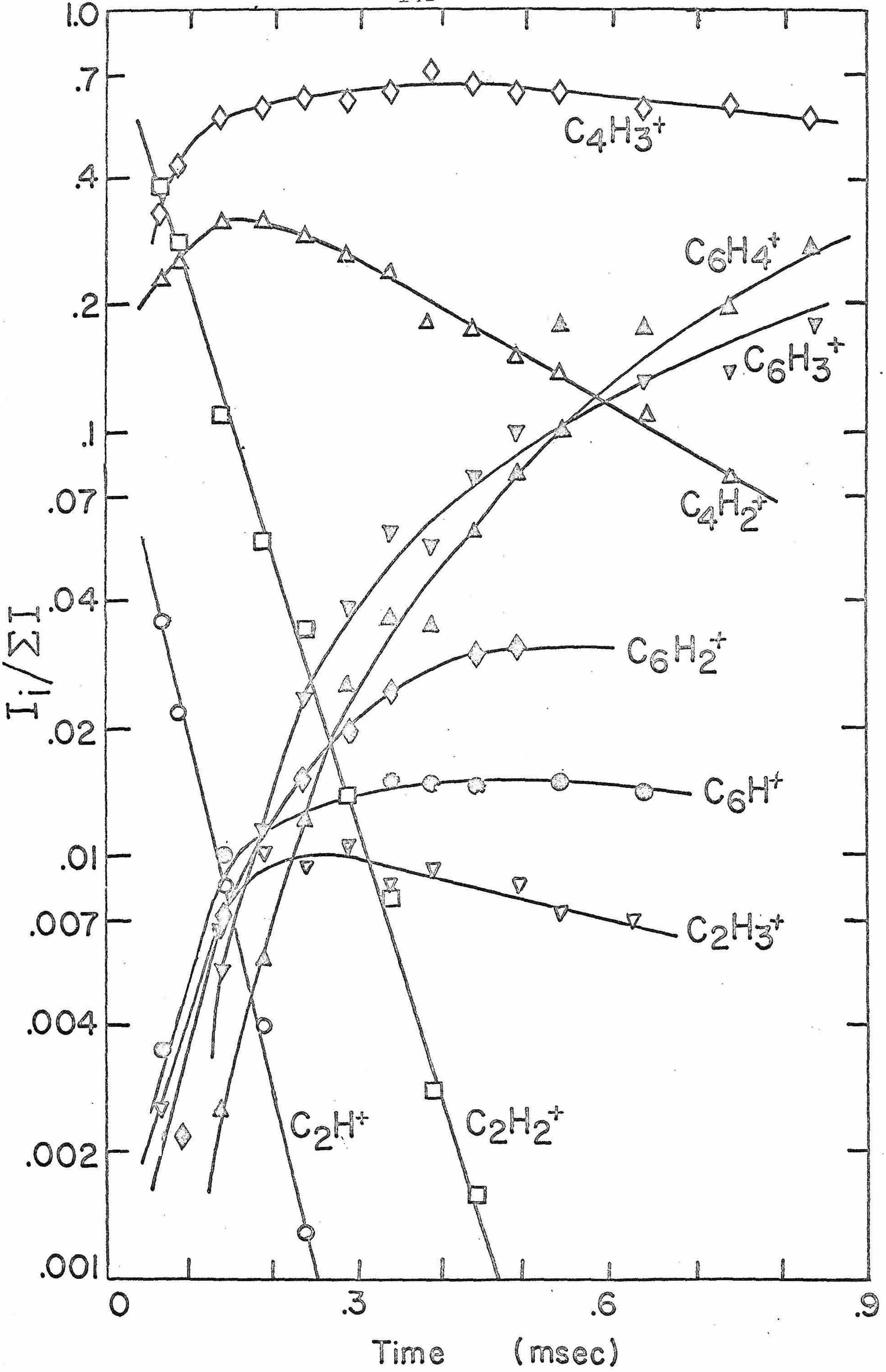
1.0
.7
.4
.2
.1
.07
.04
.02
.01
.007
.004
.002
.001
$I_i/\Sigma I$
0
.3
.6
.9
Time (msec)
$C_4H_3^+$
$C_6H_4^+$
$C_6H_3^+$
$C_4H_2^+$
$C_6H_2^+$
C_6H^+
$C_2H_3^+$
C_2H^+
$C_2H_2^+$

The slightly larger value of 0.50 found in this study thus reflects the contribution of the C_2H^+ ion to these abundances. In addition, it has been shown that an excited state of $C_2H_2^+$, formed at electron energies greater than 16 eV reacts predominately to give $C_4H_2^+$.[3, 4, 6] The ion-molecule reactions of interest are thus

$$C_2H_2^+ + C_2H_2 \longrightarrow \left[\begin{array}{ll} \longrightarrow C_4H_3^+ + H & \qquad \text{(R1)} \\ \longrightarrow C_4H_2^+ + H_2 & \qquad \text{(R2)} \end{array} \right.$$

$$C_2H^+ + C_2H_2 \longrightarrow C_4H_2^+ + H \qquad \text{(R3)}$$

An additional secondary ion $C_2H_3^+$ is formed in very low yield and has been shown[6, 7] to arise primarily from reaction (R4), involving an excited state of $C_2H_2^+$ with an appearance potential of about 16 eV.

$$C_2H_2^{+*} + C_2H_2 \longrightarrow C_2H_3^+ + C_2H \qquad \text{(R4)}$$

Futrell and Tiernan,[4] using a tandem mass spectrometer, have reported that about 8% of the C_2H^+ ions undergo charge exchange with C_2H_2 giving $C_2H_2^+$. This should introduce a slight initial curvature in the $C_2H_2^+$ decay. The extent of $C_2H_2^+$ production by this mechanism was too small to be seen.

The major tertiary ions observed at long reaction times were $C_6H_4^+$ and $C_6H_3^+$, arising primarily from $C_4H_3^+$ and $C_4H_2^+$ via reactions (R5) and (R6).

$$C_4H_3^+ + C_2H_2 \longrightarrow C_6H_4^+ + H \qquad \text{(R5)}$$

$$C_4H_2^+ + C_2H_2 \longrightarrow C_6H_3^+ + H \qquad \text{(R6)}$$

From Figure 1 it is seen that the sum of the $C_4H_2^+$ and $C_6H_3^+$ abundances is constant at .26 ± .02 of the total ionization in the time interval between 300 and 800 μsec. This suggests that $C_6H_3^+$ is not formed by R7 to a measurable extent.

$$C_4H_3^+ + C_2H_2 \longrightarrow C_6H_3^+ + H_2 \qquad (R7)$$

Alternatively, the concurrent formation of $C_6H_4^+$ directly from $C_4H_2^+$ *via* a mechanism involving collisional stabilization of the $[C_4H_2 \cdot C_2H_2]^+$ cluster would obscure this inference. However the failure to observe the analogous $C_6H_5^+$ formation from $C_4H_3^+$ suggests that the lifetimes of these complexes are too short to be stabilized at the pressures employed in this study.

The observed absence of Reaction (R7) is in contrast to the results of Derwish *et al.*[8] and Futrell and Tiernan.[4] However, it may be remarked that, in general, there is considerable uncertainty about the mechanism of formation of many of the third and higher order products in acetylene. Derwish *et al.*, for instance, determined that $C_6H_4^+$ is exclusively a fourth order product, formed by collisional stabilization of $[C_4H_2 \cdot C_2H_2]^+$. This also is in marked disagreement with the present results. The comparison of the higher order product distributions and mechanisms found in this work with those found by Munson,[3] Derwish *et al.*,[8] or Futrell and Tiernan[4] is difficult, since the latter studies were undertaken at pressures between 20 and 200 μ. At these pressures, collisional stabilization of $[C_4H_3 \cdot C_2H_2]^+$ and $[C_4H_2 \cdot C_2H_2]^+$ is extremely efficient and obscures the dissociation reactions that are the dominant mechanisms at lower pressures. The qualitative agreement of the present results with those of Herod and Harrison,[5] performed using a trapped ion technique at .2 μ, is excellent.

The absolute values of the measured disappearance rate constants are given in Table I. In general, the agreement is satisfactory, though the absolute values obtained by Herod and Harrison are substantially larger. It is of interest to compare the primary ion reaction rates with those calculated from the Langevin model. These values are given in Table II. While the reaction rate for $C_2H_2^+$ is close to the Langevin value, that for C_2H^+ is substantially larger. Futrell and Tiernan,[4] in a tandem mass spectrometric investigation of the reactions of $C_2H_2^+$ with C_2D_2 at 0-0.4 eV ion energies found that 7.6% of the total product intensity comprised $C_2D_2^+$ and 3.6% comprised C_2HD^+. The first of these products arises from a charge-transfer reaction, while the second must involve a complex mechanism with H–D exchange. If the charge-transfer mechanism involves rapid electron-electron exchange between C_2H_2 and C_2D_2, then an equal abundance (.076) of $C_2H_2^+$ should be formed upon encounter between these two ions. These would represent non-reactive collisions. In pure acetylene, all three processes, representing roughly .19 of all encounters between $C_2H_2^+$ and C_2H_2, are undetectable. Thus the rate constant for $C_2H_2^+$ reported above represents only .81 of the total encounter rate for this ion. The corrected total rate constant for $C_2H_2^+$ is reported in Table II, and is also significantly larger than the

Table I

Rate Constants in Acetylene

Reactant ion	Rate constant ($cm^3 molecule^{-1} sec^{-1} \times 10^{-9}$)		Relative rate constants				
	This work	Trapped ion m. s. [a]	This work	Trapped ion m. s. [a]	High press m. s. [b]	High press m. s. [c]	High press m. s. [d]
C_2H^+	1.47 ± .05	2.45	1.3	1.7	1.5	1.7	1.1
$C_2H_2^+$	1.15 ± .05	1.41	1.0	1.0	1.0	1.0	1.0
$C_2H_3^+$	~.085		.1				
$C_4H_2^+$	.23 ± .03	.1	.2	.1		.4	
$C_4H_3^+$	~.036		~.03				

[a] Reference 5. [b] Reference 3.

[c] Reference 4. [d] Reference 8.

Table II

Observed and Theoretical Rate Constants in Acetylene [d]

Reactant ion	Rate constants		Langevin rates	
	observed	corrected [a]	α [b]	$\alpha_{\parallel}$ [c]
C_2H^+	1.47	1.47	1.20	1.49
$C_2H_2^+$	1.15	1.42	1.18	1.46

[a] Rate constant for $C_2H_2^+$ corrected as discussed in text.

[b] Angle average value of α used (3.33 Å^3).

[c] Axial value of α used (5.12 Å^3).

[d] All values reported in cm^3 molecule^{-1} sec^{-1} $\times 10^{-9}$.

Langevin value.

Considerably better agreement of the total rate constants with the Langevin model is obtained when the axial value of the electric polarizability ($\alpha_{\parallel}$) replaces α in the Langevin equation. This implies that some degree of ion-neutral alignment along the direction of the maximum polarizability occurs in this system. Evidently, this alignment is durable enough to significantly alter the shape of the potential energy surfaces of the reactants and thus enhance the reaction rate. This is demonstrated in Figure 2, where two effective potential curves of particular interest have been plotted as a function of r, the interparticle distance. This effective potential, V_{eff}, is a sum of the induced dipole interaction described in Chapter 2 and a centrifugal potential, which arises from the requirement of conservation of angular momentum, L. The centrifugal term

$$V_{eff}(r) = \frac{-e^2\alpha}{2r^4} + \frac{L^2}{2\mu r^2} \tag{1}$$

introduces a potential energy barrier to the approach of the two particles.

The curves of Figure 2 were calculated for thermal energy $C_2H_2^+$ ions colliding with C_2H_2 with a mean relative velocity $\bar{g} = \sqrt{\frac{3kT}{\mu}}$ and an impact parameter of 7.4 Å. Under these conditions, curve A, using the angle averaged value of α, has a barrier height of 4.7×10^{-2} eV. The total available energy, indicated by the dashed line, is only 3.9×10^{-2} eV. Accordingly, the distance of closest

Figure 2

Effective potential curves for the collision of $C_2H_2^+$ with C_2H_2 as a function of r, the interparticle distance. Curve A employs an angle averaged polarizability of C_2H_2 while curve B uses the maximum value of this polarizability. The total energy of the system is indicated by the dashed line. Relative velocity of the particles = $\sqrt{\frac{3\,kT}{\mu}}$, impact parameter = 7.4 Å.

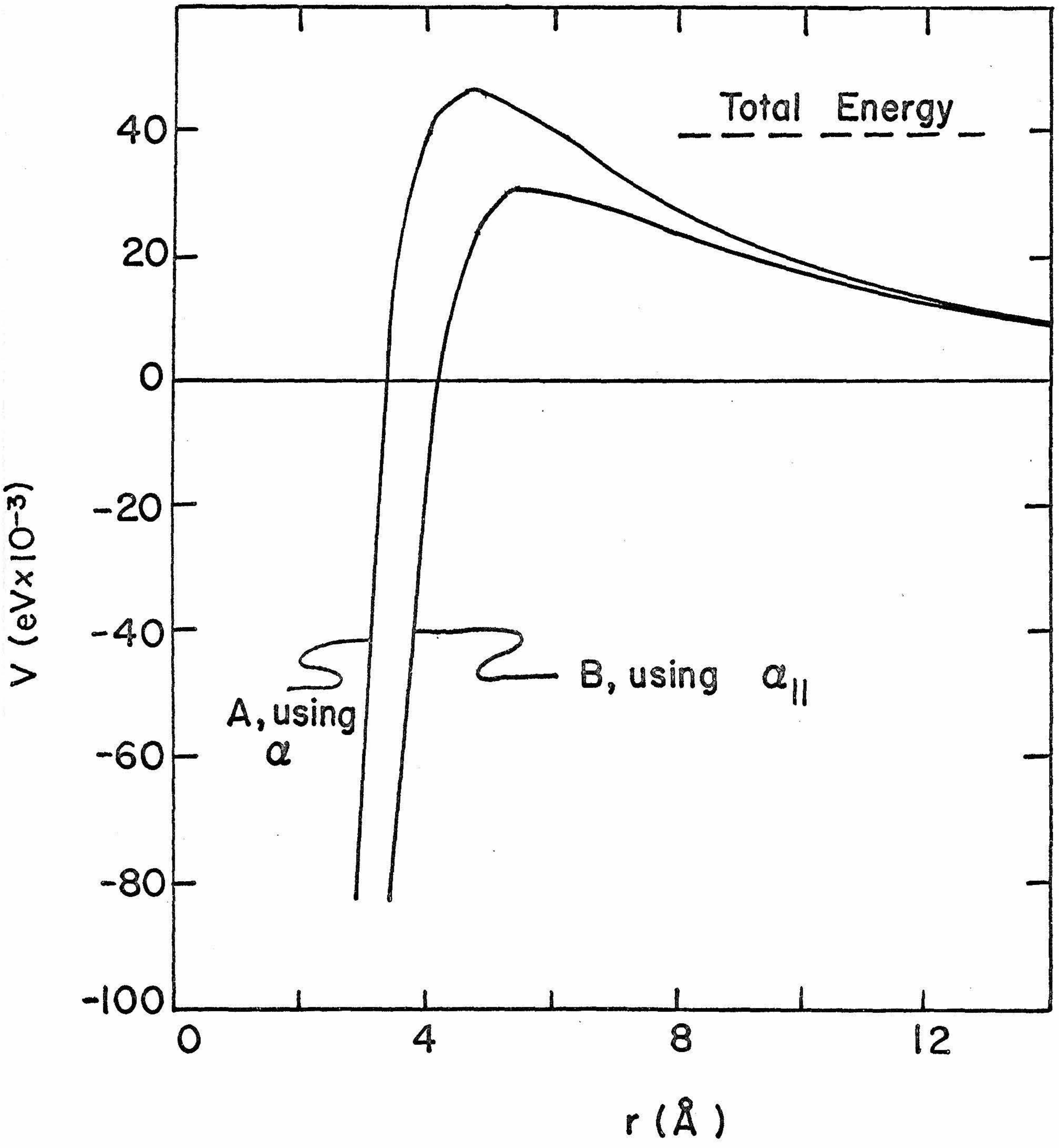
Total Energy
40
20
0
-20
-40
-60
-80
-100
V (eV×10⁻³)
0
4
8
12
r (Å)
A, using α
B, using α∥

approach can only be 6 Å, which is too far for reaction to occur easily. This barrier height is lowered by 1.5×10^{-2} eV upon the replacement of α by $\alpha_{\parallel}$, which is sufficient to permit the system to cross the barrier and undergo a hard collision at short distances.

Ion-molecule collisional effects attributable to an anisotropic polarization interaction have been noted by other workers. Dunbar[10] has recently studied the momentum transfer rates between Cl^- and a variety of anisotropic molecules (but not C_2H_2) and has observed correlations between the collision frequency for momentum transfer and the maximum component of the diagonalized polarizability tensor, $\alpha_{\parallel}$. The momentum transfer rate is very sensitive to the nature of grazing collisions, those involving long-range "reflection" off the centrifugal barrier. In this case, the nature of these distant encounters is altered by even a small degree of ion-neutral alignment. Thus the correlations he observed are understandable. By contrast, more intimate collisions are generally required for chemical reaction. Gioumousis and Stevenson[11] observed an enhancement of the rate of reaction between O_2 and H_2^+ or D_2^+ which they attributed to the anisotropic polarizability of O_2. The presence of a similar effect in the acetylene system, involving more complex reactions, is rather remarkable.

The absolute reaction rates for the secondary ions are listed in Table I. It is interesting that $C_4H_2^+$ disappears much more rapidly than $C_4H_3^+$. The former ion is an odd-electron species and reacts to produce an even-electron entity. By contrast $C_4H_3^+$ is an even-electron ion and produces $C_6H_4^+$, having an odd number of electrons. Since even-electron species are generally more stable than their odd-electron counterparts, this effect may be due to the different stabilities of these ions.

References

1. See, for example, R. C. Dunbar, J. Chem. Phys., **52**, 3204 (1970).
2. J. O. Hirshfelder, C. F. Curtiss, and R. B. Bird, "Molecular Theory of Gases and Liquids", Wiley, New York, 1954.
3. M. S. B. Munson, J. Phys. Chem., **69**, 572 (1965).
4. J. H. Futrell and T. O. Tiernan, J. Phys. Chem., **72**, 158 (1968).
5. A. A. Herod and A. G. Harrison, Int. J. Mass Spec. Ion. Phys., **4**, 415 (1970).
6. R. M. O'Malley and K. R. Jennings, Int. J. Mass Spec. Ion Phys., **2**, 257 (1969).
7. J. J. Myher and A. G. Harrison, Can. J. Chem., **46**, 1755 (1968).
8. G. A. W. Derwish, A. Galli, A. Giardini-Guidoni, and G. G. Volpi, J. Amer. Chem. Soc., **87**, 1159 (1965).
9. S. Wexler, A. Lifshitz, and A. Quattrachi, Adv. Chem., **58**, 193 (1966).
10. R. C. Dunbar, J. Chem. Phys., in press.
11. G. Gioumousis and D. P. Stevenson, J. Chem. Phys., **29**, 294 (1958).

Chapter 8

Ion-Molecule Processes in Ethylene

I. Primary Ion Reactions

The ion-molecule reactions of ethylene have been studied utilizing a variety of mass spectrometric techniques, including high pressure mass spectrometry,[1-6] tandem mass spectrometry,[6] ICR spectroscopy,[7] and trapped ion mass spectrometry.[8] In addition, a considerable amount of information has been derived from radiation chemistry studies.[9] Consequently there has emerged general agreement as to the identification of the reactions occurring. However there is some uncertainty about the reactivity and lifetimes of the intermediate collision complexes that characterize the ethylene system. These clusters are readily stabilized by collision even at relatively low pressures, in contrast to the acetylene system. This study presents additional information about the participation and lifetimes of these complexes. In addition, the absolute disappearance rates of the various ions in ethylene are reported, and used to derive the rates of particular ion-molecule reactions.

A typical intensity-reaction time plot for the ions formed in ethylene by a 70 eV electron pulse is given in Figure 1. Mass discrimination effects were investigated as for the acetylene system and were found to be minimal. Three important primary ions were observed, which initiate the reaction sequence[7] summarized in

Figure 1

Variation of ion abundance with reaction time for the ions in ethylene. Electron energy = 70 eV, ionizing pulse width = 15 μsec, pressure = 5.5×10^{-4} torr, trapping well depth = 4 volts.

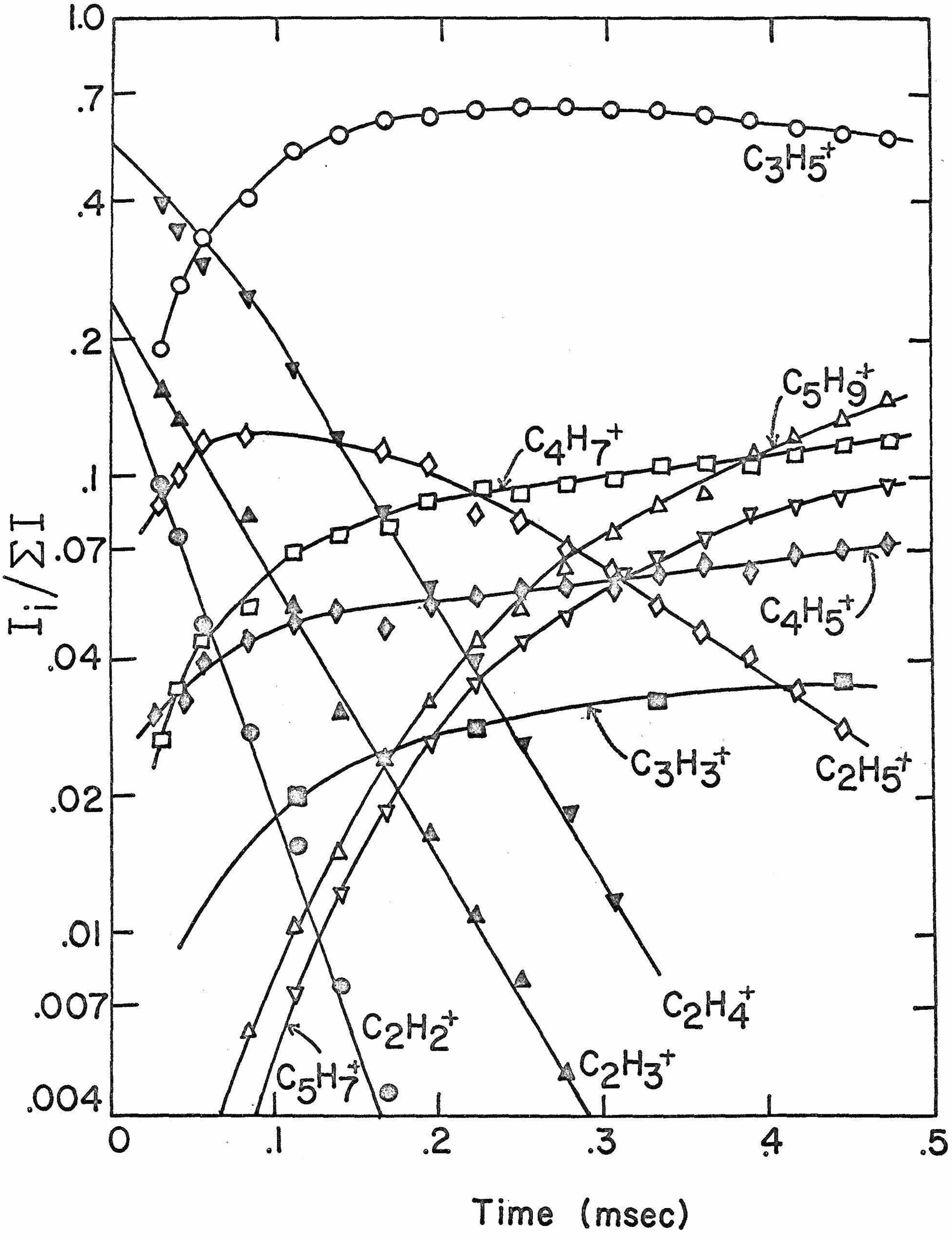
1.0
.7
.4
.2
.1
.07
.04
.02
.01
.007
.004
$I_i/\Sigma I$
0
.1
.2
.3
.4
.5
Time (msec)
$C_3H_5^+$
$C_5H_9^+$
$C_4H_7^+$
$C_4H_5^+$
$C_3H_3^+$
$C_2H_5^+$
$C_2H_4^+$
$C_2H_2^+$
$C_5H_7^+$
$C_2H_3^+$

Figure 2

Reaction sequence in C_2H_4, with $C_2H_2^+$, $C_2H_3^+$, and $C_2H_4^+$ as primary ions (taken from Reference 7).

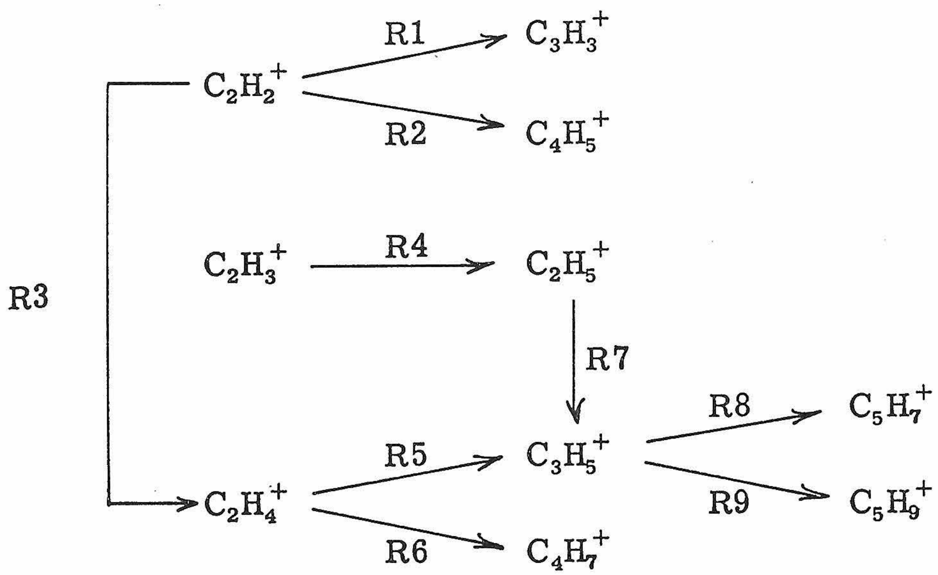
C2H2+
C3H3+
C4H5+
C2H3+
C2H5+
C3H5+
C5H7+
C5H9+
C2H4+
C4H7+
R1
R2
R3
R4
R5
R6
R7
R8
R9

Figure 2. The initial curvature in the $C_2H_4^+$ decay probably arises from the charge-exchange reaction

$$C_2H_2^+ + C_2H_4 \xrightarrow{R3} C_2H_4^+ + C_2H_2. \qquad (1)$$

Herod and Harrison,[8] in a trapped ion study under conditions similar to those of Figure 1, report a similar curvature for $C_2H_3^+$ resulting from the formation of this ion from reactions of $C_2H_2^+$ and C_2H^+. The effect of any such reactions was not observed.

The $C_2H_2^+$ ion participates in three reactive channels (R1-R3). The relative probabilities of each may be ascertained from Figure 1. Both $C_3H_3^+$ and $C_4H_5^+$ are unreactive, achieving ultimate concentrations of about .035 and .07 of the total ion current, respectively. To estimate the extent of R3, it is convenient to consider a straight line, drawn parallel to the $C_2H_4^+$ decay and having the same zero-time intercept as the actual $C_2H_4^+$ decay. This line would represent the abundance of $C_2H_4^+$ if there were no production of $C_2H_4^+$ via R3. The difference between the two abundances is thus the extent of the R3 contribution to the $C_2H_4^+$ abundance. The maximum difference, attained at 80 μsec, is .085 of the total ionization, and this excess decreases gradually as reaction proceeds. While not entirely rigorous, this value is a good estimate of the extent of charge exchange. If one now adds this value to the $C_3H_3^+$ and $C_4H_5^+$ abundances, the total is .19, in excellent agreement with the initial $C_2H_2^+$ abundance of .19. Accordingly, the relative rates of reactions

R1-R3 must be in the ratio R1:R2:R3 = .035:.07:.09, and the sum of these rates should be the total disappearance rate for $C_2H_2^+$.

The rate constants for reactions R4 and R7 are directly derived from the slopes of the $C_2H_3^+$ and $C_2H_5^+$ decays. The sum of the rates for R5 and R6 is given by the slope of the $C_2H_4^+$ decay. The relative values of these two rates is just the ratio of the $C_4H_7^+$ abundance to the total of the $C_3H_5^+$, $C_5H_7^+$ and $C_5H_9^+$ abundances taken at short times where the effect of R7 is small. This ratio is found to be R6:R5 = .13:1.

In this fashion, the rate constants for the bimolecular reactions R1-R7 are quantitatively determined. Reactions R8 and R9 are more complex since they involve a termolecular process and will be treated in more detail later. Table I lists the absolute disappearance rate constants for the various ions of interest, as well as the derived rate constants R1-R7. Included for comparison are the results of Herod and Harrison[8] and the relative rates obtained in this and other investigations. In general the agreement is satisfactory, the best agreement being with that of Herod and Harrison. The only significant area of discrepancy resides in the determination of the rates of R1-R3. The results of our work are quite definite in this regard and the present results are accepted with confidence.

It is of interest to compare the observed disappearance rate constants with those of the Langevin model. This is done in Table I. Both $C_2H_3^+$ and $C_2H_4^+$ exhibit rates considerably below the Langevin value, suggesting the reversion of the intermediate complex back to

Table I

Total Disappearance Rates in C_2H_4

Reactant ion	Total rate cm^3 molecule^{-1} sec^{-1} × 10^{-9}			Relative rates						
	This work	Trapped ion	Langevin rate	This work	Trapped ion[a]	High press[b]	High press[c]	High press[d]	High press[e]	ICR[f]
$C_2H_2^+$	1.37	1.58	1.32	1.7	1.9	3.3	3.3	1.5	1.6	1.1
$C_2H_3^+$	.83	.84	1.30	1.0	1.0	1.2	1.5	.8	.7	.8
$C_2H_4^+$	.81	.85	1.29	1.0	1.0	1.0	1.0	1.0	1.0	1.0
$C_2H_5^+$	.32	.32	1.28	.4	.4	.5	.9	.5		
$C_3H_5^+$	~.07	–	1.19							

Table I (Cont'd)

Individual Reaction Rates in C_2H_4

		Absolute reaction rate (this work) $cm^3\ molecule^{-1}\ sec^{-1} \times 10^{-9}$	Relative rates		
			This work	High press m.s.[e]	ICR[f]
$C_2H_2^+ + C_2H_4 \rightarrow C_3H_3^+ + CH_3$	(R1)	.25	.3	.5	.45
$C_2H_2^+ + C_2H_4 \rightarrow C_4H_5^+ + H$	(R2)	.49	.7	.3	.3
$C_2H_2^+ + C_2H_4 \rightarrow C_2H_4^+ + C_2H_2$	(R3)	.63	.9	.9[g]	.45
$C_2H_3^+ + C_2H_4 \rightarrow C_2H_5^+ + C_2H_2$	(R4)	.83	1.1	.8	.8
$C_2H_4^+ + C_2H_4 \rightarrow C_3H_5^+ + CH_3$	(R5)	.72	1.0	1.0	1.0
$C_2H_4^+ + C_2H_4 \rightarrow C_4H_7^+ + H$	(R6)	.09	.1	.1	.1
$C_2H_5^+ + C_2H_4 \rightarrow C_3H_5^+ + CH_4$	(R7)	.32	.4	.1	.1

[a] Reference 8. [b] Reference 3. [c] Reference 6.

[d] Reference 2. [e] Reference 4. [f] Reference 7.

[g] Value for R3 taken from Reference 5.

reactants. Myher and Harrison[1] have confirmed this by observing isotopically mixed ethylene ions in C_2H_4-C_2D_4 mixtures. By contrast, the $C_2H_2^+$ rate is quite close to its Langevin limit. This very likely reflects the importance of the charge-transfer process in the disappearance of $C_2H_2^+$. It is well established that electron jump processes can occur at distances outside the critical radius for orbiting, thus increasing the reaction cross section. This differs from the intimate collisions required for transfer of one or more atoms.

II. Production of $C_5H_7^+$ and $C_5H_9^+$

The detailed mechanism for the production of $C_5H_7^+$ and $C_5H_9^+$ is apparently quite complicated. Both ions result solely from the formation of an excited cluster $[C_3H_5 \cdot C_2H_4^+]^*$ which can either decompose back to $C_3H_5^+ + C_2H_4$, or decompose into $C_5H_7^+ + H_2$ or be collisionally stabilized forming $C_5H_9^+$. As noted from Figure 1, the disappearance rate of $C_3H_5^+$ is very slow, reflecting the importance of this reverse reaction. Tiernan and Futrell[6] have investigated the reactions of $C_3H_5^+$ with C_2D_4 in a tandem mass spectrometer and noted significant deuterium incorporation at a neutral pressure of 5 μ. This suggests the existence of a long-lived collision complex. Bowers et al.[7] have constructed two distinct mechanisms that qualitatively explain the pressure dependence of $C_5H_7^+$ and $C_5H_9^+$.

In mechanism M1, the basic assumption is that

$$\begin{tikzcd}
 & C_3H_5^+ \arrow[d, shift left, "k_1[C_2H_4]"] & \\
 & (C_5H_9^+)^{\ddagger} \arrow[u, shift left, "k_{-1}"] \arrow[d, "k_2"] \arrow[dr, "k_4"] & \\
C_5H_9^+ & (C_5H_9^+)^* \arrow[l, "k_5[C_2H_4]"'] \arrow[r, "k_3"] & C_5H_7^+ + H_2
\end{tikzcd} \qquad (M1)$$

the reaction of $C_3H_5^+$ with C_2H_4 forms an excited $(C_5H_9^+)^{\ddagger}$ ion which can decompose to $C_5H_7^+ + H_2$ or rearrange to a metastable $(C_5H_9^+)^*$ ion of different internal structure. All of the $C_5H_7^+$ in mechanism M1 comes from $(C_5H_9^+)^{\ddagger}$ or $(C_5H_9^+)^*$ through unimolecular decomposition. Mechanism M2, on the other hand, assumes that $(C_5H_9^+)^*$ is

$$\begin{tikzcd}
 & C_2H_5^+ \arrow[d, shift left, "k_1'[C_2H_4]"] & \\
 & (C_5H_9^+)^* \arrow[u, shift left, "k_{-1}'"] \arrow[r, "k_3'"] \arrow[dl, "k_5'[C_2H_4]"'] \arrow[dr, "k_4'[C_2H_4]"] & C_5H_7^+ + H_2 \\
C_5H_9^+ & & C_5H_7^+ + H_2
\end{tikzcd} \qquad (M2)$$

formed directly from $C_3H_5^+$, and that $C_5H_7^+$ comes both from collisional decomposition of $(C_5H_9^+)^*$ as well as unimolecular decomposition.

The detailed process of stabilization in ethylene may be more complex than just a collisional phenomenon. Buttrill[10] has shown that isotopic mixing occurs in the stabilization of $(C_5H_9^+)^*$ with C_2D_4, leading to $C_5H_nD_{9-n}^+$ entities. In this case, the rate constants k_5 and k_5' would represent the rates for these processes. This is discussed in greater detail later.

The ratio $R = R(C_5H_9^+)/R(C_5H_7^+)$, where $R(C_5H_7^+)$ is the rate of formation of $C_5H_7^+$, etc. can be calculated and is given in Table II for mechanisms M1 and M2. Also included in Table II are the low- and high-pressure limits of R.

In the high-pressure limit, both mechanisms give a value of R which is independent of pressure. Myher and Harrison[1] found that $R \sim 6.5$ and that it was approximately invariant with pressure from 10 to 30 μ. This value of R is in good agreement with the tandem mass spectrometer results of Tiernan and Futrell[6], which yield $R = 6.2$ at a pressure of 60 μ. This limiting value of R can be interpreted as the ratio of k_2/k_4 or k_5'/k_4', depending on the mechanism used. From Table II, the low-pressure limits of both mechanisms are essentially identical. Accordingly, the pressure dependence of R in pure ethylene will not permit a selection of one mechanism over the other.

Certain relationships between the rate constants in mechanisms M1 or M2 can readily be established. Figure 3 shows the pressure dependence of R in pure ethylene at pressures from .2 to 4 μ. The ratio was determined by measuring the ion abundances at 200 μsec trapping time. With these conditions only a small amount of higher order products ($C_7H_n^+$) was observed. The curve exhibits the expected behaviour and appears to approach the limit of 6.5 observed

Figure 3

Variation of the ratio of the rates of formation of $C_5H_9^+$ and $C_5H_7^+$ with ethylene pressure. Electron energy = 70 eV, ionizing pulse width = 15 μsec, reaction time = 200 μsec, trapping voltage = 4 volts. The point marked with the arrow is taken from the data of Herod and Harrison.[8]

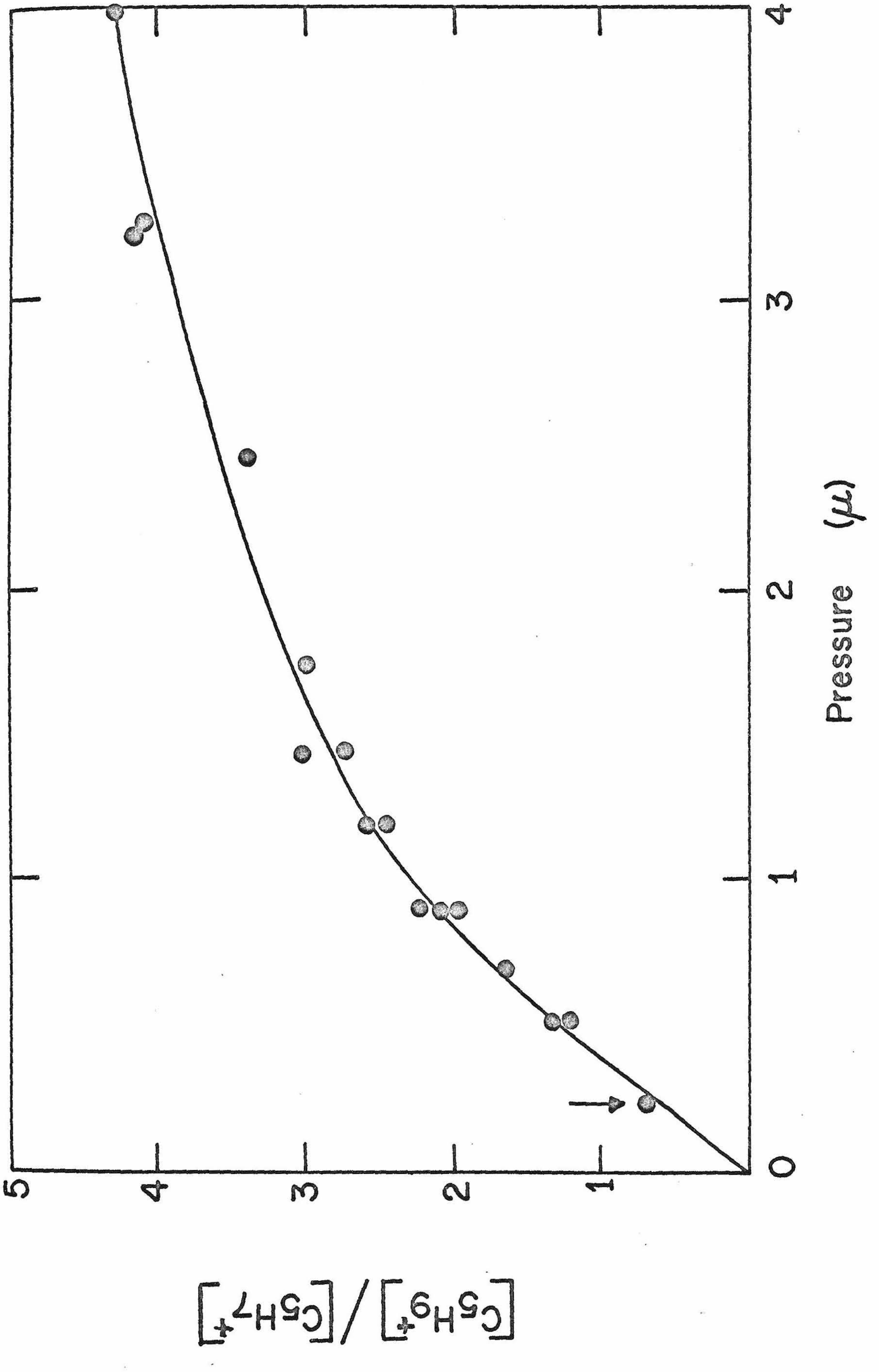
$[C_5H_9^+]/[C_5H_7^+]$
0
1
2
3
4
5
0
1
2
3
4
Pressure (μ)

Table II

Ratios of the Rates of Formation of $C_5H_9^+$ and $C_5H_7^+$ in Pure Ethylene and in Mixtures Containing Ethylene and an Inert Gas M

	$R(C_5H_9^+)/R(C_5H_7^+)$		
Mechanism	General	Low pressure	High pressure
	Pure ethylene		
M1	$\frac{k_5 k_2[C_2H_4]}{k_4(k_3 + k_5[C_2H_4] + k_3 k_2)}$	$\frac{k_5 k_2[C_2H_4]}{k_3(k_4 + k_2)}$	$\frac{k_2}{k_4}$
M2	$\frac{k_5'[C_2H_4]}{k_3' + k_4'[C_2H_4]}$	$\frac{k_5'[C_2H_4]}{k_3'}$	$\frac{k_5'}{k_4'}$
	Ethylene + M		
M1	$\frac{k_2(k_5[C_2H_4] + k_6[M])}{k_4(k_3 + k_5[C_2H_4] + k_6[M]) + k_2 k_3)}$	$\frac{k_2(k_5[C_2H_4] + k_6[M])}{k_3(k_4 + k_2)}$	$\frac{k_2}{k_4}$
M2	$\frac{k_5'[C_2H_4] + k_6'[M]}{k_3' + k_4'[C_2H_4] + k_7'[M]}$	$\frac{k_5'[C_2H_4] + k_6'[M]}{k_3'}$	$\frac{k_5'[C_2H_4] + k_6[M]}{k_4'[C_2H_4] + k_7[M]}$

by Harrison. At low pressures, the slope of R can be used to extract relationships between the other rate constants. Table III lists the results for each mechanism so derived. If an independent estimation of k_5 or k_5' can be made, as from ICR linewidths,[7] k_3, k_3' and k_4' can be calculated quantitatively.

The addition of an inert gas M to the ethylene system introduces several additional rate processes in mechanism M1 and M2. Mechanism M1 now includes a sixth process, that of collisional

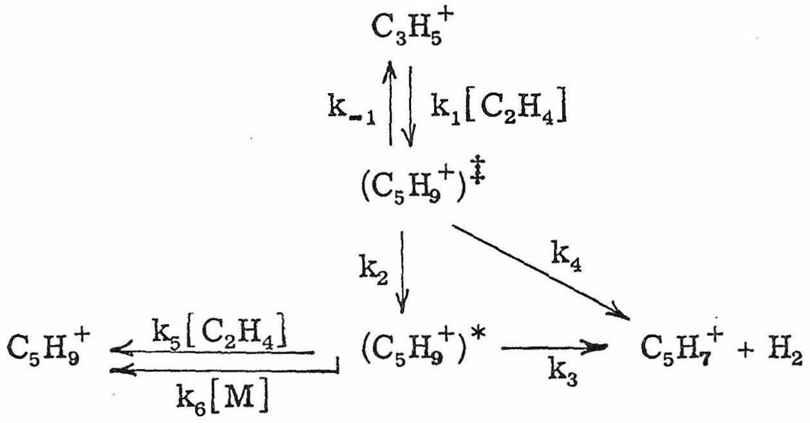

(M1)

stabilization of $(C_5H_9^+)^*$ by M. Similarly, M2 includes two additional processes, the collisional decomposition and the collisional stabilization of $(C_5H_9^+)^*$ by M.

Table III

Derived Relationships between Rate Constants

Mechanism	Low pressure (cm^3 molecule^{-1} × 10^{-14})	High pressure (dimensionless)
M1[a]	$\frac{k_5 k_2}{k_3(k_4 + k_2)} = 8.05$	$\frac{k_2}{k_4} = 6.5$
M2	$k_5'/k_3' = 8.05$	$k_5'/k_4' = 6.5$

[a] The low and high pressure relationships may be combined to give $k_5/k_3 = 9.38 \times 10^{-14}$ cm^3 molecule^{-1}.

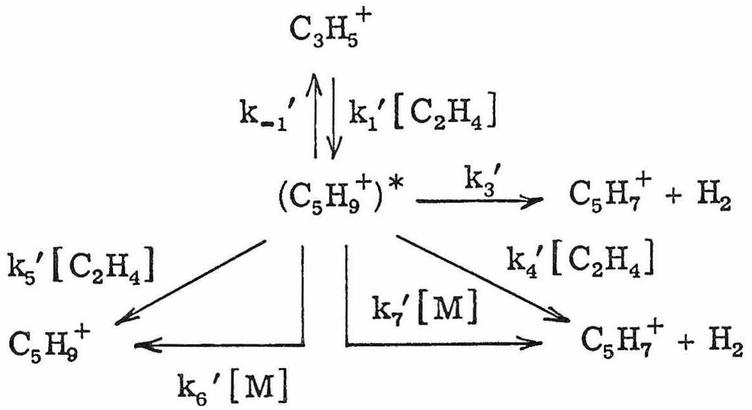

(M2)

The ratio R can be calculated and is given in Table II. In this case, the low-pressure limits for both mechanisms are still essentially identical, but the high-pressure limits have changed significantly. This affords a way of distinguishing between the two mechanisms, if sufficiently high pressures are attainable. Figure 4 shows the results of measurements of R made in pure ethylene and for mixtures of ethylene with a variety of other gases M. The pressure ratio for these mixtures was $[M]/[C_2H_4] = 6.7 \pm .1$. Mixtures were prepared in one gas bulb containing roughly 50 torr of gas. Partial pressures were measured with a Wallace and Treinan gauge. It is seen that even at the highest pressures employed, the values of R do not reach a constant value. Accordingly, the determination of the high-pressure limit of R, which would provide unequivocal evidence for either M1 or M2, is not possible with this instrument.

The calculated Langevin collision rates of these four gases with $C_5H_9^+$ are given in Table IV. The rates are all within 20% of each other and about 65% of the $(C_5H_9^+)^*$-C_2H_4 collision rate.

Figure 4

Variation of R with total pressure in pure ethylene and in mixtures of ethylene with an inert gas M. The mixture ratio was $[M]/[C_2H_4] = 6.7 \pm .1$. Electron energy = 70 eV, ionizing pulse width = 15 μsec, reaction time = 200 μsec, trapping voltage = 4 volts.

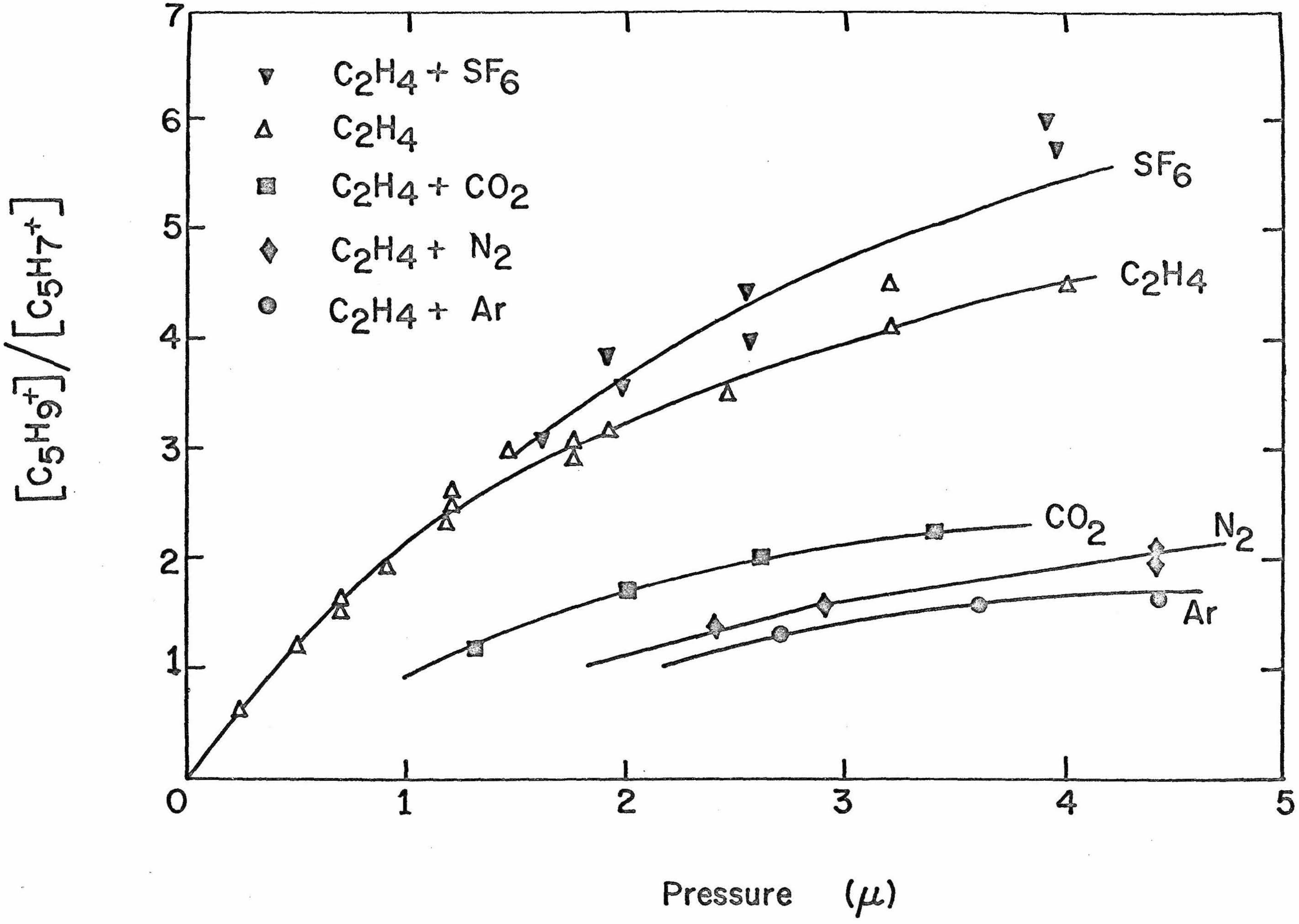
$C_2H_4 + SF_6$
C_2H_4
$C_2H_4 + CO_2$
$C_2H_4 + N_2$
$C_2H_4 + Ar$
SF_6
C_2H_4
CO_2
N_2
Ar
$[C_5H_9^+]/[C_5H_7^+]$
7
6
5
4
3
2
1
0
1
2
3
4
5
Pressure (μ)

Table IV

Collision Rates of $C_5H_9^+$ with Ar, N_2, CO_2, SF_6, and C_2H_4 [a]

Neutral gas	Collision rate $cm^3\ molecule^{-1}\ sec^{-1} \times 10^{-10}$
Ar	5.97
N_2	6.93
CO_2	7.26
SF_6	7.25
C_2H_4	10.60

[a] Calculated from Langevin equation using $\alpha(Ar) = 1.64\ Å^3$, $\alpha(N_2) = 1.74\ Å^3$, $\alpha(CO_2) = 2.59\ Å^3$, $\alpha(SF_6) = 4.48\ Å^3$, $\alpha(C_2H_4) = 4.10\ Å^3$. These polarizabilities were taken from E. W. Rothe and R. B. Bernstein, J. Chem. Phys., **31**, 1619 (1959).

Thus with a pressure ratio $[M]/[C_2H_4] = 6.7$, the actual collision rates of $(C_5H_9^+)^*$ with M and with C_2H_4 are in the ratio ~4.5:1. It can be concluded that the observed differences in R for the various gases should reflect, to a first approximation, only their relative abilities to collisionally stabilize or collisionally decompose $[C_5H_9^+]^*$.

The curves of Figure 4 can be used to provide indirect evidence favouring mechanism M1 over M2, by showing that M2 leads to unreasonable values for k_7'(M). Using the known quantities listed in Table III together with the exact expression for R for M2 from Table II, the quantities $k_6'[M]$ and $k_7'[M]$ can readily be determined from the data shown in Figure 4. Table V lists these values.

The collisional stabilization rate for SF_6 is roughly equal to that of C_2H_4, while the values of k_6' for the remaining molecules are all much lower than k_5', as expected in view of their limited number of degrees of freedom.

By contrast, the values of k_7' listed in Table V all appear anomalously low. Since the collisional decomposition rate should depend primarily on the mass of the collision gas, it is predicted that all the values of k_7' should be similar to k_4'. It is seen that they are all substantially lower, and exhibit no trace of systematic behaviour. The inability of mechanism M2 to provide reasonable values for k_7' is evidence against M2 being the actual mechanism.

Similar calculations can be performed using mechanism M1 to provide values of k_6. For all cases but SF_6, the values so obtained were nearly constant over the entire range of the curves in Figure 4.

Table V

Calculated Values of k_6', k_7', and k_6

M	k_6' (units of k_5')	k_7' (units of k_4')
	Mechanism M2	
SF_6	.85	.39
CO_2	.33	.52
N_2	.08	.03
Ar	.09	.19

Mechanism M1

	k_6 (units of k_5)
SF_6	2.5 ± 1
CO_2	.33 ± .05
N_2	.17 ± .03
Ar	.12 ± .03

Table V lists the calculated values of k_6 and their uncertainties.

The value of $k_6(SF_6)$ seems anomalously high. This is a consequence of the large scatter in the data for this molecule. In particular, the point at 4 μ seems too high and adversely affects the calculation of k_6. If this point were lowered by 14% (to 5.0), k_6 would be reduced to $1.6 \pm .4$, which is somewhat more reasonable. The values for the remaining molecules are good and exhibit the expected dependence on the number of degrees of freedom. The results of these calculations are clear enough to permit a tentative selection of mechanism M1 as the correct mechanism.

The results of the above experiments were encouraging enough that similar work was undertaken with an ICR spectrometer. This instrument had the advantage of a dual inlet system enabling the ethylene pressure to be set at a fixed value while the pressure of the collision gas was independently varied. This simplified the subsequent analysis. Figure 5 shows the results of an experiment at 14 eV ionizing energy where the ethylene pressure was fixed at a value such that $R = 1.37 \pm .02$ when no collision gas was present. The pressure of the collision gas was successively increased until line broadening of the $C_5H_7^+$ and $C_5H_9^+$ peaks prohibited accurate intensity measurements.

A comparison between Figures 4 and 5 reveals numerous similarities as well as one striking difference. In both cases, SF_6 produces the largest stabilization (as measured by R) while N_2 produces the smallest. Argon was not run in the ICR because of

Figure 5

Variation of R with pressure of added collision gas as measured by ICR spectroscopy. Electron energy = 14 eV; ion residence time ~1 msec.

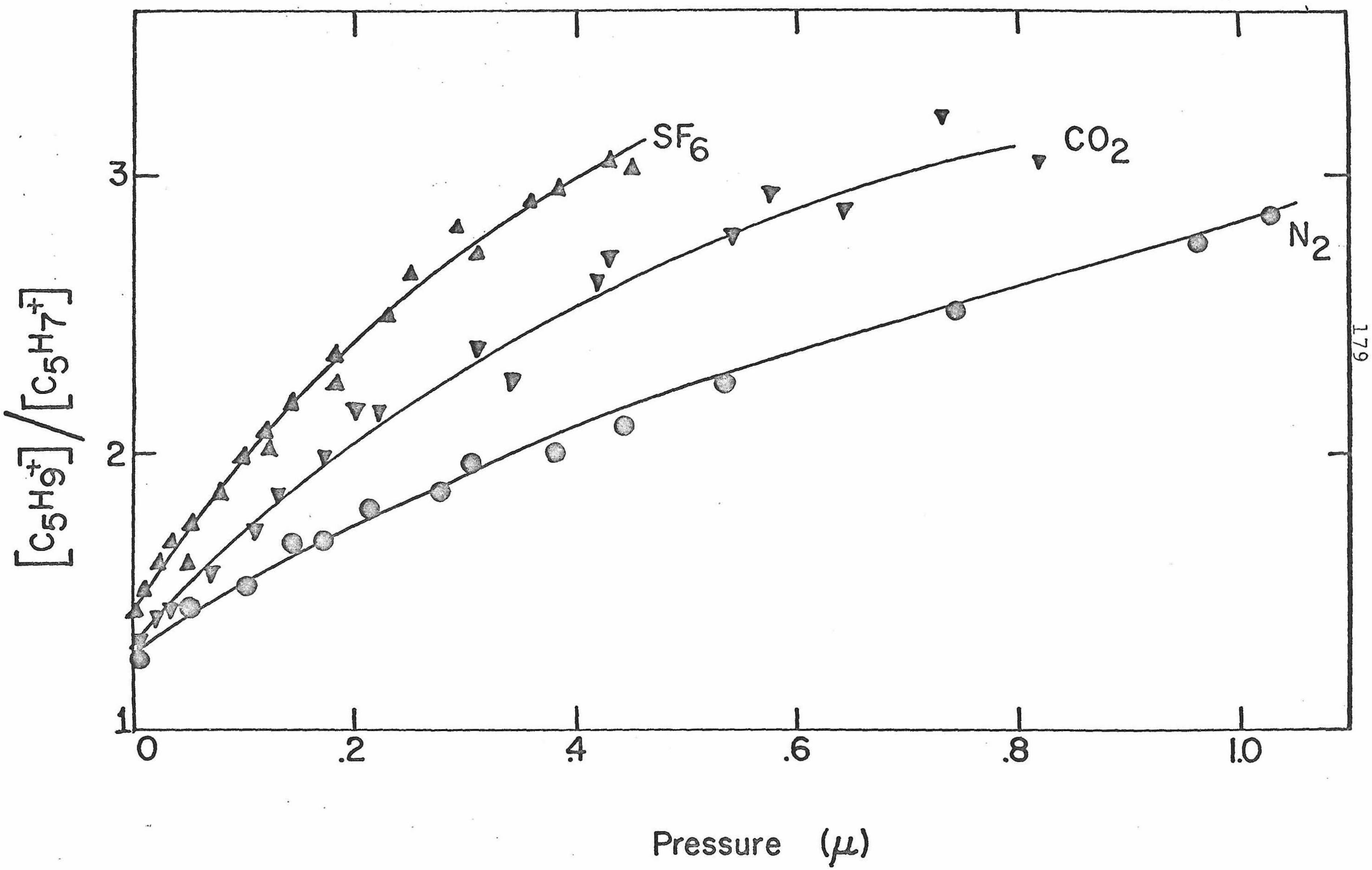
SF$_6$
CO$_2$
N$_2$
$[C_5H_9^+]/[C_5H_7^+]$
1
2
3
0
.2
.4
.6
.8
1.0
Pressure (μ)

instabilities in the pumping system. However the extent of stabilization differs markedly, as approximately twice the pressure is required in the high pressure mass spectrometer to reach an equivalent value of R. This effect has also been noted in pure ethylene; where R reaches 3 at 1 μ in the ICR while 1.6 μ are required in the high pressure mass spectrometer. This difference is too large to be merely an error in pressure measurement. It may reflect either the difference in electron energies or the difference in observing times--200 μsec in the high pressure mass spectrometer versus 1 msec in the ICR. This anomaly does not affect the determination of relative rates of stabilization of the various collision gases, nor does it affect any attempt to distinguish between M1 and M2. However it precludes the quantitative determination of the lifetime of $(C_5H_9^+)^*$ and it is for this reason that is has not been attempted.

The data in Figure 5 can be analyzed to determine the rate constants k_6 and k_6' and k_7'. The method is identical to that used previously and essentially consists of a curve fitting procedure wherein the quantities k_6 or k_6' and k_7' are selected to duplicate the curves of Figure 5. In this analysis, use is made of the known value of the high-pressure limit of R.[11]

The results of this analysis are presented in Table VI for both mechanisms. The rate constants are given relative to k_6 or k_6' for N_2. The uncertainties listed for each quantity represent the variations in the magnitude of that quantity needed to adequately reproduce the

Table VI

Calculated Values of k_6, k_6' and k_7'

Mechanism M1

M	k_6[a]
SF_6	4.2 ± .2
CO_2	2.0 ± .1
N_2	1.0

Mechanism M2

M	k_6'[a]	k_7'[a]
SF_6	3.2 ± .6	$.6_2$ ± .50
CO_2	2.0 ± .2	$.4_6$ ± .06
N_2	1.0	$.1_6$ ± .02

[a] Reported relative to k_6 or k_6' for N_2.

curves. Mechanism M1 achieves a good fit for all three gases, but M2 suffers difficulties, particularly for k_7' (SF_6). In addition, the value for k_7' (N_2) again seems anomalously low.

On this basis one may again draw the tentative conclusion that mechanism M2 is wrong. On the other hand, mechanism M1 reproduces the data faithfully.

The values of k_6 obtained in the ICR experiment are in reasonable agreement with those from the high pressure mass spectrometer. It is of interest to compare our results with those of Rabinovitch and co-workers[12] and Setser and co-workers.[13] These latter studies investigated collisional stabilization and energy transfer of chemically activated neutral molecules in a variety of bath gases. Table VII presents a summary of our results and compares them to those of Rabinovitch and Setser. For Ar, N_2 and CO_2, the agreement is excellent, particularly in view of the large difference in the nature of the activated species. For SF_6, the agreement with the result of Setser is poor. Setser has commented on the similarity of his measured rate for SF_6 to those of smaller molecules and concludes that it is consistent with a model having an upper limit to the amount of excess energy trasferred on one collision. This effect does not appear to be present in the deactivation of $(C_5H_9^+)^*$.

Our value for the stabilization rate of C_2H_4 seems anomalously high. This is likely a consequence of a unique mechanism of deactivation present for this molecule. Buttrill[10] has observed that stabilization of $(C_5H_9^+)^*$ by C_2D_4 exhibits deuterium incorporation into

Table VII

Relative Deactivation Rates [a]

Neutral gas	This work	Rabinovitch [b]	Setser [c]
Ar	.7 ± .2	.9, .8, .7	.6
N_2	1.0	1.0	1.0
CO_2	2.0 ± .2	1.6, 1.4, 1.4	–
SF_6	4.2 ± .4	–	1.0
C_2H_4	5.9 ± .6	2.2, 1.5, 1.6	–

[a] Rates reported relative to those for N_2.

[b] Reference 12. Values are for stabilization of $(C_2H_5CN)^*$ and $(CH_3CH)^*$ formed by thermal isomerization of C_2H_5NC and CH_3NC at temperatures of 231°C and 281°C.

[c] Reference 13. Values are for stabilization of $(C_2H_4Cl_2)^*$ formed by the combination of $\cdot CH_2Cl$ radicals. The internal energy of the cluster is 88.3 kcal/mole.

the deactivated species, resulting in $C_5H_nD_{9-n}^+$ entities. Evidently deactivation by C_2H_4 is not a simple collisional phenomenon, but involves formation of a $(C_7H_{11})^*$ cluster that is sufficiently long lived to permit H-D exchange. Clearly this must be a very efficient deactivation channel.

III. Thermochemical Predictions

These studies of the reaction processes in ethylene suffer from a lack of knowledge regarding the structures and heats of formation of the various ions. The following paragraphs represent our speculations on this subject. We are aware of the pitfalls of such an endeavour, but feel that our suggestions are reasonable and provide chemical insight into the processes.

The results of the present studies indicate that mechanism M1, involving two structures of excited $C_5H_9^+$, adequately describes the formation of $C_5H_7^+$ and $C_5H_9^+$. The precursor ion, $C_3H_5^+$, is undoubtedly allyl cation and should have minimal excess internal energy, due to the numerous nonreactive collisions that it suffers with C_2H_4. As discussed earlier, Tiernan and Futrell [6] have shown that these collisions involve hydrogen scrambling. Thus they should efficiently deactivate the cation.

Allyl cation can readily add ethylene to form either a linear or ring complex. While the ring complex cannot be discounted, it cannot easily be reconciled with the two structures of $C_5H_9^+$, as only one ring structure of this stoichiometry, I, appears plausible.

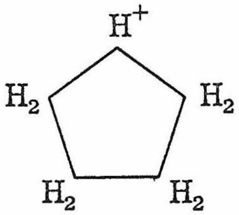

I

If a linear complex is then assumed, then the $C_5H_9^+$ ion may initially have structure II, which is a primary carbonium ion and thus is not

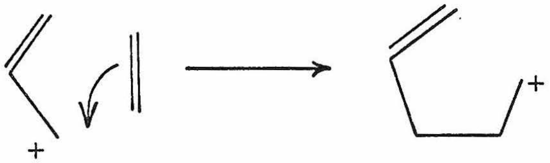

II

very stable. Elimination of H_2 would result in an ion of structure III,

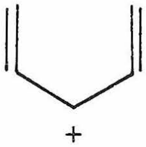

III

representing pentadienyl cation. The ion of structure II can also rearrange by a 1, 3 hydride shift, giving IV which resembles an allyl cation and probably represents the structure of stable $C_5H_9^+$.

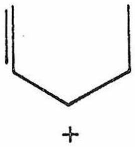

IV

Assuming that structures II and IV are those of $(C_5H_9^+)^\ddagger$ and $(C_5H_9^+)^*$, respectively, it is then possible to predict the enthalpy changes for the various processes in mechanism M1. Lossing[14] has recently measured the heat of formation of allyl cation using energy-resolved electron beams impacting on allyl radicals. He obtained $\Delta H_f(C_2H_5^+) = 226$ kcal/mole, which we will take as the heat of formation of the ground state allyl cation formed in ethylene.

The heats of formation of ions II, III and IV are not known with certainty, but can be estimated from molecular heats of formation, C–H bond strengths and hydrocarbon radical ionization potentials. Many of these latter quantities are also unknown, but reasonable estimates can be made in each case. Table VIII presents the assumed values of these parameters and the derived heats of formation of the ions.

The total exothermicity of the processes forming $C_5H_7^+$ (R8 in Figure 2) is calculated from these values to be 4 ± 15 kcal/mole. The uncertainty in this quantity arises primarily from the imprecision in $\Delta H_f(C_5H_7^+)$. If kinetic energy effects in these reactions are unimportant, then the observation of this reaction permits a more precise estimation of $\Delta H_f(C_5H_7^+) = 235\,^{+4}_{-15}$ kcal/mole. This enables the upper limit of the ionization potential of the pentadienyl radical to be assigned as 7.8 eV, while the lower limit remains at around 7.4 eV. This ionization potential has not previously been measured.

Table VIII

Thermochemical Parameters of Various Unsaturated Hydrocarbon Radicals[a]

Radical	$\Delta H_f(RH)$[b]	D(R–H)	IP(R·)	$\Delta H_f(R^+)$
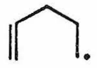	-5	98 ± 1[c]	8.0 ± .2[e]	226 ± 5
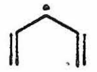	25	82 ± 5[d]	7.8 ± .4[f]	235 ± 15
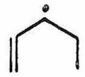	-5	83 ± 5[d]	7.8 ± .4[f]	205 ± 15
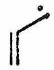	–	–	–	226[g]

[a] All thermochemical data in kcal/mole at 298°K except ionization potentials which are given in eV.

[b] Heats of formation of 1-C_5H_{10} and CH_2=$CHCH_2CH$=CH_2 taken from Reference 15.

[c] Assumed bond energy for terminal aliphatic C–H bond (Reference 16).

[d] Bond energy assumed to be 2 kcal/mole lower than an allyl C–H bond (Reference 16).

[e] Ionization potential assumed to be close to that for n-butyl and n-propyl radical (Reference 17).

[f] The limits of this quantity were established as follows. The lower limit is that of S-butyl radical (7.4 eV). The upper limit is 8.2 eV, slightly higher than allyl radical (8.07 eV) (References 14, 17).

[g] Reference 14.

The excess energy present in $(C_5H_9^+)^‡$, with respect to its ground state, can be determined from Table VIII to be 13 ± 5 kcal/mole, plus any contributions arising from the ion-neutral attraction. Fragmentation to $C_5H_7^+ + H_2$ has an enthalpy change $\Delta H = +9 \pm 20$ kcal/mole, and thus may well be endothermic for ground state $C_5H_9^+$ since the excess energy gained from the ion-neutral attraction is expended when $C_5H_7^+$ and H_2 separate. Accordingly, the fragmentation occurs only as a result of sufficient internal energy in the complex.

Rearrangement of $(C_5H_9^+)^‡$ to $(C_5H_9^+)^*$ is accompanied by an increase in the excess energy to 21 ± 20 kcal/mole (plus any kinetic energy contributions). Evidently some portion of this excess energy is lost by unreactive deactivating collisions or *via* the complex proton scrambling process observed by Buttrill. The extent of energy loss required to stabilize $C_5H_9^+$ is unknown and cannot readily be estimated.

References

1. J. J. Myher and A. G. Harrison, Can. J. Chem., 46, 101 (1968).
2. S. Wexler and R. Marshall, J. Amer. Chem. Soc., 86, 781 (1964).
3. S. Wexler, A. Lifshitz, and A. Quattrachi, Adv. Chem. Ser., 58, 243 (1966).
4. F. H. Field, J. L. Franklin, and F. W. Lampe, J. Amer. Chem. Soc., 79, 2419 (1957).
5. F. H. Field, ibid., 83, 1523 (1961).
6. T. O. Tiernan and J. H. Futrell, J. Phys. Chem., 72, 3080 (1968).
7. M. T. Bowers, D. D. Elleman, and J. L. Beauchamp, J. Amer. Chem. Soc., 72, 3599 (1968).
8. A. A. Herod and A. G. Harrison, Int. J. Mass Spec. Ion Phys., 4, 415 (1970).
9. G. G. Meisels, Adv. Chem. Ser., 58, 243 (1966).
10. S. E. Buttrill, private communication.
11. Fortunately this limit is known with some certainty and appears to be independent of the type of instrument used. A high pressure ICR study appears to yield the same value of R ~6.5. (T. B. McMahon, personal communication)
12. S. P. Pavlou and B. S. Rabinovitch, J. Phys. Chem., 75, 3037 (1971).
13. D. W. Setser and E. E. Siefert, J. Chem. Phys., 57, 3623 (1972).
14. F. P. Lossing, Can. J. Chem., 49, 357 (1971).

15. J. L. Franklin, J. G. Dillard, H. M. Rosenstock, J. T. Herron and K. Draxl, "Ionization Potentials, Appearance Potentials, and Heats of Formation of Gaseous Positive Ions", National Bureau of Standards Publication NSRDS-NBS 26, June 1969.

16. J. A. Kerr, *Chem. Rev.*, **66**, 465 (1966).

17. F. P. Lossing and G. P. Semeluk, *Can. J. Chem.*, **48**, 955 (1970).

Chapter 9

Ion-Molecule Processes in the Methyl Halides

The ion-molecule reactions of the methyl halides have been the subject of much recent work. McAskill[1, 2] and Herod et al.[3] have studied the kinetics of reactions in CH_3F and CH_3Cl using trapped ion mass spectroscopy. Beauchamp et al.[4] have determined reaction pathways, product distributions and rate constants for all the methyl halides using ICR spectroscopy. There is general agreement about the nature and rates of the major reactions that occur in these systems. The rate constants determined in the present work are in excellent agreement with the published values, providing essentially no new information. Accordingly, only a cursory summary of this work will be given, while the main attention will be focussed on two separate aspects of the ion chemistry of the methyl halides that have received little attention. These topics concern first, the kinetics of symmetric proton and charge transfer in the methyl halides and second, the determination of the kinetic energy distribution of CH_3^+ fragments from methyl halides.

I. Ion-Molecule Reactions in CH_3F

In CH_3F, the three major primary ions at 70 eV are CH_3F^+, CH_2F^+ and CH_3^+. The CH_2F^+ ion is unreactive, while the other two ions initiate the reaction scheme S1.

$$\begin{tikzcd}
 & & CH_2F^+ \\
 & CH_3FH^+ \arrow[ur, "R5"] \arrow[dr, "R3"'] & \\
CH_3F^+ \arrow[ur, "R1"] \arrow[dr, "R2"'] & & (CH_3)_2F^+ \\
 & C_2H_4F^+ &
\end{tikzcd}$$

(S1)

$$CH_3^+ \xrightarrow{R4} CH_2F^+$$

Beauchamp et al.[4] have stated that the CH_2F^+ ion formed by R5 arises from the partial decomposition of the initially formed excited fluoronium ion.

$$CH_3FH^+ + CH_3F \xrightarrow{R3} \underset{+HF}{[CH_3F^+CH_3]^*} \xrightarrow{R5} \underset{+\ CH_4}{CH_2F^+}$$

Reaction R5 is thus a unimolecular decomposition in contrast to R1-R4 which are bimolecular. McAskill[1] suggests a second possibility wherein CH_2F^+ is formed directly from CH_3FH^+ via R5′, in competition to the $(CH_3)_2F^+$ formation

$$CH_3FH^+ + CH_3F \xrightleftharpoons{R5'} [CH_3FH^+ \cdot FCH_3]^* \longrightarrow \underset{+\ HF\ +\ CH_4}{CH_2F^+}$$

He notes that comparatively more $(CH_3)_2F^+$ is formed at lower electron energies (15 eV); this is readily explained by either mechanism. The two schemes differ mainly in the identification of the intermediate complex and, as they exhibit the same pressure dependence, are indistinguishable with the present data.

An ion abundance-reaction time curve for the ions in CH_3F at at 70 eV is shown in Figure 1. The rate constants R1-R3 may be extracted in the usual fashion and are given in Table I, along with the results of other investigations.

Herod *et al.*[3] have investigated the kinetic energy dependence of the rate of R1 and found that the rate increased sharply with ion energy to a value of around 2.5×10^{-9} cm^3 $molecule^{-1}$ sec^{-1} at an average ion energy of .65 eV. The excellent agreement of the results of this work with the thermal (ICR) results of References 4 and 5 demonstrates that ions in this instrument are at near thermal energy.

The disappearance rate for CH_3F^+ is considerably greater than the calculated Langevin rate, suggesting that a significant ion-dipole interaction is present. By contrast, the rate of Reaction (R3) is somewhat below the Langevin limit. Since the same ion-dipole interaction should be present in both reactions, this implies that some non-reactive collisions occur. Alternatively some symmetric proton transfer analogous to that discussed below for CH_3Cl may occur in competition with the fluoronium ion formation.

Very little CH_3^+ was observed (less than 1% of the total ion current), though spectra taken with conventional mass spectrometers show that typically 20% of the total ionization at 70eV electron energy comprises CH_3^+. Herod *et at.*[3] have also noted that this ion was not completely trapped in their trapped ion instrument. This is a consequence of the initial kinetic energy present on formation. Detailed studies discussed in Chapter 15 of this thesis show that the

Figure 1

Variation of ion abundance with reaction time for the ions in CH_3F. Electron energy = 70 eV, ionizing pulse width = 15 μsec, pressure = 2.9×10^{-4} torr, trapping voltage = 4 volts.

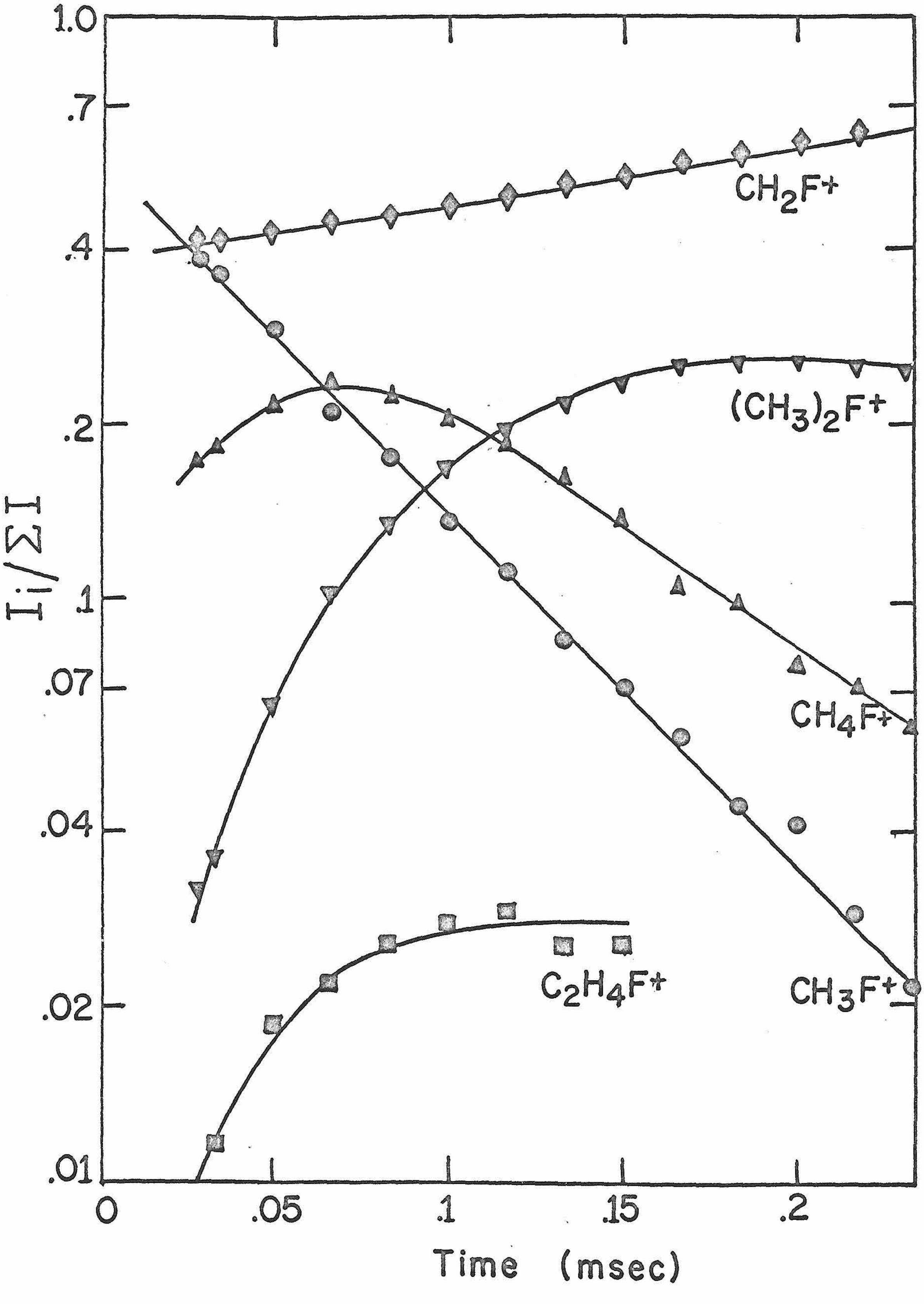
1.0
.7
.4
.2
.1
.07
.04
.02
.01
$I_i/\Sigma I$
0
.05
.1
.15
.2
Time (msec)
CH_2F^+
$(CH_3)_2F^+$
CH_4F^+
CH_3F^+
$C_2H_4F^+$

Table I

Rate Constants in CH_3F

Reaction		This work	Rate constants (cm^3 $molecule^{-1}$ $sec^{-1} \times 10^{-9}$)				
			High press m.s.[a]	High press m.s.[b]	ICR[c]	ICR[d]	Langevin rate[e]
$CH_3F^+ + CH_3F \nearrow CH_3FH^+ + CH_2F$	(R1)	1.51 ± .05	2.2	1.87	1.28	1.36	.91
$\searrow C_2H_4F^+ + HF + H$	(R2)	.14			.10	.10	
$CH_3FH^+ + CH_3F \nearrow (CH_3)_2F^+ + HF$	(R3)	1.0 ± .1	–	.9	.7	.8	.90
$\searrow CH_2F^+ + CH_4 + HF$	(R4)						

[a] Reference 1.

[b] Reference 3. Average ion energy ~ .45 eV.

[c] Reference 4.

[d] Reference 5.

[e] Langevin rate calculated using $\alpha(CH_3F) = 2.57 \text{Å}^3$.

CH_3^+ fragments carry an average of .5 eV excess kinetic energy. With an energy of ~.35 eV in directions perpendicular to the magnetic field, the cyclotron radius of CH_3^+ in our instrument can be calculated to be .5 cm. Accordingly, ions formed in the centre of the source will move a maximum distance of 1 cm from the centre. Since the radius of the ion source is only ~.9 cm, all CH_3^+ will be neutralized on the wall of the reaction chamber and will thus not contribute to the CH_2F^+ intensity. In the ICR spectrometer, cyclotron radii are much smaller and ion loss occurs only by neutralization on the trapping plates. This effect has been used to determine the kinetic energy distribution of CH_3^+ (see Chapter 15).

II. Ion-Molecule Reactions in CH_3Cl

The ion-molecule chemistry of CH_3Cl is similar to that of CH_3F. Beauchamp et al.,[4] McAskill,[2] and Herod et al.[3] have studied this system in detail. Our results are in general agreement with their studies. The parent ion CH_3Cl^+ initiates the reaction scheme S2.

$$\begin{aligned} CH_3Cl^+ + CH_3Cl &\xrightarrow{R6} CH_3ClH^+ + CH_2Cl \\ CH_3ClH^+ + CH_3Cl &\xrightarrow{R7} (CH_3)_2Cl^+ + HCl \end{aligned} \qquad (S2)$$

Only small amounts of CH_2Cl^+ or CH_3^+ were observed and their intensities were not monitored as they do not appear to participate in this reaction scheme at thermal ion energies.[3] Figure 2 shows an intensity-time plot for the major ions in CH_3Cl taken at sufficiently

Figure 2

Variation of major ion abundances with reaction time in CH_3Cl. Electron energy = 70 eV, ionizing pulse width = 15 μsec, pressure = 9.2×10^{-4} torr, trapping voltage = 3 volts. The zero-time intercept of CH_3Cl is $\sim .6$, indicating some CH_3ClH^+ formation during the electron beam pulse.

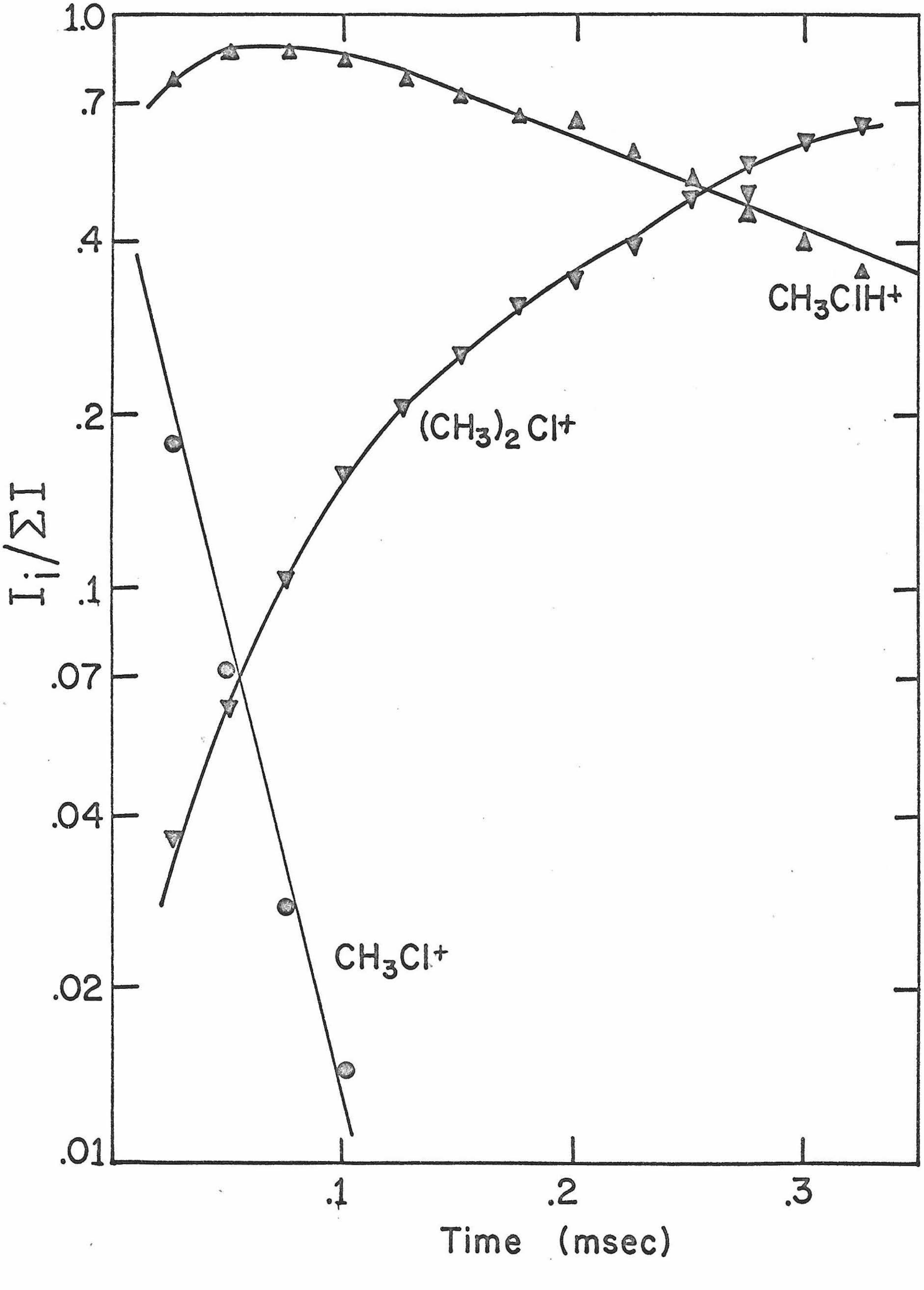
1.0
.7
.4
.2
.1
.07
.04
.02
.01
$I_i/\sum I$
.1
.2
.3
Time (msec)
CH_3ClH^+
$(CH_3)_2Cl^+$
CH_3Cl^+

low pressure that considerable chloronium ion formation occurred. Lower pressure spectra were also run to measure the rate of R6 more accurately. Table II lists the measured rate constants as well as measurements by other workers.

Again the rate of R6 is substantially larger than the Langevin limit, demonstrating a significant ion-dipole interaction as for CH_3F. However the rate of chloronium ion formation is much lower than the analogous fluoronium ion formation rate in CH_3F. This effect has been investigated in detail using a trapped ion-ion ejection ICR technique. It was found that symmetric proton transfer between CH_3ClH^+ and CH_3Cl is an important reactive channel in addition to the chloronium ion formation. These results are presented in Section IV of this chapter.

III. Ion-Molecule Reactions in CH_3Br

Methyl bromide was only briefly investigated. In contrast to CH_3F and CH_3Cl, the parent ion does not protonate the molecule but reacts directly to form $(CH_3)_2Br^+$. This very slow reaction was found to have a rate constant at 70 eV electron energy of 3×10^{-11} cm^3 $molecule^{-1}$ sec^{-1}, in excellent agreement with the value of 3.8×10^{-11} cm^3 $molecule^{-1}$ sec^{-1} determined by Sieck and Gordon[7] using photoionization at 11.7 eV. These workers have also measured the rate at 10.6 eV, obtaining a rate of 5.8×10^{-11} cm^3 $molecule^{-1}$ sec^{-1}, in good agreement with the value of Beauchamp et al. using 11.4 eV electron impact. Thus it appears that the formation of

Table II

Reaction Rates in CH_3Cl

Reaction	Reaction rates (cm^3 molecule^{-1} sec^{-1} × 10^{-9})						
	This work	High press m. s.[a]	High press m. s.[b]	ICR[c]	High press m. s.[d]	Trapped ion ICR[e]	Langevin rate[f]
$CH_3Cl^+ + CH_3Cl \rightarrow CH_3ClH^+ + CH_2Cl$	1.25 ± .1	1.94	1.53	1.25	1.21	1.20	.98
$CH_4Cl^+ + CH_3Cl \rightarrow (CH_3)_2Cl^+ + HCl$	.13		.10	.14		.18	.97

[a] Reference 2.

[b] Reference 3.

[c] Reference 4.

[e] Reference 7.

[f] Langevin rate calculated using $\alpha(CH_3Cl) = 4.44$ Å.

bromonium ion is sensitive to the internal energy content of the parent ion.

The parent ion also undergoes rapid charge transfer with the neutral. The rate constant for this process was investigated using trapped ion-ion ejection ICR spectroscopy, as reported below.

IV. Symmetric Proton Transfer in CH_3Cl

Under bombardment with 14 eV electrons, CH_3Cl forms only one important positive ion, CH_3Cl^+, which reacts rapidly with the neutral to form the protonated parent. For convenience, reaction numbers in this section commence again with R1.

$$CH_3Cl^+ + CH_3Cl \xrightarrow{k_1} CH_3ClH^+ + CH_2Cl. \qquad \text{(R1)}$$

The rate constant k_1 has been shown above to be 12×10^{-10} cm^3 molecule^{-1} sec^{-1}. This is slightly larger than the Langevin collision rate of 9.8×10^{-10} cm^3 molecule^{-1} sec^{-1}, suggesting that the actual collision (and reaction) cross section is increased somewhat by the presence of a favourable ion-dipole interaction. The magnitude of such an attractive effect is generally quite small, as conservation of angular momentum usually precludes any significant ion-dipole "locking". Accordingly, it is reasonable to assume that k_1 is very close to the collision rate and that virtually all collisions lead to reaction. This assumption will be examined in more detail later and is shown to be realistic.

The protonated parent is known to react further

$$CH_3ClH^+ + CH_3Cl \xrightarrow{k_2} (CH_3)_2Cl^+ + HCl \qquad (R2)$$

with the relatively slow rate constant of 1.3×10^{-10} cm^3 $molecule^{-1}$ sec^{-1}. The collision rate between CH_3ClH^+ and CH_3Cl should be essentially identical to that for CH_3Cl^+–CH_3Cl since the same ion-induced dipole and ion-dipole terms participate in each. This indicates that relatively few collisions between CH_3ClH^+ and CH_3Cl lead to formation of the chloronium ion and it follows, therefore, that other processes are occurring upon encounter between these two species. Only two other channels appear feasible, completely non-reactive collisiions and symmetric proton transfer. A proton transfer reaction such as R3′

$$CH_3XH^+ + CH_3X \longrightarrow CH_3X + CH_3XH^+ \qquad (R3')$$

is undetectable in most cases, but for methyl chloride we have examined the reactions

$$CH_3{}^{35}ClH^+ + CH_3{}^{37}Cl \underset{k_3'}{\overset{k_3}{\rightleftharpoons}} CH_3{}^{37}ClH^+ + CH_3{}^{35}Cl \qquad (R3)$$

using a trapped ion-ion ejection ICR technique.

Recently developed ion cyclotron resonance techniques[8, 9] have made it possible to trap ions in the source region of the spectrometer for periods up to 1 sec. Ions are formed in the source by a brief pulse of electrons, then trapped for a variable reaction time, and finally removed and detected in the analyzer region. It is possible to selectively eject an ion from the trapping region while other ions remain unperturbed. This is accomplished by applying a radio-frequency electric field between two of the plates in the source at the cyclotron frequency of the ion to be ejected. This causes the ion motion to become unbounded and after about 1 msec, it collides with the source drift plates. The time for ejection is short enough compared to reaction times that ejection can be considered as instantaneous. The ejection technique has sufficient resolution to discriminate between ions of mass 51 and 53, and was used in the study of R3.

A typical experiment involves monitoring the concentration of $CH_3{}^{35}ClH^+$ with and without continuous ejection of $CH_3{}^{37}ClH^+$ (m/e = 53). Figure 3 shows the results of such an experiment. Ejection of $CH_3{}^{37}ClH^+$ causes a marked diminution of the $CH_3{}^{35}ClH^+$ abundance, indicating that the proton transfer R3 does occur to a significant extent. The exact kinetic analysis is straightforward but tedious, and it can be shown[10] that

$$R = \frac{[CH_3{}^{35}ClH^+]_{ej}}{[CH_3{}^{35}ClH^+]} = \frac{n(k_2 - k_1)}{n(k_2 - k_1) + n_{37}k_3} \times \frac{e^{-nk_1t} - e^{-(nk_2 + n_{37}k_3)t}}{e^{-nk_1t} - e^{-nk_2t}} \qquad (1)$$

where $[CH_3{}^{35}ClH^+]$ is the abundance of that ion without ejection and $[CH_3{}^{35}ClH^+]_{ej}$ is the abundance of that ion with ejection of $CH_3{}^{37}ClH^+$.

Figure 3

Variation of ion intensity with reaction time in CH_3Cl with and without ejection of $CH_3{}^{37}ClH^+$ (m/e = 53). Electron energy = 14 eV, pressure = $1.3 \pm .15 \times 10^{-6}$ torr, ionizing pulse width = 6 msec.

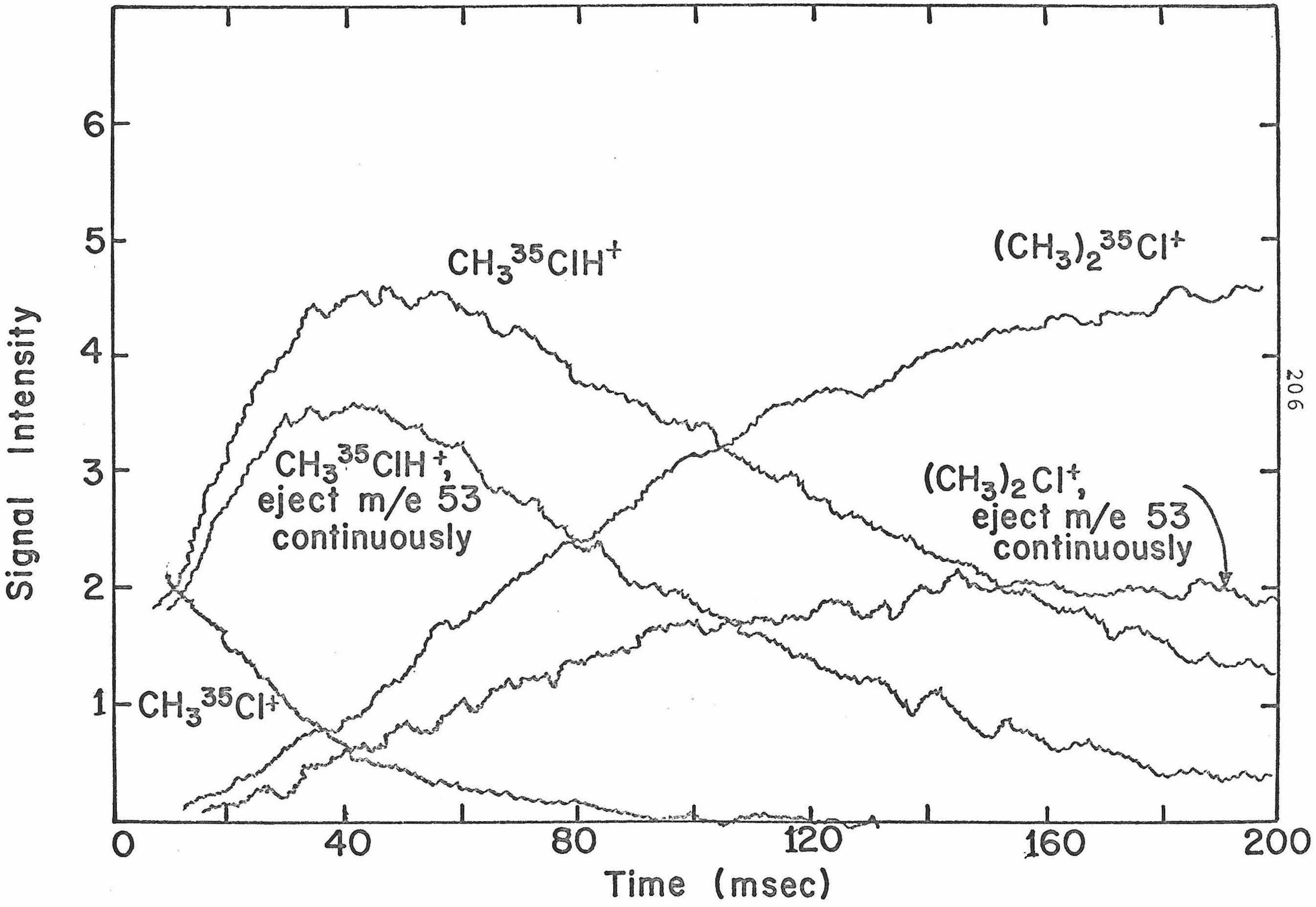
Signal Intensity
Time (msec)
0
40
80
120
160
200
1
2
3
4
5
6
$CH_3{}^{35}ClH^+$
$CH_3{}^{35}ClH^+$, eject m/e 53 continuously
$CH_3{}^{35}Cl^+$
$(CH_3)_2{}^{35}Cl^+$
$(CH_3)_2Cl^+$, eject m/e 53 continuously

The total neutral pressure is n and n_{37} represents the partial pressure of $CH_3{}^{37}Cl$. If $e^{-nk_1t} \ll e^{-(nk_2+n_{37}k_3)t}$, then Equation (1) reduces to a more convenient form

$$R \approx \frac{n(k_2+k_1)}{n(k_2-k_1)+n_{37}k_3} \; e^{-n_{37}k_3t} . \tag{2}$$

The rate constant k_3 can thus be extracted from the slope of a plot of log R versus t, if the pressure is known. The pressure was measured using a calibrated Shultz-Phelps gauge. The accuracy of this determination was checked by calculating the rate of R1 from the CH_3Cl^+ decay curve. The agreement with accepted values was within 10%. Figure 4 shows a plot of log R versus t for the data shown in Figure 3. The apparent rate constant k_3 is found to be $6.1 \pm .5 \times 10^{-10}$ cm^3 $molecule^{-1}$ sec^{-1}. For these experimental conditions, the quantity

$$\frac{e^{-nk_1t}}{e^{-(nk_2+n_{37}k_3)t}}$$

has the values .14, .02, .003 and .0004 at 50, 100, 150 and 200 msec, respectively. Thus while the above inequality is not strictly obeyed at very short times, it is valid over most of the scan. Hence the measured value of k_3 can be confidently taken to be the rate constant of R3.

Figure 4

Variation of R for $CH_3^{35}ClH^+$ and $CH_3^{37}ClH^+$ with time. Experimental conditions as for Figure 3.

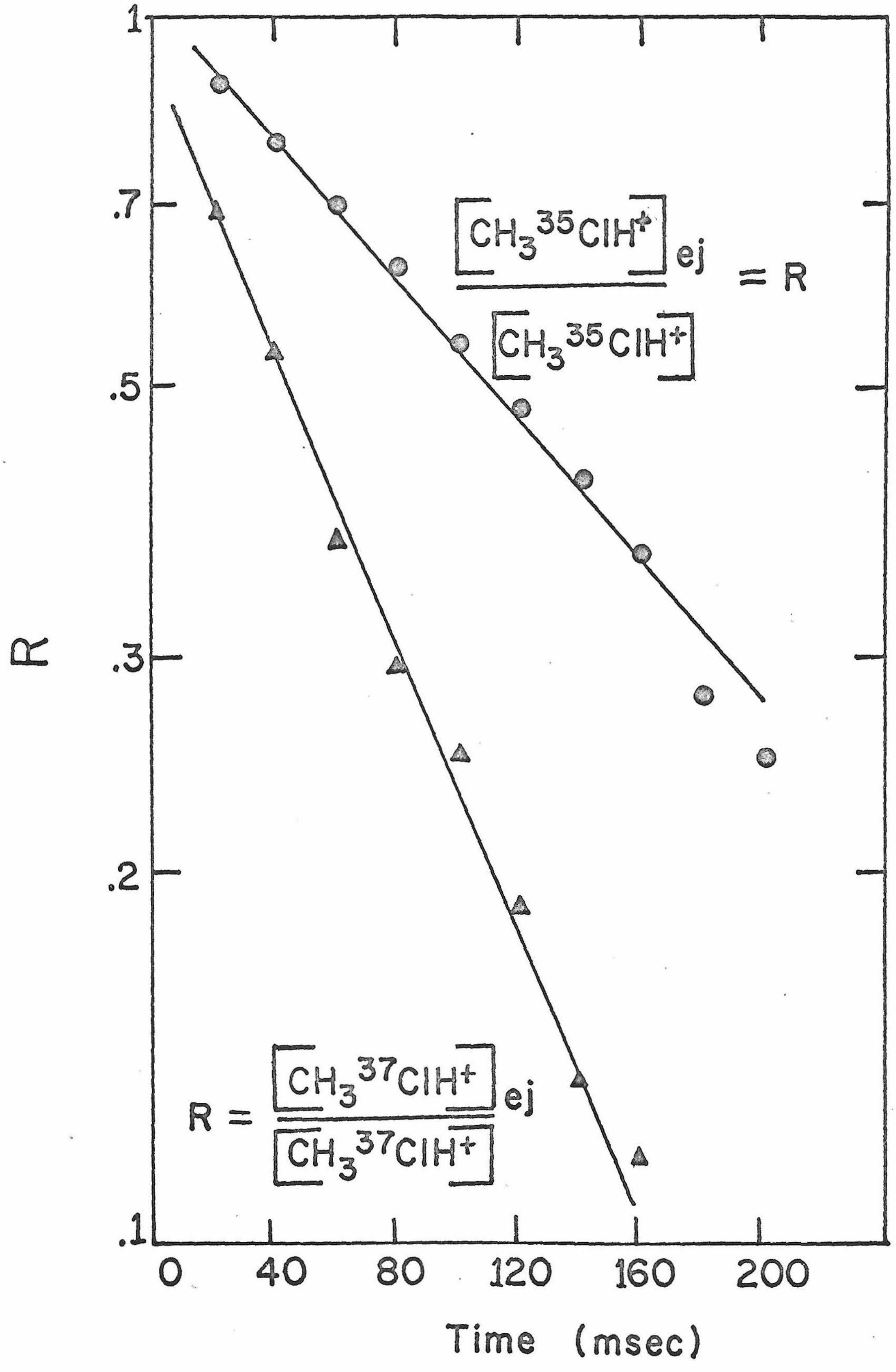
1
.7
.5
.3
.2
.1
R
0
40
80
120
160
200
Time (msec)
$\frac{[CH_3{}^{35}ClH^+]_{ej}}{[CH_3{}^{35}ClH^+]} = R$
$R = \frac{[CH_3{}^{37}ClH^+]_{ej}}{[CH_3{}^{37}ClH^+]}$

The rate constant k_3' was determined in the analogous fashion by monitoring the $CH_3{}^{37}ClH^+$. The uncertainties in k_3 and k_3' arise primarily from pressure uncertainties. If it is assumed that the differences between k_3 and k_3' are due to some small systematic error, then these rates are thus concluded to be $5.3 \pm 1.1 \times 10^{-10}$ cm^3 molecule^{-1} sec^{-1}.

Consider now the nature of the collision complex formed in R3. If it is a proton bound dimer, it follows that only half of these encounters should result in the actual transfer of a proton, while half should result in no change. Accordingly, the total encounter rate for these processes should be $10.6 \pm 2.2 \times 10^{-10}$ cm^3 molecule^{-1} sec^{-1}. Adding the rate for chloronium ion formation to this value results in a total rate of $11.9 \pm 2.2 \times 10^{-10}$ cm^3 molecule^{-1} sec^{-1}. This is in excellent agreement with the rate of R1 (12.0×10^{-10} cm^3 molecule^{-1} sec^{-1}) and increases confidence in the measured values for k_1, k_2 and k_3.

Numerous important and interesting conclusions can be drawn from these results. First, the good agreement between the known total encounter rate of CH_3ClH^+ and the measured rate of protonation, R1, suggests that the total collision rate between CH_3Cl^+ and CH_3Cl is also about 1.2×10^{-9} cm^3 molecule^{-1} sec^{-1} and that all collisions lead to protonation. This result has also been confirmed by monitoring the decay of $CH_3{}^{35}Cl^+$ with and without ejection of $CH_3{}^{37}Cl^+$. Non-reactive collisions might be expected to have a 1/2 probability of charge transfer, which would be detectable as a difference in these curves. No difference was observed.

Second, it appears that the phenomena occurring upon collision with CH_3ClH^+ and CH_3Cl have been completely characterized. The data for proton transfer suggest that at least 90% of collisions result in formation of a proton-bound dimer. Half of these encounters result in proton transfer while half result in no net change. This suggests that the dimer should have a lifetime of at least a few vibrational periods.

Roughly 10% of the collisions result in eventual chloronium ion formation. Beauchamp *et al.*[4] have demonstrated that the Cl atom in the product ion comes with equal probability from the ionic and neutral reactant species. Our ion ejection results are in agreement with this. A proton-bound dimer structure, I, is again implicated and forms the chloronium ion by simple bond shifts.

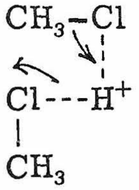

(I)

Since it thus appears that all collision complexes initially have the same structure, I, the interesting question arises as to the nature of the determining factors governing chloronium ion formation versus mere symmetric proton transfer. Perhaps the significant factor is the CH_3–($ClCH_3$) distance designated as r in structure II.

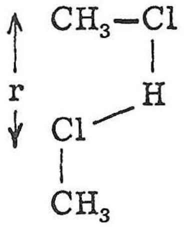

(II)

The CH_3–Cl–H bond angles are probably between 90° and 120°, while in most systems, such as H_2O, proton bridge angles generally are close to 180°. In this case, the critical parameter could be this Cl–H–Cl bond angle, and chloronium ion formation should be sensitive to the amount of energy E* present in the bending vibration of this angle. This energy should be related to the original configuration of Cl–H–Cl immediately following bond formation, as the more oblique collisions should introduce more energy into this mode. This model predicts that chloronium ion formation is a random event depending critically on the extent of a collinear collision.

V. Symmetric Charge Transfer in CH_3Br

Under electron impact at 15 eV, CH_3Br forms only one important ion, CH_3Br^+. Although no protonated parent is formed, this ion reacts extremely slowly with the neutral, forming $(CH_3)_2Br^+$

$$CH_3Br^+ + CH_3Br \longrightarrow (CH_3)_2Br^+ \ CH_3 . \qquad \text{(R4)}$$

It was felt that charge exchange between ion and neutral could easily be a very significant reactive channel. Charge exchange in the reaction

$$CH_3{}^{79}Br^+ + CH_3{}^{81}Br \underset{k_5'}{\overset{k_5}{\rightleftharpoons}} CH_3{}^{81}Br^+ + CH_3{}^{79}Br \qquad (R5)$$

can readily be studied using the same ion ejection techniques described above. Figure 5 shows typical results when $CH_3{}^{81}Br^+$ (m/e = 96) was ejected. The charge exchange rate is seen to be many times faster than the $(CH_3)_2Br^+$ formation rate.

The kinetic analysis is much simpler than for CH_3Cl since these ions approximate non-reactive primary ions. In this case

$$R = \frac{[CH_3{}^{79}Br^+]_{ej}}{[CH_3{}^{79}Br^+]} = e^{-n_{81} k_5 t} \qquad (3)$$

where the terms are defined analogously to those in Equation (1). Figure 6 shows the dependence of log R with time for both ions. The rate constants k_5 and k_5' are found to be $9.7 \pm .2 \times 10^{-10}$ cm^3 molecule^{-1} sec^{-1}.

If it is assumed that the charge-transfer reaction proceeds via a transient intermediate complex and that the probability of charge transfer to change identity is 1/2, then the total charge-transfer encounter rate is 19.4×10^{-10} cm^3 molecule^{-1} sec^{-1}.

This is considerably larger than the calculated Langevin rate of 7.9×10^{-10} cm^3 molecule^{-1} sec^{-1}, and indicates either that charge transfer occurs at distances greater than those causing a spiraling collision, or that there is significant ion-dipole enhancement of the collision rate. There is no a priori way to distinguish these two

Figure 5

Variation of ionic abundances in CH_3Br with and without ejection of $CH_3{}^{81}Br$ (m/e = 96). The $(CH_3)_2{}^{79}Br^+$ curve when m/e = 96 was ejected is not shown. Electron energy = 15 eV, pressure = 1.45×10^{-6} torr, ionizing pulse width = 6 msec.

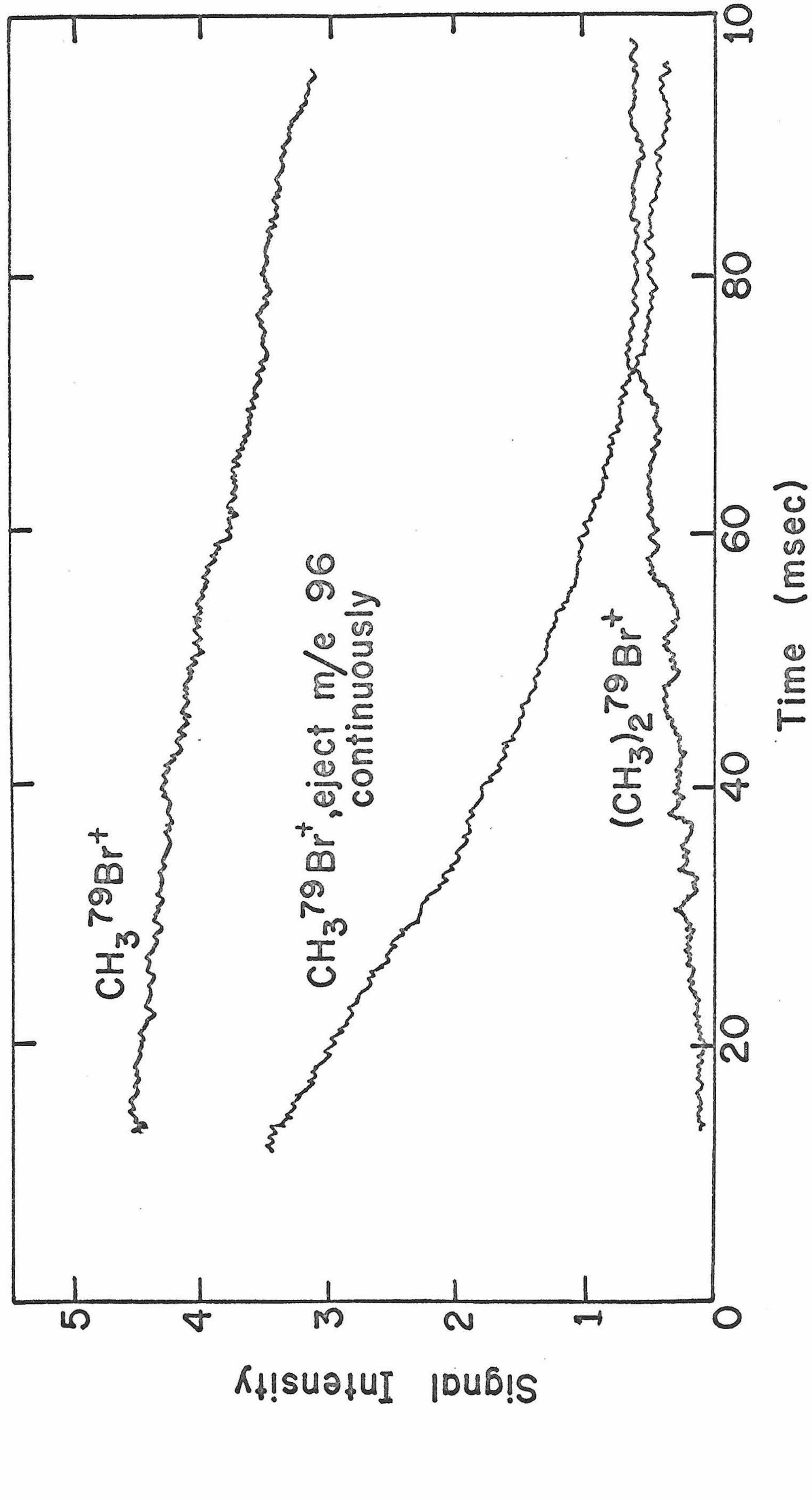
Signal Intensity
0
1
2
3
4
5
Time (msec)
0
20
40
60
80
100
CH$_3$^{79}Br$^+$
CH$_3$^{79}Br$^+$,eject m/e 96 continuously
(CH$_3$)$_2$^{79}Br$^+$

Figure 6

Variation of R for $CH_3{}^{79}Br^+$ and $CH_3{}^{81}Br^+$ with reaction time. Experimental conditions as for Figure 5.

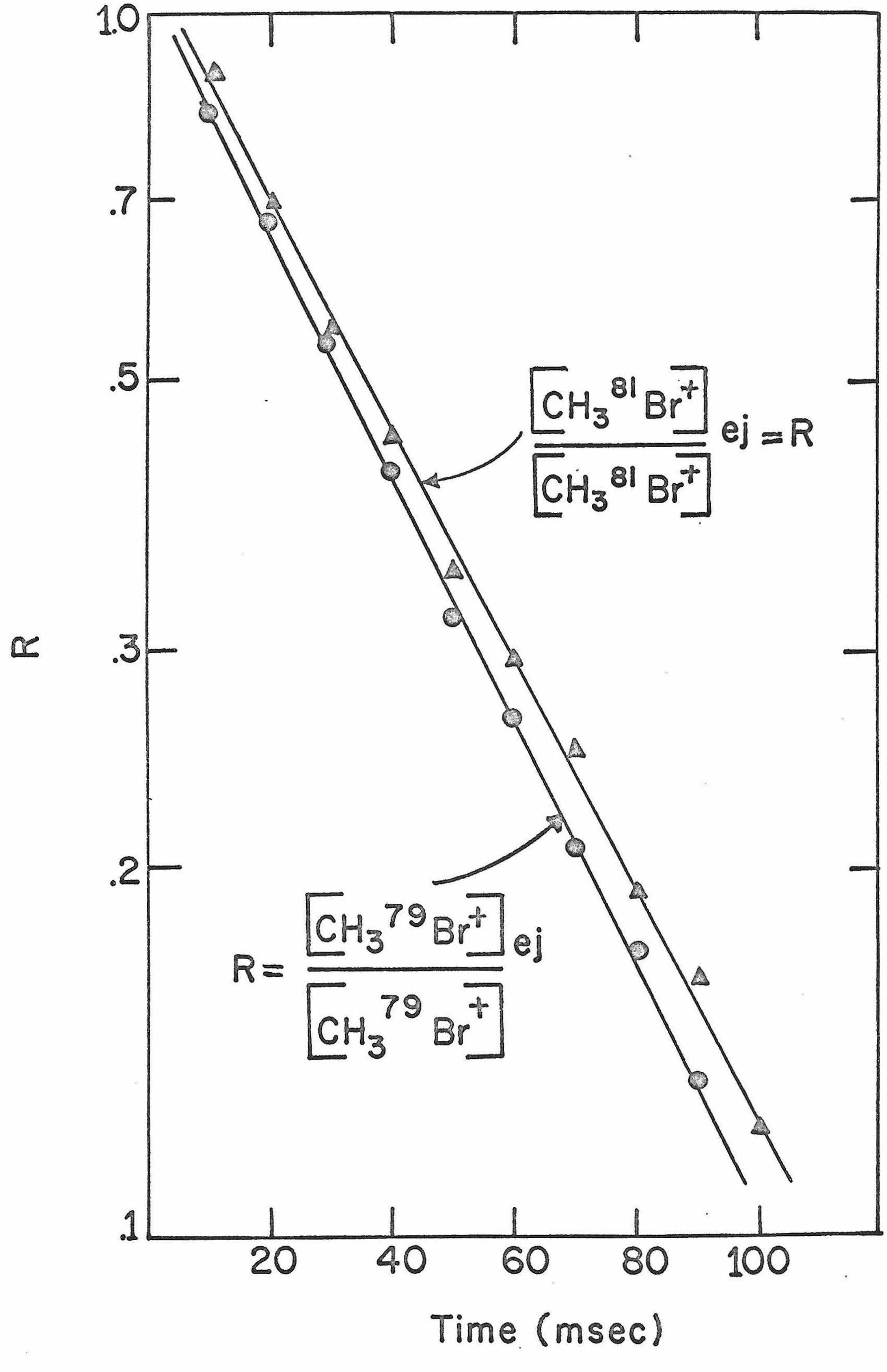
1.0
.7
.5
.3
.2
.1
R
20
40
60
80
100
Time (msec)
$\frac{[CH_3{}^{81}Br^+]_{ej}}{[CH_3{}^{81}Br^+]} = R$
$R = \frac{[CH_3{}^{79}Br^+]_{ej}}{[CH_3{}^{79}Br^+]}$

possibilities. However, it may be significant that long-range electron jump processes are a common occurrence in systems such as N_2 and CO_2.[11]

References

1. N. A. McAskill, *Aust. J. Chem.*, **23**, 2301 (1970).
2. N. A. McAskill, *ibid.*, **22**, 2275 (1969).
3. A. A. Herod, A. G. Harrison, and N. A. McAskill, *Can. J. Chem.*, **49**, 2217 (1971).
4. J. L. Beauchamp, D. Holtz, S. D. Woodgate, and S. L. Patt, *J. Amer. Chem. Soc.*, **94**, 2798 (1972).
5. A. G. Marshall and S. E. Buttrill, *J. Chem. Phys.*, **52**, 2752 (1970).
6. S. K. Gupta, E. G. Jones, A. G. Harrison, and J. J. Myher, *Can. J. Chem.*, **45**, 3107 (1967).
7. L. W. Sieck and R. Gordon, *Int. J. Chem. Kin.*, in press.
8. T. B. McMahon and J. L. Beauchamp, *Rev. Sci. Instr.*, **43**, 509 (1972).
9. T. B. McMahon, R. J. Blint, and J. L. Beauchamp, *J. Amer. Chem. Soc.*, in press.
10. Gratitude is expressed to T. B. McMahon for performing this analysis.
11. P. G. Miasek, this thesis, Chapter 13.

Chapter 10

Ion-Molecule Reactions in Methanol

The ion-molecule chemistry of methanol is a rich and interesting blend of elementary proton transfers, complex condensations and stabilization of collision complexes. The kinetics of the proton transfer reactions have been the subject of much investigation in both CH_3OH and CD_3OH and the mechanisms and rates of these processes are well characterized.[1-3] By contrast, little quantitative kinetic study has been undertaken on the subsequent reactions of the protonated molecule in forming condensation reactions and collision stabilized dimers, though the nature of these reactions is understood.[4, 5]

Under impact of 70 eV electrons, three major primary ions are formed which initiate the reaction sequence[5] outlined in Figure 1. The structure of $C_2H_7O^+$ has been confirmed[5] to be protonated dimethyl ether

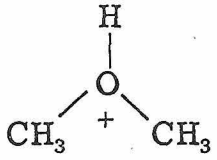

while $C_2H_9O_2^+$, the collision stabilized product of $CH_3OH_2^+ + CH_3OH$ has the likely structure II.

Figure 1

Reaction scheme in methanol (adapted from Henis [5]). Each step involves methanol as the neutral reactant. Henis has also reported reactions R11 and R13, which are collision induced decompositions of the complexes $[C_3H_{12}O_3^+]^*$ and $[C_3H_{11}O_2^+]^*$, respectively. Our kinetic data provided little evidence for these processes, which may become important only for translationally excited complexes.

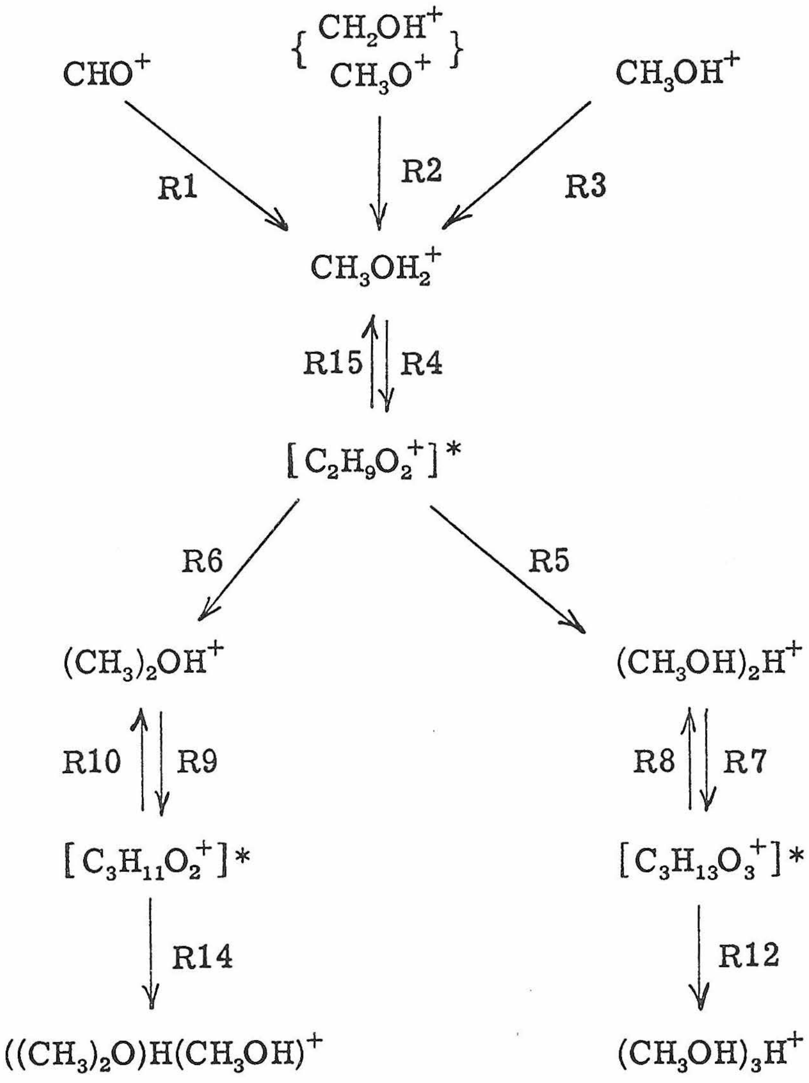
CHO$^+$
$\{CH_2OH^+$ / $CH_3O^+\}$
CH_3OH^+
R1
R2
R3
$CH_3OH_2^+$
R15
R4
$[C_2H_9O_2^+]^*$
R6
R5
$(CH_3)_2OH^+$
$(CH_3OH)_2H^+$
R10
R9
R8
R7
$[C_3H_{11}O_2^+]^*$
$[C_3H_{13}O_3^+]^*$
R14
R12
$((CH_3)_2O)H(CH_3OH)^+$
$(CH_3OH)_3H^+$

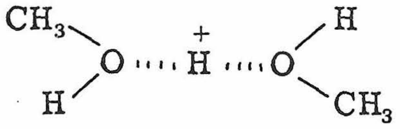

(II)

Similarly $C_3H_{11}O_2^+$ is likely the proton bound dimer of dimethyl ether and methanol, structure III

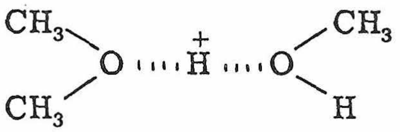

(III)

while $C_3H_{13}O_3^+$, formally the proton bound trimer,possible has two proton bridges. No ions of heavier mass have been observed in CH_3OH, supporting Munson's [4] suggestion that the maximum number of strongly bound solvent molecules about a proton is three for methanol.

Until recently there has been some doubt about the number of collisions involved in the production of $C_2H_7O^+$, $C_2H_9O_2^+$, and the higher mass ions. For instance, Sieck et al. [3] report that $C_2H_7O^+$ and $C_2H_9O_2^+$ are both third-order ions. However, the pressure dependence of our trapped ion curves agrees well with the scheme of Figure 1.

In Figure 1 it is seen that all three primary ions react to produce the protonated parent. Analysis of the reactions of CH_3OH and CD_3OH shows that this occurs via proton and hydrogen transfer from both the carbon and oxygen sites. [2, 6]

The transfer reactions are rapid, but are readily studied at fairly low pressures in the high pressure mass spectromer. Figure 2 shows typical low pressure results. In every case it was found that the abundance of CHO^+ and CH_3^+ was substantially lower than would be predicted from low pressure mass spectra.[5] The absence of CH_3^+ may arise from excess kinetic energy released on fragmentation, causing this ion to be lost in analogy with the CH_3^+ loss from CH_3F. The small amount of CHO^+ observed may result from a similar occurrence in this fragmentation. Clearly the excess kinetic energy carried by CHO^+ will be much smaller, but calculations show that even a small amount of excess energy should severely decrease the extraction efficiency.

The measured rate constants are given in Table I and compare favourably with those measured by other investigators. The primary uncertainty in our experiments is in the measurement of the total pressure. Gupta et al.[1] found that the disappearance rate of CH_2OH^+ at 50 eV was significantly lower than at 11-18 eV. They attributed this to the formation of this ion by reactions of CH_3^+ and CHO^+

$$CH_3^+ + CH_3OH \longrightarrow CH_2OH^+ + CH_4$$

$$CHO^+ + CH_3OH \longrightarrow CH_2OH^+ + CH_2O$$

Our disappearance rate for CH_2OH^+ is in excellent agreement with their low energy value, a consequence of the poor trapping efficiency for CH_3^+ and CHO^+.

Figure 2

Ion abundance versus trapping time for ions in methanol. Electron energy = 70 eV, ionizing pulse width = 15 μsec, pressure = 6×10^{-5} torr, trapping voltage = 3 V.

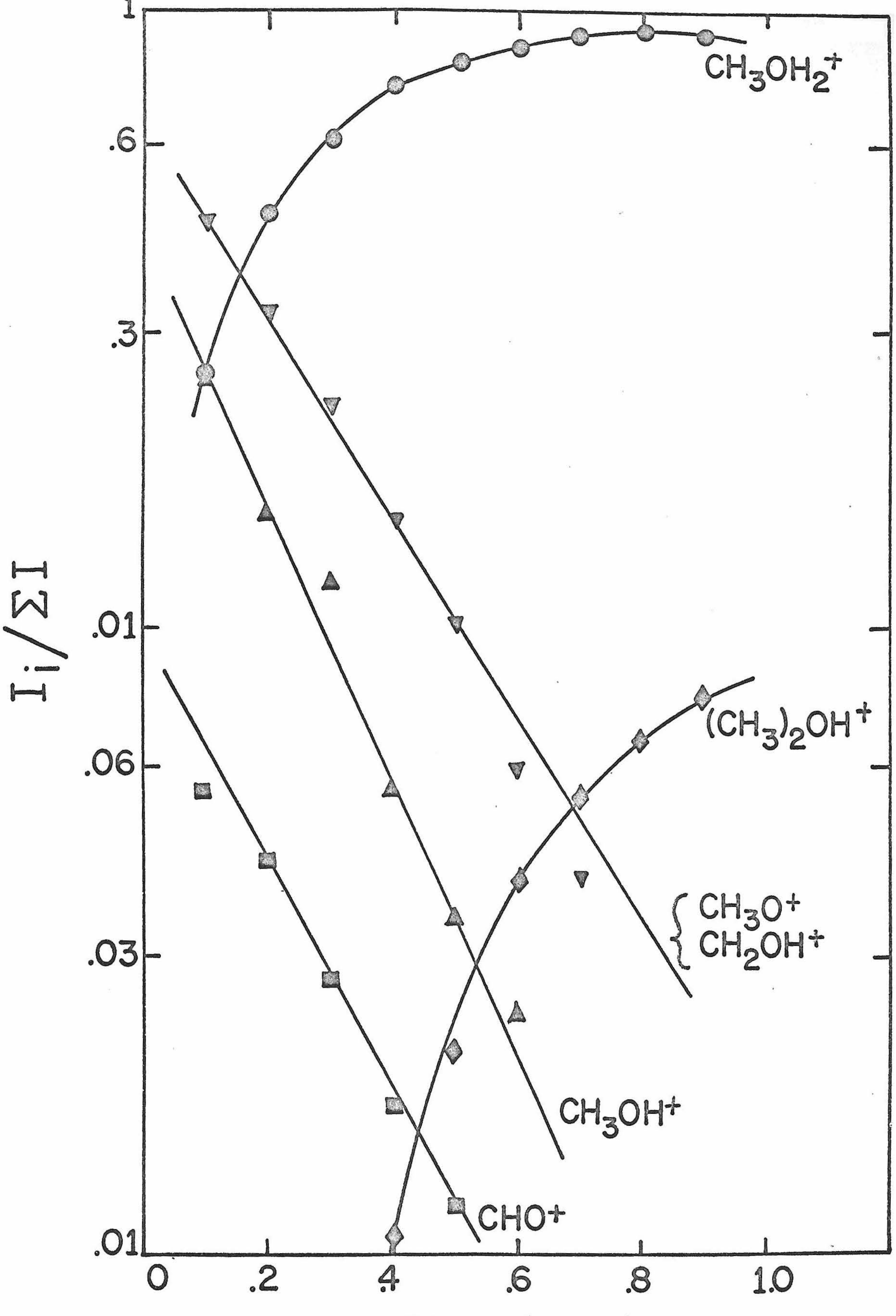

1
.6
.3
.01
.06
.03
.01
$I_i/\Sigma I$
0
.2
.4
.6
.8
1.0
Time (msec)
$CH_3OH_2^+$
$(CH_3)_2OH^+$
CH_3O^+
CH_2OH^+
CH_3OH^+
CHO^+

Table I

Primary Ion Reaction Rate Constants in CH_3OH

Reaction	Rate constant cm³ molecule⁻¹ sec⁻¹ × 10⁻⁹			
	This work	High press m.s.[a]	High press m.s.[b]	High press m.s.[c]
$CH_3OH^+ + CH_3OH \rightarrow CH_3OH_2^+ + \left\{\begin{matrix} CH_2OH \\ CH_3O \end{matrix}\right.$	$2.3 \pm .2$	2.53	2.45	2.0
$\left.\begin{matrix} CH_2OH^+ \\ CH_3O^+ \end{matrix}\right\} + CH_3OH \rightarrow CH_3OH_2^+ + CH_2O$	$2.0 \pm .2$	2.11	.7	
$CHO^+ + CH_3OH \rightarrow CH_3OH_2^+ + CO$	$1.8_5 \pm .2$	1.75		

[a] Reference 1.

[b] Reference 2.

[c] Reference 7.

It is interesting to compare the rates of protonation by the parent ions in CH_3OH and CH_3F. These two isoelectronic molecules have very similar polarizabilities and dipole moments, yet they react at substantially different rates. Table II lists some properties of interest for these molecules, and also for CH_3NH_2 and CH_3Cl.

Methanol and methyl fluoride have two important differences, one of which should account for the differing protonation rates. These are:

(a) The lowest ionization potential of CH_3F is for loss of an electron from the CH_3 molecular orbitals, while ionization in CH_3OH occurs from a lone pair on oxygen.

(b) Either the hydroxylic proton or the methyl proton can be transferred in CH_3OH, while only a methyl proton is available in CH_3F.

The site of ionization cannot be an important factor in the rate of the proton transfer, since in CH_3Cl, which exhibits virtually identical behaviour to CH_3F, the ionization occurs from the chlorine lone pairs.

We conclude that ability to transfer the hydroxylic proton or hydrogen must be responsible for the faster rate in CH_3OH. Numerous workers have studied the relative probabilities of transferring the hydroxylic and methyl H-entities in methanol. Using deuterated species, Ryan et al.[2] found that $k_{hydrox} = 11.0 \times 10^{-10}$, $k_{methyl} = 13.5 \times 10^{-10}$, while Gupta et al.[1] measured $k_{hydrox} = 9.9 \times 10^{-10}$, $k_{methyl} = 12.0 \times 10^{-10}$, with all rates in cm^3 $molecule^{-1}$

Table II

Properties of CH_3OH, CH_3F, CH_3Cl and CH_3NH_2

	α (Å^3)	μ (debeye)	Rate constant (cm^3 molecule^{-1} sec^{-1} × 10^{-9})		
			k_{Lang}^{a}	k_{LD}^{b}	k_{Prot}^{c}
CH_3OH	3.25	1.70	1.02	4.80	2.3 [d]
CH_3NH_2	3.92	1.27	1.18	4.14	2.1 [e]
CH_3F	2.57	1.79	.91	4.89	1.5 [f]
CH_3Cl	4.44	1.87	.99	4.62	1.2 [f]

[a] Langevin rate.

[b] Locked dipole rate.

[c] Rate of protonation by parent ion.

[d] This work.

[e] E. G. Jones and A. G. Harrison, Can. J. Chem., 45, 3119 (1967).

[f] This thesis, Chapter 9.

sec^{-1}. The sum of these rates is in good agreement with the total measured disappearance rate of CH_3OH^+. In addition, and of considerable importance, k_{methyl} is very close to the protonation rates in CH_3F and CH_3Cl.

Similar conclusions can be drawn from the methyl amine protonation rate, which, in view of the slightly reduced collision frequency, is again roughly twice as fast as the methyl fluoride rate.

These results present an interesting picture concerning the collision dynamics in these three gases. First, it is assumed that the site of ionization is not an important factor in H-entity transfer. This follows from a comparison of CH_3F and CH_3Cl. Apparently, as far as the neutral is concerned, the ion is an isotropic charged sphere and the site of collision at the ion is randomly chosen.

It is evident that in CH_3OH and CH_3NH_2, the protonation rate is very rapid, because H-entities on both the methyl group and on the heteroatom site are available and readily transferred. Probably the reaction has almost unit efficiency per collision. In CH_3F, exhibiting a similar collision rate, about 50% of the ion-neutral encounters must then be unreactive, probably those where halogen collides only with halogen. The transfer of a methyl H-entity is again a very favourable process, and occurs whenever a suitable collision has occurred. Interestingly, the similarities in the rates for CH_3OH and CH_3NH_2 suggests that one hydrogen on the heteroatom is sufficient to ensure that all collisions at that site are reactive.

Returning to CH_3OH alone, the rates of all three primary ions are substantially above the Langevin, angle-averaged value and indicate a large degree of ion-dipole locking. The rate of primary ion disappearance is among the faster ion-molecule reactions known,[1] a consequence of the availability of two reactive sites.

At higher pressures, the reactions of the primary ions are fast enough and complete enough that $CH_3OH_2^+$ can be treated as a primary ion initiating the remainder of the reaction sequence in Figure 1. A typical ion abundance-reaction time curve is given in Figure 3. Pressures ranging from 1 μ to 10 μ were employed, but no $(CH_3OH)_3H^+$ was detected in any of these runs. This ion was observed in small abundance by Henis in an ICR spectrometer at a pressure of 1 μ and a reaction time of around 100 msec. Evidently the reaction times in our experiments were too small for this ion to be formed to an appreciable extent.

If $CH_3OH_2^+$ is treated as a primary ion, then the disappearance rate of this ion is readily shown to be $k_4 \frac{nk_5 + k_6}{k_{15} + nk_5 + k_6}$, where n is the neutral pressure. At low pressures $nk_5 \ll k_6$, and the rate of the $CH_3OH_2^+$ disappearance is simply $\frac{k_4\, k_6}{k_{15} + k_6}$. This quantity was determined to be $1.0 \pm .1 \times 10^{-10}$ cm^3 molecule^{-1} sec^{-1}. The rate of complex formation (k_4) can reasonably be assumed to be similar to the rate of protonation, since the parameters determining the collision rate are nearly the same in each. If k_4 is thus assumed to be about 2.0×10^{-9} cm^3 molecule^{-1} sec^{-1}, then the quantity $k_6/(k_6 + k_{15}) \sim 1/20$, or $k_6/k_{15} \sim 1/20$. It is noted that k_{15} is a measure of the rate of

Figure 3

Variation of ion abundance with reaction time in methanol. Electron energy = 70 eV, ionizing pulse width = 15 μsec, pressure = 4.5×10^{-3} torr, trapping voltage = 3 V.

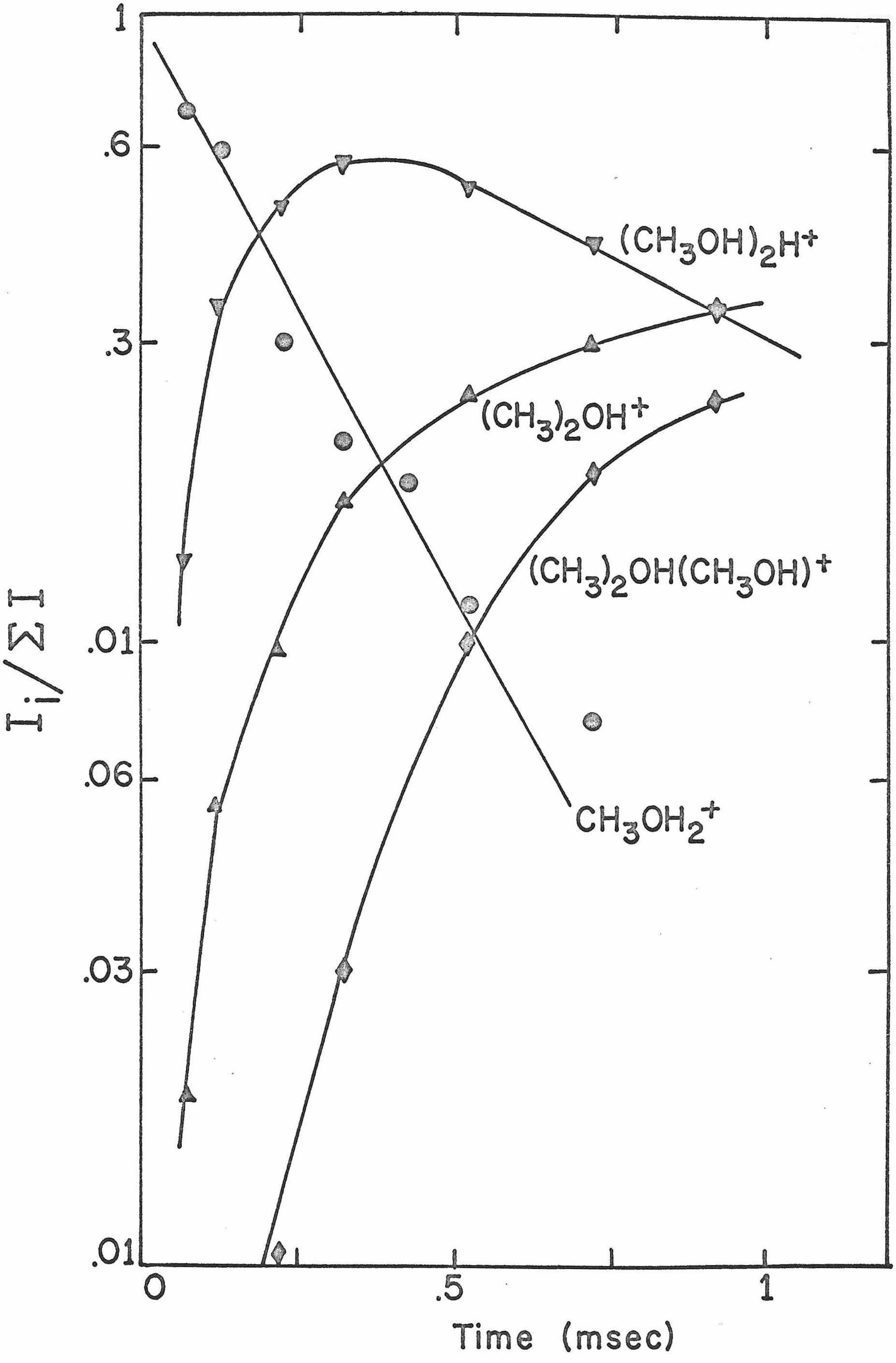
1
.6
.3
.01
.06
.03
.01
$I_i/\Sigma I$
0
.5
1
Time (msec)
$(CH_3OH)_2H^+$
$(CH_3)_2OH^+$
$(CH_3)_2OH(CH_3OH)^+$
$CH_3OH_2^+$

symmetric proton transfer in methanol, which is known to occur in a somewhat analogous fashion to symmetric proton transfer in the alkyl halides. Using CD_3OH, investigators have determined the rate of symmetric proton transfer by monitoring

$$CD_3OHP^+ + CD_3OH \xrightarrow{k_{sym}} CD_3OH_2^+ + CD_3OH \qquad (R16)$$

the $[CD_3OHD^+]/[CD_3OH_2^+]$ ratio as a function of pressure. The only absolute measurement of this rate has been made by McMahon,[9] who found $k_{sym} = 4.4 \times 10^{-10}$ cm^3 $molecule^{-1}$ sec^{-1}.

There are two possible intermediate complexes for reaction R16. The first of these, containing a linear proton bridge, would result

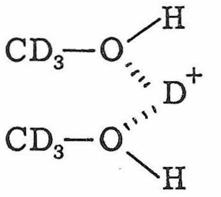

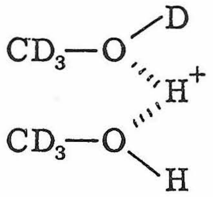

in $CD_3OH_2^+$ on one encounter in four, if no isotope effect is present. Alternatively, a four membered ring complex could be formed

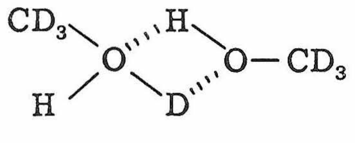

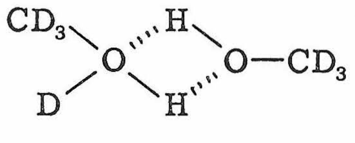

which would fragment to $CD_3OH_2^+$ on one encounter in three in the absence of isotope effects. Using McMahon's value for k_{sym}, the total encounter rate for proton transfer is thus either 1.76×10^{-9}

cm^3 molecule^{-1} sec^{-1} or 1.32×10^{-9} cm^3 molecule^{-1} sec^{-1}, depending on the model used. Referring back to the analysis in pure methanol, this encounter rate is also given by

$$k_4 \frac{k_{15}}{k_6 + k_{15}} \sim .95\, k_4$$

Assuming again that $k_4 \sim 2.0 \times 10^{-9}$ cm^3 molecule^{-1} sec^{-1}, the encounter rate for symmetric proton transfer is thus 1.9×10^{-9} cm^3 molecule^{-1} sec^{-1}, in good agreement with the rate measured by McMahon. It is impossible to distinguish between the two complexes for proton transfer, as the isotope effect is unknown.

Under conditions where minimal further reaction of $(CH_3)_2OH^+$ or $(CH_3OH)_2H^+$ is expected, the ratio $[(CH_3OH)_2H^+]/[(CH_3)_2OH^+]$ is expected to give the quantity $[CH_3OH]k_5/k_6$. These conditions are achieved at low and intermediate pressures, and a plot of $[(CH_2OH)_2H^+]/[(CH_3)_2OH^+]$ versus pressure is a straight line of slope $k_5/k_6 = 2.0 \pm 1 \times 10^{-15}$ cm^3 molecule^{-1}. The uncertainty in this number is due to an unexplainable change in this ratio with reaction time of about 50% above and below the mean value. This result predicts that at a pressure of $\sim 15\ \mu$, the initial rates of formation of $(CH_3)_2OH^+$ and $(CH_3OH)_2H^+$ from $[C_2H_9O_2^+]^*$ should be equal.

An upper limit to the rate of $[C_2H_9O_2^+]^*$ stabilization, k_5, can be estimated by using for this quantity the collision rate between an ion of mass 65 and CH_3OH. This number is again about 2.0×10^{-9} cm^3 molecule^{-1} sec^{-1}, and would represent k_5 if all collisions were effective in stabilizing the excited dimer. These results permit a lower limit on the lifetime of $(C_2H_9O_2^+)^*$ to be estimated as $\sim 5 \times 10^{-8}$ sec. Henis has estimated the lifetime of this ion to be $\sim 2 \times 10^{-6}$ sec; however his qualitative analysis is erroneous as it fails to consider the statistical implications inherent in the definition of a lifetime. It may be remarked that his data, subject to the above analysis, gives a lifetime of 8×10^{-8} sec.

An estimation of the lifetime of $(C_3H_{11}O_2^+)^*$, the methanol-dimethyl ether complex, can also be made. For this determination, it is convenient to consider the time when the $C_2H_7O^+$ ion abundance reaches a maximum. At this point, the rates of formation and reaction of this ion are identical, and a kinetic analysis with appropriate approximations, shows that

$$\frac{n k_{14}}{k_{10} + n k_{14}} = \frac{k_4}{20\, k_9} \frac{[CH_3OH_2^+]}{[(CH_3)_2OH^+]} \cdot \qquad (1)$$

Since k_4 and k_9 represent the collision rates of $CH_3OH_2^+$ and $C_2H_7O^+$, they can be assumed to be nearly identical and the quantity on the right side of Equation (1) reduces simply to .05 of the abundance ratio of $CH_3OH_2^+$ and $(CH_3)_2OH^+$. Typical values of this ratio over the pressure interval studied ranged from 1/5 to 2/3. Hence the right side of Equation (1) is very small, implying that $k_{10} \gg n k_{14}$. Accordingly, Equation (1) may be simplified to

$$\frac{n k_{14}}{k_{10}} = \frac{1}{20} \frac{[CH_3OH_2^+]}{[(CH_3)_2OH^+]} . \qquad (2)$$

A plot of the ionic ratio versus pressure yields k_{14}/k_{10} directly. If k_{14} can again be assumed to be the collision rate of $(C_3H_{11}O_2^+)^*$, then k_{10} can be found to be $2.2 \pm .7 \times 10^7$ sec^{-1}.

This analysis was also repeated including an additional process, R13, involving the collisional dissociation of the dimethyl ether-methanol complex to form $CH_3OH_2^+$. This channel was included by Henis in his reactive scheme for methanol (Figure 1). In this case, Equation (2) becomes

$$\frac{n k_{14}}{k_{10}} + \frac{k_{13}}{k_{10}} = \frac{1}{20} \frac{[CH_3OH_2^+]}{[(CH_3)_2OH^+]} \qquad (2a)$$

and a plot of the ionic ratio versus pressure yields k_{13}/k_{10} as the zero intercept. The rate k_{13} was found to be $2 \pm 2 \times 10^{+5}$ sec^{-1}, or only about 1% of k_{14}. This suggests that R13 is only a very improbable dissociative channel of $(C_3H_{11}O_2^+)^*$.

The slow rate of R13 is not surprising, since, for ground state dimethyl ether and methanol, it is endothermic by ~6 kcal/mole. Accordingly, this process can only occur for $(CH_3)_2OH^+$ with excess internal energy. The lifetime of $(C_3H_{11}O_2^+)^*$ is determined to be $4.5 \pm 1.5 \times 10^{-8}$ sec, which is comparable to the lifetime of $(C_2H_9O_2^+)^*$.

The rate constants k_{10} and k_{13} can also be determined, with suitable approximations, from the slope of the $(CH_3)_2OH^+$ decay curve at long times. This method gave the same results as those above.

A summary of all the rate constants determined in methanol is given in Table III. The values of k_1-k_3, k_{15} and k_6 are known with some certainty, but more accurate determination of k_{10} and k_{13} are required. If the present values are correct, they would be of considerable chemical interest, as they would indicate that the additional degrees of freedom in $(C_3H_{11}O_2^+)^*$ do not substantially increase its lifetime over that of $(C_2H_9O_2^+)^*$. The excess internal energy, E*, with respect to the ground state of the complex, is simply the energy of the proton bond plus any kinetic energy present initially or gained from the ion-neutral attraction. For $(CH_3OH)_2H^+$, the bond energy has been measured by Kebarle et al.[10] to be 31 kcal/mole. For $(CH_3)_2OH(CH_3OH)^+$, this bond energy is unknown but is probably close to this value, just as the bond strength in $(H_2O)_2H^+$ is similar to that for $(CH_3OH)_2H^+$. The extent of energy loss to effect a stable complex is unknown.

The lifetimes of the collision complexes formed in methanol all appear to be about 5×10^{-8} sec. They are markedly higher than the lifetimes of collision complexes in the alkyl halides, where no collision complexes have been observed in our investigations of these systems. A comparison of the reactions of the protonated parents is particularly illustrative. In each case, symmetric proton transfer efficiently deactivates the protonated parent to its ground state. The excess internal energy E* present in the complex, with respect to the ground state, is the sum of any kinetic energy of the reactants plus the dissociation energy of the proton bridge bond, typically 20-30

Table III

Rate Constants in Methanol

	Rate constant cm^3 molecule^{-1} sec^{-1} [a]
k_1	1.85×10^{-9}
k_2	2.0×10^{-9}
k_3	2.3×10^{-9}
k_4	2.0×10^{-9} (assumed)
k_{15}	2×10^{7} sec^{-1}
k_5	2.0×10^{-9} (assumed)
k_6	1×10^{6} sec^{-1}
k_9	2.0×10^{-9} (assumed)
k_{10}	$2.2 \pm .7 \times 10^{7}$ sec^{-1}
k_{13}	$2 \pm 2 \times 10^{5}$ sec^{-1}
k_{14}	2.0×10^{-9} (assumed)

[a] Except where otherwise specified.

kcal/mole.[10] Evidently in methanol this energy is sufficiently delocalized over other vibrational modes of the complex, while in the alkyl halides enough of this energy remains localized to effect rapid dissociation. These two systems differ only in that methanol has an additional O–H bond. This suggests that the presence of this bond is the critical factor leading to the long lifetime of $[(CH_3OH)_2H^+]^*$. The availability of this additional O–H bond for further hydrogen bonding provides a facile route for the deactivation of the complex. Thus the deactivation mechanism M1 is implicated

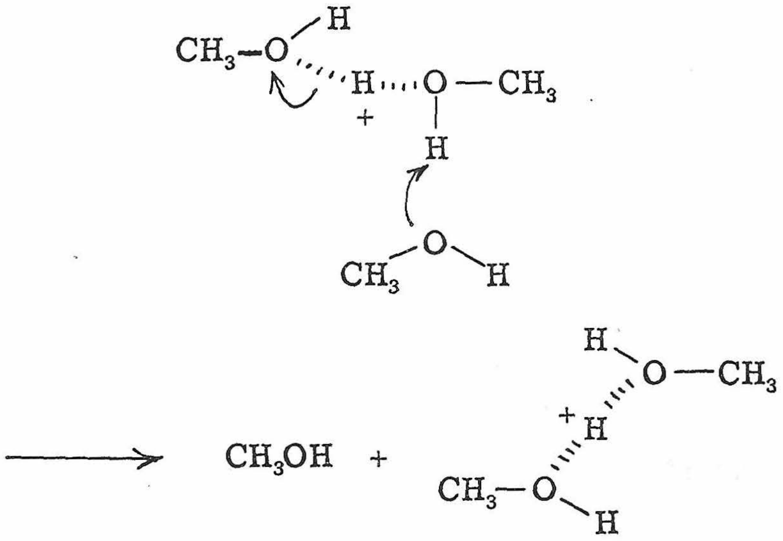

(M1)

The analogous process in the alkyl halides is not possible.

References

1. S. K. Gupta, E. G. Jones, A. G. Harrison, and J. J. Myher, Can. J. Chem., 45, 3107 (1967).
2. K. R. Ryan, L. W. Sieck, and J. H. Futrell, J. Chem. Phys., 41, 111 (1964).
3. L. W. Sieck, J. H. Futrell, and F. P. Abramson, J. Chem. Phys., 45, 2859 (1966).
4. M. S. B. Munson, J. Amer. Chem. Soc., 87, 5313 (1965).
5. J. M. S. Henis, J. Amer. Chem. Soc., 90, 844 (1968).
6. E. Lindholm and P. Wilmenius, Arkiv. Kimi, 20, 255 (1963).
7. D. J. Hyatt, E. A. Dodman, and M. J. Henchman, Adv. Chem. Ser., 58, 131 (1966).
8. J. L. Beauchamp, D. Holtz, S. D. Woodgate, and S. L. Patt, J. Amer. Chem. Soc., 94, 2798 (1972).
9. T. B. McMahon, Candidacy Report, California Institute of Technology, 1971.
10. P. Kebarle, R. N. Haynes, and J. G. Collins, J. Amer. Chem. Soc., 89, 5753 (1967) have measured the hydrogen bond strength in $(CH_3OH)_2H^+$ to be 31 kcal/mole.
11. D. P. Ridge and J. L. Beauchamp, J. Amer. Chem. Soc., 93, 5125 (1971) and references therein.

Chapter 11

Ion-Molecule Reactions in CH_2F_2 and CHF_3

The gas phase ion chemistry of the fluoromethane has recently been the subject of considerable investigation in these laboratories.[1, 2] Using ion cyclotron resonance spectroscopy, the kinetics of reactions involving parent and fragment ions have been studied. Fluoride transfer reactions are the most prevalent processes, and their detailed examination has provided information relating to carbonium ion stabilities.

These results are complemented by those obtained from a study of the same systems using the high pressure mass spectrometer. The different observation times of the two instruments lead, in some cases, to significant differences in the ion chemistry.

The investigation of the ion molecule reactions of CH_3F has been reported in detail in Chapter 9. Thermochemical inferences are presented in Reference 2.

I. Methylene Fluoride

At 70 eV electron energy, CH_2F_2 fragments to produce mainly CF_2H^+ and CH_2F^+. In addition, small amounts of CF^+ and parent ion, $CF_2H_2^+$, are present. Mass discrimination at the electron multiplier was investigated by comparing a low pressure-short time mass spectrum of a mixture of N_2, H_2S, CO_2 and CH_3Cl with a low pressure ICR spectrum of the same mixture. No systematic discrimination was found over this mass range. The variation of ion abundance with time is shown in Figure 1.

The parent ion reacts rapidly to form the protonated parent by reaction R1

$$CH_2F_2^+ + CH_2F_2 \longrightarrow CH_2F_2H^+ + CHF_2 \qquad (R1)$$

Blint et al.[2] report that this ion reacts further producing $(CH_2F)_2F^+$, as in methyl fluoride, but this ion could not be measured due to its low abundance at long times. The ion CF_2H^+ reacts via fluoride transfer producing CH_2F^+, which becomes the dominant ion at long times. The final ion, CF^+, disappears by an unknown mechanism,

$$CHF_2^+ + CH_2F_2 \longrightarrow CH_2F^+ + CHF_3 \qquad (R2)$$

though several feasible reactions are potentially available (R3-R5).[3]

$$CF^+ + CH_2F_2 \longrightarrow CF + CH_2F_2^+ \qquad \Delta H = -320 \text{ kcal/mole} \qquad (R3)$$

$$CF^+ + CH_2F_2 \longrightarrow CH_2 + CHF_2^+ \qquad \Delta H = -250 \text{ kcal/mole} \qquad (R4)$$

$$CF^+ + CH_2F_2 \longrightarrow CH_2F^+ + CF_2 \qquad \Delta H = -20 \text{ kcal/mole} \qquad (R5)$$

The charge exchange reaction (R 3) would be expected to produce a significant initial curvature in the $CF_2H_2^+$ decay curve. Since none was observed, this suggests that either the hydride or fluoride

Figure 1

Variation of ion abundance with reaction time in CH_2F_2. Electron energy = 70 eV, pressure = 6.7×10^{-4} torr, trapping voltage = 4 volts. Protonated parent abundance not shown.

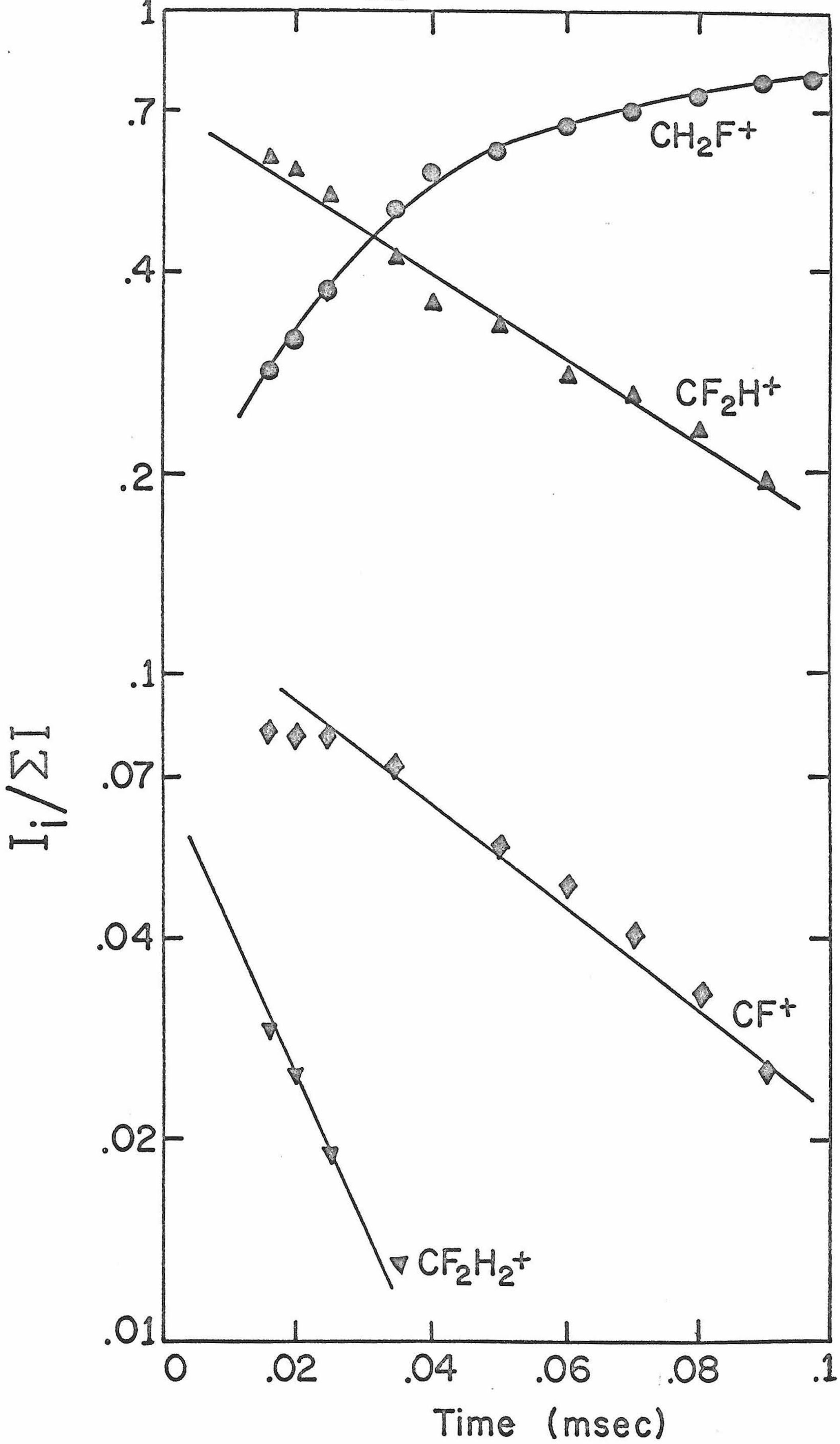
1
.7
.4
.2
.1
.07
.04
.02
.01
$I_i/\Sigma I$
0
.02
.04
.06
.08
.1
Time (msec)
CH_2F^+
CF_2H^+
CF^+
$CF_2H_2^+$

transfer reactions must occur. Any resulting curvature in either the CH_2F^+ or CF_2H^+ curves would be too small to be seen.

The measured rate constants are given in Table I together with the rates measured by Blint et al. and by Harrison and McAskill[3] using high pressure mass spectrometry. The rate of protonation is considerably larger than the Langevin rate and is, in fact, rather close to the rate of protonation in methyl fluoride. Interestingly, methyl fluoride has an electric polarizability and dipole moment within 10% of those of methylene fluoride. Evidently considerable dipole locking enhances these protonation reaction rates.

The rate of fluoride transfer is roughly half that of the protonation rate, and similar to the disappearance rate of CF^+. The disappearance rates of these two ions are exactly in the ratio of their Langevin rates, suggesting that the same process occurs in each. This would be evidence favouring R5 as the disappearance route for CF^+. The rate of R2 is in marked disagreement with the results of the low pressure, ICR investigations. The difference was large enough that twelve separate determinations of this rate were made, over pressures ranging from .1 to 1.1 μ and reaction times from .1 msec to .5 msec. In addition, the rate constant was determined by varying the pressure and using constant reaction times of .1 and .2 msec. There was no systematic variation in the rates with either reaction time or pressure, although this is not unexpected since the dynamic range of these variables was not large. The average of all these determinations gave $6 \pm 1.5 \times 10^{-10}$ cm^3 $molecule^{-1}$ sec^{-1}.

Table I

Rate Constants in CH_2F_2

Reaction	Rate constant (cm^3 molecule^{-1} sec^{-1} × 10^{-9})				
	This work	ICR[b]	High press m. s.[c]	k_{Lang}^{d}	k_{LD}^{e}
$CH_2F_2^+ + CH_2F_2 \rightarrow CH_2F_2H^+ + CHF_2$	1.5 ± .1	1.3	1.99	.76	4.30
$CF_2H^+ + CH_2F_2 \rightarrow CH_2F^+ + CF_3H$	.60 ± .15	.19	.40	.77	4.33
$CF^+ + CH_2F_2 \rightarrow CH_2F^+ + CF_2$[a]	.75 ± .15	—	.75	.90	4.98

[a] Assumed products, as discussed in text.

[b] Reference 2.   [c] Reference 3.

[d] Langevin rate, using $\alpha(CH_2F_2) = 2.69\ \mathring{A}^3$.

[e] Locked-dipole rate, using $\mu = 1.96$ D.

The difference between the high pressure results and those obtained by ICR is large enough that it cannot easily be attributable to random error. It appears that it must be a direct consequence of the nature of the experimental parameters. The experiments differed in three significant ways. First, while the high pressure experiments used an electron energy of 70 eV, the ICR experiments used ionizing energies of 17 eV. Second, the typical observation times in the high pressure instrument were 20-500 μsec, which are at least two orders of magnitude shorter than those used for the trapped-ion ICR experiments. Finally, the reactant kinetic energies are somewhat lower, with centre of mass energies in the ICR being typically .1 eV (for a trapping voltage of 1 volt) as compared to .4 eV in the high pressure instrument. As the fluoride transfer reaction, R2, is nearly thermoneutral ($\Delta H = -0.3$ kcal/mole [1]), the additional kinetic energy could be sufficient to enhance the rate.

If kinetic energy effects are unimportant, then these results provide evidence for the existence of different states of CF_2H^+ with significantly different efficiencies of fluoride transfer. The radiative lifetimes of excited electronic states are generally short enough [5] (10^{-8} sec) that all ions should be in their ground electronic states in both experiments. The lifetimes of vibrational states may be estimated from the Einstein A coefficient for spontaneous emission, [5]

$$A_{mn} = \frac{64\pi^4\nu^3}{3hc^3}|R_{mn}|^2, \qquad (1)$$

where ν is the transition frequency, R_{mn} is the matrix element of the dipole moment between states m and n, and the other symbols have their usual meaning. For a harmonic oscillator only transitions between adjacent vibrational states can take place, and[6]

$$|R_{n,\,n-1}|^2 = \frac{e^2 h n}{8\pi^2 \mu \nu}, \tag{2}$$

where μ is the reduced mass. Thus

$$A_{n,\,n-1} = \frac{8\pi^2 \nu^2 e^2 n}{3\mu c^3}. \tag{3}$$

While not directly applicable to CF_2H^+, this quantity nevertheless should give an order of magnitude estimation for the infra-red lifetime of CF_2H^+. Using a vibrational frequency of 2000 ± 1000 cm^{-1}, a reduced mass between 1 and 10 amu and n between 1 and 5, the lifetime τ of vibrationally excited CF_2H^+ is found to be between .5 msec and 200 msec. Typically, radiative lifetimes are about 10 msec.[5] Thus the likelihood of the participation of vibrationally excited CF_2H^+ in the high pressure instrument is considerable. Since observing times in the ICR were typically 100 msec, it is likely that only ground state ions were present in those experiments.

As the fluoride transfer reaction is nearly thermoneutral, excess vibrational energy could easily have a significant effect on this rate. Thus the different results in the two experiments can be qualitatively rationalized. In addition, preliminary ICR results[7] using short trapping times (10 msec) seem to indicate that the fluoride transfer rate increases at these short times. This lends credence to a mechanism involving the participation of excited vibrational states.

II. Fluoroform

The principal fragment ions derived from CHF_3 at all electron energies are CF_3^+ and CHF_2^+. No parent ion was detected. Only the fluoride reaction R6 was observed, where the product ion CHF_2^+ is unreactive.

$$CF_3^+ + CF_3H \longrightarrow CF_2H^+ + CF_4 \qquad (R6)$$

The rate constant was determined at a variety of reaction times and pressures similar to those employed in the study of R2. In addition, runs at constant reaction times and variable pressures were again used. All determinations were in good agreement, yielding a rate constant of $5.3 \pm .5 \times 10^{-10}$ cm^3 molecule^{-1} sec^{-1}. This value again is more than twice as fast as the value of 2.1×10^{-10} cm^3 molecule^{-1} sec^{-1} measured by Blint et al.,[2] but in excellent agreement with McAskill's[8] high pressure result of 5.9×10^{-10} cm^3 molecule^{-1} sec^{-1}. A mechanism involving vibrationally excited states of CF_3^+ with lifetimes between .1 and 20 msec is again implicated.

III. Methylene Fluoride and Fluoroform

The reaction sequences in CH_2F_2 and CHF_3 lead to the formation of CH_2F^+ and CHF_2^+, respectively, as the most abundant ions at long times. In a mixture of these two gases, reaction R2 can occur reversibly. This behaviour is

$$CHF_2^+ + CH_2F_2 \rightleftharpoons CH_2F^+ + CHF_3 \qquad (R2)$$

observed in the variation of ionic abundance with pressure at 70 eV, shown for a 1.85:1 mixture of CH_2F_2 and CHF_3 in Figure 2. Above 8×10^{-4} torr, the relative concentrations attain a constant value, leading to an equilibrium constant for R2 as written of .80 ± .03. Similar measurements were made with other mixtures. In addition, the variation of ionic abundance with time at a constant pressure was examined, as in Figure 3. At pressures between .5 and 1 μ, equilibrium was generally reached after 200 μsec.

The good agreement between the equilibrium constant determined in this work and that found by Blint et al. of .69 ± .05 suggests that the participation of states with lifetimes comparable to or slightly greater than the observing time at high pressures is not significant. Evidently, if these excited ionic states exist, they deactivate to the ground state by successive fluoride transfers.

The equilibrium constant $K_{303} = .80$ corresponds to $\Delta G^\circ_{303} = .15$ kcal/mole for reaction R2 as written. The entropy change ΔS°_{303} can be estimated to be -1.86 eu,[1] giving $\Delta H^\circ_{303} = -.4$ kcal/mole.

The temperature dependence of the equilibrium constant was briefly investigated. The ion source and gas inlet system was heated to 110°C by wrapping heating tape around the vacuum housing. Aluminum foil was used to thermally insulate this portion of the system. The temperature was measured with a thermometer in contact with the vacuum housing. The uncertainty in this temperature

Figure 2

Variation of ion abundance with pressure in a 1.85:1 mixture of CH_2F_2 and CHF_3. The electron energy was 70 eV and the observing time was 200 μsec. The ion CF_3^+, present in small abundance at low pressures, is not shown.

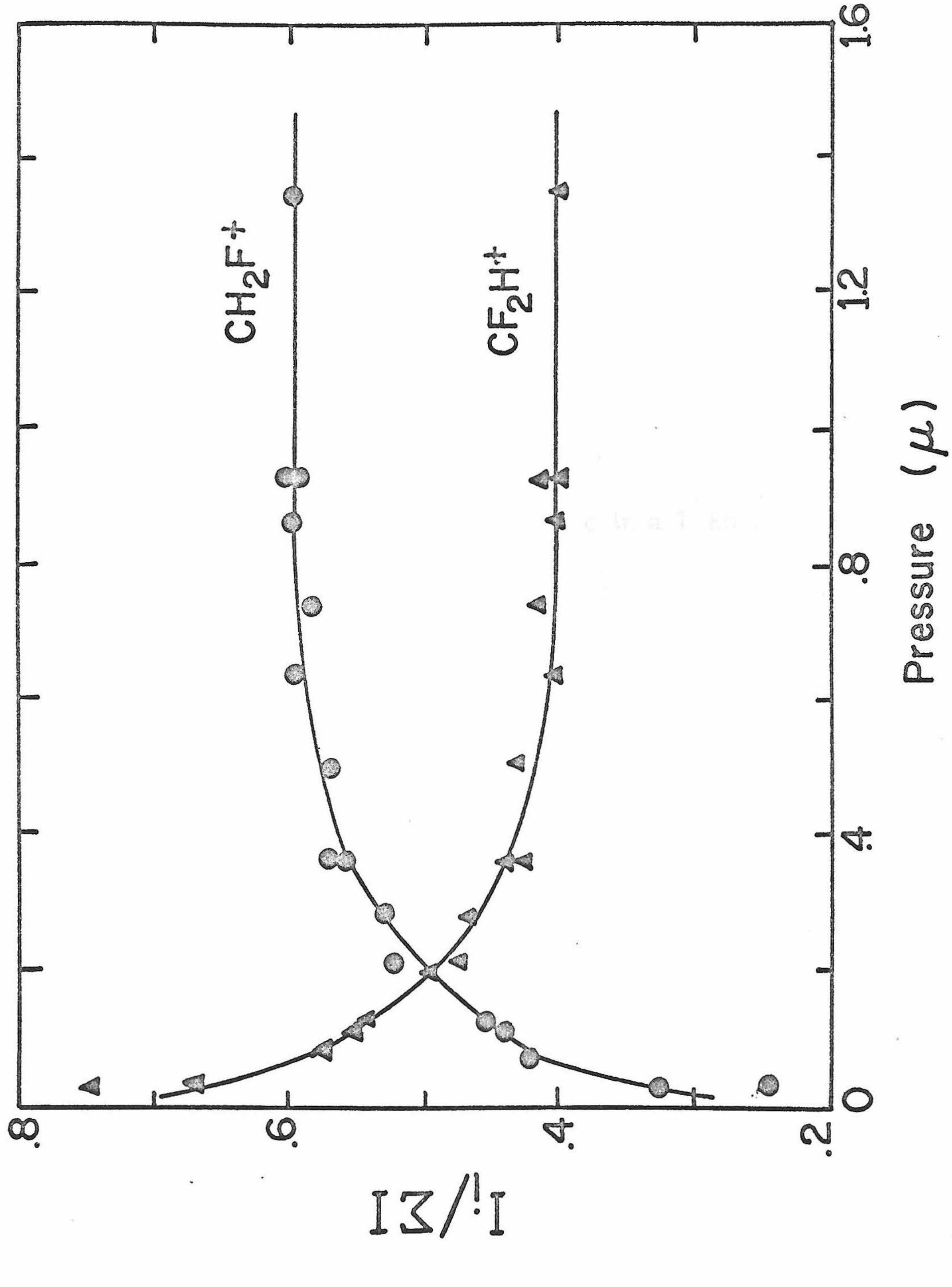
CH_2F^+
CF_2H^+
Pressure (μ)
$I_i/\Sigma I$
0
.4
.8
1.2
1.6
.2
.4
.6
.8

Figure 3

Variation of ion abundance with time in a 1.85:1 mixture of CH_2F_2 and CHF_3 at 30°C and 110°C. The electron energy was 70 eV and the pressure, as measured by a capacitance manometer kept at 30°C, was 5.6×10^{-4} torr.

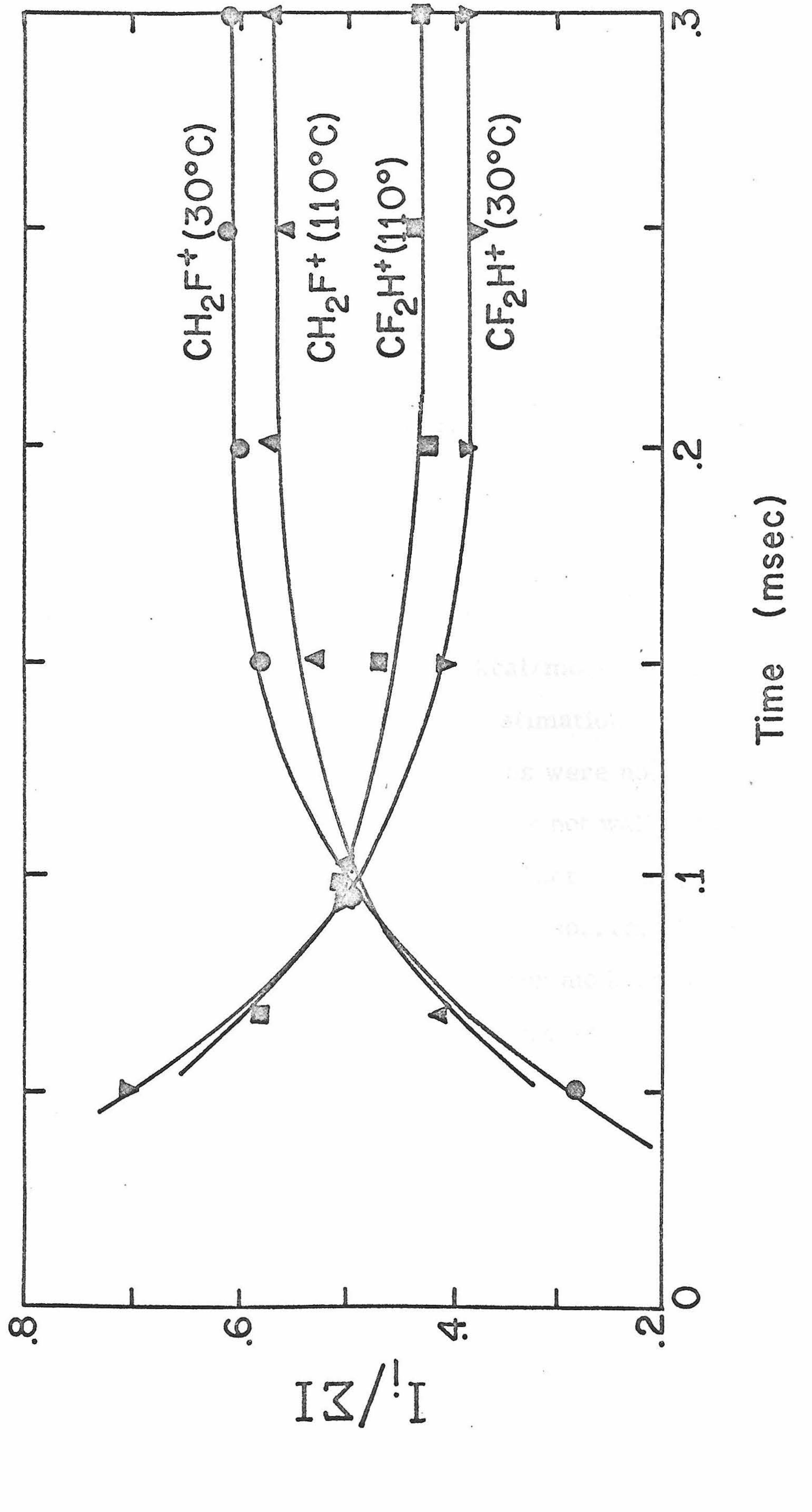
CH_2F^+ (30°C)
CH_2F^+ (110°C)
CF_2H^+ (110°)
CF_2H^+ (30°C)
$I_i/\Sigma I$
.2
.4
.6
.8
0
.1
.2
.3
Time (msec)

should be less than 20°C. The long gas inlet tube and the good thermal contact between the ion source and the external flanges ensures that thermal equilibrium between the gas and the vacuum housing should be attained. Figure 2 illustrates the time dependence of the ionic concentrations for the mixture described previously. The equilibrium constant was found to be $K_{383} = .70 \pm .03$. Using the von't Hoff equation

$$\ell n \frac{K_2}{K_1} = -\frac{\Delta H}{R}\left(\frac{1}{T_2} - \frac{1}{T_1}\right) \tag{1}$$

the enthalpy change of R2 is found to be -.38 kcal/mole, in excellent agreement with the value calculated using an estimation of ΔS°_{303}.

More comprehensive temperature studies were not undertaken as the reaction chamber and gas inlet system are not well designed for uniform heating of the system. In addition, there is no provision for directly measuring the temperature of the ion source. Elimination of these objections would not require major modifications to the instrument. The present studies already demonstrate many of the inherent advantages of this instrument for variable temperature studies.

The calculation of the entropy change in ion-molecule reactions is often very dependent on the assumed ion structures. For example, in the case of R2, the rotational entropy difference of the ions was the dominant term in ΔS°_{303}. The absolute determination of ΔS from the temperature dependence of ion-molecule reactions is thus a useful tool in the elucidation of ion structures.

References

1. T. B. McMahon, R. J. Blint, D. P. Ridge, and J. L. Beauchamp, J. Amer. Chem. Soc., **94**, 8934 (1972).
2. R. J. Blint, T. B. McMahon, and J. L. Beauchamp, J. Amer. Chem. Soc., in press.
3. A. G. Harrison and N. A. McAskill, Aust. J. Chem., **24**, 1611 (1971).
4. Heats of formation for species in R3-R5 taken from Reference 2 and from "Ionization Potentials, Appearance Potentials, and Heats of Formation of Gaseous Positive Ions," National Bureau of Standards Publication, NSRDS-NBS26.
5. T. L. Cottrell, "Dynamic Aspects of Molecular Energy States," Oliver and Boyd, London, 1965.
6. L. Pauling and E. B. Wilson, "Introduction to Quantum Mechanics," McGraw-Hill, New York, 1935.
7. T. B. McMahon, personal communication.
8. N. A. McAskill, Aust. J. Chem., **23**, 893 (1970).

Chapter 12

Ion-Molecule Reactions in Trifluoro Propyne

The ion chemistry of 1, 1, 1 trifluoro propyne has been investigated in this laboratory as part of a continuing programme of research into fluoride and hydride affinities of positive ions. However the kinetics of the ion-molecule reactions in this compound have not previously been investigated in detail.

At 14 eV ionizing energy, only the parent ion is formed and reacts with the neutral via two major reaction channels[1] to produce the P-19 ion, $C_3F_2H^+$ and a condensation product $C_5H_3H_2^+$. Reaction R1 is probably a fluoride transfer reaction similar to those observed in the fluoromethanes.

$$H{-}C{\equiv}C{-}CF_3^+ + H{-}C{\equiv}C{-}CF_3$$

$$\xrightarrow[65\%]{k_1} H{-}C{\equiv}C{-}CF_2^+ + \text{neutrals} \qquad \text{(R1)}$$

$$\xrightarrow[35\%]{k_2} C_5F_3H_2^+ + CF_3 \qquad \text{(R2)}$$

Reactions R1 and R2 were studied at 16 eV electron energy in the high pressure mass spectrometer, and typical results are shown in Figure 1. Mass discrimination at the electron multiplier was investigated by comparing a low pressure, 70 eV spectrum of trifluoro propyne with that obtained at low pressure with an ICR spectrometer. The ICR results[1] indicated that at 70 eV, ions of

Figure 1

Variation of ion abundances with time in 1, 1, 1 trifluoro propyne. Electron energy = 16 eV, ionizing pulse width = 15 μsec, pressure = 3.6×10^{-4} torr, trapping voltage = 3 volts.

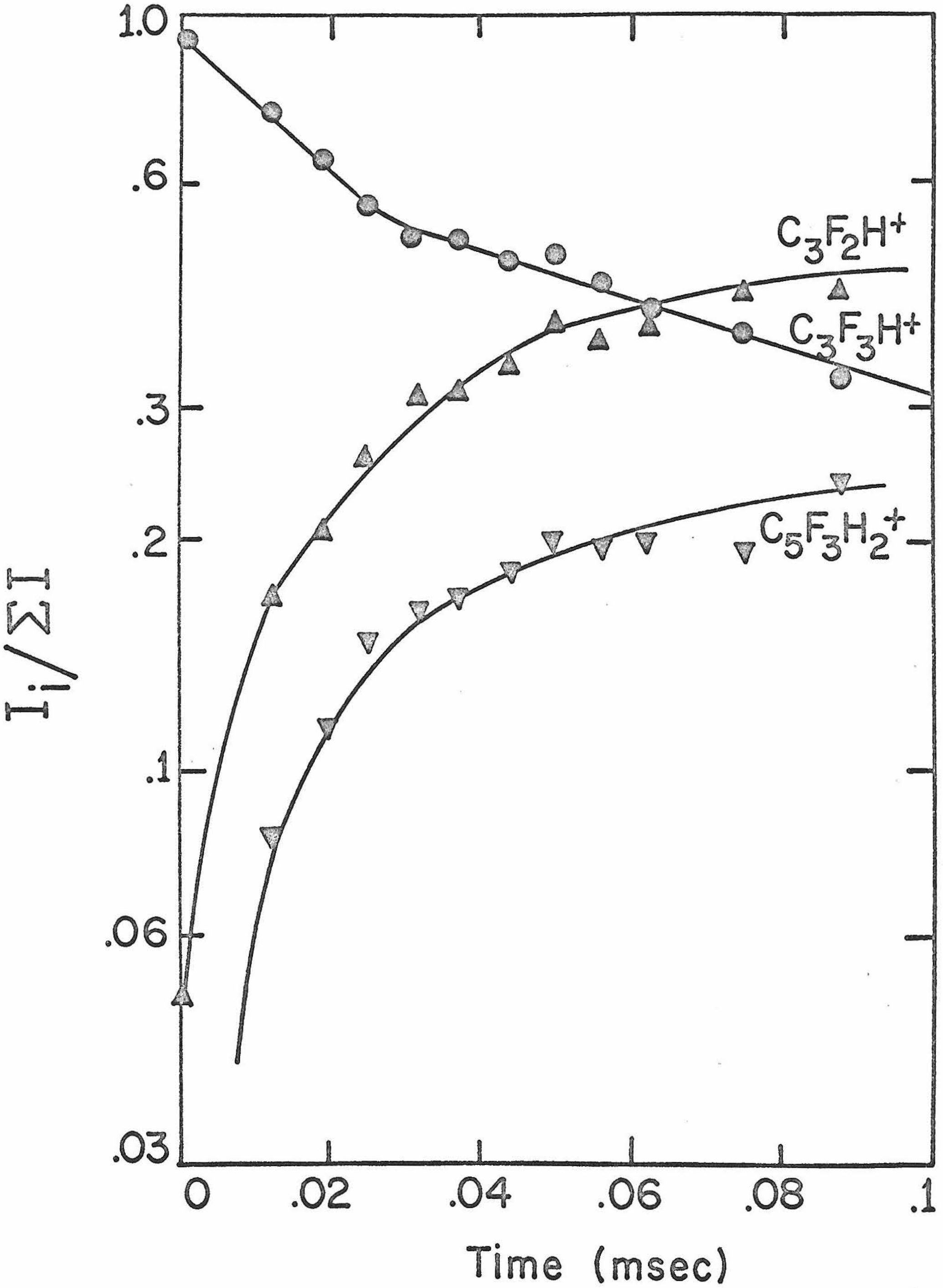
1.0
.6
.3
.2
.1
.06
.03
$I_i/\Sigma I$
0
.02
.04
.06
.08
.1
Time (msec)
$C_3F_2H^+$
$C_3F_3H^+$
$C_5F_3H_2^+$

mass 94 and 75 were equally abundant, representing 70% of the total ionization. The equivalent spectrum on the high pressure instrument gave an abundance ratio [P]/[P-19] = 3.3. This would imply an apparent mass discrimination factor of 3.3, which is anomalously large in view of the relatively small mass difference. In addition, as shown in Figure 1, the ratio of products, $[C_3F_2H^+]/[C_5F_3H_2^+]$, was about 2 under all conditions, in good agreement with the results of Beauchamp. This implies minimal mass discrimination between masses 75 and 119, in direct contradiction with the results inferred from the 70 eV primary ion spectrum. The disagreement is best resolved if it is assumed that $C_3F_2H^+$ is initially formed with some excess kinetic energy. As demonstrated in earlier chapters, excess kinetic energy substantially increases ion loss rates and significantly impairs extraction efficiencies. Excess kinetic energy ions are a common feature in the fragmentation of fluoroalkanes.[2] Accordingly it was assumed that mass discrimination was negligible.

Inspection of Figure 1 reveals a pronounced change in the parent ion decay slope at 25 μsec. If this effect is real, then it probably arises from one of two separate causes. The curvature could result either from a time dependent rate constant for R1-R2, or the parent ion could be formed in more than one reactive state. These two effects can be distinguished by examining the decay at different pressures, as reported below. The parent ion abundance at zero time was found by operating the source in a continuous mode.

Very little $C_3F_2H^+$ was observed. The relative rates of R1 and R2 can be estimated by comparing the abundance of the product ions. This method gives $k_2/k_1 \sim .6$, in good agreement with the results of Beauchamp.

The decay curves for $C_3F_3H^+$ at different pressures are shown in Figure 2. The change in slope is evident except at low pressures. The absence of such an inflection at 9×10^{-5} torr indicates that the disappearance rate of $C_3F_3H^+$ is not time dependent. However, the curves provide strong evidence for the existence of two long-lived states of the ion reacting at different rates. Table I lists the rate constants obtained from the initial and final slopes of each curve.

The agreement between the various runs is good. This self-consistency suggests that, at 16 eV, two states $\tilde{A}$ and $\tilde{B}$ of $C_3F_3H^+$ are formed, where state $\tilde{A}$ reacts with neutral C_3F_3H approximately three times faster than state $\tilde{B}$. The fraction of ions formed in each state may be estimated by extrapolating the decay curves at long times back to zero time. The approximate concentration of $\tilde{B}$ determined in this way is .65, resulting in $[\tilde{A}] \sim .30$, or $([\tilde{B}]/[\tilde{A}])_{t=0} \simeq 2$.

The time dependence of the $C_3F_3H^+$ abundance has also been investigated by Beauchamp[1] using ICR spectroscopy. A nonlinear decay was again observed, though the data was not sufficiently precise to enable rate constants to be determined.

Figure 2

Time dependence of $C_3F_3H^+$ abundance (normalized) at different pressures. Concentrations of $C_3F_2H^+$ and $C_5F_3H_2^+$ not shown. Electron energy = 16 eV, ionizing pulse width = 15 μsec. An additional run, at 4.5×10^{-4} torr, is omitted for clarity, but also exhibited a pronounced break in slope at ~25 μsec.

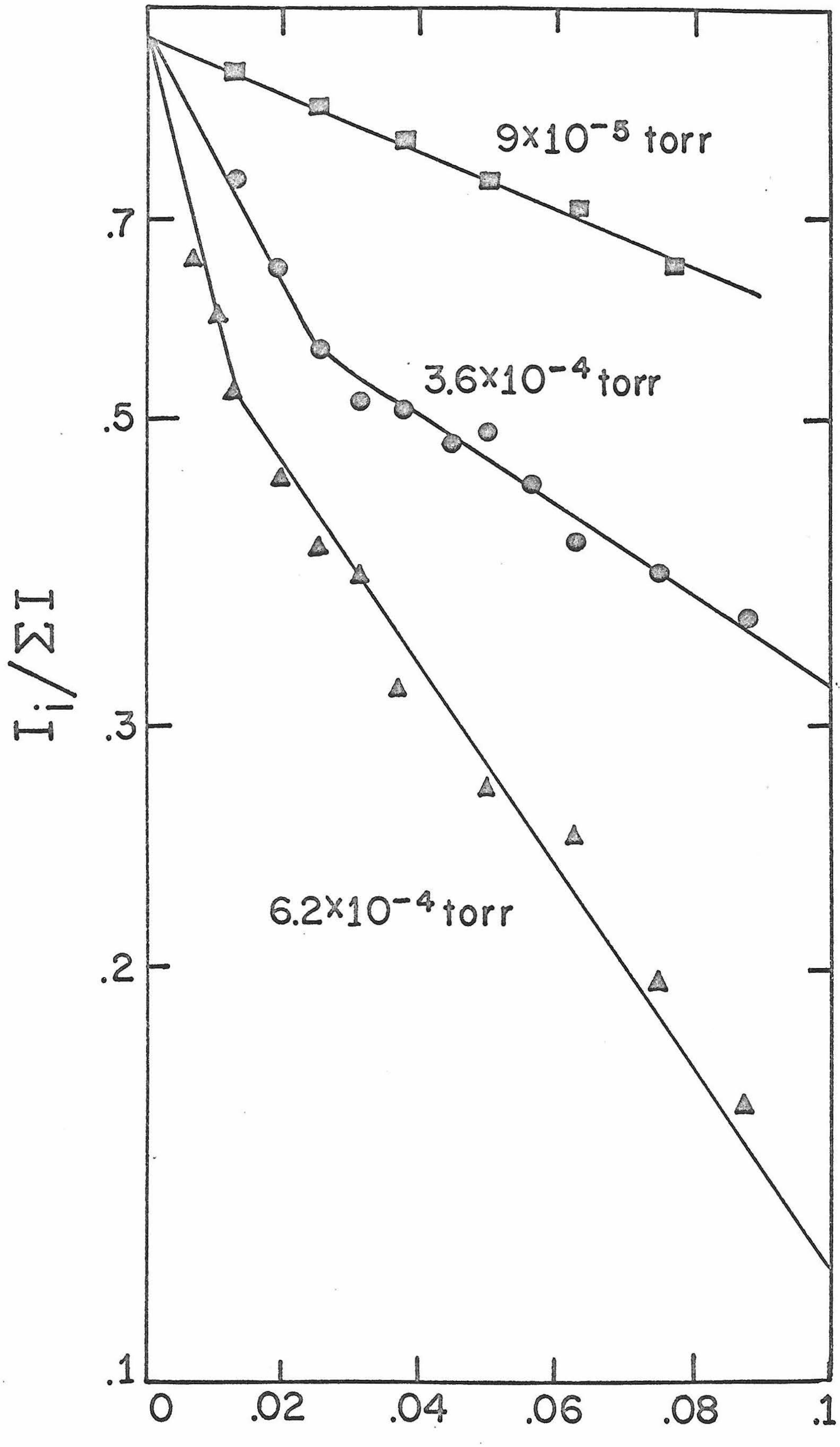
9×10⁻⁵ torr
3.6×10⁻⁴ torr
6.2×10⁻⁴ torr
I_i/ΣI
.7
.5
.3
.2
.1
0
.02
.04
.06
.08
.1
Time (msec)

Table I

Rate Constants for Parent Ion in Trifluoro Propyne

Pressure (torr)	Rate (cm^3 $molecule^{-1}$ $sec^{-1} \times 10^{-9}$) Initial slope	Final slope
9×10^{-5}	1.75	–
3.6×10^{-4}	1.88	.68
4.5×10^{-4}	2.39	.69
6.2×10^{-4}	2.30	.81
Average	2.05 ± .25	.73 ± .07
Langevin rate	.80[a]	
Locked-dipole rate	3.94[b]	

[a] Polarizability of C_3F_3H calculated from known bond and group polarizabilities listed by J. O. Hirshfelder, C. F. Curtiss and R. B. Bird, "Molecular Theory of Gases and Liquids", Wiley, New York, 1954. It was found that $\alpha = 5.48 Å^3$.

[b] $\mu_D = 2.36 D$. (National Bureau of Standards publication, NSRDS-NBS 10).

The photoelectron spectrum of trifluoropropyne has recently been investigated by Cullen et al.[3] The two lowest bands, commencing at 10.9 and 11.8 eV were assigned to ionization of CF_3 orbitals and C≡C orbitals, respectively. The lower band exhibited vibrational structure arising from both a C≡C stretch (2016 cm^{-1}) and a C–F stretch (1081 cm^{-1}). The infrared radiative lifetimes of these vibrational modes are probably sufficiently long that they will retain their excitation energy for the duration of the time scan. The two reactive states of the trifluoropropyne ion may be related to the vibrational energy present in these modes. Further speculation about our data would be unwarranted, as the rates at ionizing energies just above threshold were not measured.

References

1. J. L. Beauchamp, unpublished results.
2. Chapter 15, this thesis, and references contained therein.
3. W. R. Cullen, D. C. Frost and W. R. Leeder, J. Fluorine Chem., **1**, 227 (1971/72).

Chapter 13

Charge Exchange in N_2 and CO_2

Charge exchange in simple systems such as N_2 and CO_2 can be studied using the same trapped-ion, ion-ejection ICR technique employed for CH_3Br, as described in Chapter 9. Ionizing energies were 70 eV. The studies were conducted using appropriate isotopic mixtures. Partial pressures were obtained from the peak heights of single resonance spectra at low pressures. The rate constants were found from a plot of log I_{ej}/I versus time. Typical data for N_2^+ is given in Figure 1. The results are reported below in units of 10^{-10} cm^3 $molecule^{-1}$ sec^{-1}.

(1) N_2:

$$^{14}N_2^+ + {}^{15}N_2 \underset{k_r}{\overset{k_f}{\rightleftharpoons}} {}^{15}N_2^+ + {}^{14}N_2$$

$k_f = 5.7 \pm .3$

$k_r = 6.6 \pm .3$

(2) CO_2:

$$^{12}CO_2^+ + {}^{13}CO_2 \underset{k_r}{\overset{k_f}{\rightleftharpoons}} {}^{13}CO_2^+ + {}^{12}CO_2$$

$k_f = 4.8 \pm .4$

$k_r = 4.7 \pm .4$

Figure 1

Variation of R for $^{15}N_2^+$ and $^{14}N_2^+$ with reaction time. Electron energy = 70 eV. Mole fractions of $^{15}N_2$ = .57, $^{14}N_2$ = .43. Total pressure = 9.5×10^{-7} torr.

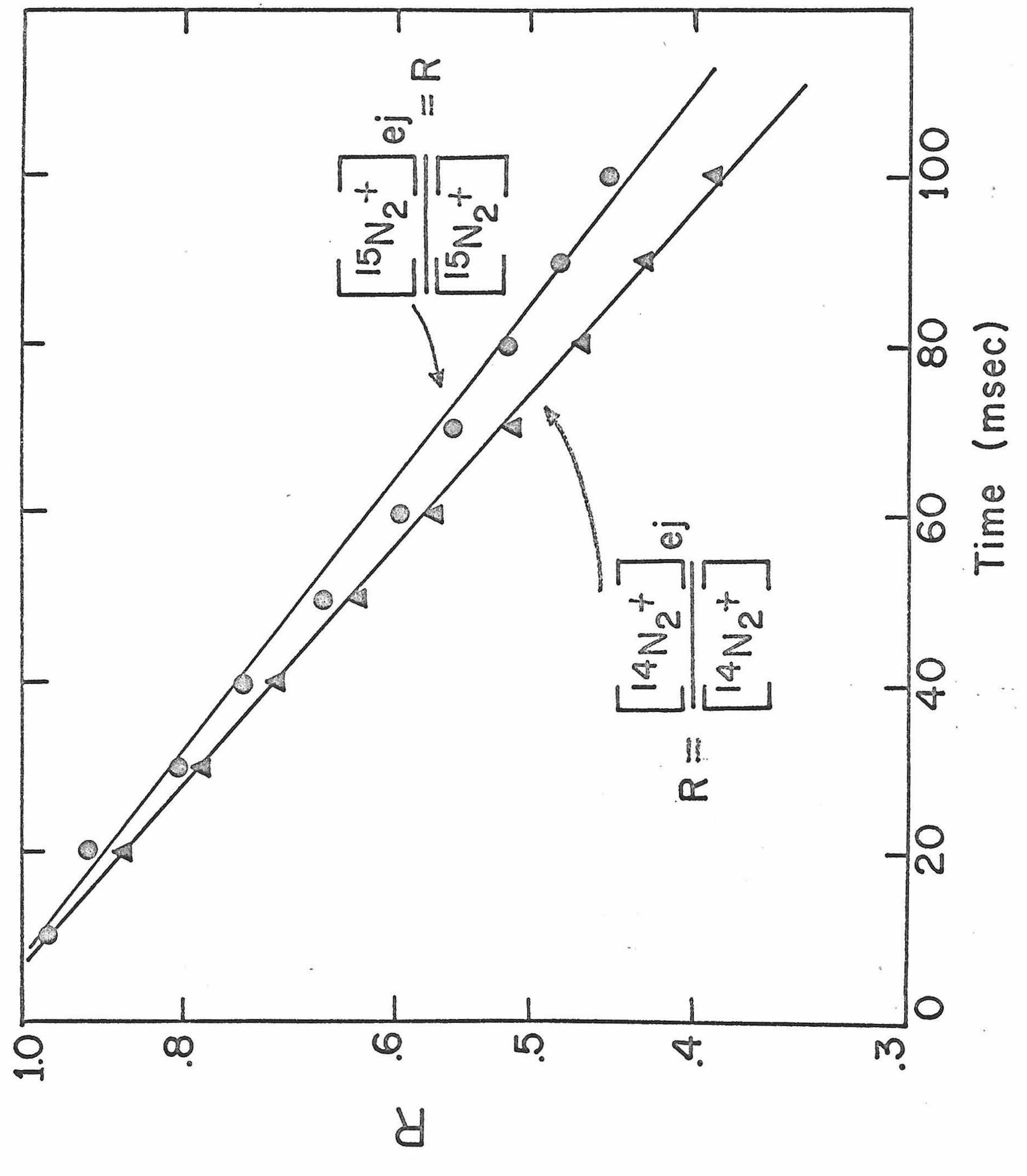

R
1.0
.8
.6
.5
.4
.3
0
20
40
60
80
100
Time (msec)
$\frac{[^{15}N_2^+]_{ej}}{[^{15}N_2^+]} = R$
$R = \frac{[^{14}N_2^+]_{ej}}{[^{14}N_2^+]}$

The accuracy of the results does not warrant attaching great significance to the differences in k_f and k_r for N_2.

Assuming that charge transfer occurs on every second collision, the total encounter rate in these systems will be roughly double this rate. Accordingly, the calculated Langevin rate should then represent twice the charge exchange rate. Table I reports the charge-transfer rates and those calculated from the Langevin equation using this simple model. While the rate of charge transfer for CO_2 is in good agreement with the Langevin rate, the experimental rate in N_2 is considerably larger than the Langevin value. This indicates that the electron jump can occur over distances larger than those required for "hard" collisions.

A symmetric charge-transfer occurrence is equivalent to an event in which an ion undergoes momentum transfer. Accordingly, the large charge-transfer cross sections reported here should markedly influence the ICR linewidths of N_2^+ and CO_2^+ at high pressure, as this parameter is directly related to the momentum transfer cross section.[1] Huntress[2] has measured ICR linewidths for N_2^+ and CO_2^+ in their parent gases. The results from that investigation are given in Table I. Good agreement is observed in the case of N_2. Factors other than charge transfer must be responsible for the enhanced momentum transfer of CO_2^+.

The rapidity of charge exchange in these systems is of considerable chemical importance, as these processes provide facile routes for the de-excitation of ions formed in excited states.

Table I

Charge Exchange Rates in N_2 and CO_2

System	Rate (cm^3 $molecule^{-1}$ $sec^{-1} \times 10^{-9}$)		
	This work	Langevin model	Reference 2[a]
N_2	6.2 ± .5	4.1	6.7
CO_2	4.7 ± .4	4.0	6.7

[a] Obtained from ICR linewidths.

References

1. J. L. Beauchamp, Ann. Rev. Phys. Chem., **22**, 527 (1971).
2. W. T. Huntress, J. Chem. Phys., **55**, 2146 (1971).

Chapter 14

Thermoneutral Proton Transfer in CH_2D_2

Protonated methane is known to undergo no further reaction with methane. However, thermoneutral proton transfer processes, such as R1, have been postulated as the chain propagation step in the

$$CH_4D^+ + CH_4 \longrightarrow CH_3D + CH_5^+ \qquad \text{(R1)}$$

radiation induced exchange of isotopic methanes.[1] These reactions occur reversibly and are thus undetectable in conventional single source mass spectrometers. Recently developed time-delayed ion ejection ICR techniques[2] have permitted a measurement of the rates of thermoneutral proton and deuteron transfer in CH_2D_2. This technique, described in more detail in Chapter 9, permits the selective removal of one ion from the ICR cell without perturbing the motion of other ions.

Ionization of CH_2D_2 at 70 eV energy results in parent ion formation and eventually in the production of $CH_3D_2^+$ and $CD_3H_2^+$ to slightly different extents via reactions R2a and R2b

$$CH_2D_2^+ + CH_2D_2 \longrightarrow \begin{cases} \xrightarrow{60\%} CH_3D_2^+ + CD_2H & \text{(R2a)} \\ \xrightarrow[40\%]{} CD_3H_2^+ + CH_2D & \text{(R2b)} \end{cases}$$

These two products can interconvert by thermoneutral proton or deuteron transfer, shown in R3.

$$CH_3D_2^+ + CH_2D_2 \xrightarrow{k_{3a}} CD_3H_2^+ + CH_3D \qquad (R3a)$$

$$CD_3H_2^+ + CH_2D_2 \xrightarrow{k_{3b}} CH_3D_2^+ + CD_3H \qquad (R3b)$$

Ejection of one of these ions causes the system to respond at the rate of reaction to achieve a new equilibrium. Hence by monitoring the decay in ion abundance of one ion while the other is continuously ejected, the rate constants for R3a and R3b can readily be determined. This procedure is carried out for $CH_3D_2^+$ in Figure 1. The quantity log I_{ej}/I is plotted as a function of time after ejection and the rate constants k_3 are determined from the slope.

The rate constants k_{3a} and k_{3b} were found to be $3 \pm 1 \times 10^{-11}$ cm^3 molecule^{-1} sec^{-1}. The large uncertainty in this quantity arises primarily from the complicating effects due to H_3O^+ and H_2DO^+ formation at long times. The accuracy of our results was insufficient to determine whether k_{3a} and k_{3b} were identical.

If protons and deuterons are equivalent in these ions, then the rates k_{3a} and k_{3b} represent only 2/5 of the total rate of proton or deuteron transfer in this system, since transfer processes resulting in no change in chemical identity remain undetected. Accordingly, the total rate of symmetric proton transfer for a reaction such as R4 is on the order of 7×10^{-11} cm^3 molecule^{-1} sec^{-1}, demonstrating

$$CH_5^+ + CH_4 \longrightarrow CH_4 + CH_5^+ \qquad (R4)$$

that only one collision in 20 results in the transfer of a proton.

Figure 1

Variation of ion abundances in CH_2D_2 with and without continuous ejection of $CD_3H_2^+$ after 100 msec. The $CD_3H_2^+$ curve is not shown. Electron energy = 70 eV, pressure = 2.3×10^{-6} torr. The anomalous feature in the decay curves results from transients generated by turning on the irradiating oscillator in the timing sequence.

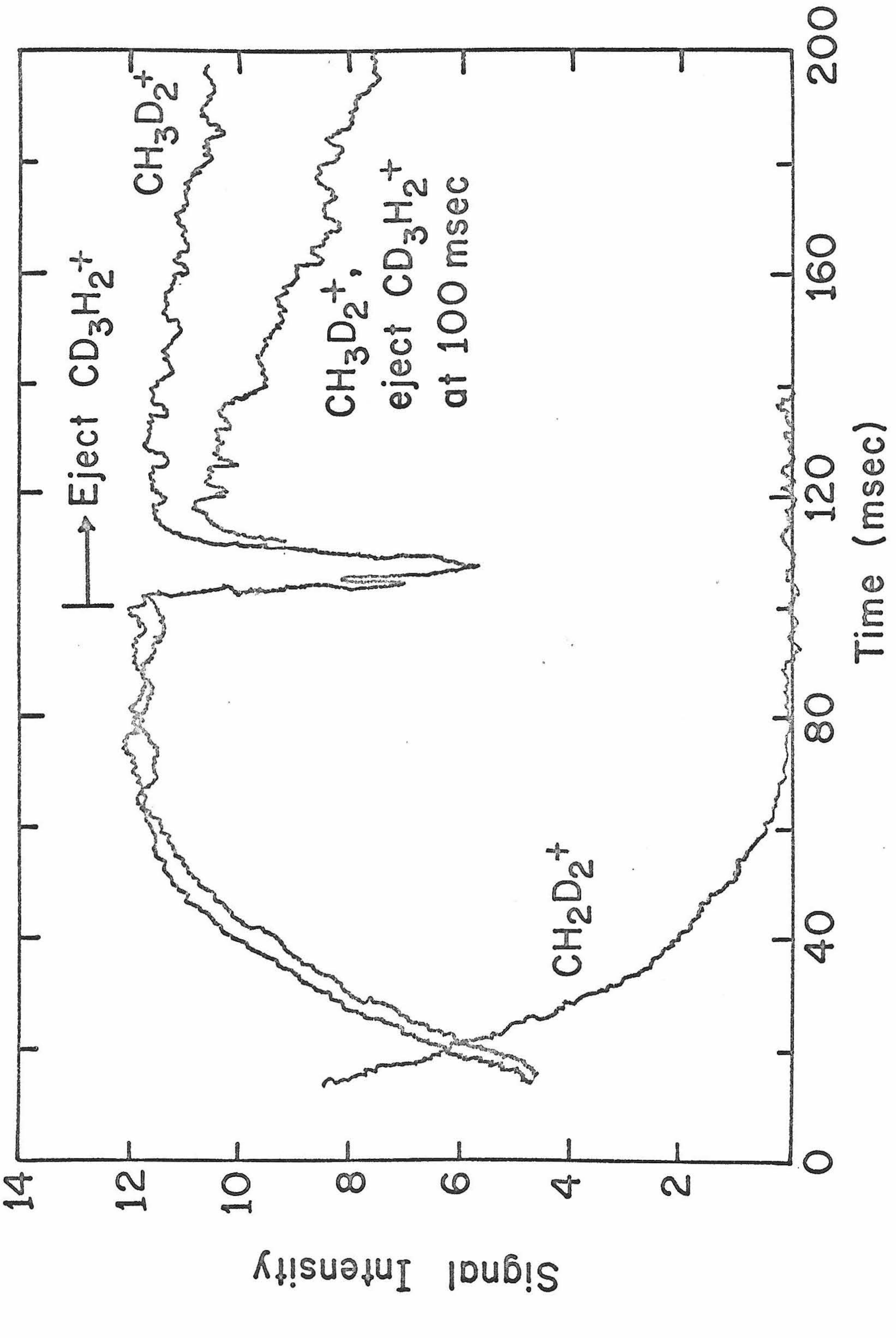
Signal Intensity
14
12
10
8
6
4
2
0
40
80
120
160
200
Time (msec)
Eject $CD_3H_2^+$
$CH_3D_2^+$
$CH_3D_2^+$, eject $CD_3H_2^+$ at 100 msec
$CH_2D_2^+$

The slow rate of this process is in marked contrast to that in HD, where similar transfers involving H_2D^+ and D_2H^+ are known to occur.[3] In HD, proton transfer appears to occur on almost every collision. The difference may arise because the transfer in methane involves a substantial structural rearrangement. Thus CH_5^+ resembles $(CH_3 \cdot H_2)^+$, and must undergo a large structural change to assume the tetrahedral geometry of CH_4^+.

References

1. R. H. Lawrence, Jr., and R. F. Firestone, J. Amer. Chem. Soc., **87**, 2288 (1965).
2. T. B. McMahon, R. J. Blint, D. P. Ridge, and J. L. Beauchamp, J. Amer. Chem. Soc., **94**, 8934 (1972)
3. T. B. McMahon and P. G. Miasek, unpublished results.

Chapter 15

Determination of Ion Kinetic Energy Distributions Using ICR Spectrometry

I. Introduction

It has long been known that fragment ions from diatomic and polyatomic ions often have excess kinetic energy.[1] In some cases,[2-5] interpretation of this effect was based upon the ideas of Hustrulid _et al._,[6] who attributed the excess kinetic-energy ions to the dissociation of doubly charged parent ions into two singly charged fragments. This mechanism characteristically predicts a kinetic energy distribution that is sharply peaked around an energy corresponding to the Coulomb repulsion of the two fragments, generally 1-3 eV. Since in most cases the same fragment ions are formed by other (thermal) processes as well as by the doubly charged parent mechanism, the energy distribution of these ions typically shows two sharp peaks, one at near-thermal energies and the other near the Coulombic energy mentioned above.

There are also numerous instances[7-10] where high energy fragment ions arising from a singly charged parent have been studied. One of the most important of these, with respect to our own studies, was undertaken by Hagustrum and Tate,[11, 12] who measured the kinetic energy distribution of fragment ions from electron impact on various diatomic molecules. From their data they were successful in deducing certain features about the ionic states responsible for the dissociation. They demonstrated that markedly different kinetic energy distributions may arise, depending on the position and shape of the ionic potential surface. This is illustrated by the potential energy diagram in Figure 1. Transitions to curve 2 yield ions of initial kinetic energy including zero, whereas all ions from transitions to curve 3 passes appreciable kinetic energies.

More recently Noutary[13] has observed that CF_3^+ is formed with excess energy on photoionization of several fluorocarbons and trifluoromethylhalides. Appell and Kubach[14] have recently measured the kinetic energy distribution of energetic H^+ fragments from CH_4, and concluded that translationally excited H^+ arises from the dissociation of the first excited state of CH_4^+.

The first detailed investigation on the excess kinetic energy of CH_3^+ in methyl halides was undertaken by Dibeler and Reese.[15] The largest effects were observed for CH_3F, where it was found that the appearance potential for the formation of translationally excited methyl cations by electron impact (EI) was 16.3 ± .3 eV.

$$CH_3F + e^- \longrightarrow CH_3^+ + F + 2e^- \qquad \text{(R1)}$$

From the shape of the CH_3^+ peak recorded at low ion accelerating voltages, they estimated the total kinetic energy of the dissociation process to be 1.3 eV.

Figure 1

Typical potential energy curves involved in the dissociative ionization of a diatomic molecule by electron impact (Reference 12). Curve 1 is the potential curve of the ground molecular state of XY, curves 2 and 3 are stable and repulsive states of XY^+, respectively. Curves 4 and 5 are reflections of the square of the ground state vibrational eigenfunction in the potential curves 2 and 3, respectively, and give the kinetic energy distribution of X^+.

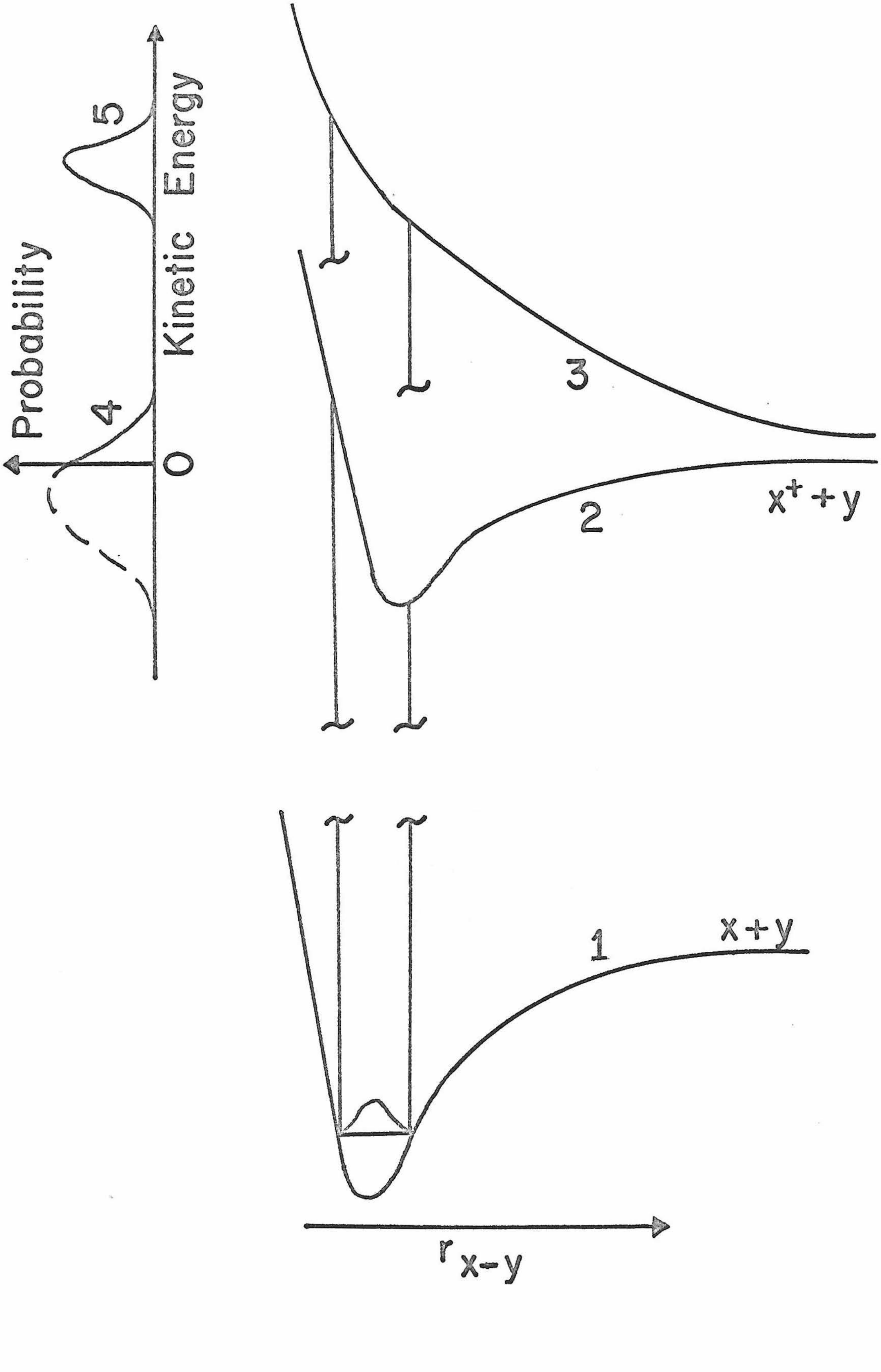
Probability
Kinetic Energy
0
4
5
3
2
$x^+ + y$
1
$x + y$
r_{x-y}

Smaller effects were observed in CH_3Cl, where translationally excited CH_3^+ was found to have an appearance potential of 13.7 ± .2 V. The total kinetic energy of the dissociation process was estimated as less than .7 eV. The other methyl halides produced no observable effect.

The production of CH_3^+ from methyl halides _via_ the photoionization (PI) process in R2 has recently been examined by Krauss, Walker and Dibeler.[16] Figure 2 is a reproduction of their data.

$$h\nu + CH_3X \longrightarrow CH_3^+ + X\cdot + e^- \qquad \text{(R2)}$$

They obtained appearance potentials of 16.25 eV and 13.87 eV for CH_3F and CH_3Cl, respectively, in good agreement with the earlier electron impact study. From various known thermochemical heats of formation, they ascertained that these thresholds were 1.7 eV and .5 eV, respectively higher than the predicted thresholds. They ascribed these differences at threshold to excess energy carried by the products. For CH_3Br, the methyl cation appearance potential was 12.77 eV, leading to an excess energy of less than .2 eV.

Photoelectron (PE) studies on the methyl halides have been undertaken by Turner and co-workers[17] and by Potts _et al._[18] The two groups obtained virtually identical spectra in every case. Figure 3 shows Turner's results. For CH_3F, the first two bands occur in the ranges 12.5-14.5 eV and 16.2-18.0 eV. This latter band is Gaussian shaped with virtually no irregularities. Potts _et al._ have stated that this second band is associated with CH_3^+ formation.

Figure 2

Photoionization yield curves for the molecules and some fragment ions of methyl fluoride, methyl chloride and methyl bromide (taken from Reference 16).

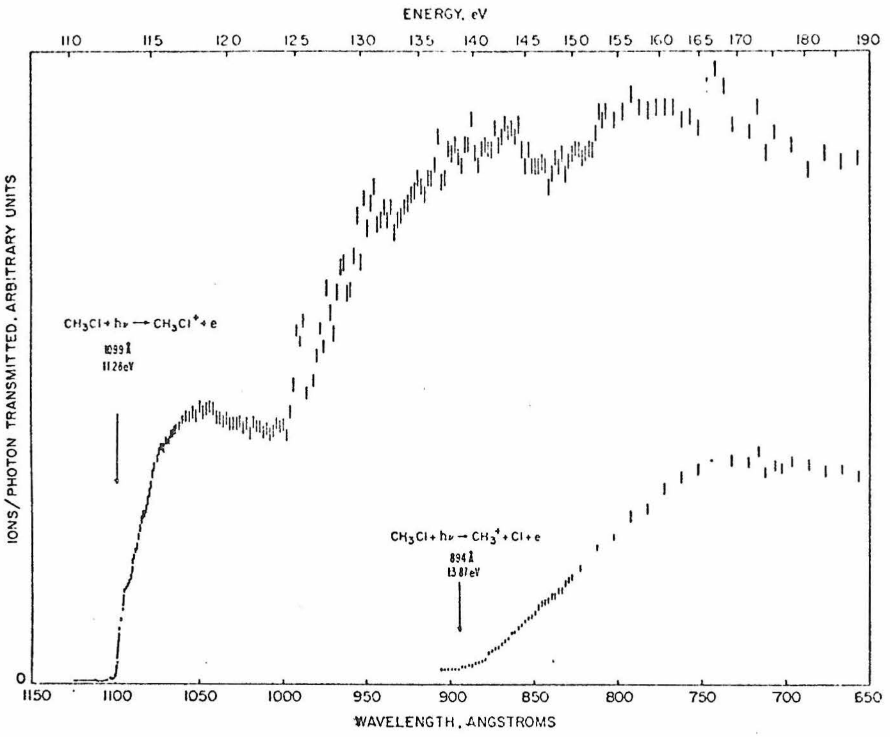

Photoionization yield curves of the CH_3Cl^+ *and the* CH_3^+ *ions of methyl chloride.*

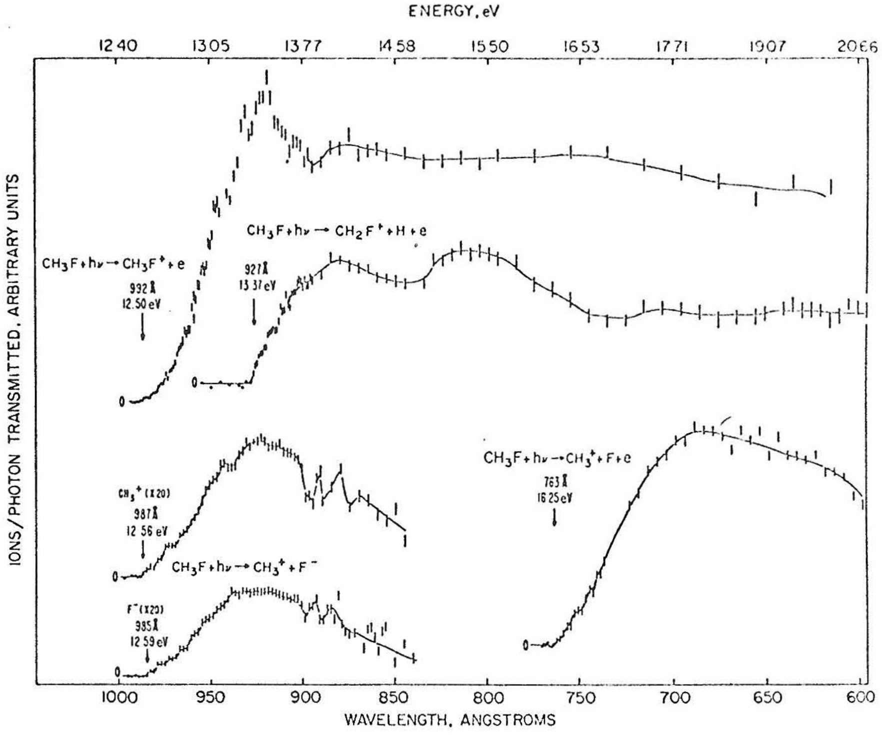

Photoionization yield curves for the molecule and some fragment ions of methyl fluoride.

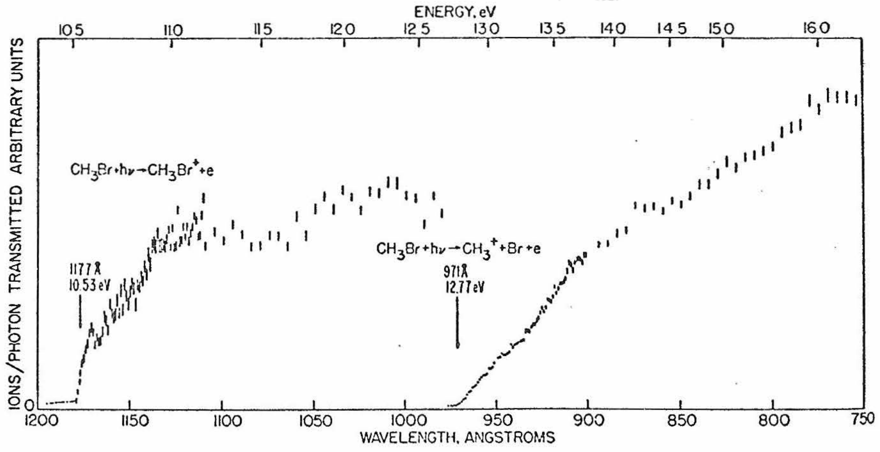

Photoionization yield curves for the molecule and methyl ions of methyl bromide.

Figure 3

Photoelectron spectra of methyl fluoride, methyl chloride and methyl bromide (taken from Reference 17).

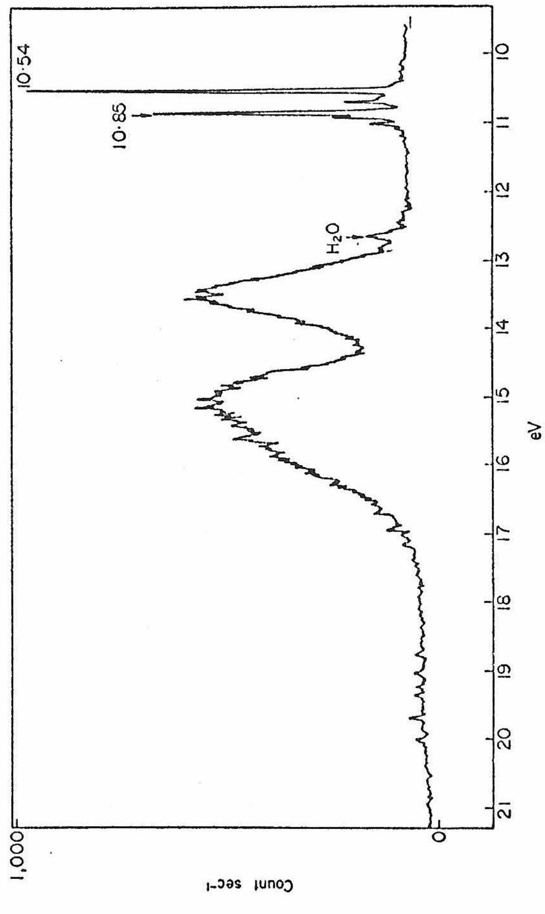

Methyl bromide (full spectrum)

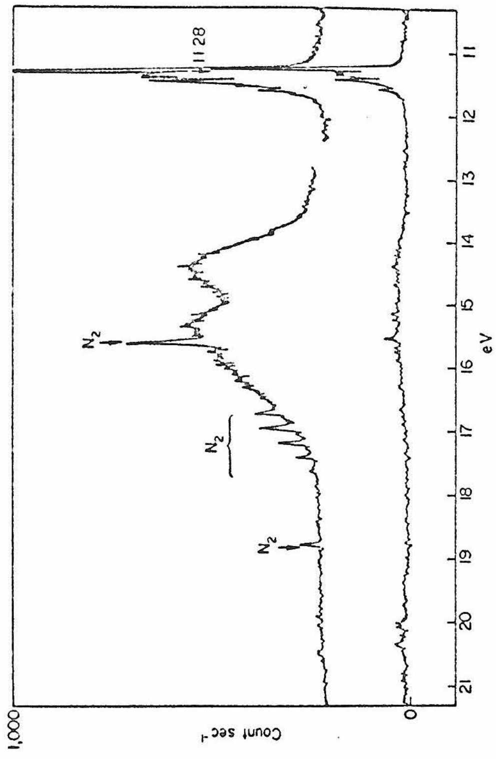

Methyl chloride (full spectrum)

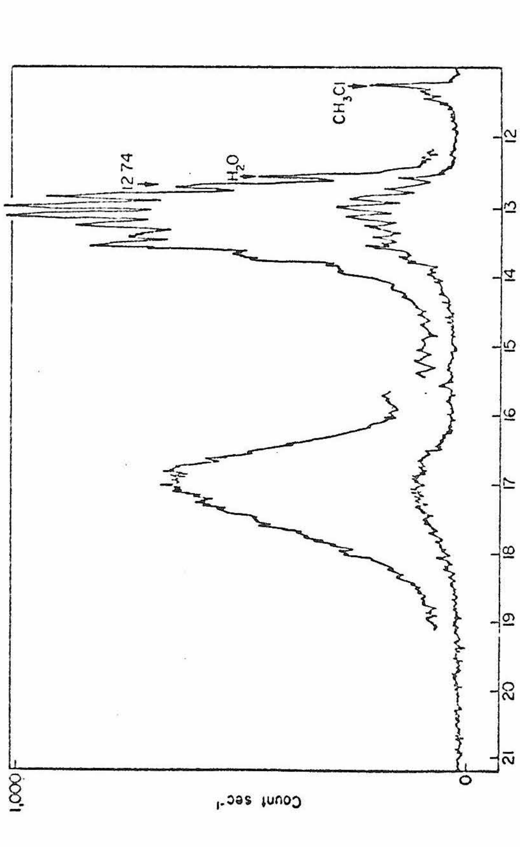

Methyl fluoride (full spectrum)

In this case, the agreement with the PI work of Krauss et al. is excellent, and these two studies would jointly predict excess energies ranging from 1.7 eV at threshold to 3.5 eV at maximum.

In PE studies on CH_3Cl and CH_3Br, Gaussian shaped bands compatible with CH_3^+ formation are observed at threshold energies of 13.6 eV and 12.75 eV, respectively. No vibrational structure is evident. While the agreement with the corresponding PI appearance potentials is excellent for CH_3Br, there is a discrepancy of .3 eV for CH_3Cl. The origin of this difference is discussed later.

The molecular orbital interpretation of the mechanism of CH_3^+ formation has been subject to some controversy, particularly for CH_3F. Krauss et al. found no evidence that the vibrationally excited ground state of CH_3F^+ or autoionizing Rydberg states contributed to CH_3^+ production in CH_3F. Instead they claimed that the dissociation involves excitation from the (σa_1) molecular orbital of CH_3F (primarily the C–F bond) to an ionic state that dissociates into CH_3^+ and F.

Potts et al. offer a similar explanation for their results, claiming that the broad band in the range 16.2-18.0 eV results from a superpositon of the (σa_1) band and one corresponding to the $(\Pi e)^4$ orbitals (largely localized on fluorine). The latter ionized state is greatly modified by a repulsive curve associated with the former. This unstable state of the ion dissociates into $CH_3^+ + F$.

Turner et al. present an alternate interpretation of the PE spectrum of CH_3F, suggesting that the band between 12.5 and 14.5 eV is the one containing the (σa_1) excitation, while the band at 16.2-18.0 eV arises solely from the $(\Pi e)^4$ orbital. In view of the closeness between the threshold of the second band and the appearance potential of CH_3^+ from PI work, it appears that this second band should be the one containing the (σa_1) excitation. This experimental evidence thus favours the first interpretation. It is important to identify the σa_1 band with certainty, since its width is used in later calculations to determine the total excess energy of the dissociation.

Carlson and White[19] have commented on the different interpretations of Turner et al. and Potts et al., but their investigations using variable angle PE spectroscopy did not give a means to decide the question.

For CH_3Cl and CH_3Br, Krauss et al. suggest that ionization of the σa_1 orbital should produce an abundance of vibrationally excited CH_3^+-Cl molecules. These excited ions are also produced by autoionization of the Rydberg states having the $(\Pi e)^{-1}$ limit. The notation[16] $(\Pi e)^{-1}$ describes the ionic state resulting from ionization from the (Πe) orbital (primarily the C–H bond). Krauss et al. suggest that CH_3^+ is produced from the σa_1^{-1} surface, but that there is no evidence for autoionization contributing to this process. The PE spectra are clearly interpreted as the ionization of the σa_1 orbital.

We have undertaken both PI and EI experiments to measure directly the excess kinetic energy carried by the CH_3^+ fragment from ionization of the methyl halides. This should provide information about the nature of the dissociative state, which can be correlated with results from the PI and PE work described above.

This study is the outgrowth of the observation that the abundance of CH_3^+ from CH_3F as measured in an ion cyclotron resonance (ICR) mass spectrometer depended on the trapping voltage. We used ICR for the EI experiments as ICR has very low mass discrimination compared to other techniques. In addition, no consideration of excess kinetic energy ions has been undertaken with this technique. This study should thus aid in the understanding of ion motion in an ICR spectrometer.

II. Experimental

The electron impact studies were done at 70 eV electron energy on an ion cyclotron resonance (ICR) mass spectrometer that has been previously described.[20] The pressure was low enough (5×10^{-7} torr) that no ion-molecule reaction products were observed. The CH_3^+ kinetic energy distribution was determined by monitoring the relative concentrations of CH_3^+ and CH_3X^+ as a function of V_T, the trapping voltage. Balanced drift voltages were maintained in the source and resonance region. The ion concentrations were measured from their single resonance peak heights using electron energy modulation, and were converted to absolute intensities by dividing by mass.

Photoionization studies were undertaken on CH_3F only using two instruments. The first of these is a conventional photoionization spectrometer,[21] newly constructed at the Jet Propulsion Laboratory. These experiments used the He resonance line at 586 Å (21.2 eV) for photoionization. The ion source, sketched in Figure 4, comprises a U-shaped repeller located in a box shaped ionization chamber. The size and location of the photon beam is indicated by the circle. Normally the repeller is held at a large positive potential for efficient ejection of the ions, but in this case negative voltages were often used so the plate acted as a retarder. The variation of the ion current with this retarding potential was measured for both CH_3^+ and CH_3F^+.

Studies on CH_3F were also undertaken using a photoelectron spectrometer newly constructed in these laboratories,[22] which was biased in these experiments to count ions rather than electrons. In this case, ions were formed in a field free region by 21.2 eV photoionization, and their kinetic energy was measured directly using a cylindrical electrostatic analyzer.

Methyl fluoride was obtained from Peninsular Chemresearch Inc., methyl chloride from Matheson and methyl bromide from Union Carbide. Except for degassing with freeze-pump-thaw cycles, all gases were used as supplied. Mass spectral analysis indicated acceptable purities.

Figure 4

Sketch of photoionization ion source looking along the path of the photon beam. The U shaped electrode is the repeller. Equipotentials are shown as fractions of retarding voltage, relative to the potential of the ionization chamber. The size and location of the photon beam are indicated by the circle.

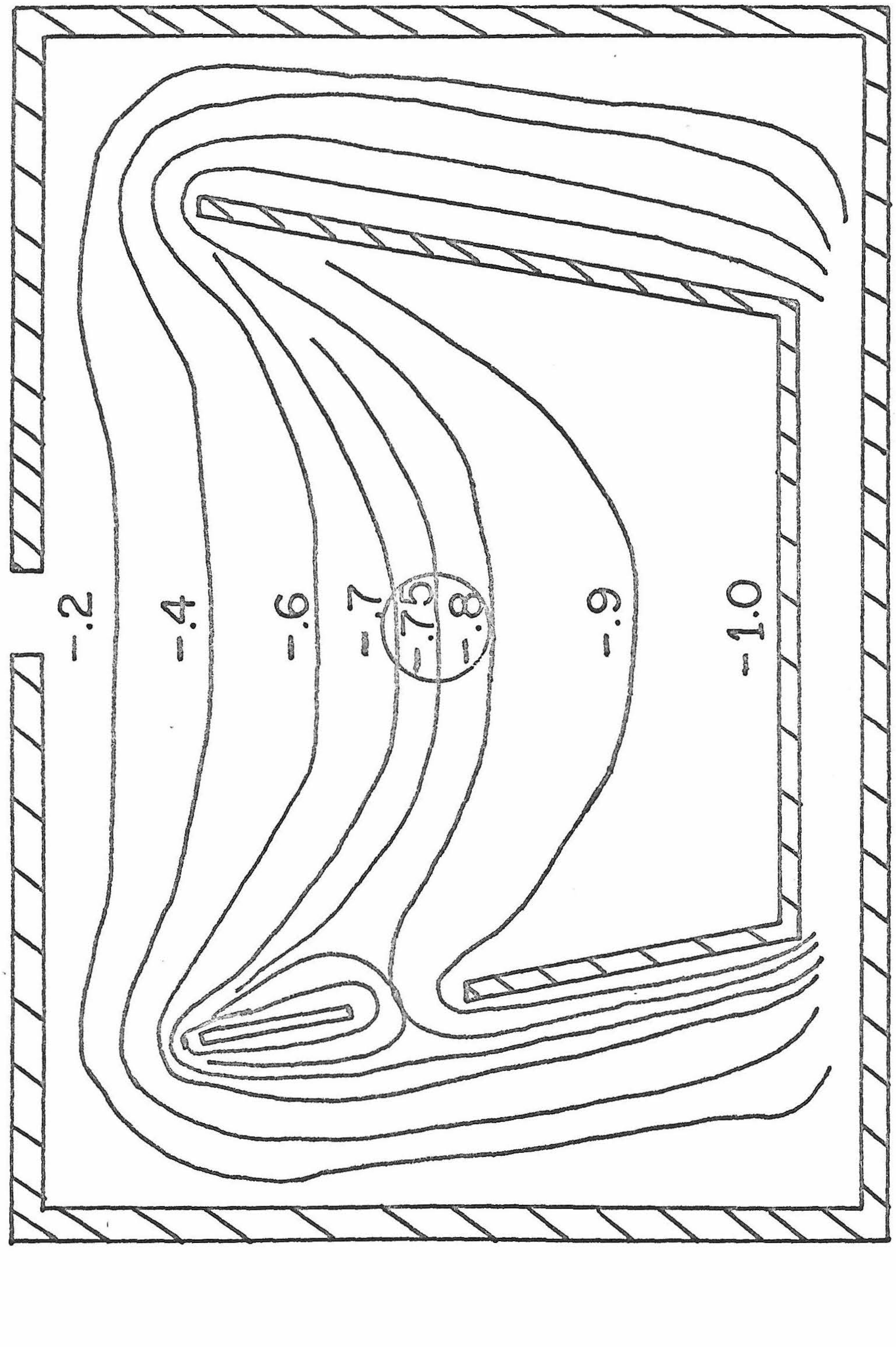
-.2
-.4
-.6
-.7
-.75
-.8
-.9
-1.0

III. Results

Electrostatic equipotentials in the photoionization ion source were determined by painting the electrode configuration on resistance paper, then applying the appropriate voltages to the electrodes and measuring the corresponding potentials at interior points. The resulting equipotential curves are presented in Figure 4. It is seen that the actual retarding barrier felt by ions formed in the centre of the source is .75 of the retarding voltage.

Typical results for this photoionization experiment are presented in Figure 5. Both the CH_3F^+ and CH_3^+ ion currents decreased markedly as the retarding potential increased, and at positive retarding potentials, no CH_3F^+ ions were detected, indicating that they possessed only thermal kinetic energy. By contrast, a CH_3^+ ion current was observed with retarding voltages exceeding 1.2 V, demonstrating that a sizeable portion of these ions were formed with excess kinetic energy. The magnitude of this maximum retarding barrier is at least $1.0 \pm .1$ V which demonstrates that the maximum kinetic energy that a CH_3^+ fragment from CH_3F may possess is at least 1.0 eV.

The results obtained in a typical ICR experiment on CH_3F are shown in Figure 6. At trapping voltages below ~1 V, the ratio $[CH_3^+]/[CH_3F^+]$ fell, implying that proportionally more of the high energy CH_3^+ ions then escaped ana were not detected. It is significant that the ratio extrapolates exactly to zero at zero trapping voltage, indicating the absence of any thermal CH_3^+ ions. This type of energy distribution is typical of a dissociative process similar to

Figure 5

Ion currents versus retarding potential for photoionization experiment.

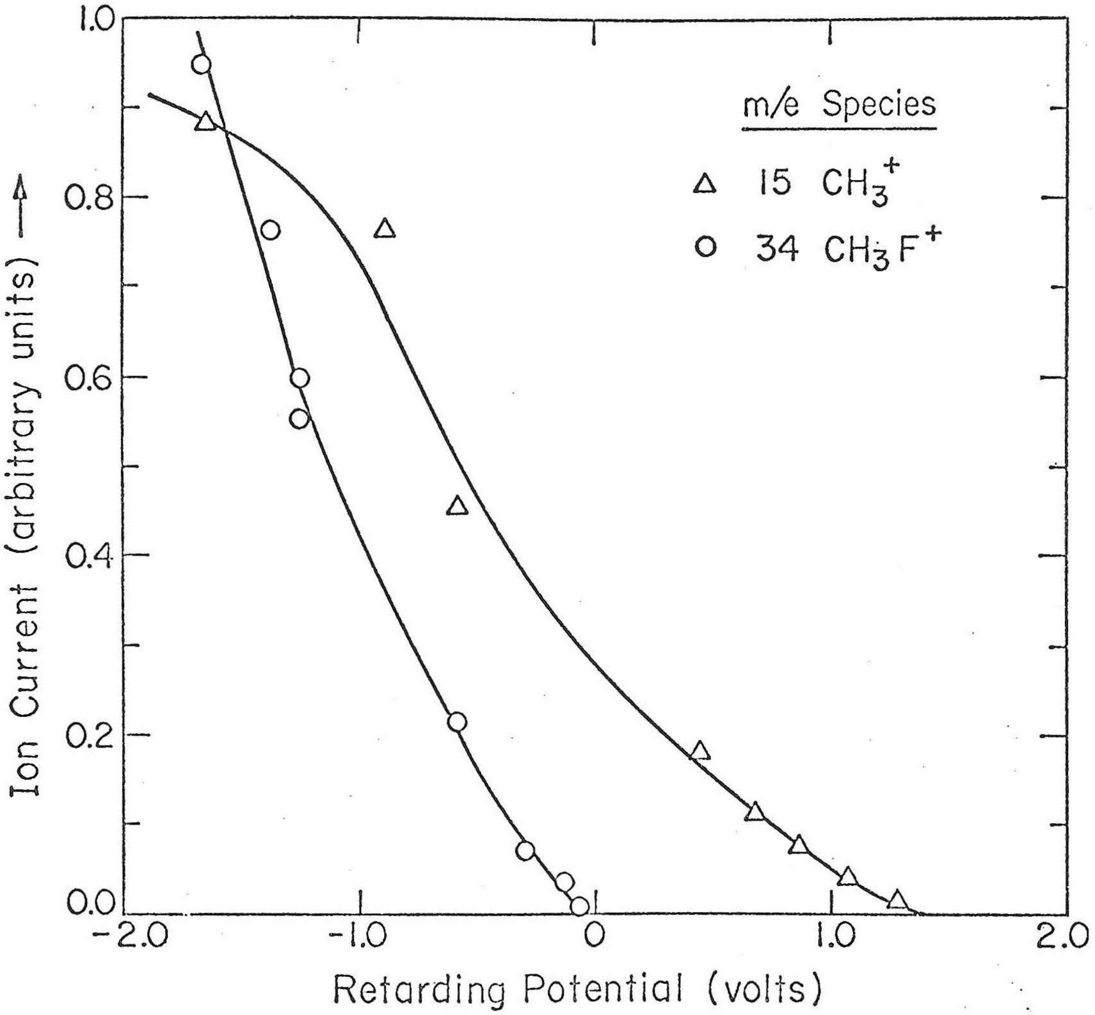
1.0
0.8
0.6
0.4
0.2
0.0
-2.0
-1.0
0
1.0
2.0
Ion Current (arbitrary units) →
Retarding Potential (volts)
m/e Species
△ 15 CH_3^+
○ 34 CH_3F^+

Figure 6

Relative CH_3^+ concentration in CH_3F versus trapping voltage. The points are experimentally determined, the three curves are fits using a Gaussian-type distribution and three different average energies, as described in the text. These Gaussians all were chosen to have zero probability at $E = 0$. The width of the distributions is thus $2\,\overline{E}$.

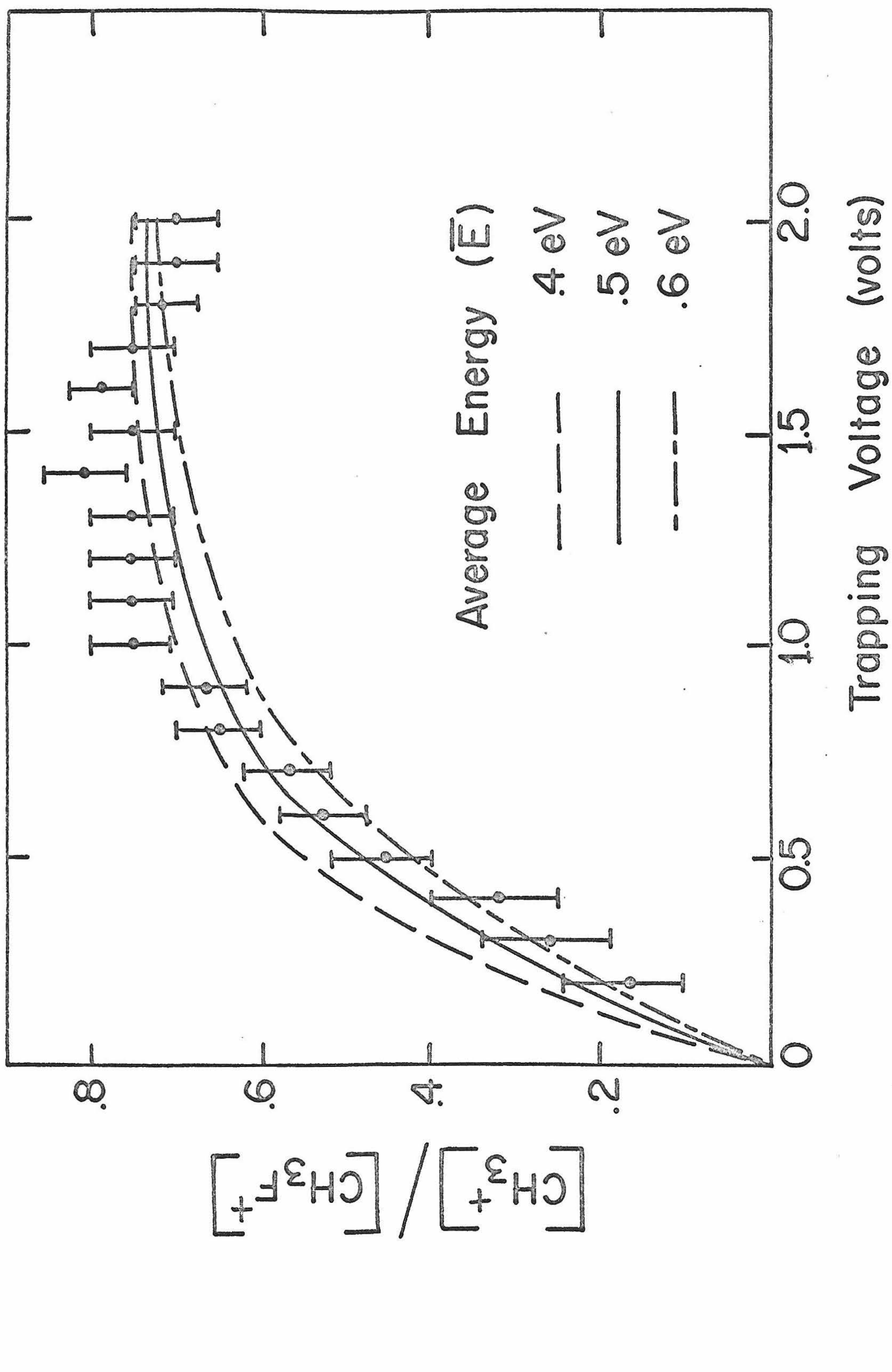

[CH$_3^+$] / [CH$_3$F$^+$]
.8
.6
.4
.2
0
0.5
1.0
1.5
2.0
Trapping Voltage (volts)
Average Energy (Ē)
.4 eV
.5 eV
.6 eV

Figure 7

Relative CH_3^+ concentration in CH_3Cl and CH_3Br versus trapping voltage. The points are experimentally determined, the curve is a fit using a "truncated" Gaussian distribution, as described in the text.

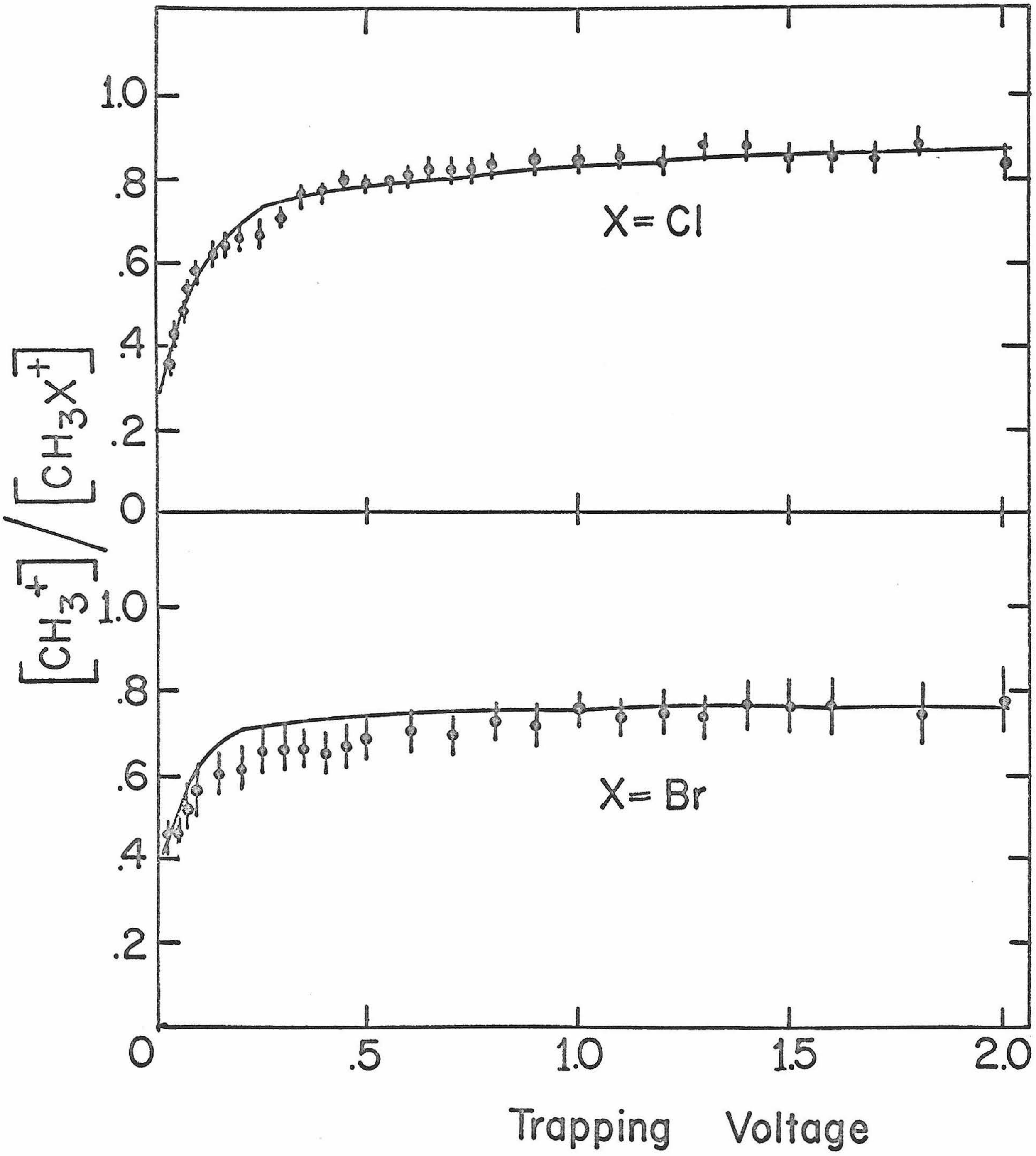
$[CH_3^+]/[CH_3X^+]$
X= Cl
X= Br
1.0
.8
.6
.4
.2
0
0
.5
1.0
1.5
2.0
Trapping Voltage

Figure 8

Variation of total ion signal with kinetic energy of the ions. This data was obtained using an appropriately altered photoelectron spectrometer, as described in the text.

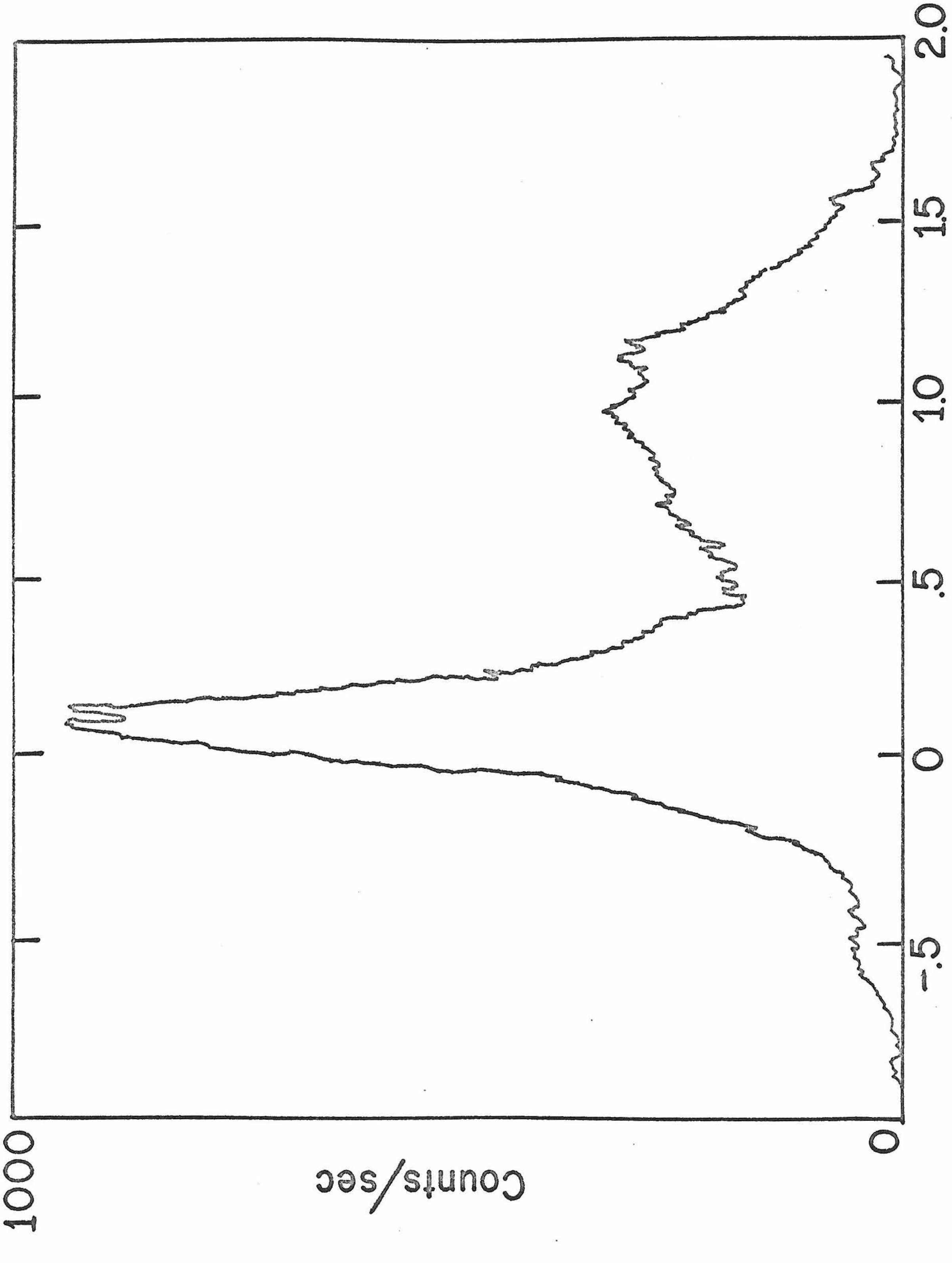
1000
0
Counts/sec
-.5
0
.5
1.0
1.5
2.0
Kinetic Energy

that involving transition to curve 3 in Figure 1.

The results of ICR experiments on CH_3Cl and CH_3Br are shown in Figure 7. Although the relative methyl cation abundances do decrease at low trapping voltages, the two curves differ markedly from their CH_3F counterpart as they do not appear to pass through zero. This suggests the presence of a substantial number of thermal methyl cations, and may imply a dissociative process similar to that involving transition to curve 2 in Figure 1. Quantitative analysis based on these two models are presented in the next section.

The results of our direct kinetic energy analysis-photoionization experiment are presented in Figure 8. Ionic masses cannot be measured in this experiment but must be inferred from other considerations. The large peak near 0 eV corresponds to thermal ions (mostly CH_3F^+ and CH_2F^+). This peak is not symmetric about zero, as only ions possessing thermal energy in a specific direction (towards the cylindrical analyzer) can be detected. The broad peak centered at 1.0 eV evidently represents excess energy CH_3^+ ions. The distribution appears to resemble a symmetric Gaussian, having a minimum energy near zero and a maximum energy near 1.8 eV.

IV. Kinetic Energy Distribution of CH_3^+

Although a quantitative interpretation of the PI results is difficult, the kinetic energy distribution of CH_3^+ can be determined from the ICR results.

When the drift plates are balanced, the electric potential along the line of the electron beam can be shown from Laplace's equation to be

$$V(z) = V_T - \frac{4V_T}{\pi} \sum_{\substack{n \\ \text{odd}}} (-1)^{(n-1)/2} \frac{1}{n \cosh \frac{n\pi}{4}} \cos \frac{n\pi z}{\ell} \tag{1}$$

where ℓ is the width of the cell and V_T is the trapping voltage. Following McMahon and Beauchamp,[20] an approximate form for this potential can be used

$$V(z) = V_T \left[.11 + 3.52 \left(\frac{z}{\ell}\right)^2 \right] \tag{2}$$

which follows the exact solution very closely. The well depth W(z) experienced by an ion formed at a point z is defined as the potential barrier preventing it from striking the trapping plates, and is simply

$$W(z) = V_T - V(z) = .89\, V_T \left[1 - 4 \left(\frac{z}{\ell}\right)^2 \right]. \tag{3}$$

If the ions are formed uniformly across the width of the cell, then the fraction $F(E_Z)$ of ions having an energy E_Z in the z direction that will remain trapped in the spectrometer can be shown to be

$$\begin{aligned} F(E_Z) &= \sqrt{1 - \frac{E_Z}{.89\, V_T}} \qquad (E_Z \leq .89\, V_T) \\ &= 0 \qquad (E_Z > .89\, V_T). \end{aligned} \tag{4}$$

Assume now that the distributions of excess energies obeys a distribution P(E), defined so that P(E) dE is the probability that an ion has kinetic energy between E and E + dE. This distribution is normalized such that

$$\int_0^{\infty} P(E)\, dE = 1 . \qquad (5)$$

The velocity vector defining E can have any spatial orientation, however only its z component is trapped. For a particular kinetic energy T, the probability that its z component is between E_z and $E_z + dE_z$ is

$$P_T(E_z)\, dE_z = \frac{dE_z}{2\sqrt{TE_z}} \qquad E_z \leqslant T \quad . \qquad (6)$$

Again, this is normalized so that

$$\int_0^{\infty} P_T(E_z)\, dE_z = 1 . \qquad (7)$$

Now the kinetic energy distribution along the z axis arising from a distribution of total energies P(E) is simply the logical extension of Equation (6),

$$P_z(E_z)\, dE_z = \int_0^{\infty} \frac{dE_z}{2\sqrt{EE_z}}\, P(E)\, dE \quad . \qquad (8)$$

The lower limit of the integral arises because the total energy (E) must be larger than or equal to its z component (E_Z).

Finally it is necessary to relate this distribution to the actual variation of the total current with trapping voltage, $I(V_T)$. Consider a population of ions, formed uniformly along the width of the cell, all with kinetic energy along the z axis of E_Z. Then the fraction of these ions remaining trapped in the spectrometer is $F(E_Z)$, where F is defined in Equation (4). For a distribution of energies along this axis, $P(E_Z)$, the variation of $I(V_T)$ will then be

$$\begin{aligned} I(V_T) &= \int_0^\infty P(E_Z)\,F(E_Z)\,dE_Z \\ &= \int_0^\infty P(E_Z)\sqrt{1 - \frac{E_Z}{.89\,V_T}}\,dE_Z \qquad \text{for } E_Z \leqslant .89\,V_T \\ &= 0 \qquad \text{for } E_Z > .89\,V_T. \end{aligned} \tag{9}$$

The most direct way to employ Equation (9) is to assume a form for P(E), then calculate $P(E_Z)$ from Equation (8) and finally compare the calculated $I(V_T)$ with the experimental data. The closeness of the fit should indicate how accurately the assumed P(E) describes the actual energy distribution. We have used this procedure for three different energy distributions:

(1) All fragments are assumed to have an equal amount of kinetic energy T. In this case

$$P(E_z)\,dE_z = dE_z/2\sqrt{TE_z} \qquad (E = T) \tag{10}$$

$$= 0 \qquad (E \neq T) \ .$$

(2) The distribution of kinetic energies is similar to a Gaussian. This is appropriate for a vibrational probability function reflected off a repulsive potential that is nearly linear, as shown by curve 5 of Figure 1. For a repulsive wall that is curved, the energy distribution will be skewed, but the relative insensitivity of the experimental curves to small changes in P(E) will obscure this effect. For computational ease, only a first-order expansion of a Gaussian was used,

$$P_G(E)\,dE = \frac{3}{4\bar{E}}\left[1 - \frac{(E-\bar{E})^2}{\bar{E}^2}\right] dE, \tag{11}$$

$$(\text{for } 0 \leqslant E \leqslant 2\bar{E})$$

$$= 0 \qquad (\text{for } E > 2\bar{E}) \ .$$

This distribution, plotted in Figure 10, preserves the main features of an exact Gaussian distribution but introduces two energies where $P_G(E)\,dE$ drops to zero. One of these zero-intercepts was chosen to be $E = 0$, while the other was defined as $2\bar{E}$. Thus the average energy of this distribution is simply $\bar{E}$. The corresponding kinetic energy distribution along the z direction follows from Equation (8), and can be shown to be

Figure 10

Plots of the energy distribution functions used in the analysis of the ICR data. Curve A represents our approximation to a Gaussian distribution, and falls to zero at energies 0 and $2\bar{E}$, where $\bar{E}$ is the average energy. Curve B represents our approximation to a truncated Gaussian, and was fixed to be maximum at zero energy and to fall to zero at an energy E_{max}.

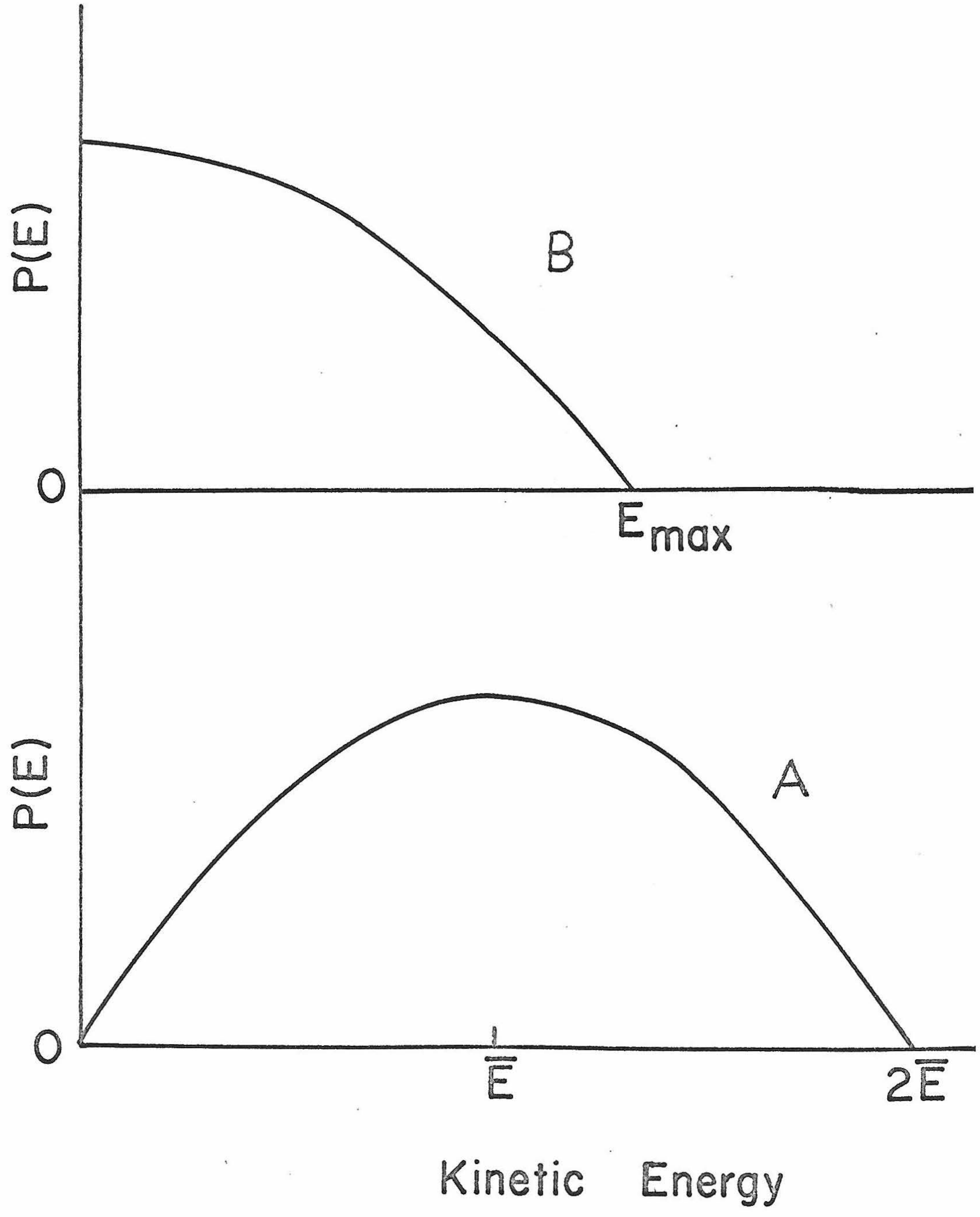
P(E)
B
0
E_{max}
P(E)
A
0
$\overline{E}$
$2\overline{E}$
Kinetic Energy

$$P_G(E_z)\,dE_z = \frac{1}{\overline{E}}\left[0.67\sqrt{\frac{\overline{E}}{E_z}} + 0.15\,\frac{{E_z}^2}{\overline{E}^2} - 0.5\,\frac{E_z}{\overline{E}}\right] dE_z \; . \quad (12)$$

(3) The distribution of kinetic energies is a truncated Gaussian. This is appropriate for a vibrational probability function convoluted with an ionic curve having a potential minimum, and is exemplified by curves like curve 4 of Figure 1. Only one such Gaussian was investigated, as the sensitivity of the data did not warrant a more detailed study. The distribution chosen was a Gaussian having its maximum probability at zero energy and decaying uniformly for larger energies. For computational ease, only a first-order expansion of a Gaussian was used, as shown in Figure 10

$$\begin{aligned} P_{TR}(E)\,dE &= \frac{3}{2E_{max}}\left[1 - (E/E_{max})^2\right] dE \\ & \qquad\qquad (\text{for } 0 \leq E \leq E_{max}) \qquad (13) \\ &= 0 \qquad\qquad (\text{for } E > E_{max}) \, . \end{aligned}$$

As with the full Gaussian, this distribution introduces an energy E_{max} where $P_{TR}(E)\,dE$ is zero. The corresponding distribution for E_z is found from Equation (8) to be

$$P_{TR}(E_z)\,dE_z = \frac{1}{E_{max}}\left[1.2\sqrt{\frac{E_{max}}{E_z}} + 0.3\,\frac{{E_z}^2}{{E_{max}}^2} - 1.5\right] dE_z \, . \quad (14)$$

The equations expressing the variation of $[CH_3^+]$ with trapping voltage now follow directly from Equation (9). We varied the energies T, $\bar{E}$, and E_{max} and examined the resulting curves $I(V_T)$.

It was found that curves arising from the first (single energy) distribution were virtually identical to those from the Gaussian distribution if the average energy $\bar{E}$ in the latter equalled the energy T used in the former. Since the single energy distribution can be considered as a sharply peaked Gaussian, this demonstrates that $I(V_T)$ is independent of the width of the Gaussian. This is a dramatic illustration of the insensitivity of $I(V_T)$ to certain changes in P(E). Figure 6 shows three curves resulting from the use of the Gaussian distribution at three different average energies. From these plots it is apparent that the experimental data for CH_3F is reproduced fairly well using any symmetric Gaussian-type distribution with an average kinetic energy of .5 ± .1 eV and arbitrary width (up to a minimum energy of zero, and, thus, a maximum energy of 1.0 eV).

There is thus an entire family of suitable Gaussian distributions with no *a priori* method to distinguish between them using the ICR data. However if it is assumed that photoionization at 21.2 eV produces an ionization pattern in CH_3F similar to that from electron impact ionization at 70 eV, then the PI results may be used to good advantage. They indicate that the maximum kinetic energy of CH_3^+ is at least 1.0 eV, and this accordingly restricts the number of permissible Gaussians to those having this maximum energy. Thus the kinetic energy distribution of CH_3^+ will be a Gaussian that drops to zero at

0 eV and 1.0 eV.

From conservation of linear momentum, the kinetic energy of F· in this dissociation is simply

$$E_F = \frac{m_{CH_3}}{m_F} E_{CH_3^+} \qquad (15)$$

where E_X and m_X represent the kinetic energy and mass of X. The total kinetic energy released upon dissociation will thus have a Gaussian-type distribution with an average energy of .9 eV, a maximum energy of about 1.8 eV, and a minimum energy of zero.

For CH_3Cl and CH_3Br, the experimental data is best reproduced using the truncated Gaussian distributions, with maximum energies E_{max} of ~.2 and ~.1 eV, respectively, as shown in Figures 7 and 8. Upon including the energy carried by X·, the maximum kinetic energies of dissociation are around .3 eV and .1 eV, respectively.

Finally it is appropriate to discuss the results of the direct kinetic energy analysis--photoionization experiment on CH_3F, shown in Figure 9. This data yields the kinetic energy distribution of CH_3^+ directly. The distribution resembles a Gaussian having an average energy of 1.0 eV and falls to zero near 0 and 1.8 eV. Including the energy carried by F, the maximum is found to occur at 1.8 eV, with extremums at 0 and 3.4 eV. The agreement with the ICR results is only fair.

There are two significant differences between the two experiments which may make a direct comparison of the results invalid, or at best difficult. First, the method of ionization was different. Second, the ICR experiments measured the z-component of the kinetic energy and this component is parallel to the direction of the ionizing radiation. This z-distribution was related to the total kinetic energy distribution by assuming that this total distribution was isotropic (i.e., had no angular dependence). By contrast, the photoionization results measured the energy distribution perpendicular to the photon beam.

Variable angle electron impact studies[23] of the formation of translationally excited H^+ ions from H_2 exhibit a marked angular dependence at electron energies below 200 eV. Thus, relatively more protons are detected in directions parallel to the beam. This anisotropy in number density of ions may also introduce an angular anisotropy in the kinetic energy distribution and could invalidate the original assumption of an isotropic distribution.

Similarly, the transition moment for excess energy CH_3^+ production via photoionization may well exhibit an angular dependence, thus precluding any extension of these results to the determination of an isotropic kinetic energy distribution.

V. Conclusions

We have observed that methyl cation formation in CH_3X involves the appearance of excess kinetic energy. For CH_3F the excess kinetic energy has a Gaussian distribution with zero probability for thermal ions. Significant differences between the electron impact ICR results and those obtained from photoionization are evident. These differences may arise from the different methods of ionization or from the different directions of detection of CH_3^+. The two kinetic energy distributions are shown in Figure 11.

The absence of thermal energy ions suggests that the dissociative ionic state resembles curve 3 of Figure 1. This is in agreement with the assertions of Krauss et al.

The distribution of total excess energy, both kinetic and vibrational, can be obtained from the PE spectrum, assuming the $(\sigma a_1)^{-1}$ ionic state to be entirely dissociative, and is also shown in Figure 11. A comparison of this distribution of total energy and the photoionization kinetic energy distribution should be meaningful, as both arise from the same process. The good agreement between the maximum total energy and the maximum kinetic energy implies that all the excess energy is released as kinetic energy at this point. Accordingly, the excess energy at threshold must be entirely vibrational. This demonstrates that at energies above threshold, vibrational-kinetic energy interconversion must occur and suggests that the lifetime of CH_3F^+ in the $(\sigma a_1)^{-1}$ state must be at least a few vibrational periods.

Figure 11

Excess energy distributions for CH_3^+ + F formation in CH_3F. The solid curves represent results from the photoionization experiment. P(KE) is the experimentally derived kinetic energy distribution, while P(KE + E_{vib}) is the total excess energy distribution, taken from the PE spectrum. The dashed curve represents the kinetic energy distribution from the ICR experiment.

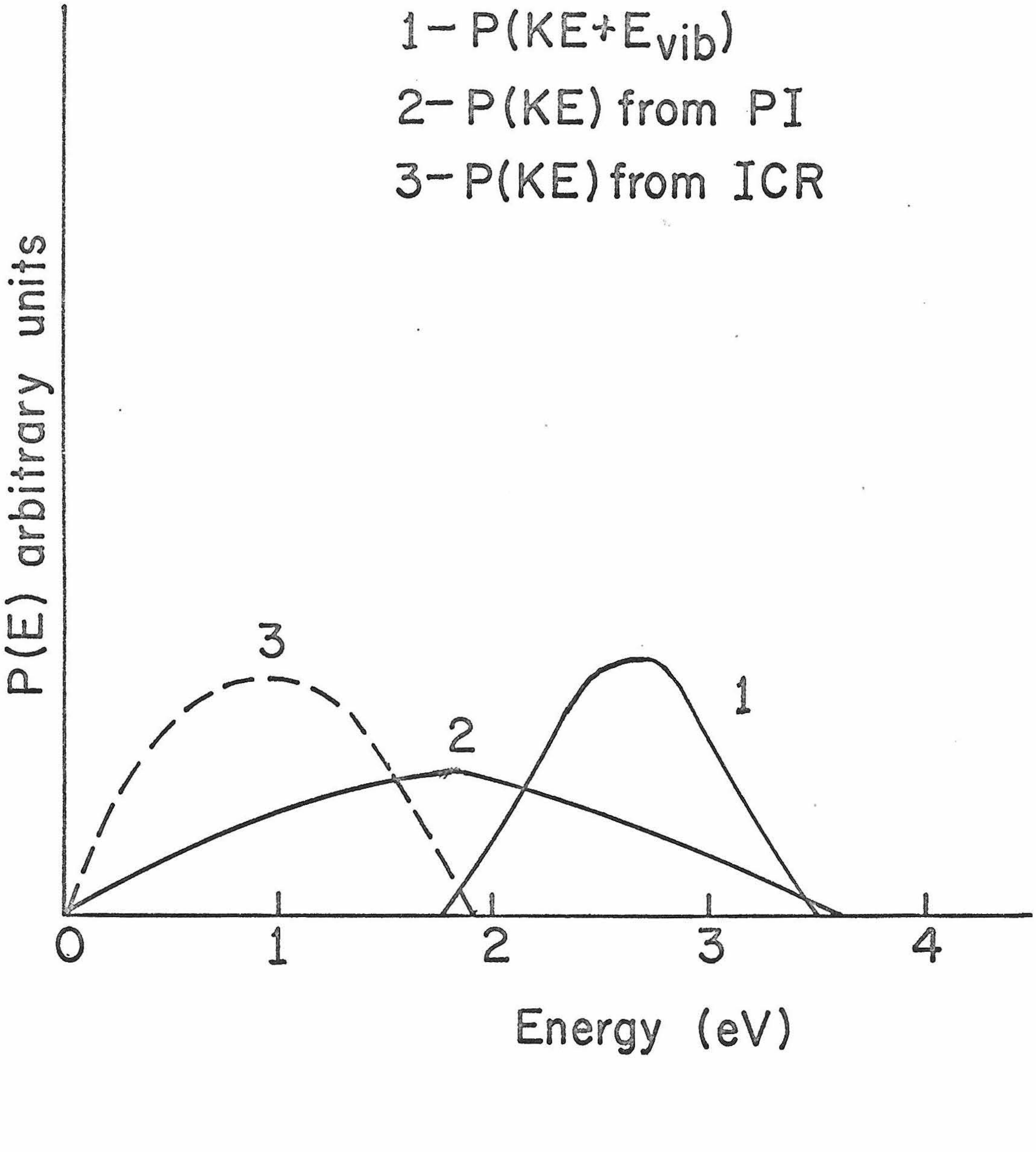
1– P(KE+E$_{vib}$)
2– P(KE) from PI
3– P(KE) from ICR
P(E) arbitrary units
3
2
1
0
1
2
3
4
Energy (eV)

The kinetic energy distribution of $CH_3^+ + X\cdot$ from CH_3Cl and CH_3Br derived from ICR data is shown in Figure 12. These curves demonstrate that thermal CH_3^+ ions are present, suggesting that the dissociation may occur from a bound ionic state similar to curve 2 in Figure 1. Alternatively, other ionic states that are sufficiently long lived to permit a delocalization of the excitation energy over various vibrational modes may contribute to the thermal CH_3^+ population. This could be the major mechanism of CH_3^+ production in CH_3Br, where virtually no kinetic energy was released.

As noted earlier, the onset of the PE band in CH_3Cl compatible with CH_3^+ formation (13.6 eV) is .3 eV below the appearance potential of CH_3^+ from the PI work (13.9 eV). This suggests the existence of a bound state of CH_3^+-Cl between 13.6 and 13.9 eV, and that at photon energies above 13.9 eV, enough vibrational energy is present for dissociation to occur. There is some evidence for this suggestion from the PI spectrum of CH_3Cl^+, which exhibits a pronounced rise near 13.5 eV that appears to level off near 14.0 eV as expected. Thus a bound ionic state resembling curve 2 of Figure 1 is implicated for CH_3Cl.

There may be important consequences of the excess kinetic and vibrational energy of CH_3^+ with respect to its reactivity. For example, ion intensity versus pressure and time plots for ions in CH_3F as studied by ICR[24, 25] have shown that CH_3^+ apparently undergoes a period of nonreactivity before reacting in a normal manner.

Figure 12

Experimentally derived kinetic energy distribution P(KE) for CH_3^+ + X· formation in CH_3Cl and CH_3Br. These results are from the ICR experiment.

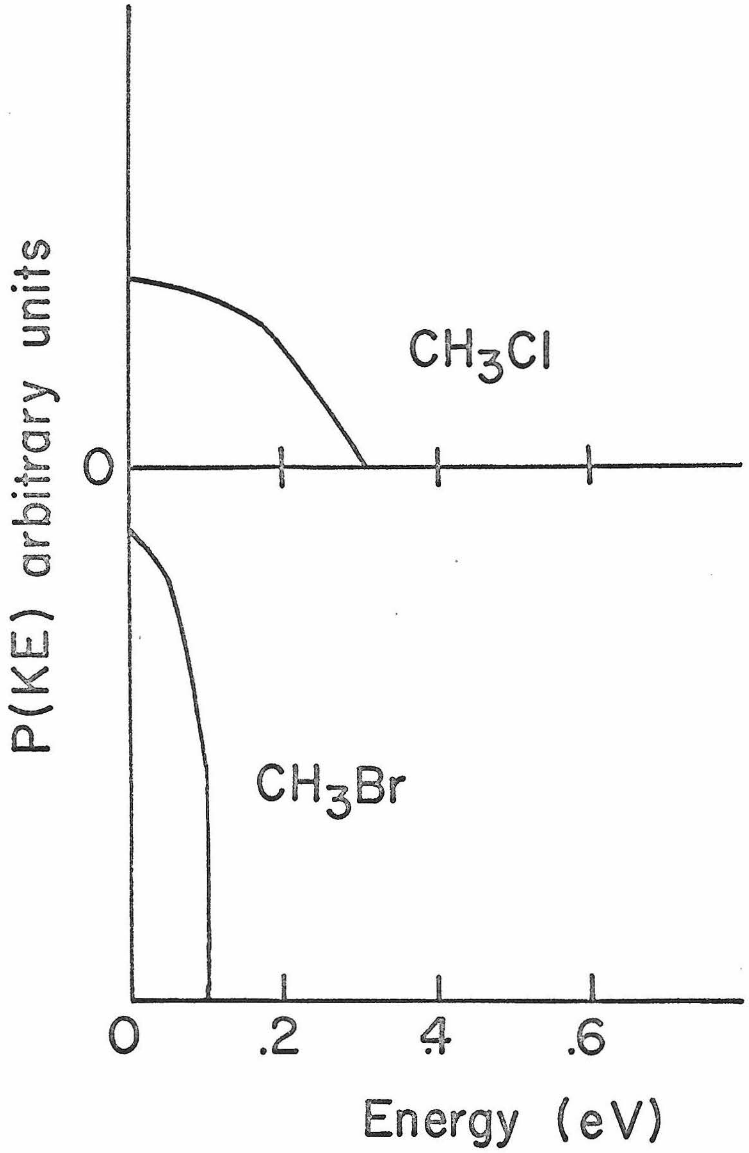
P(KE) arbitrary units
0
CH3Cl
CH3Br
0
.2
.4
.6
Energy (eV)

Using collision frequencies calculated from the Langevin model (Chapter 2), it is found that this nonreactive period allows enough time for about two collisions. This behaviour could be due to the excess energy that CH_3^+ possesses. The implication would then be that CH_3^+ requires several unreactive collisions involving vibrational or translational energy transfer before it cools down sufficiently to react.

As this work represents the first attempt to calculate ionic kinetic energy distributions using ICR spectroscopy, a few comments on the suitability of this technique are appropriate. Because of the large distribution of trapping wells, this method is unable to provide a detailed kinetic energy distribution. Thus, asymmetries in the distributions remain undetected. However, our results are qualitatively consistent with those inferred from photoionization and photoelectron spectroscopy. But the quantitative correlation of the ICR results with those from photon impact studies may be unreliable in those cases where anisotropic energy distributions are present.

References

1. W. Bleakney, Phys. Rev., 35, 1180 (1930).
2. F. L. Mohler, V. H. Dibeler and R. M. Reese, J. Chem. Phys., 23, 394 (1954).
3. W. Higgins and K. R. Jennings, Trans. Faraday Soc., 62, 97 (1965).
4. J. Olmsted III, K. Street, Jr. and A. S. Newton, J. Chem. Phys., 40, 2114 (1964).
5. T. Tsuchiya, J. Chem. Phys., 36, 568 (1962).
6. A. Hustrulid, P. Kusch and J. T. Tate, Phys. Rev., 54, 1037 (1938).
7. C. E. Berry, Phys. Rev., 78, 597 (1950).
8. C. R. Lagergren, Phys. Rev., 96, 823 (1954).
9. R. K. Curan and R. E. Fox, J. Chem. Phys., 34, 1590 (1961).
10. C. A. McDowell and B. C. Fox, J. Chem. Phys., 20, 1496 (1952).
11. H. D. Hagustrum and J. T. Tate, Phys. Rev., 59, 354 (1941).
12. H. D. Hagustrum, Rev. Mod. Phys., 23, 185 (1951).
13. C. J. Noutary, J. Rev. NBS, 72A, 479 (1968).
14. J. Appell and C. Kubach, Chem. Phys. Lett., 11, 486 (1971).
15. V. H. Dibeler and R. M. Reese, J. Res. NBS, 54, 127 (1955).
16. M. Krauss, J. A. Walker and V. H. Dibeler, J. Res. NBS, 72A, 281 (1968).
17. D. W. Turner, C. Baker, A. D. Baker and C. R. Brundle, "Molecular Photoelectron Spectroscopy," Wiley-Interscience, London, 1970.
18. A. W. Potts, H. J. Lampka, D. G. Streets and W. C. Price,

Phil. Trans. Roy. Soc., London, A268, 59 (1970).

19. T. A. Carlson and R. M. White, Disc. Faraday Soc., 54, 1 (1972).

20. T. B. McMahon and J. L. Beauchamp, Rev. Sci. Instr., 42, 1632 (1971).

21. A. D. Williamson, P. le Breton, W. T. Huntress and J. L. Beauchamp, to be published.

22. R. H. Staley and J. L. Beauchamp, to be published.

23. G. H. Dunn and L. J. Kieffer, "Fifteenth Annual Gaseous Electronic Conference," Boulder, Colorado, 1962.

24. J. L. Beauchamp, D. Holtz, S. D. Woodgate and S. L. Patt, J. Amer. Chem. Soc., 94, 2798 (1972).

25. R. J. Blint, T. B. McMahon and J. L. Beauchamp, J. Amer. Chem. Soc., in press.

Chapter 16

Comparison of Trapped-Ion Instruments

In this concluding chapter, it is appropriate to summarize the various features of the trapped-ion high pressure mass spectrometer (HPMS) and to compare it to trapped-ion ICR spectrometry (ICR) and, whenever possible, to the space charge trapping (SCT) apparatus of Herod and Harrison.[1]

Other ion-trapping instruments have been devised, including one utilizing a three dimensional, rotationally symmetric, quadrupole field.[2] Trapping times as long as several days were obtained at low pressures ($\sim 10^{-10}$ torr). This instrument has not been applied to the study of ion-molecule reactions (see however Reference 3).

Table I lists the principal feature of the first three instruments which pertain to the study of ion-molecule reactions. Features of particular interest are discussed in more detail below.

I. Discrimination

To correct for possible mass discrimination of the electron multiplier, it is necessary to independently calibrate the mass sensitivity of this detector. This is usually effected by recording primary ion spectra of known compounds or mixtures.

While ICR spectrometry suffers only minimal loss of total trapped-ion current at typical operating pressures, significant ion loss in the high pressure instrument is evident except at very low

Table I

Properties and Applications of Trapped-Ion Instruments

	HPMS	ICR	SCT
Method of trapping	crossed field	crossed field	space charge
Mass range	in principle, no limit	1-500	in principle, no limit
Discrimination	can be appreciable	negligible	may be negligible
Pressure range	10^{-5} to 10^{-2} torr or more	10^{-7} to 10^{-5}	probably similar to HPMS
Ion residence time	.01-10 msec	.01-10 sec	.01-~100 msec
Temperature range	subthermal to ~400°C	ambient only	?
Negative ions	yes	yes	no
Average ion kinetic energy	~.5 eV	~.1 eV	~.5 eV
Direct study of reaction of specific ion	needs minor modification	yes double resonance	no
Energy dependence of ion-molecule reactions	yes qualitatively by varying trapping voltage	yes qualitatively by varying trapping voltage	no
Metastable decompositions	yes	no	yes

pressures. In agreement with theoretical predictions, trapping efficiencies also deteriorate for heavier mass ions. If all ions in a particular reactive system have masses within a factor of ~ 3, then discriminatory ion loss is not apparent. Accordingly, normalization of the total trapped ion signal at each reaction time is a valid procedure to aid in extracting rate constants. For systems have ions of greatly differing masses (viz. H_2-CH_4 mixture, Chapter 6), discriminatory ion loss is evident at short times, thus precluding many kinetic inferences.

Primary ions formed with excess kinetic energy cannot be trapped efficiently in the high pressure instrument. This effect has also been observed in the trapped-ion mass spectrometer of Herod and Harrison, but is not usually evident in the ICR.

The different ion loss characteristics of the two instruments arise primarily from the differences in magnetic fields. Sharp et al.[4] have investigated ion motion in the trapped-ion ICR cell of McIver et al.[5] and have qualitatively determined the average ultimate trapping time of an ion in this instrument. Ion loss is assumed to occur solely via a series of collisions causing the ion to random walk to one of the drift plates. Their analysis is directly applicable to the trapped-ion cell of this laboratory. The average ultimate trapping time τ was found to be

$$\tau_{\mathrm{ICR}} \approx \frac{D^2 q^2 B^2}{2.4\, m k T n K c^2} \tag{1}$$

where D is the distance from the origin to the drift plates, m is the ionic mass, n is the neutral pressure, K is the collision frequency of the ion and the other symbols have their usual meaning. The quantity 2.4 arises from including collisions displacing the ion in the direction (drift direction). For Ar^+, with B = 10000 gauss, D = 0.5", n = 1.0×10^{-4} torr and K = 1.0×10^{-9} cm^3 $molecule^{-1}$ sec^{-1}, the average retention time is determined to be ~3 sec.

A similar analysis using the geometry of the high pressure source yields

$$\tau_{hp} \approx \frac{D^2 q^2 B^2}{2 m k T n K c^2}, \tag{2}$$

where only radial ion loss has been considered. With a magnetic field of 700 gauss, D = .375" and other conditions as above, τ_{hp} is found to be 5.7 msec. The difference is almost 3 orders of magnitude, and arises almost exclusively from the difference in magnetic fields. Thus the differing ion loss characteristics of the two instruments is understood.

II. Pressure range

Source pressures as high as 10 μ have been employed in the present studies using the high pressure instrument, and higher pressures could easily be reached if the source aperture sizes were reduced. Accordingly, processes involving collisional stabilization of intermediates can routinely be investigated. Trapped-ion studies of these processes have not previously been reported. The high pressure limit of trapped ion ICR is determined by collisional broadening of the resonance lines (usually significant at pressures above 1 μ) and by the long time required for product ion analysis (1 msec). If ion-molecule reactions in the detection region are to be avoided, this restricts the high pressure limit to about .1 μ. Minimal collisional stabilization is usually observed at these pressures.

III. Ion Residence Times

Typical ion residence times in the high pressure instrument are between .1 and 1 msec, considerably shorter than the infrared radiative lifetimes of most ions. Thus the ion-molecule reactions of vibrationally excited ions can be studied. This capability is not present for ICR.

IV. Direct Study of Reactions of Specific Ions

The ability of the ICR to determine complex reaction pathways using double resonance has no counterpart at present in the high pressure mass spectrometer. The double resonance technique has been used to good advantage to selectively eject ions from the trapping region and thus observe processes that are undetectable in the high pressure instrument.

The double resonance feature can readily be incorporated into the HPMS through use of a "split" ion source. This simply involves modifying the cylindrical ion source screen to electrically insulate two halves of this screen, as shown in Figure 1. Application

Figure 1

Sketch of the split ion source potentially useful for the study of reactions of specific ions.

F -- Filament
P1 -- Anode plate
P2 -- Control plate
P3 -- Electron-entry plate
P4 -- Ion-exit plate
P5 -- Drawout plate
S -- Ion energy screen. This element is split as shown to permit an rf field to be applied to the chamber.

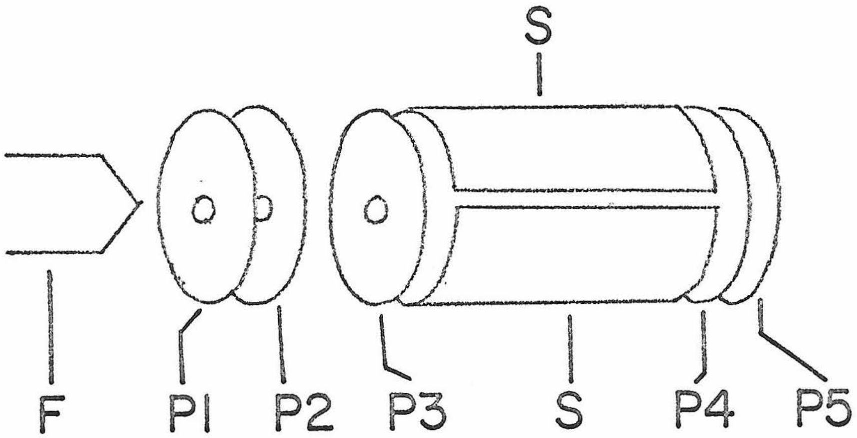
S
F
P1
P2
P3
S
P4
P5

of an rf electric field to these elements at the cyclotron frequency of an ion will cause that ion to be accelerated in analogy to ICR double resonance. The effect on the reactive system can then be ascertained.

V. Metastable Decompositions

The flight time of ions between the ion source and the quadrupole spectrometer is typically about 50 μsec and variable over a wide range. It is thus possible to observe metastable decompositions occurring during this flight period. Ions arising from such decompositions will be characterized by anomalous arrival times at the detector. Introduction of a fast-response electron multiplier would permit a quantitative study of these processes.

VI. Conclusions

The major advantages of ICR spectrometry at present are the absence of ion loss and the availability of the double resonance technique. The high pressure instrument is well suited for the accurate determination of ion-molecule rate constants, the study of collisional stabilization processes and the study of temperature dependences of ion-molecule processes. Introduction of a solenoidal electromagnet having a higher ultimate field would remove many of the difficulties associated with its operation. Incorporation of a "split" ion source would duplicate the advantages of ICR double resonance.

References

1. A. A. Herod and A. G. Harrison, *Int. J. Mass Spec. Ion Phys.*, **4**, 415 (1970).
2. P. H. Dawson and N. R. Whetten, *J. Vacuum Sci. Tech.*, **5**, 1 (1967).
3. R. F. Bonner, G. Lawson and J. F. J. Todd, *Int. J. Mass Spec. Ion Phys.*, **9**, 421 (1972) have used quadrupole trapping up to 3 msec to observed ion-molecule reactions in methane and ethylene.
4. T. E. Sharp, J. R. Eyler and E. Li, unpublished results.
5. R. T. McIver, *Rev. Sci. Instr.*, **41**, 555 (1970).